NUCLEAR INSTRUMENTS AND METHODS

GREGG M. SINCLAIR LIBRARY
UNIVERSITY OF HAWAII

EDITORIAL BOARD:

J. B. ADAMS (CERN)
F. A. ALSINA (Buenos Aires)
E. AMALDI (Rome)
H. L. ANDERSON (Chicago)
K. T. BAINBRIDGE (Cambridge, Mass.)
P. R. BELL (Oak Ridge)
R. E. BELL (Montreal)
A. BERTHELOT (Saclay)
H. BRINKMAN (Groningen)
E. H. COOKE–YARBOROUGH (Harwell)
S. DE BENEDETTI (Pittsburgh)
M. DE HEMPTINNE (Louvain)
A. DE-SHALIT (Rehovoth)
M. DEUTSCH (Cambridge, Mass.)
S. DU TOIT (Pretoria)
B. S. DŽELEPOV (Leningrad)
W. GENTNER (Heidelberg)
F. S. GOULDING (Berkeley)
P. C. GUGELOT (Amsterdam)
H. HALBAN (Paris)
O. HAXEL (Heidelberg)
P. HUBER (Basel)
S. KIKUCHI (Tokyo)
J. KOCH (Copenhagen)
M. S. KOZODAEV (Moscow)
S. LIVINGSTON (Cambridge, Mass.)
E. M. MCMILLAN (Berkeley)
M. G. MEŠČERJAKOV (Moscow)
P. B. MOON (Birmingham)
M. L. OLIPHANT (Canberra)
W. PAUL (Bonn)
A. S. RAO (Bombay)
G. SALVINI (Rome)
P. SAVIĆ (Belgrade)
P. SCHERRER (Zürich)
CH. SCHMELZER (CERN)
R. TANGEN (Oslo)
D. TAYLOR (Northampton)
V. I. VEKSLER (Moscow)
G. VON DARDEL (CERN)
O. WERNHOLM (Stockholm)
R. R. WILSON (Cornell)
S. D. WINTER (Saclay)

NUCLEAR INSTRUMENTS & METHODS

A JOURNAL ON ACCELERATORS, INSTRUMENTATION
AND TECHNIQUES IN NUCLEAR PHYSICS

EDITOR: K. SIEGBAHN - UPPSALA

VOLUME 14

NOVEMBER 1961 — JANUARY 1962

NORTH-HOLLAND PUBLISHING COMPANY — AMSTERDAM

PRINTED IN THE NETHERLANDS
DRUKKERIJ MEIJER N.V. - WORMERVEER AND AMSTERDAM

NOVEMBER 1961 VOLUME 14 (1961) No. 1

GREGG M. SINCLAIR LIBRARY
UNIVERSITY OF HAWAII
8-7-62

NUCLEAR INSTRUMENTS & METHODS

A JOURNAL ON ACCELERATORS, INSTRUMENTATION AND TECHNIQUES IN NUCLEAR PHYSICS

EDITOR: K. SIEGBAHN - UPPSALA

CONTENTS

J. B. PARKER, J. H. TOWLE, D. SAMS and P. G. JONES, Multiple scatter corrections by Monte Carlo 1

A. ALBERIGI-QUARANTA, B. RIGHINI, V. PRODI and O. RIMONDI, On a 2π gas-flow counter for low-level counting 13

L. VARGA, Pulse shape discrimination 24

MILORAD MLADJENOVIĆ, Some new proposals for design of Compton spectroscopes 33

G. BRUNHART, C. D. GALL, C. VITTITOE, K. SCHNEIDER and V. P. KENNEY, Scanning apparatus for bubble chamber data analysis 38

B. CONRAD, Das Raumwinkelfilter, Ein Blendensystem zur Messung geladener Teilchen aus Kernreaktionen 41

M. O. DEIGHTON, Statistical errors arising from use of a gated pulse train for total live time measurement during pulse amplitude analysis 48

C. F. COLEMAN, A network analogue for a quadrupole lens system 53

O. M. BILANIUK, B. B. MARSH, A. K. HAMANN and J. C. HEURTLEY, An array of solid state counters with delay line pulse sorting 63

W. C. PARKER and Y. GRUNDITZ, Rapid carrier free separation technique 71

H. J. RIJKS, Stabilizing a scintillation spectrometer by means of a low frequency modulated light source 76

P. H. ROSE, A. B. WITTKOWER, R. P. BASTIDE and A. GALEJS, Quantitative measurements of ion beam properties 79

THOMAS FRIESE, Tragbarer Pulsgenerator für Prüfzwecke 83

JUICHI AKUTSU, A mechanism of the propagation of Geiger discharge in halogen-quenched G.M. counters 87

K. V. VLADIMIRSKY and B. A. LABZOV, Single sample spin generator spectrometer 94

A. CITRON, L. HOFFMANN and C. PASSOW, Investigation of the nuclear cascade in shielding materials 97

NORTH-HOLLAND PUBLISHING COMPANY — AMSTERDAM

NUCLEAR INSTRUMENTS AND METHODS

A journal on accelerators, instrumentation and techniques in nuclear physics

EDITOR: K. SIEGBAHN, UPPSALA

EDITORIAL BOARD:

J. B. ADAMS (CERN)
F. A. ALSINA (Buenos Aires)
E. AMALDI (Rome)
H. L. ANDERSON (Chicago)
K. T. BAINBRIDGE (Cambridge Mass.)
P. R. BELL (Oak Ridge)
R. E. BELL (Montreal)
A. BERTHELOT (Saclay)
H. BRINKMAN (Groningen)
E. H. COOKE-YARBOROUGH (Harwell)
S. DE BENEDETTI (Pittsburgh)
M. DE HEMPTINNE (Louvain)
A. DE-SHALIT (Rehovoth)
M. DEUTSCH (Cambridge Mass.)
S. DU TOIT (Pretoria)
B. S. DŽELEPOV (Leningrad)
W. GENTNER (Heidelberg)
P. C. GUGELOT (Amsterdam)
H. HALBAN (Paris)
O. HAXEL (Heidelberg)
P. HUBER (Basel)
S. KIKUCHI (Tokyo)
J. KOCH (Copenhagen)
M. S. KOZODAEV (Moscow)
S. LIVINGSTON (Cambridge Mass.)
E. M. MCMILLAN (Berkeley)
M. G. MEŠČERJAKOW (Moscow)
P. B. MOON (Birmingham)
M. L. OLIPHANT (Canberra)
W. PAUL (Bonn)
A. S. RAO (Bombay)
G. SALVINI (Rome)
P. SAVIĆ (Belgrade)
P. SCHERRER (Zürich)
CH. SCHMELZER (CERN)
R. TANGEN (Oslo)
D. TAYLOR (Northampton)
V. I. VEKSLER (Moscow)
G. VON DARDEL (CERN)
O. WERNHOLM (Stockholm)
R. R. WILSON (Cornell)
S. D. WINTER (Saclay)

INSTRUCTIONS FOR CONTRIBUTORS

Contributions may be sent to the Editor, Professor K. Siegbahn, Institute of Physics, University of Uppsala, Sweden, either directly or through the intermediation of one of the members of the Editorial Board. Contributions may be written in English, French or German but should always, except for very short papers, be supplied with a brief abstract in English. Figures should be in inked original drawings or glossy prints and they should be sufficiently large. Contributors should make sure that important details in drawings and photographs will show up clearly in the diminished copy used by the publisher.

Books for review should be sent to Professor Siegbahn.

Objective and descriptive material on endeavours and product developments from the industry for the section "Spotlight on Industry" should be sent directly to the publishers, North-Holland Publishing Company, P.O. Box 103, Amsterdam.

Nuclear Instruments and Methods is published monthly. The subscription price of a volume of 360 pages is $ 17.00 (130s), postage free.

Subscriptions should be sent to the publishers, North-Holland Publishing Company, P.O. Box 103, Amsterdam, or to any subscription-agent.

No part of this issue may be reproduced in any form, by print, photoprint, microfilm or any other means without written permission from the publisher.

65-24542

Ten.
QC786
N883
U. 14-15

PHILIPS

nuclear reactor instrumentation

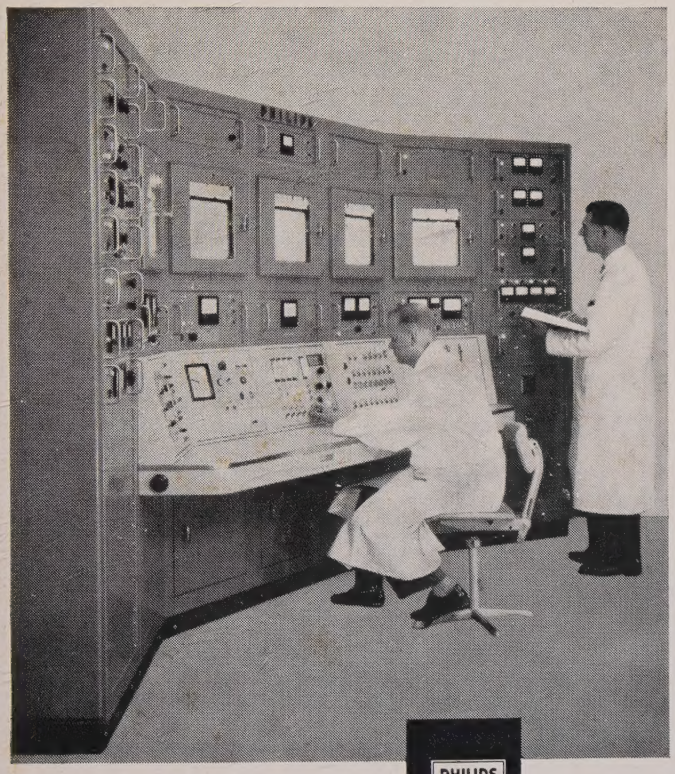

Philips have designed and supplied complete systems for the operation of nuclear reactors.
Such control and monitoring instrumentation is aimed at operation of the reactor to fulfil its function and providing adequate protection against radiation hazards.
To obtain co-ordinated functioning of the control devices, circuits are incorporated for combining information from the instruments used for measuring, recording, and control.
Shown here are the combined control console and equipment racks for the swimming pool type research facility, recently delivered to the Technische Hogeschool, Delft, The Netherlands.

PHILIPS

PHILIPS NUCLEAR EQUIPMENT

N.V. PHILIPS' GLOEILAMPENFABRIEKEN - EINDHOVEN - THE NETHERLANDS - SCIENTIFIC EQUIPMENT DEPARTMENT

SCINTILLATION SPECTROMETRY

NON-OVERLOADING LINEAR PULSE AMPLIFIER NE 5202:

with 5 microsecond recovery for 100 times overload. Designed for scintillation spectrometry and pulse height analysis studies, this amplifier features high gain (50,000), high gain stability (better than 0.25% per week), good linearity, low noise (less than 40 microvolts at input), excellent overload characteristics, and operation at high duty cycles. Rise time 0.2 microseconds and integral linearity 0.15%. Preamplifier NE 5202A also available. Based on the double delay line differentiated Fairstein system, it consits of three high gain feedback groups, and a White cathode follower output.

SINGLE CHANNEL PULSE HEIGHT SELECTOR NE 5102

Resolving time 1.2 microsecs; 3–140 volts operating range with energy zero drift less than 0.05 volts per day; 0 to 10 volt gate width with less than 0.01 volts per day drift; maximum counting rate, 2×10^5 c.p.s.; Larger gate widths and automatic scanning facilities available.

E.H.T. SUPPLY UNIT NE 5302

Output stability 0.01%; low noise and ripple—less than 3 mV; output voltage continuously variable from 500–1,500 V; output current 5 mA.

E.H.T. SUPPLY UNIT NE 5303:

As NE 5302, but with output voltage range from 1,000–5,000 V.

SHIELDED SCINTILLATION HEAD UNITS NE 5501–3:

containing White cathode follower preamplifiers with noise level of 25 microvolts; photomultipliers of 1″ or 2″ can be accomodated; for general use or for C14 and H3 investigations with special rotary light locking device.

OTHER UNITS AVAILABLE:

Precision Ratemeter NE 5401.

Scanning scintillation spectrometer Ne 8601. Complete human body monitors and low level counting facilities.

Multi-channel scintillation spectrometer NE 8201 for industrial tracer investigations. Scintillometers for geophysical exploration, including transistorised airborne and carborne equipment.

C14 and H3 counting unit HE 8301.

Exclusive concessionaire for C.D.C./Bendix 100-channel Transistorised Kicksorter in Great Britain.

Sole agent for Harshaw Sodium Iodide Crystals in the United Kingdom.

Write for new catalogue and price list

For full details of the above and of our SCINTILLATION PHOSPHOR PRODUCTS (plastic, liquids, loaded liquids, crystals, gels, neutron detectors, and chemiclas) write to:

Nuclear Enterprises (G.B.) Ltd.

BANKHEAD MEDWAY, SIGHTHILL, EDINBURGH 11, SCOTLAND. (TEL. CRA 5262)

Associate Company: Nuclear Enterprises Ltd., 550, Berry Street, Winnipeg 12, Canada.

(nuh) 1406

efficient 4-input, 400-channel pulse height analyzer is easy to use, has many "system" features, weighs 37 lbs., occupies one cubic foot, operates on 110 or 220 volts, 50 to 400 cycles AC.

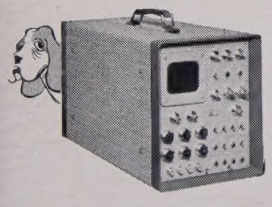

Each input has its own linear amplifier and gain control. Information can be stored in four 100-channel groups, two 200-channel groups or one 400-channel group. Direct readout on TMC Model 500 Decimal Printer, X-Y or strip chart recorder, IBM computer typewriter or paper tape punch. Add these facts (and the moderate price of the instrument) to the versatility suggested by front panel photo — and you have the reason for the TMC 404's popularity. Write for Bulletin 400.

TMC TECHNICAL MEASUREMENT CORPORATION
441 WASHINGTON AVENUE, NORTH HAVEN, CONN. — CE 9-2501

Bendix TIME-OF-FLIGHT MASS SPECTROMETER

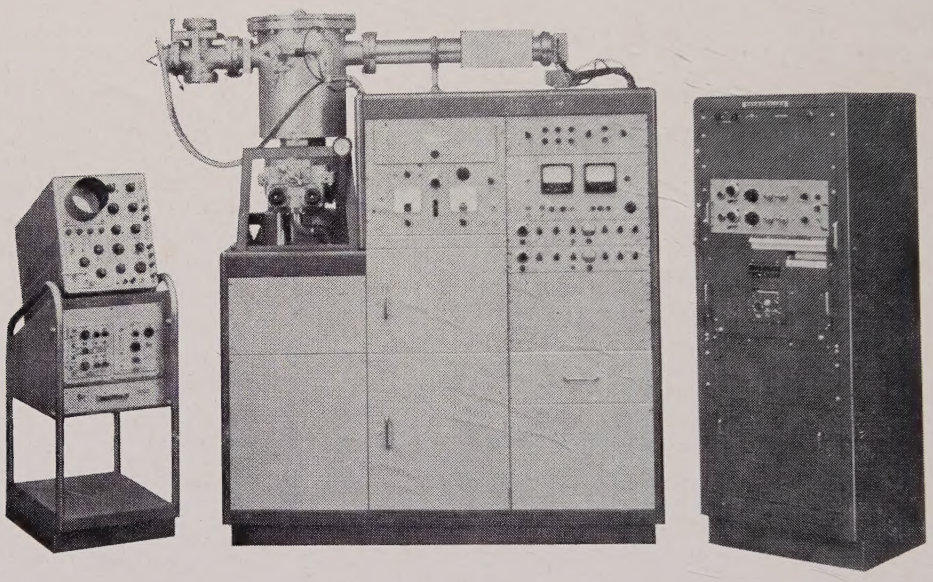

BENDIX MODEL 14-101 MASS SPECTROMETER SHOWN WITH AN OSCILLOSCOPE AND AN ANALOG RECORDER

The Bendix* Time-of-Flight Mass Spectrometer combines high speed and sensitivity with extreme versatility. 10,000 complete mass spectra are presented each second covering a mass range of m/e 1 to m/e 5000 with unit resolution to mass 200. The instrument exhibits the unique ability to handle a wide range of samples from the usual low boiling gases and liquids to solids with vapor pressure as low as 10^{-9} atmospheres at 2500°K. The versatility of the mass spectrometer coupled with a wide variety of Bendix engineered sample inlet systems make it particularly suited to such application as Monitoring chromatograph output, determinations of vapor pressures, heats of vaporization, free radical studies, solids' analyses, shock tube research, appearance potential measurements, photoionization, molecular structure studies, photochemical reaction studies, combustion analyses and plasma jet analyses.

*Registered Trademark

SPECIAL Bendix International FEATURES

• 10,000 complete mass spectra per second • Parts per million sensitivity • Wide mass range—1-5000 • High resolution • Multi-Channel recording • Modular plug-in electronics • Wide sample range • Analyzes liquids, solids, gases • Open source and detector geometry • Wiley electron multiplier • Stainless steel vacuum system • Getter-type pump (Optional) • Wide variety of sample inlet systems • No volume restricting magnets • Low noise level multiplier • Oscilloscope readout • Line of sight inlets • Variable electron energy

Technical Sales and Service Representatives located in most major countries.

Bendix International DIVISION THE Bendix CORPORATION

205 E. 42ND ST., NEW YORK 17, N.Y., U.S.A. CABLE ADDRESS: "BENDIXINT", N.Y.

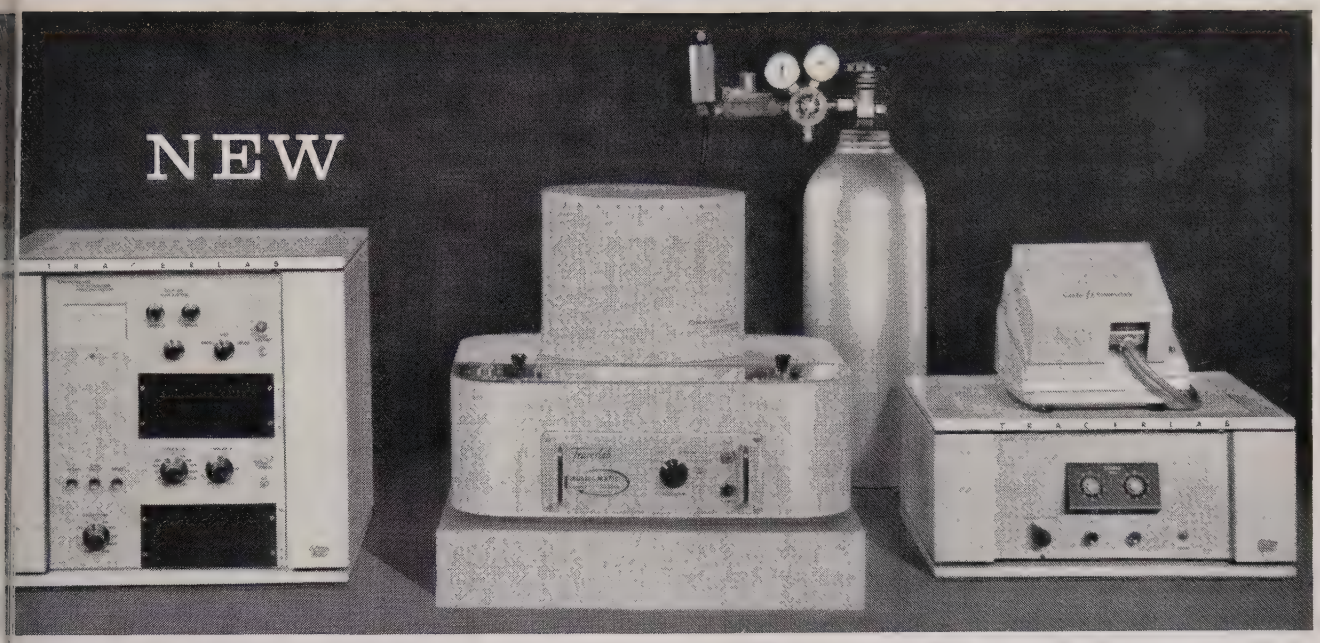

Tracerlab

Low Background Beta Counting System

omni/guard

- **BACKGROUND LESS THAN 0.3 CPM**
- **1″ OR 2″ SAMPLES**
- **MANUAL OR AUTOMATIC SYSTEMS**

Guaranteed ultra low background, *guaranteed* high efficiency counting, compact shielding, automatic or manual operation, a choice of sample sizes . . . all these advantages are combined in the new Omni/Guard System from Tracerlab. This new system utilizes the very latest Tracerlab instruments . . . the new Multi/Matic Sample Changer, the Omni/Guard Anti-Coincidence Flow Counter and the new Omni/Guard Scaler. Each is the most advanced in its field. Small wonder the new Tracerlab Omni/Guard System outperforms all other low background Beta counting systems.

With the new Tracerlab Omni/Guard System it is possible to assay solid beta samples *with counting rates of less than 1 c.p.m.* You'll get superb counting efficiency (even for low energy beta rays, C^{14}, S^{35} etc.) because of the ultra thin Mono/Mol Windows of the Omni/Guard Flow Counter (<125 $\mu g/cm^2$). Very low background coupled with high counting efficiency means less starting material is needed, lower activity levels can be measured and counting time is substantially reduced. Yet the new Tracerlab Omni/Guard System is moderately priced and economical to operate and maintain.

The Tracerlab Omni/Guard System may be combined with a variety of standard readouts; Tracer/Matic timers; Time and Count printers and Time, Count and Count Per Minute printers.

By extending the range of detection sensitivity further than ever before, the new Tracerlab Omni/Guard System opens a new era of instrumental analysis. You should have complete information on this latest Tracerlab development. *Write for Tracerlab Omni/Guard Bulletin*

Tracerlab

Tracerlab Kelvinet

1601 Trapelo Road, Waltham 54, Massachusetts
2030 Wright Avenue, Richmond 3, California

European address: **TRACERLAB, S. A.** 277, Chaussée d'Anvers, Malines, Belgium

NANOSECOND PULSES? - MICROSECOND PULSES?

MODEL 414

CALIBRATION PULSER

Decay Times	*Ranges*
0.003 microseconds	0 - 1 millivolts
0.01 microseconds	0 - 5 millivolts
0.03 microseconds	0 - 10 millivolts
0.1 microseconds	0 - 50 millivolts
0.3 microseconds	0 - 100 millivolts
1. microseconds	0 - 500 millivolts
3. microseconds	0 - 5 Volts
10. microseconds	0 - 10 Volts
100. microseconds	0 - 50 Volts
	0 - 100 Volts

Dual purpose- manual or motor driven slider.
Dual 50 ohm output permits coincidence circuit applications.
Internal standard cell calibration.
Polarity switch for positive or negative pulses.
0.1% helical potentiometer.
High pressure hermetically sealed mercury relay.

Write for details.

$ 785 f.o.b. factory

RADIATION INSTRUMENT CO.

P.O. BOX 733

SILVER SPRING, MARYLAND, U.S.A.

NORTH-HOLLAND BOOKS

Plasma Physics

by

J.G. Linhart

CERN, Geneva

"The author of the present work, who is well known for his contributions in the C.T.R. field, has given in his book an interesting presentation of the complementary approaches of (1) individual particle motion, and (2) a fluid description of a plasma in relation to the study of high temperature discharges.
This book can be highly recommended."

Institute of Physics Bulletin

6×9″ 290 pp. 125 figs. Gld. 25.00 (50 s.)

NORTH-HOLLAND PUBLISHING COMPANY AMSTERDAM

Sole distributor U.S.A.: Interscience Publishers Inc. New York

NORTH-HOLLAND BOOKS

Imperfections in Crystals

by H. G. VAN BUEREN, *Philips Laboratories, Eindhoven*

CONTENTS

Part I: General properties of lattice imperfections
Part II: Imperfections in metals
Part III: Imperfections in non-metallic crystals

Just out second revised edition

XVIII + 675 PAGES, NUMEROUS PHOTOGRAPHS - GUILDERS 55.— (10S.)

ASK YOUR BOOKSELLER OR:

NORTH-HOLLAND PUBLISHING COMPANY - AMSTERDAM

SOLE DISTRIBUTION IN U.S.A.: INTERSCIENCE PUBLISHERS INC. - NEW YORK

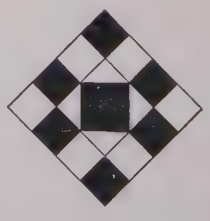

When it's a matter of using ACCELERATOR RADIATIONS . . . Discuss it with HIGH VOLTAGE ENGINEERING

High Voltage Engineering stands out as the group to talk to when a problem involving the application of accelerator radiations is on the agenda. High Voltage Engineering and Applied Radiation Corporation have unparalleled experience in this field. Accelerator applications *today* include:

ELECTRONS AND X-RAYS FOR:

Radiation sterilization of medical and surgical materials ■ Preservation of foods ■ Radiation cross-linking of plastic film and wire ■ Initiation of chemical reactions ■ Modification of semiconductors ■ X-ray therapy ■ Radiography of castings, weldments, reactor components or solid fuel rocket engines ■ Fundamental chemical, biological and nuclear research.

POSITIVE IONS AND NEUTRONS FOR:

Rapid, sensitive analysis by neutron activation ■ Materials evaluation, environmental simulation, solid state physics, wear and corrosion studies ■ Reactor engineering, pulsed sources for subcritical reactors and shielding studies ■ Neutron cross-sections ■ Physics research and teaching.

Reliability from experience with more than 250 particle accelerators in the field.

HIGH VOLTAGE ENGINEERING

HVEC — arco

BURLINGTON, MASSACHUSETTS, U. S. A.

APPLIED RADIATION CORPORATION
HIGH VOLTAGE ENGINEERING (EUROPA) N.V.

n de Graaff electron celerator and x-ray urce — for research processing up to 4 ev, 4 kw — 15″ to)″ scanning.

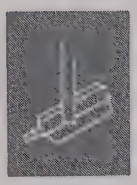

Van de Graaff and Linac x-ray generators for radiography 1 to 15 Mev up to 6000 r/min.

Insulating Core Transformer (ICT) High Voltage dc power supply and electron accelerator. 300 to 600 kv up to 30 ma.

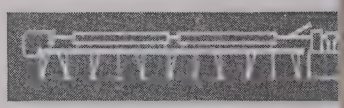

ARCO
S and L-Band microwave linear electron accelerators for research. 4 to 100 Mev. — up to 40 Kw average electron power.

New 165 cm electromagnetic isotope separator for nuclear chemistry.

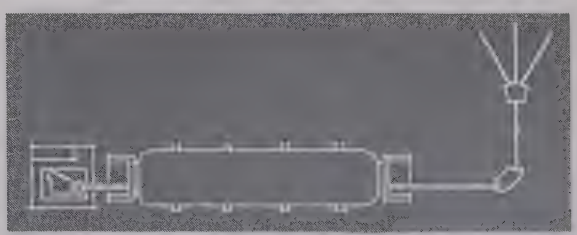

Tandem Van de Graaff Positive Ion Accelerator — 6 to 20 Mev. (3-stage) with 90° beam analyzer and 3-portal switching magnet.

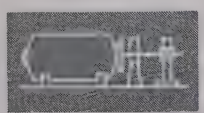

Van de Graaff Positive Ion Accelerator and neutron source — for research and activation analysis. Pulsed or continuous operation. 0.4 to

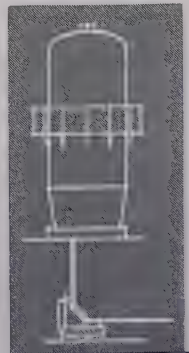

Van de Graaff Positive Ion Accelerator with heavy ion sources, nano-second pulsing — 5.5 Mev. with 90° beam analyzer.

600 kV Generator

Research Centres and Industry alike find the modern, polished solution to the problem of continued high voltage in the

SAMES ELECTROSTATIC GENERATOR

Electrostatic Paintin
with the STATRON

HIGH VOLTAGE GENERATORS

* 50 kV to 600 kV
* 20 W to 3 kW
* Positive or negative polarity
* Medium or high stability for
* Electrostatic precipitation
* Electrical testing
* Electronic optics
* X-rays
* Nuclear Physis, etc.

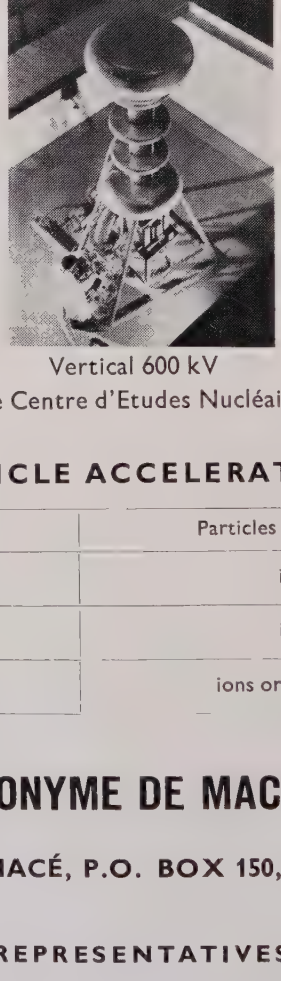

Vertical 600 kV
Accelerator at the Centre d'Etudes Nucléaires de Grenoble

ELECTROSTATIC PAINTIN

The STATRON is a portable equipme
for electrostatic painting, featuring

* 90 kV voltage
* Complete safety, owing to use electrostatic generator.
* Paint output: 15 litres/hour
* Supply: 110 or 220 V, single phase.
* Consumption: 110 Watts

PARTICLE ACCELERATORS

Type	Acceleration Voltage	Particles Accelerated	Application
J	150 kV	ions	Neutron Generator b
L	300 kV	ions	D/T or D/D reaction
S	600 kV	ions or electrons	All applications

SOCIETE ANONYME DE MACHINES ELECTROSTATIQUE

21, RUE JEAN MACÉ, P.O. BOX 150, TEL: 44.77.64 GRENOBLE, FRAN

REPRESENTATIVES

GENERATORS AND ACCELERATORS

Austria: AUSTRONIK, Salzburg – Belgium: CENTRONICS, Brussels – Chinese People's Republic: Cie OLIVIER, Paris – Denmark: DANSK SCIENTA, Copenhagen – Great Britain: MILES HIVOLT LTD., Shoreham by Sea – Italy: SECI, Milan – Netherlands: PROJECTO, Amsterdam – Norway: LEHMKUHL, Oslo – Portugal: A.G.M.E., Lisbon – Spain: CRESA, Barcelona – Sweden: SCIENTA SCANDIA, Gothenburg – Switzerland: OMNIRAY, Zurich – Western Germany: DR. NAMUR, Darmstadt – Bulgaria, Czechoslovakia, Eastern Germany, Hungary, Poland, Rumania, U.S.S.R.: CIFAL, Paris.

ELECTROSTATIC PAINTING EQUIPMENT

Algeria: FAMPA, Algiers – Austria: PETER PETERSEN, Vien
Belgium: DURMECO, Brussels – Chinese People's Republic:
OLIVIER, Paris – Denmark: DANKS SCIENTA, Copenhage
Eire: HODGES & SONS, Dublin – Great Britain: AEROST
LDT., London – Italy: TRASMETAL, Milan – Netherlands: STU
MAN, Wormerveer – Norway: LEHMKUHL, Oslo – Portu
RAMADA, Ovar – Spain: INSTITUTO ELECTROQUIMICO,
celona – Sweden: SCIENTA SCANDIA, Gothenburg – Swit
land: REGSA, Lausanne – Western Germany: A. WIRTH, R
lingen – Bulgaria, Czechoslovakia, Eastern Germany, Hung
Poland, Rumania, U.S.S.R.: CIFAL, Paris.

Accuracy

Stability

Linearity

Flexibility

256-Channel Pulse Height Analyzer - mod. A 45 - CISE

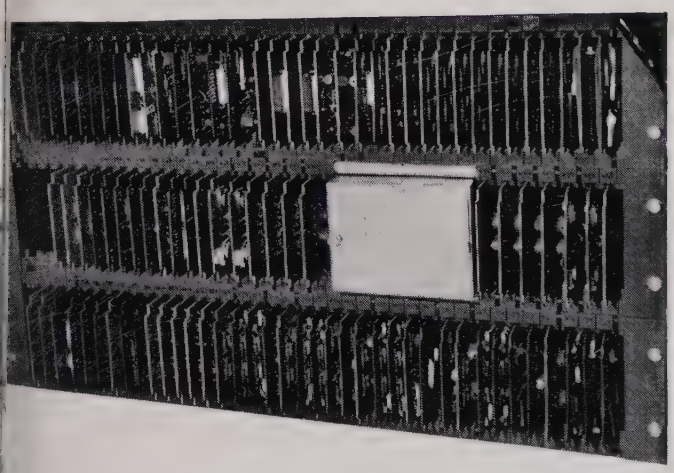

SPECIFICATIONS

- 256-channel Ferrite core memory.
- Linearity: better than 0,5 %.
- Stability: better than ½ channel per day.
- Dead time: 16 + 0,25N + T μs. (Where N = channel number; T = rise time protection).
- Automatic bi-directional storage.
- Tridimensional analysis: 8 x 32; 16 x 16.
- Memory subgrouping (manually or electronically selected); 2 x 128; 4 x 64; 8 x 32; 16 x 16.
- Coincidence and anticoincidence operation.
- Crystal controlled live timer.
- Internal automatic programmer.
- Spectrum transfer: 128' - 128'' and viceversa.
- Continous readout during measures.
- Multiscaler operation.
- Time-of-flight plug-in unit.
- Spectrum stripping operations.
- Readout by IBM electric typewriter (other high speed printing devices can be used) or punched paper tape.

Construction for maximum reliability and servicing facilities

BEFORE YOU DECIDE contact our technical staff

LABEN

Laboratori Elettronici e Nucleari S.r.l.

MILANO - VIA EDOARDO BASSINI 15 - TELEFONO 236.4.101/3

-how to sell your nuclear products internationally-

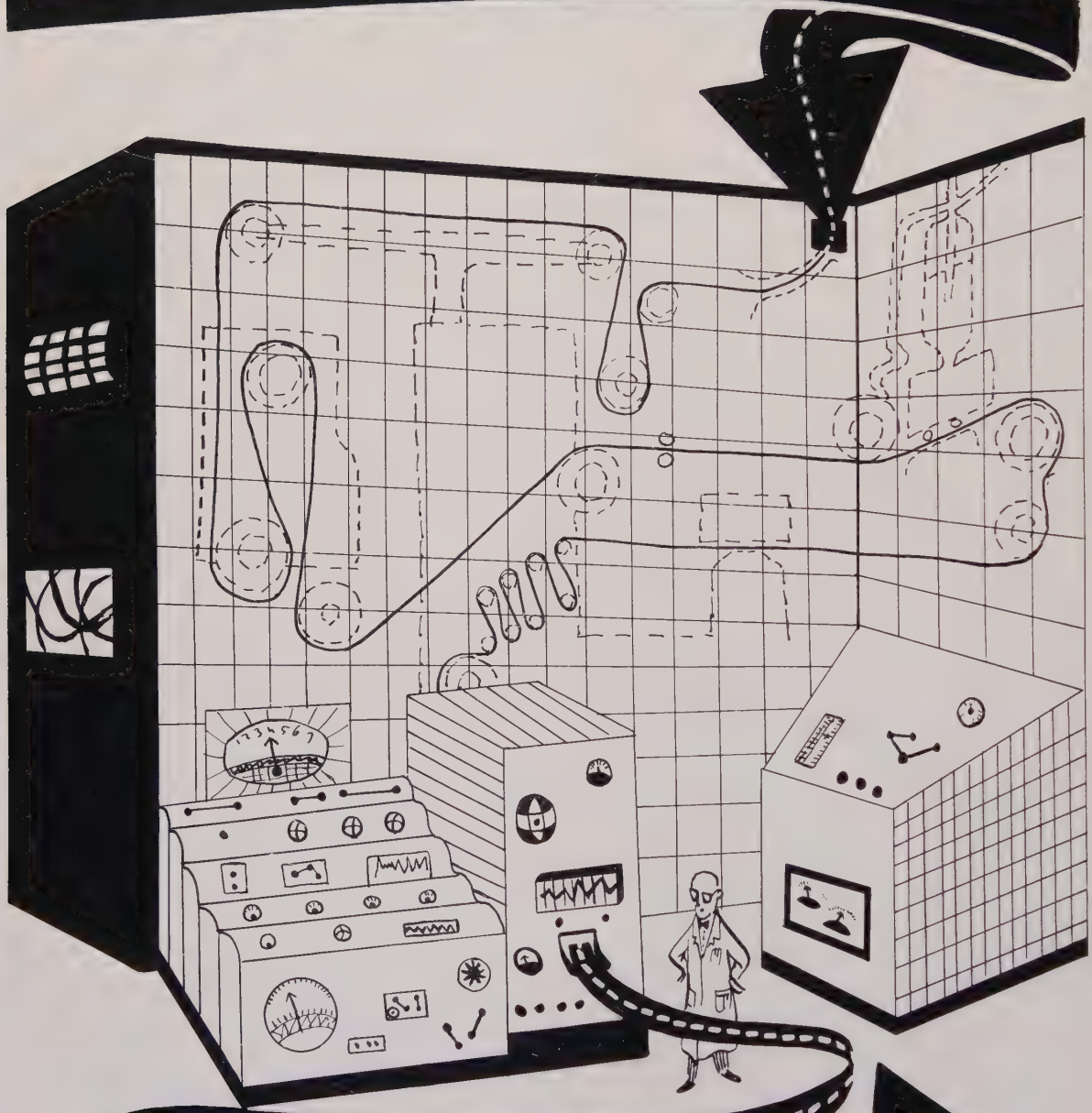

-advertise in nuclear instruments & metho

Go International with your Sales Program today-Write

William F. Baars-Advertising Manager, North-Holland Publishing Company

P.O. Box 103, Amsterdam, The Netherlands

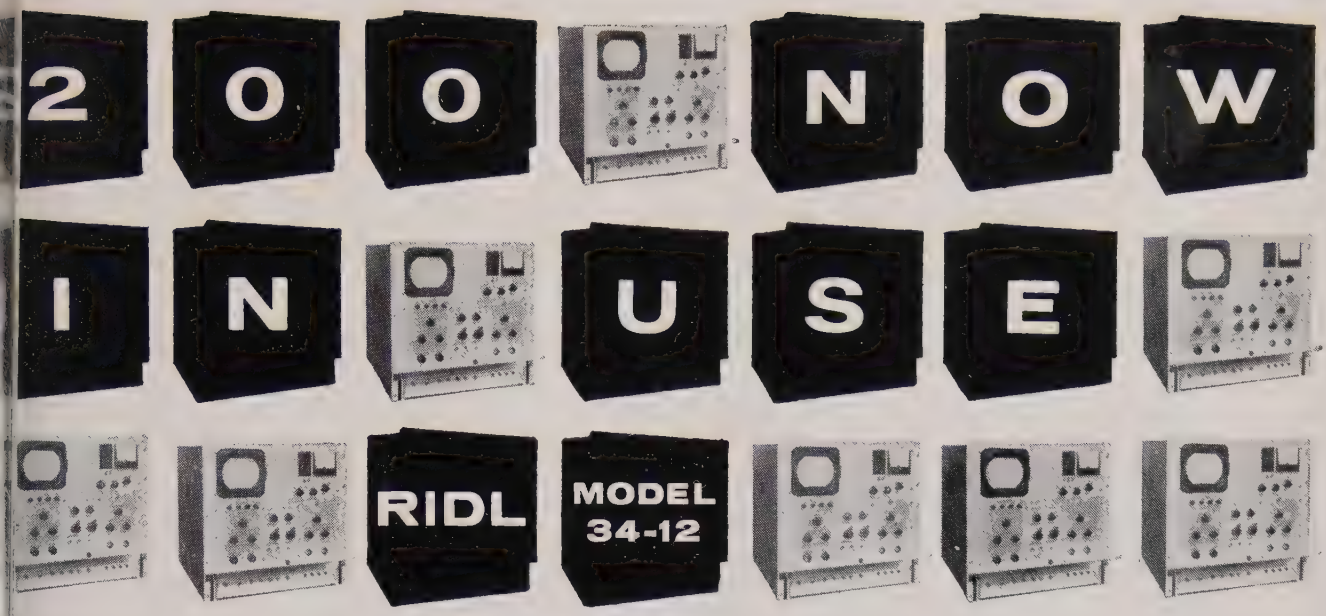

RANSISTORIZED 400 CHANNEL PULSE HEIGHT ANALYZER

CONTACT RIDL FOR NEW LOW PRICES

- Live Display (logarithmic opt.)
- 5" built-in C. R. T.
- Prompt and delayed coincidence
- Automatic programming including:
  - auto-print
  - auto-record
  - auto-transfer
- Memory subgrouping
- 10^5 count capacity (10^6 opt.)
- External programming
- Crystal controlled live timer
- Free course of instruction
- Failsafe channel identification
- High voltage power supply
- Multiple detector operation
- Add-subtract logic

See this analyzer at the Atomfair in Chicago— Booth number 308-309.

WIDEST CHOICE OF READOUTS—typewriter, X-Y plotter, punched paper tape, H.P. printer, Magnetic Tape, Manual Digital Display.

WIDEST CHOICE OF INPUTS—either transistorized or vacuum tube amplifiers including A61, A8, DD2, A1D, etc., and Magnetic Tape.

WIDEST CHOICE OF APPLICATIONS—pulse height analysis, time mode, multichannel scaler, Mossbauer studies, spectrum stripping.

WIDEST CHOICE OF ACCESSORIES AND OPTIONS

- IBM Typewriter
- Tally Paper Tape Punch
- Manual Meter Readout
- 4-Channel Mixer Amplifier
- 8 Subgroups of 50 channels
- Log Display and Readout
- Mobile Analyzer Table
- Hewlett-Packard Printer
- Friden Adding Machines
- Magnetic Tape
- 10^6 Count Capacity
- Random Access Memory

RIDL

Radiation Instrument Development Laboratory, Inc.

4501 WEST NORTH AVENUE • MELROSE PARK, ILLINOIS

PHONE: MUrray 1-2323 • Cable Address: RADILAB

• • • ORTEC presents the latest evolution in semiconductor detectors; featuring improved resolution, lower noise, deeper depletion depths, simplified connections, a more rugged and compact design, larger range of sensitive areas and negligible dead layer. Warranted performance. Each unit accompanied by test data and instruction manual. From forty-five dollars. Delivery: Stock to two weeks.

For further product information, write to:

OAK RIDGE TECHNICAL ENTERPRISES CORP.

P. O. BOX 485 OAK RIDGE, TENNESSEE

ORTEC INSTRUMENTS FOR RESEARCH:

- ☐ Charged Particle Detection and Spectroscopy
- ☐ Neutron Detection and Spectroscopy
- ☐ Low Noise Amplifier Systems
- ☐ Sum and Coincidence Circuits
- ☐ R. F. and Duo Plasmatron Ion Sources and other Accelerator Terminal Electronics

UCLEAR INSTRUMENTS AND METHODS 14 (1961) 1–12; NORTH-HOLLAND PUBLISHING CO.

MULTIPLE SCATTER CORRECTIONS BY MONTE CARLO

J. B. PARKER, J. H. TOWLE, D. SAMS and P. G. JONES

Atomic Weapons Research Establishment, Aldermaston, Berks.

Received 17 August 1961

his paper describes two Monte Carlo programmes which have een written to correct measurements of neutron scattering ross sections for effects due to the finite dimensions of the cattering sample. The first programme calculates multiple catter corrections to be applied to the experimentally deter-hined ratio $\sigma_{in}:\sigma_{el}$, and also obtains the flux attenuation correction. The second enables the shapes of the experimentally determined differential elastic and inelastic cross sections to be corrected for multiple scatter. An account of an application of the programmes to measurements of the scattering of 1.5 MeV neutrons by Na^{23} is also given.

1. Introduction

Measurements of differential cross sections for the lastic and inelastic scattering of fast neutrons are arried out by allowing neutrons from a source effectively a point), to impinge on a sample which s generally in the form of a cylindrical shell, and by counting the emergent neutrons. The detector, which can be moved on a circle centred on the sample, is well shielded from neutrons coming direct from the source. The inelastic events are distinguished from the elastic events provided that the final energy of the inelastically scattered neutron falls within certain limits. In some experiments, for example, these neutrons are not distinguished from those scattered elastically if they have lost less than 0.25 MeV energy, and are not detected at all if their energy is less than 0.4 MeV.

In order to distinguish the scattered neutrons from background, and also to obtain data at a reasonable speed, it is necessary to employ, within limits, a large scattering sample. These limits are imposed by two effects, multiple scattering and flux attenuation, for which corrections to the data have to be applied. Keeping these corrections within reasonable bounds, a suitable compromise is reached with approximately a mole of material, which, in the form of a hollow cylinder usually has a fairly uniform transmission of some 75 per cent.

Since the actual mean flux F within the sample cannot be directly measured, it is convenient to measure the cross sections in terms of the flux F_0 at a point corresponding to the centre of the sample when the sample is removed. Thus the apparent elastic cross section $\sigma_{el}(\phi)$ plotted from the experimental data is defined by†

$$X_{el}(\phi) = \sigma'_{el}(\phi) n F_0 \, d\Omega$$

where $X_{el}(\phi)$ is the number of neutrons scattered into solid angle $d\Omega$ and n is the number of atoms. Due to flux attenuation the value of σ'_{el} will be too small by a factor F/F_0.

Apart from this, corrections for multiple scatter in the sample are necessary. A singly scattered neutron will (subject to the considerations listed above) be correctly identified as elastic or inelastic. However, a neutron which subsequently collides again before being counted may be incorrectly classified if this second collision is inelastic. Usually the ratio $\sigma_{in}:\sigma_{el}$ will be overestimated in the experiment. Also the variation in neutron count with detector position will not represent the true differential cross section owing to multiple scatter.

The programmes described here have been used to correct scatter cross sections for Na^{23} measured recently at AWRE[1]). In sections 4 and 6 we give the results of the calculations for the case of 1.5 MeV incident neutrons.

† Strictly this implies a sample of spherical symmetry. The general case will be discussed further in section 5.

[1]) J. H. Towle and W. B. Gilboy, (to be published).

2. The Monte Carlo Approach

By tracing neutron histories by the Monte Carlo method, the effects of flux attenuation and multiple scatter are automatically taken into account. A Monte Carlo calculation, using the correct physical nuclear data, will therefore parallel the physical process, apart from statistical fluctuations. The problem is therefore to find out what nuclear data, when put into the Monte Carlo calculation, simulates the experiment. In the next two sections we shall describe the basis on which two IBM 7090 Monte Carlo programmes, called B3 and B4, are constructed.

3. Programme B3-Flux Correction and Overall Multiple Scatter Correction

This is a straightforward Monte Carlo programme which enables the flux attenuation factor referred to in section 1 together with the overall multiple scatter correction to be calculated. The geometry is that of fig. 1. We have assumed the source to be situated at a point S and have taken the neutrons impinging on the cylindrical sample to be mono-energetic. These approximations incur negligible error. The programme simply tracks the neutrons from S by straightforward Monte Carlo methods and catalogues the neutrons leaving the sample

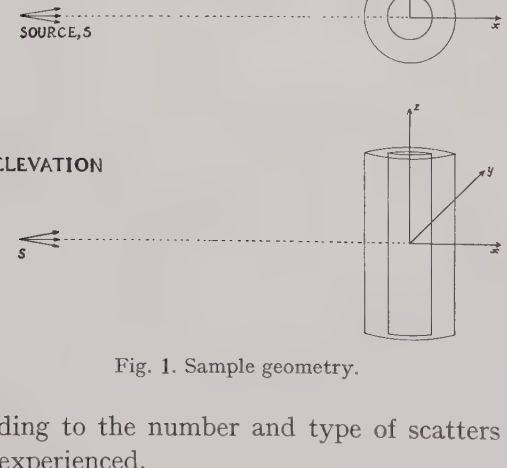

Fig. 1. Sample geometry.

according to the number and type of scatters (if any) experienced.

With this sort of problem there are two lines of attack. The first is to simulate the physics as accurately as possible, starting neutrons, in accordance with the prescribed experimentally determined angular distribution at S. A proportion of these will miss the cylinder altogether and such tracks will be wasted; of the remainder, several tracks will not interact with the sample, passing straight through, and will likewise fail to contribute. A Monte Carlo employing this first philosophy would therefore in a sense be uneconomic, a relatively small amount of valuable information being obtained for a large initial number of neutrons.

In the second approach this wastage is overcome by using special techniques to ensure that all initial particles collide at least once in the sample. Such techniques are well known and have been used before in this type of problem[2]). However, since they involve neutron weighting, the processing time for each track is increased.

With fast machines the arguments in favour of sophisticated methods for this simple programme are less compelling and we have adopted the first approach. Neutrons are started in a cone that includes the largest sample under consideration. The output is straightforward and a specimen is illustrated in table 1. The programme recognizes all possible scatter types and detailed nuclear data for the tracking are available in high speed stores. A typical calculation, for 10000 neutrons penetrating the sample, requires about $5\frac{1}{2}$ minutes of IBM 7090 computing time.

The nuclear data input is an assumed one (section 2). The experimental ratio $\sigma'_{el}:\sigma'_{in}$ can be corrected as follows. If a fraction f_1 of the neutrons which at first collision undergo an elastic scatter, subsequently undergo an inelastic scatter, then the inelastic counts are enhanced at the expense of the elastic counts, which are reduced by a factor $(1 - f_1)$. Further, if a fraction f_2 of neutrons which at first collision have an inelastic scatter, subsequently undergo a further inelastic scatter, the number of inelastic events is underestimated by a factor $(1 - f_2)$. We have assumed here for argument's sake that double inelastic events are not detected. Thus if primed quantities refer to experi-

[2]) E. D. Cashwell and C. J. Everett, A Practical Manual on the Monte Carlo method for random walk problems (Pergamon Press, 1959).

TABLE 1
Scattering corrections for 1.5 MeV neutrons in a Na sample

	Run										All runs
	1	2	3	4	5	6	7	8	9	10	
Number started	13151	13338	13243	13155	13156	13226	13250	13164	13237	13240	132200
Number penetrating sample	10000	10000	10000	10000	10000	10000	10000	10000	10000	10000	100000
Collided tracks	1806	1795	1744	1722	1738	1828	1799	1765	1779	1841	17817
Single scatters	1576	1549	1503	1525	1483	1561	1565	1501	1552	1594	15409
Double scatters	198	210	214	175	219	231	205	222	192	210	2076
Triple scatters	29	31	23	16	30	30	25	38	28	29	279
Four or more scatters	3	5	4	6	6	6	4	4	7	8	53
No. of elastic first collisions	1524	1477	1476	1433	1458	1546	1519	1475	1459	1533	14900
No. of these that subsequently had inelastic scatter	29	27	22	24	31	36	26	27	32	31	285
f_1	0.0190	0.0183	0.0149	0.0167	0.0213	0.0233	0.0171	0.0183	0.0219	0.0202	0.0191
No. of inelastic first collisions	282	318	268	289	280	282	280	290	320	308	2917
No. of these that subsequently had a further inelastic scatter	6	6	8	3	10	11	13	6	6	9	78
f_2	0.0213	0.0189	0.0299	0.0104	0.0357	0.0390	0.0464	0.0207	0.0188	0.0292	0.0267
F_0/F	1.126	1.149	1.174	1.181	1.171	1.119	1.142	1.153	1.151	1.112	1.148

mental determinations and unprimed quantities refer to the correct physical values.

$$\frac{\sigma'_{el}}{\sigma'_{in}} = \frac{(1-f_1)}{(1-f_2)\dfrac{\sigma_{in}}{\sigma_{el}} + f_1}. \tag{3.1}$$

The Monte Carlo results from which f_1 and f_2 are calculated, are obtained on the basis of assumed elastic and inelastic cross-sections. If the assumed values are close to the physical truth, f_1 and f_2 will be determined sufficiently accurately; if not it would be necessary to repeat the calculations with new nuclear data input.

To correct for the flux attenuation in the sample, we require to estimate F_0/F (section 1) to get

$$\sigma_T = \sigma_{in} + \sigma_{el} = \frac{F_0}{F}\left[\frac{\sigma'_{in}}{1-f_2} + \frac{\sigma'_{el}}{1-f_1}\left(1 - \frac{f_1}{1-f_2}\right)\right].$$

This factor can be calculated simply from the Monte Carlo results and the starting data, as follows. F_0 is the flux per cm^2 of neutrons tracked from the source, which would obtain at a point corresponding to the centre of the sample if the sample is removed. F is equal to $N/n\sigma_T$ where N is the number of neutrons which had at least one collision in the sample, n is the number of atoms, and σ_T is the assumed total cross-section. The correction F_0/F will be subject to error; first there is the purely statistical error which can be controlled by arranging for replicate runs; secondly if the assumed σ_T is incorrect, F_0/F will be incorrectly estimated, errors in $[(F_0/F) - 1]$ being roughly proportional to the error made in estimating σ_T.

4. Results of Programme B3 calculations

The sample is a solid cylinder of Na weighing 70.89 g of diameter 4.5 cm and height 4.6 cm, located with its centre 11 cm away from the source.

The neutrons were started according to an angular distribution obtained experimentally. The nuclear data input for the Monte Carlo were taken from[3]) save that the cross-sections in the energy range 1.3–1.9 MeV were estimated by applying a rough correction to the experimental results. These

[3]) B. R. S. Buckingham, K. Parker and E. D. Pendlebury, AWRE Report No. 0-28/60 (1960).

cross-sections were taken to be $\sigma_T = 2.45$ barns; $\sigma_{el} = 2.05$ barns; $\sigma_{inel} = 0.40$ barns. The differential elastic cross-section used in the calculation was the experimentally determined one, uncorrected for multiple scatter, and the inelastic scattering was taken to be isotropic in the laboratory system.

Ten runs were carried out. For each run a sufficient number of neutrons are started at S in a cone of semi angle 16°.44 to ensure that 10000 neutrons penetrate the sample. This cone is chosen so as just to embrace the sample.

Results for each run are given in table 1. From them we compute, using the methods of section 3, $f_1 = 0.0191$ (s.d. 0.0007), $f_2 = 0.0268$ (s.d 0.0028) and $F_0/F = 1.148$ (0.006). The uncorrected experimental results were

$$\sigma'_{el} = 1.794; \quad \sigma'_{inel} = 0.375$$

and an application of the f_1, f_2, and F_0/F corrections gives

$$\sigma_T = 2.50; \quad \sigma_{el} = 2.10; \quad \sigma_{inel} = 0.40\,.$$

5. Programme B4-Multiple Scatter corrections to the differential elastic cross sections

In section 3 a Monte Carlo programme for counting the neutron tracks in various categories was described. For correcting the differential cross-sections (elastic and inelastic) we are interested not only in how many neutrons in these categories escape, but in what direction. A straightforward Monte Carlo simulation of the problem would be very inefficient, since physically the detector is situated a long way from the sample, and subtends a very small solid angle at it; thus few neutrons would actually hit it. This situation can be alleviated to some extent by using in the calculation a "detection band" subtending a much larger solid angle than exists in the experiment. Even with this technique (which is used at the expense of introducing some error), however, the computation time for a statistically reliable result is very lengthy.

The crux of the programme described here lies in the calculation of the *density* (number per unit area) of neutron tracks in a given category, at the centre of a detector situated at a prescribed point on a semicircle surrounding the sample (fig. 2). This is done by examining each neutron immediately before collision and calculating the chance that it would leave the sample after the collision and contribute to the detector in question, either as an elastic or as an inelastic event. Each neutron collision is therefore employed to estimate some

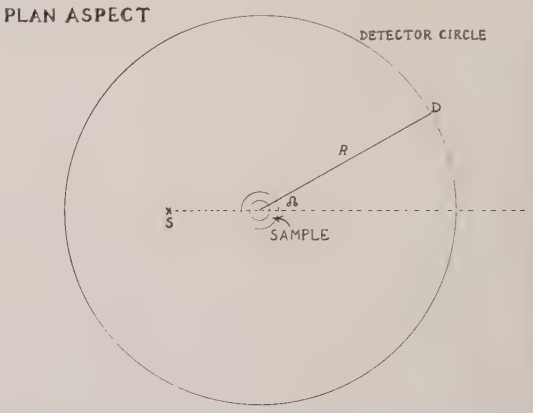

Fig. 2. Detector circle.

quantity for each of a number of detector positions (actually thirty are catered for in the programme).

Conceptually, the occurrence of a collision in the sample switches on a torch, as it were, whose axis is coincident with the neutron's incident track. This torch produces light whose spectrum and intensity follow the shape and size of $\sigma_{el}(\phi)$ and $\sigma_{in}(\phi)$, the input data to the Monte Carlo programme, where ϕ is the scattering angle about the torch axis. The whole sphere on which the counter circle lies is illuminated with light from the torch, but in this application the only concern is to measure the light density at the thirty positions around the counter circle. These densities are accumulated, in appropriate categories, for each position as tracking proceeds.

To consider a specific example, we imagine a scattering sample of Na^{23} subjected to a source of 1.5 MeV incident neutrons, for which the only actions are elastic and inelastic scatter, capture being negligible. To estimate the density of neutrons hitting a detector whose co-ordinates (fig. 2) are ($R\cos\Omega$, $R\sin\Omega$, 0) which are detected as *elastic events* we start by considering all *first* collisions, whether elastic or inelastic. Independently of what type of collision does in fact occur, we know that a proportion $p = \sigma_{el}(1.5)/\sigma_{tot}(1.5)$ will be elastic and a

roportion $(1 - p)$ inelastic. The expected number f elastic first collisions will therefore be

$$\sum_{i=1}^{N} p = Np ,$$

here N is the number of observed first collisions. or each point of first collision in the sample, P, here will be some definite direction $\mathbf{d}$ (P, Ω) in which the neutron must emerge if it is to strike the entre of the detector. If it be assumed (as is the ase in most practical applications) that the radius f the detector circle be large compared with the limensions of the sample we may write

$$\mathbf{d}(P, \Omega) = \mathbf{d}(\Omega)$$

For each first collision, therefore, a score is lefined for each detector position. This score is the roduct of three quantities

(a) the chance, p, that the scatter is elastic;

(b) the chance, $\exp\{ - r(\mathbf{d})/m(E) \}$, that the emergent neutron (of energy E) will not be further scattered before leaving the target;

(c) the differential elastic cross-section used in the Monte Carlo input data, $\sigma_{el}(\phi)$, where ϕ is the angle between the initial neutron track and the direction $\mathbf{d}(\Omega)$.

Here $r(\mathbf{d})$ is the distance of travel in the sample of a neutron leaving P with direction $\mathbf{d}$, and m is the neutron mean free path, a function of the emergent energy E and hence, for elastic scatter, of the known incident energy $E_0 = 1.5$ MeV and the scatter angle ϕ.

The programme computes the score $p\,\sigma_{el}(\phi) \exp\{ - r(\mathbf{d})/m(E) \}$ for each counter position and accumulates this over all first collisions. In the actual calculation $\sigma_{el}(\phi)$ is normalized by first dividing by

$$\sigma_{el} = \int_{-1}^{+1} \sigma_{el}(c)\, \mathrm{d}c ,$$

where $c = \cos\phi$. The final result will be proportional to the actual number of first elastic collision events that would be detected experimentally in the event that the Monte Carlo differential elastic cross-section input had been correct.

No attempt has been made to average these scores over the finite extent of the actual counters. This is because in the experiments under consideration the angle subtended by the counter is very small ($\sim 5 \times 10^{-4}$ sterad) and contributes virtually nothing to the angular resolution of the scattering geometry. Further, such a consideration in the programme would be applicable to only one detector geometry.

A slightly more complex analysis is needed when estimating the density of multiple scattered neutrons arriving at the detector. Let us consider again neutrons detected as elastic —i.e. those which have undergone a sequence of elastic scatters. In the Monte Carlo neutrons are examined immediately before their second collision, provided that at the first collision the scatter was elastic. The score $p\,\sigma_{el}(\phi) \exp\{ - r(\mathbf{d})/m(E) \}$ is evaluated, noting that p, $\sigma_{el}(\phi)$ and $m(E)$ are functions of the incident energy, which may be less than the initial energy if the scatter is with a light element. This score is the density corresponding to a neutron having had one elastic scatter being succeeded by a further elastic event, independently of the actual type of the second collision or the fate of the neutron thereafter.

Tracking now proceeds; if the neutron escapes there are no more scores for this track. If there is a third scatter it is reprocessed in exactly the same way providing always that the second collision had been elastic, and the results are added to the detector scores. This process is continued until the neutron leaves the sample; the final score is the mathematical expectation of the density of multiple elastic events that have been detected at a given detector position. The technique is illustrated in the flow diagram given in fig. 3.

In a similar way, scores for neutrons detected as inelastic may be accumulated. Here the first factor in the score is $(1 - p)$ or p depending on whether an inelastic collision or a subsequent elastic collision from a track containing a previous inelastic collision is being considered. Again, the quantities p, $\sigma(\phi)$ are appropriate to the energy prior to collision, and $m(E)$ to that after collision.

At present, the programme estimates, for each detector position, the following quantities

(a) The density of elastically scattered one collision events.

(b) The density of inelastically scattered one collision events.

(c) The density of multiple scatter elastic events.

(d) The density of neutrons, with first scatter elastic, which in (one or more) subsequent collisions undergo one inelastic scatter before hitting the detector (fig. 3; multiple inelastic score 1).

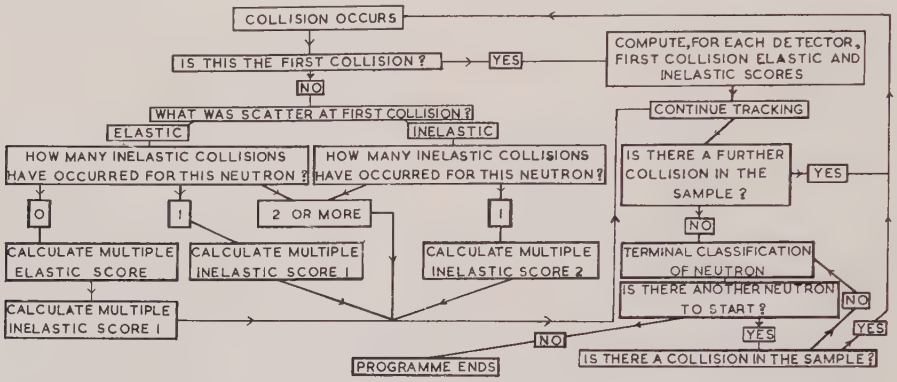

Fig. 3. Analysis flow diagram. Multiple inelastic score 1: first collision elastic, one subsequent inelastic scatter. Multiple inelastic score 2: first collision inelastic, all subsequent scatters elastic.

(e) The density of neutrons whose first scatter is inelastic and whose subsequent scatters are all elastic (fig. 3; multiple inelastic score 2).

The knowledge of the aggregate scores in each of these classes is sufficient to enable multiple scatter corrections to be applied in the usual case where neutrons with more than one inelastic scatter are not detectable experimentally. The way in which this is done is as follows. With an assumed differential elastic cross-section, the single collision elastic score is calculated for each counter position. When these scores are plotted as a function of detector angle the input differential cross-section for elastic scatter will be reproduced [apart from small effects due to the finite source distance in fig. 1 (which results in a nonparallel beam of incident neutrons) and the variation with scatter angle of average track length in the sample]. Next the multiple scatter elastic scores are added, for each detector position, to the single elastic scores. This estimates what the experimenters actually measure. When plotted, the new curve will not parallel the input curve, and the problem is to deduce that input which will yield a curve everywhere proportional to the experimental results. A good ad hoc method of deducing the input is to reflect the new Monte Carlo plot (when normalized) about the experimental curve in a manner which will be described more accurately in the next section. The result is an estimate of the new input. A second Monte Carlo is now run, and the new elastic scatter (single plus multiple) curve is obtained. This should be sensibly proportional to the experimental curve; if not, a further iteration is necessary.

There is a feature in the programme, as written, which enables one to avoid iteration. At one time it was considered that a series of Monte Carlo runs, with converging nuclear data input, would be computationally preclusive and it was arranged to subdivide each score at each counter position into groups depending on the initial scatter angle. The idea was then to estimate the correct input by weighting these groups so as to sum to the experimentally determined value. The weighting factors are then used to correct this input data. This method justifiably assumes that negligible error is made in omitting to correct the scattering laws at subsequent collisions. In practice however no more than one Monte Carlo iteration has been found necessary, and as the programme is quick (just over 2 minutes IBM 7090 time for 1000 initial neutrons) no use has been made of this facility.

It is readily seen that this programme also enables a correction to be made for the differential inelastic cross-section. In practice, however, this is often so close to isotropy that the corrections are very much smaller than the experimental errors, and therefore need not be applied.

The strength of the B4 programme is in its

bility to provide accurate estimates of the relative cores for the several detector positions, for a nodest number of neutron tracks. The accuracy of he absolute scores is rather less (section 7), but nevertheless is sufficient for a useful comparison to be made between the integrated scores (Σ (score) 1 [cos Ω]), and the number of collisions of corresponding type in the sample. In the case of a scattering sample of spherical symmetry, these two quantities must be equal. In the case of a long thin cylindrical sample however, with its symmetry axis perpendicular to the plane of the detector circle, one expects the integrated detector scores to exceed the number of collisions. This is because, physically, a neutron which (after a single collision say) is travelling towards the curved surface, is more likely to escape without further collision, than a similar neutron travelling lengthwise in the cylinder. This effect must be allowed for when obtaining the total scatter cross-sections by integrating the differential cross-sections (section 1) if the sample used departs substantially from spherical symmetry.

In the B4 Monte Carlo run for the Na^{23} sample (section 6), the ratio of the total integrated scores to the total number of collisions was 1.00 ± 0.01. This is as expected since the departure from sphericity of this sample is small, and no allowance for non sphericity was required. It is of interest to note that a similar B4 run for 1 MeV neutrons incident on a sample of cerium in the form of a cylinder 2.5 cm diam. and 5 cm long gave a ratio of 1.05 ± 0.01, and an experimental measurement of the total scatter cross-section would thus be 5 per cent high on this account.

6. Results of Programme B4 calculations

Ten runs, each of 1000 neutrons (these were neutrons that actually penetrated the sample) were carried out on the assembly of section 4. The same nuclear data as described there were used, the differential elastic scatter input being taken as the uncorrected experimental results. The whole run took 22 minutes on the 7090. Neutron for neutron, this is about four times slower than the B3 programme.

Results are presented, as a function of detector position, in tables 2–4. Table 2 lists the single elastic collision scores, table 3 the multiple elastic collision scores, and table 4 the sum of the two. For brevity the results for only five of the thirty detector positions are included.

Preceding the scores are given first the actual number of tracks in the appropriate category that left the sample and next the number of collisions used in estimating the scores. For example in table 2 the first quantity is the total number of neutrons in the Monte Carlo that had just one elastic scatter, and the second quantity is the total number of neutrons that had at least one collision. This latter number is larger, but not considerably so, than the first; if we had been interested in estimating *in-*

TABLE 2
Single elastic scores

Run	No. of observed events	No. of contributing collisions	Detector position (cos Ω)				
			— 0.875	— 0.5	0.01	0.5	0.875
1	127	172	37.7	35.9	46.7	79.1	132.8
2	114	166	36.5	35.0	46.1	78.0	128.5
3	125	176	39.5	37.2	47.4	78.9	130.9
4	115	159	35.3	33.7	43.7	73.6	121.7
5	140	185	41.3	39.3	51.1	85.6	140.6
6	140	185	40·7	39.1	51.3	86.9	143.6
7	111	150	33.2	31.8	41.7	70.3	115.9
8	130	179	39.2	37.3	48.4	82.0	137.0
9	137	192	42.7	40.7	52.9	88.9	147.0
10	153	192	42.8	40.4	51.8	86.7	144.0
Mean	129.2	175.6	38.89	37.04	48.11	81.00	134.20

TABLE 3
Multiple elastic scores

Run	No. of observed events	No. of contributing collisions	Detector position (cos Ω)				
			— 0.875	— 0.5	0.01	0.5	0.875
1	13	21	6.6	6.3	6.4	7.1	8.2
2	18	20	4.7	5.0	6.0	8.0	10.4
3	16	23	7.8	10.3	11.1	10.7	9.8
4	22	29	8.1	8.7	9.9	11.6	13.3
5	14	21	7.2	6.7	7.2	8.4	10.3
6	14	20	6.5	6.3	6.9	8.4	10.8
7	11	16	6.6	7.6	7.6	7.2	6.6
8	25	27	8.1	8.7	9.6	10.8	12.7
9	15	23	7.4	6.7	7.1	9.0	12.3
10	14	21	5.3	6.3	7.5	8.7	10.0
Mean	16.2	22.1	6.83	7.26	7.93	8.99	10.44

TABLE 4
Elastic events

Run	No. of observed events	No. of contributing collisions	Detector position (cos Ω)				
			— 0.875	— 0.5	0.01	0.5	0.875
1	140	193	44.3	42.2	53.1	86.2	141.0
2	132	186	41.2	40.0	52.1	86.0	138.9
3	141	199	47.3	47.5	58.5	89.6	140.7
4	137	188	43.4	42.4	53.6	85.2	135.0
5	154	206	48.5	46.0	58.3	94.0	150.9
6	154	205	47.2	45.4	58.2	95.3	154.4
7	122	166	39.8	39.4	49.3	77.5	122.5
8	155	206	47.3	46.0	58.0	92.8	149.7
9	152	215	50.1	47.4	60.0	97.9	159.3
10	167	213	48.1	46.7	59.3	95.4	154.0
Mean	145.4	197.7	45.72	44.30	56.04	89.99	144.64

elastic scores, the second figure would be unchanged but the first considerably smaller, and the advantage of using all possible information to estimate the scores would have been considerably greater. In table 3 the number of collisions contributing to the score includes all scatters subsequent to the first, up to and including the first inelastic scatter of a chain. This again is rather higher than the number of neutrons in the Monte Carlo that emerged as multiple elastic scattered events.

It is the sum of the data of tables 2 and 3 that is of interest (table 4). This would be proportional to the experimenters' result if the Monte Carlo nuclear data input had been correct. In fig. 4 the experimenters' uncorrected curve (the Monte Carlo input) together with the Monte Carlo output (table 4), arbitrarily normalized so as to lie close to the experimenters' curve, are shown as a function of detector position. Since the subsequent scattering produces a more isotropic distribution than single scattering (tables 2 and 3), the Monte Carlo output is a curve that is not proportional (i.e. parallel on the log scale used in fig. 4) to the input, being low at the forward scatter end. We deduce, therefore, that the input should have been more sharply peaked. A good way of correcting the input is to reflect the Monte Carlo output curve about the first curve, by stepping off, for each ordinate, a *distance* equal to the distance apart of the two curves, thus defining a new curve such that the old

ut is equidistant from this and the old output. s new curve, when normalized, will yield an ended Monte Carlo input for the next run. The cess is repeated until the Monte Carlo output curve is indistinguishable (apart from a constant factor of proportionality) from the experimental result.

After the second Monte Carlo the two curves were in fact virtually parallel (fig. 5). In table 5 the

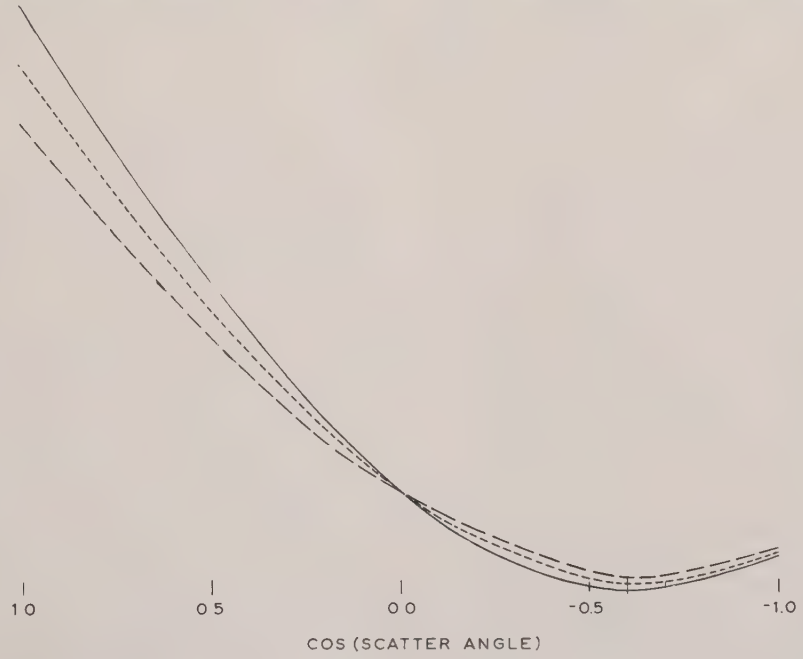

Fig. 4. Differential elastic cross section (sodium: 1.5 MeV neutrons).

- - - - - - Monte Carlo input (≡ experimental result) – – – – Monte Carlo output arbitrarily normalised
——— Revised Monte Carlo input for next run

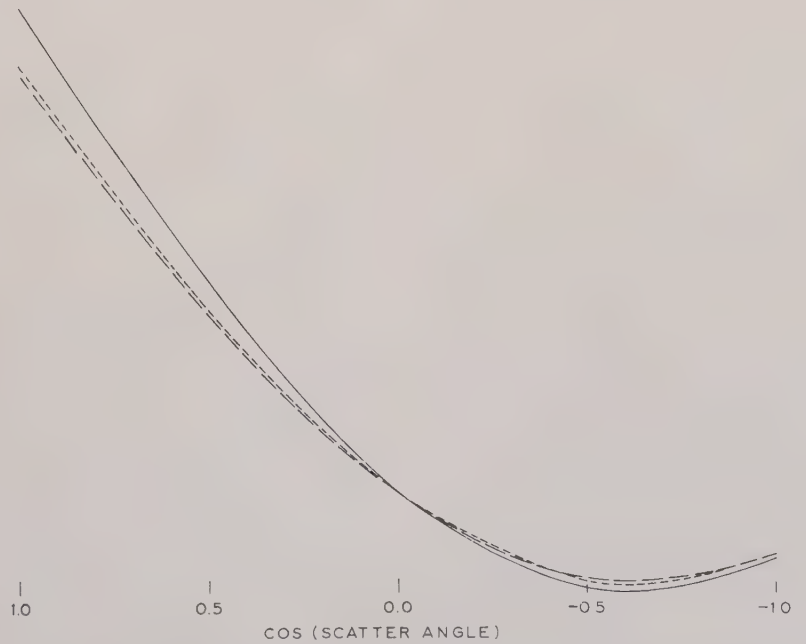

Fig. 5. Differential elastic cross section.

——— Monte Carlo input – – – – Monte Carlo output arbitrarily normalised - - - - - - Experimental result (fig. 4)

process of converging the differential elastic scatter cross-section is shown numerically. In the Monte Carlo calculations the differential cross-section is fed in as 32 discrete scatter angle cosines, computed in such a way that a random sampling from these 32 values correctly represents the input distribution. Naturally these cosines are tightly bunched at

TABLE 5
Equiprobable scatter cosines

Run 1		Run 2	
−0.95	0.42	−0.95	0.46
−0.85	0.47	−0.84	0.51
−0.75	0.52	−0.73	0.56
−0.65	0.57	−0.62	0.61
−0.54	0.61	−0.51	0.65
−0.44	0.66	−0.40	0.69
−0.34	0.70	−0.29	0.72
−0.25	0.73	−0.19	0.76
−0.15	0.77	−0.09	0.79
−0.07	0.81	−0.01	0.82
0.02	0.84	0.08	0.86
0.09	0.87	0.15	0.88
0.17	0.90	0.23	0.91
0.24	0.93	0.29	0.94
0.30	0.96	0.35	0.96
0.36	0.99	0.41	0.99

the maximum of the input curve (i.e. near $\cos\phi = 1$). In table 5 the two sets of cosines are shown for the two Monte Carlo runs, the first set being based on the uncorrected experimental curve.

7. Errors

We now discuss errors which fall under two heads.

7.1. APPROXIMATIONS MADE IN THE PROGRAMME

The programme computes a quantity that is proportional to the density of neutrons around the detector circle. In this calculation it is assumed, for the purpose of computing the chance that the ray hits the detector (though not for the purpose of computing the chance that no further collision occurs in the sample) that the ray originates from the centre of the sample. If the detector were at an infinite distance from the cylinder this treatment would be exact.

If the distance of the detector from the cylindrical sample is R, and $2h$, $2r$ are respectively the height and diameter of the sample, the maximum error i scatter angle due to the collision point not being a the centre of the sample is $(1/R)\sqrt{r^2 + h^2}$ radians In the experiments, R is about a metre, $2h$ = 4.6 cm, and $2r$ = 4.5 cm, and this error in scatte angle is therefore less than 0.3 degrees, which ca be ignored.

7.2. STATISTICAL ERRORS

For the purpose of correcting the shape of th experimentally determined differential cross-sec tions we are interested only in the *relative* errors o the curve obtained by summing the mean first col lision and the mean multiple collision curves. Th contributing sources of error are

(7.2.1) the errors in the shape of the mean curv for the first collision,

(7.2.2) the errors in the shape of the mean curv for multiple collisions,

(7.2.3) the error in the ratio of the mean numbe of first collisions to the mean number of contri buting multiple collisions.

For interest, we estimate these errors separately In table 2 are shown the first collision elastic score as a function of detector position (cos Ω) for ten independent runs and five selected detector posi tions. The variation in these figures consists o three parts, the systematic detector to detecto variation (due to anisotropic scattering), the run t run variation (due to some runs having more col lisions than others) and a residual component tha measures the shape error. An analysis of variance shows that the latter quantity is 0.4% (standard deviation).

A similar analysis on the data of table 3 measures the shape error of the multiple collision curve as 3.9% (standard deviation), and the ratio of the mean number of first collisions to the mean numbe of contributing multiple collisions is 8.0 with a standard deviation of 6%.

The way in which these errors should be com bined depends on the difference in shape between the first collision curve and the multiple collision curve. Obviously, if there were very little difference between these shapes, even a big error in estimating the ratio would have little effect on the shape error of the combined curve. We therefore present, in

le 4, the combined scores (single plus multiple) d subject these to the same analysis. The varia- n in these figures consists again of a systematic ector to detector variation, a run to run varia- n, and a residual variation which measures the

The relatively large shape error for multiple scattering arises mainly because the way the scores are distributed from one detector position to the next may very considerably from event to event, the direction of the track before collision deter-

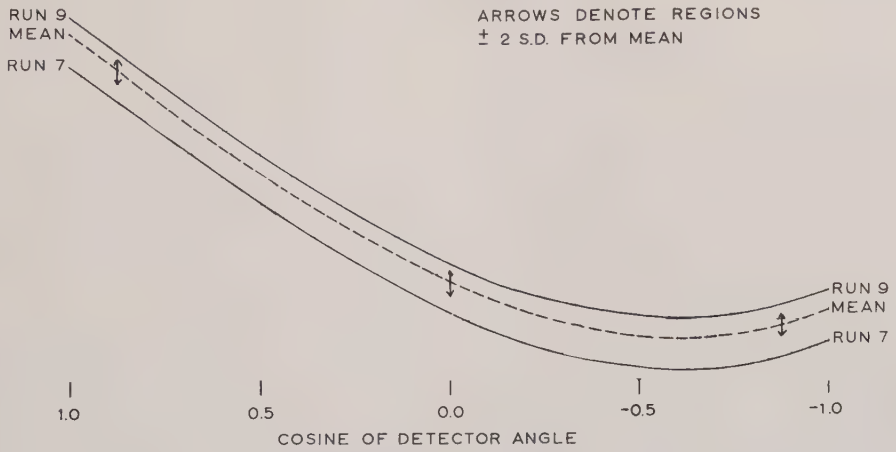

Fig. 6. Distribution of first collision scores.

ape error of the final curve; this quantity is presented by a standard deviation of 0.6%. This andard deviation includes contributions due to 2.1 and 7.2.2 above, plus a proportion of 7.2.3 which high or low depending on how widely the shapes

mining this. For first collisions these directions are virtually the same (to within the angle subtended by the sample at the source). However, when the scores are combined the shape error is satisfactorily small, this being dominated by the shape error of

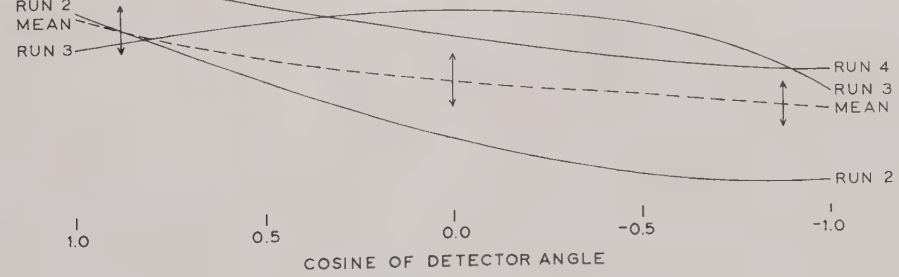

Fig. 7. Distribution of multiple collision scores.

the two component curves differ from one another. Summarizing, the various errors are listed below:

	First scatter (%)	Multiple scatters(%)	Overall (%)
cale error (s.d)	2.5	5.1	3.2
hape error (s.d)	0.4	3.9	0.6

the more sizeable proportion of first scatter events. Since the corresponding experimental results with which these data are to be compared have shape errors (s.d) of an estimated 1.5%, this accuracy is quite satisfactory.

These phenomena are illustrated in figs. 6 and 7. Fig. 6 shows the mean first collision score together with those for two extreme runs. Fig. 7 shows the

relative wide fluctuation from run to run for the multiple elastic scores.

8. Discussion

In the past, Monte Carlo multiple scatter programmes have served their purpose as a useful tool for calculating corrections to experimental data, but their utility has been greatly restricted by the large computing effort required. The basic philosophy behind these programmes is that of Cashwell and Everett[2]). Neutrons are tracked from a point source either conventionally or by the "forced first collision" technique, a device that guarantees that every neutron started will interact with the sample and hence contribute to the results. The detectors, imagined as a series of abutting regions lying on the detector circle of fig. 2, are replaced by a band, coaxial with the sample, and whose height is equal to the diameter of the detector. The band is divided into zones corresponding to the different scatter angles, and when a neutron hits the band it is classified by zone and collision type (e.g. single inelastic, double elastic, etc). Since the detector diameter is very small when compared with the radius of the detector circle, the solid angle subtended by the band is small and a large initial sample of neutrons must be run in order to obtain reliable statistics; this drawback is palliated (at the expense of some error) but not overcome, by increasing the band height beyond the detector dimension.

Perhaps for these reasons, other workers have attempted the problem analytically, using Monte Carlo simply as a check on the validity of the approximations used in the analysis[4]). A similar technique is used, the band height being increased to three times the detector diameter to obtain better statistics. To obtain better information of the effect of multiple scatter, a subset of those neutrons suffering two collisions were retracked from the second collision.

The programme described here is conceptuall different, the aim being to calculate the densities c neutrons in different categories at various point around the detector circle. The number of initia neutrons required for this programme need only b sufficient to give a good representation of th relative numbers and types of collision occurring i the sample. An accuracy of $\frac{1}{2}\%$ in the estimation c the *relative* number of elastic events occurrin around the detector circle has been obtained with starting distribution of neutrons which gave onl 2000 collided tracks. The greater part of th statistical variation associated with this rathe limited number of events is shown up as a scalin error.

Previous programmes require a large number c neutrons to be counted at each detector. A count c 10^4 (for a 1% error) would require about 10^5 neu trons to actually interact in the sample for a detec tor subtending one steradian (very poor geometry).

It is clear, therefore, that this Monte Carl multiple scatter programme has substantial ad vantages over earlier such programmes an enables accurate corrections to be applied to ex perimental results at the cost of very little com puting time.

There are many possible improvements an modifications which can be made to the program mes described. Programmes B3 and B4 may b amalgamated into one composite whole, with op tions to exclude the B4 (a relatively slow pro gramme) where attention is concentrated on th overall correction (section 3). This is currentl being done.

At the moment the B4 programme is limited t non-multiplicative neutron processes; it canno handle (n, 2n) or (n, f) reactions. This is also a limitation that will be removed in due course.

[4]) M. Walt, The scattering of 1 MeV neutrons by medium an heavy elements (Thesis), University of Wisconsin (1953).

CLEAR INSTRUMENTS AND METHODS 14 (1961) 13–23; NORTH-HOLLAND PUBLISHING CO.

ON A 2π GAS-FLOW COUNTER FOR LOW-LEVEL COUNTING

A. ALBERIGI-QUARANTA and B. RIGHINI

I.N.F.N, Centro Elettronica, Istituto di Fisica dell' Università di Bologna

and

V. PRODI and O. RIMONDI

C.N.E.N., Divisione di Biologia e di Protezione Sanitaria, Sezione di Bologna

Received 5 August 1961

ow radioactivity level measuring apparatus is described: it composed by a 2π gas-flow counter without window, whose ful diameter is equal to 4 cm, an anticoincidence scintillation nter and a shield made by iron bricks and a mercury layer uated between the two counters.

Under these conditions the background is equal to $0.62 \pm$ 3 c.p.m.; the sensibility, for a counting time of 1000′ is about 0.2 c.p.m. The gas-flow counter works in the proportional region, where it presents two plateaus, the former corresponding to α-particles and the latter to electrons. The gas used is natural methane.

Entirely transistorized electronics is used for elaborating and recording the data given by the counter.

Introduction

A low level background counter should have an tremely high sensitivity, where sensitivity is fined as the minimum detectable activity. The nsitivity of a low-level counter, referred to a rtain counting time, the same for the specimen nd the background, is limited by the latter's ablute value and by its inherent statistical fluctuaons: hence the need to keep the background to a inimum by iron or lead shields and by antiincidence counters[1]).

With low counting rates one should ensure that ackground fluctuates only statistically[2]) and that ain transients or other troubles are without effect; ne latter, in fact, could alter completely the measrements due to the very low counting rates.

The above prompts induce designing the whole evice, and particularly the electronics, with special gard to reliability and reproducibility[1,3]).

Finally a low level background counting system hould obviously have a high efficiency in detecting eta particles. This directs one to choose flow couners with an extremely thin window or, better, vithout any window at all, so as to reduce aborption.

2. The Apparatus

The apparatus we have made is shown schematically in fig. 1. A photograph of the whole instrument is given in fig. 2. It consists of:

1. A gas-flow windowless 2π counter.

2. A scintillation A.C. counter that covers counter 1.

3. An iron shield that encloses counters 1 and 2.

4. Electronics: this includes the recording apparatus and the power supplies: both the high-voltage stabilized ones for the two counters and the low voltage one for the electronics proper.

Active components of these devices are all solid state.

Let us now describe the equipment just mentioned.

2.1. THE GAS-FLOW, WINDOWLESS 2π-COUNTER

Due to the scope of our instrument, it is obvious that a counter is required in which one can easily

[1]) K. van Duuren, W. K. Hofker, J. Hermsen Proc. 2nd Geneva Conf., Vol. **14** (United Nations, Geneva) p. 339.

[2]) R. D. Evans, The Atomic Nucleus (McGraw-Hill, 1955) Ch. 27, § 2.

[3]) S. D. Softky and R. E. Nather, Nucleonics **15**, No. 5 (1957) 90.

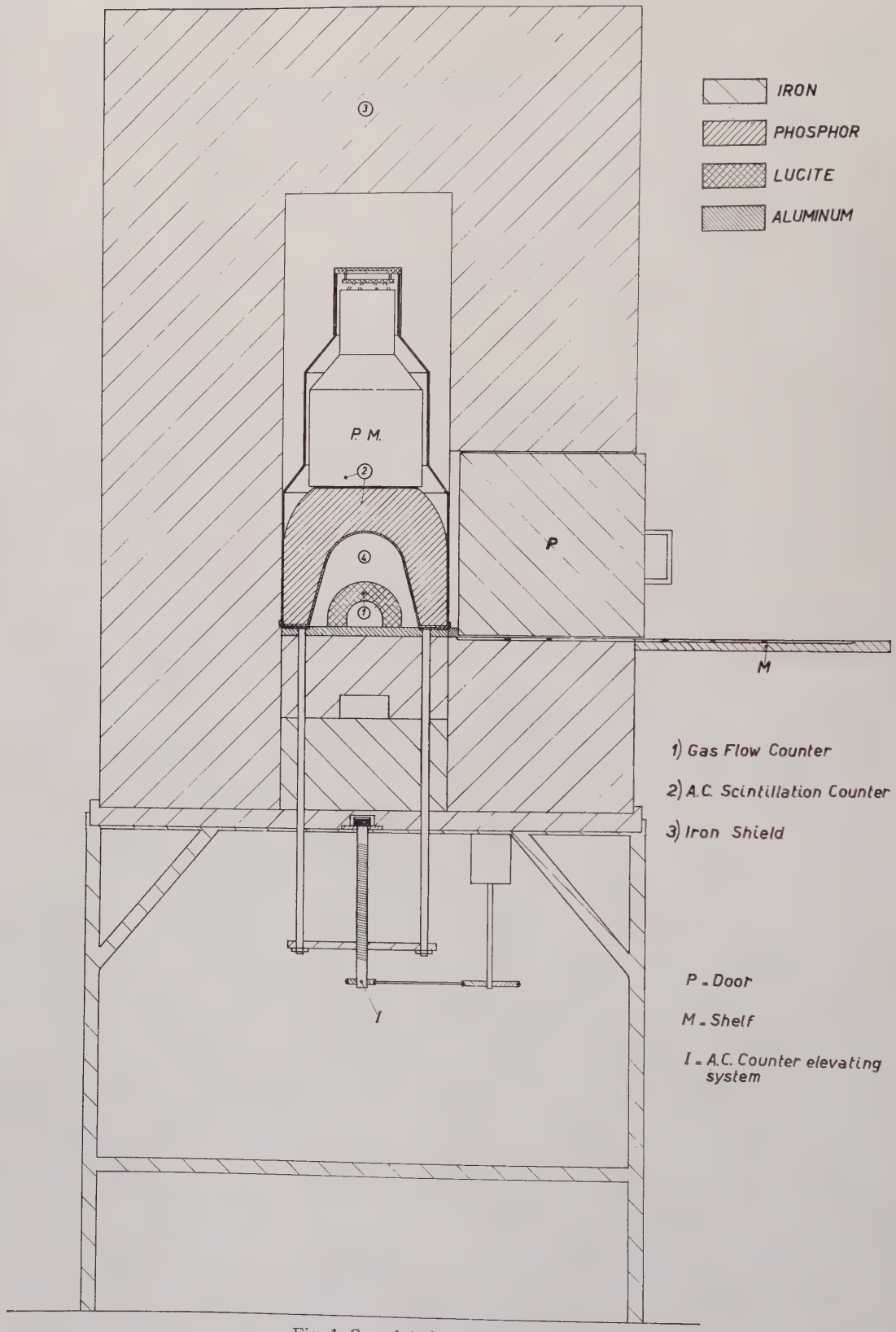

Fig. 1. Complete instrument diagram.

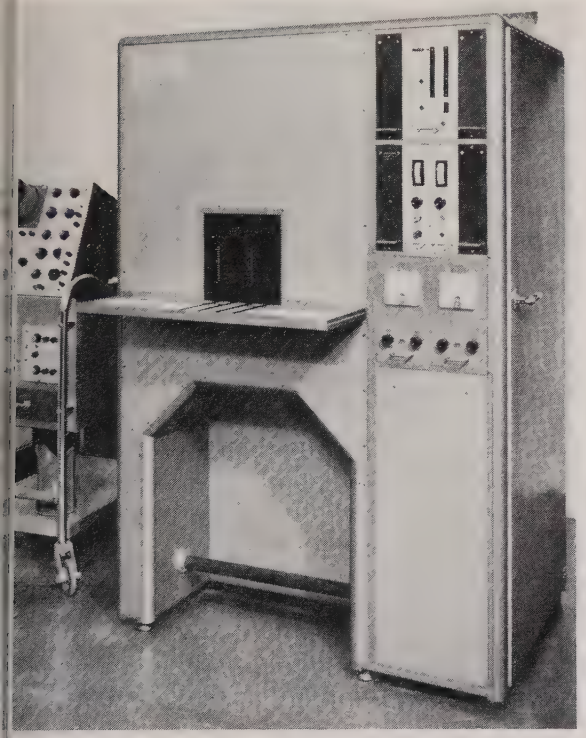

Fig. 2. Photograph of the instrument.

d speedily change the sample whose activity is to measured. For this reason a windowless gas-flow unter was decided upon. On the other hand, it is ell known that a gas-flow counter can be used as a eiger counter and as a proportional counter. If it used as a Geiger counter, high amplitude pulses actically constant are available, rendering ampli-ation unnecessary. Nevertheless we have chosen proportional counter, due to the advantages we ow quote and that will be detailed in the final ction, where results and conclusions are dis-ussed:

a. As a proportional counter, one notices two lateaus: an α plateau and a β one. This is a very arked advantage, specially when dealing with nknown sources on which one can count only α articles (also when beta rays are present), or ount both alphas and betas simultaneously.

b. In proportional counters natural methane gas an be used, which is very cheap and easy to find. ll the measurements to be reported here have been ade with natural unpurified methane gas, since ne counter worked well under these conditions. Furthermore methane can also be used when wet[4]). This allows measurements to be made on damp sources, which is a marked advantage.

As it was mentioned above, natural methane is quite cheap ($ 0.10 per m^3) while argon and He-isobuthane, that are largely used for counters of this type, are much more expensive ($ 4 and $ 50 per m^3 respectively).

c. With a windowless proportional counter absolute alpha or beta measurements are possible, since the counter has the same characteristics of a 2π counter used for preparing standard sources. The mechanical part of the counter has been studied so as to make all manual operations easy. The doors P, through which one reaches the measuring counter, rest on ball bearings that slide on shelf M (see fig. 1); when one opens the door, the anti-coincidence counter is automatically raised and the measuring counter is uncovered. To insert a source in the latter, a lever that unblocks the counters upper hemisphere is actioned: the hemisphere can then be removed; this automatically stops the flux of the gas. The source may then be put in place and the counter closed again. Measuring conditions are reestabilished within a minute.

2.2. A.C. COUNTER

In general, in most recent instruments of the type described, the measuring counter is partially surrounded by one or more Geiger counters (sometimes by scintillation counters[5,6]): pulses produced by the latter counters are placed into anticoincidence with pulses produced by the measuring counter. With this precaution background is reduced considerably, especially cosmic background.

In our device, a plastic scintillation counter was chosen: it offers noticeable advantages, both from the point of view of reliability, and because when measuring beta-gamma sources, gamma rays produce pulses in the scintillation counter that are quite different from the ones due to cosmic rays. The latter, in fact, produces pulses whose amplitudes range within 0.2 and 2 V, while gamma-induced

[4]) G. Nilsson and G. Aniansson, Nucleonics **13**, No. 2 (1955) 38.
[5]) R. P. Parker, Nucl. Instr. and Meth. **8** (1960) 339.
[6]) J. R. Gat (Gutmann) and J. Gilat, Nucl. Instr. and Meth. **8** (1960) 233.

pulses are not higher than a few hundredths of a volt. Discrimination between the two is hence quite easy, therefore preventing the anticoincidence circuit from triggering on gamma radiation.

The anticoincidence counter used is showed in fig. 3b: it consists of a single block of plastic scintillator† viewed by an E.M.I. 6099 B photomultiplier placed in optical contact. The arrangement of fig. 3a was also tried: here the photomultiplier was not placed in optical contact; both counters proved efficient.

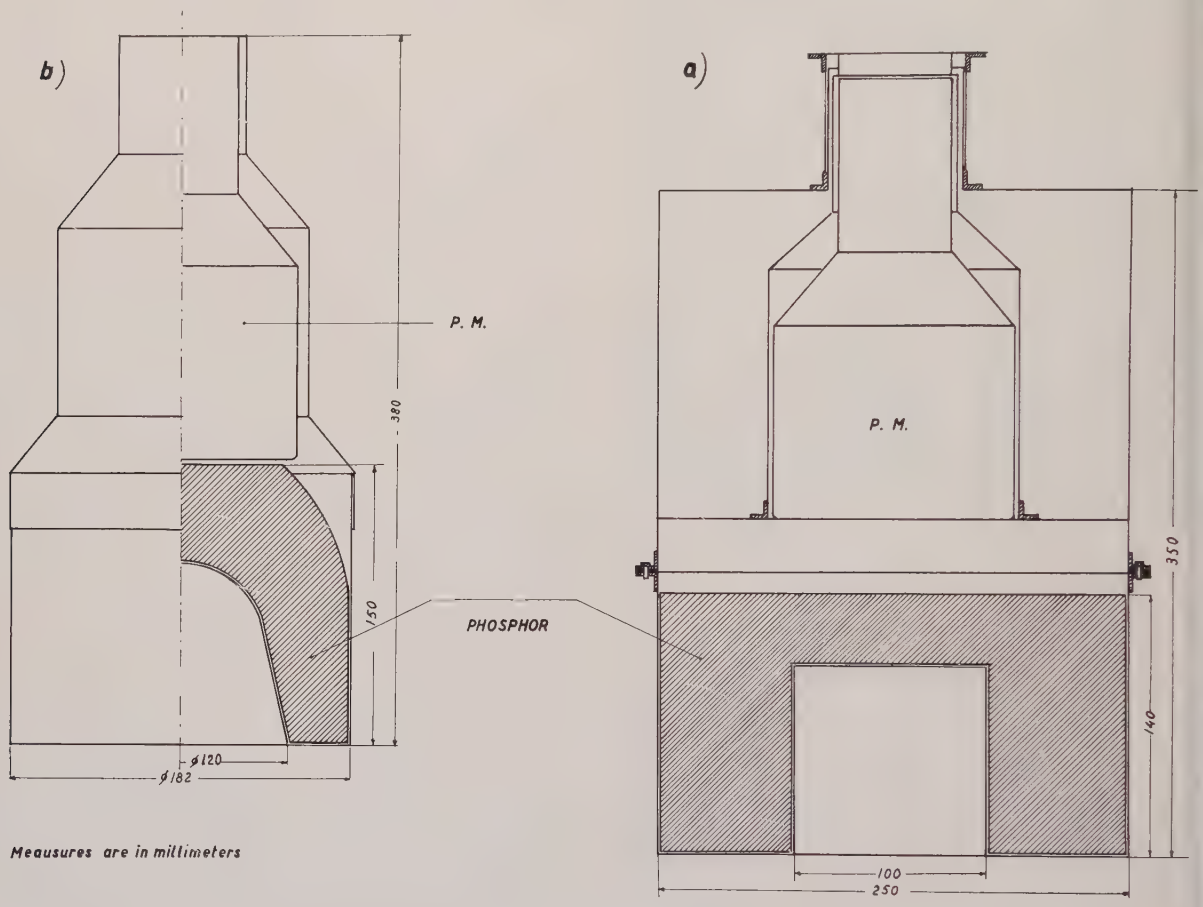

Fig. 3. Anticoincidence counters.

2.3. SHIELDING

The iron shielding reduces background component due to natural gamma radiation of the surrounding materials. The iron shield has a thickness that can vary between 10 and 20 cm; it has a window closed by two iron doors. As it was mentioned previously, when the doors are opene the A.C. counter is automatically raised and th high voltage on the measuring counter is als opened.

In the inside of the device (fig. 2) the methan gas tank is also placed.

2.4. ELECTRONICS

Electronic circuits used to handle the informa tion produced by the counters should satisfy th following requisites:

a. highly constant and reproducible functioning

b. complete elimination of spurious counts due t disturbances;

c. long maintenance-less life.

The block diagram of the electronics is given i fig. 4. Pulses coming from the scintillation counte

† The luminescent plastic material was prepared at th Istituto di Fisica of Bologna.

hannel 1) are emitter-followed, amplified and scriminated: the integral discriminator elimina- s gamma-ray induced pulses, accepting, on the ntrary, pulses produced by cosmic radiation; e discriminator output is connected to a pulse aper and to an inverter.

This choice presents also the advantage of reducing power supply and space requirements of the electronics.

Furthermore it should be noted that the high voltage supplies are also completely transistorized; stability is of 0.1% against main variations of

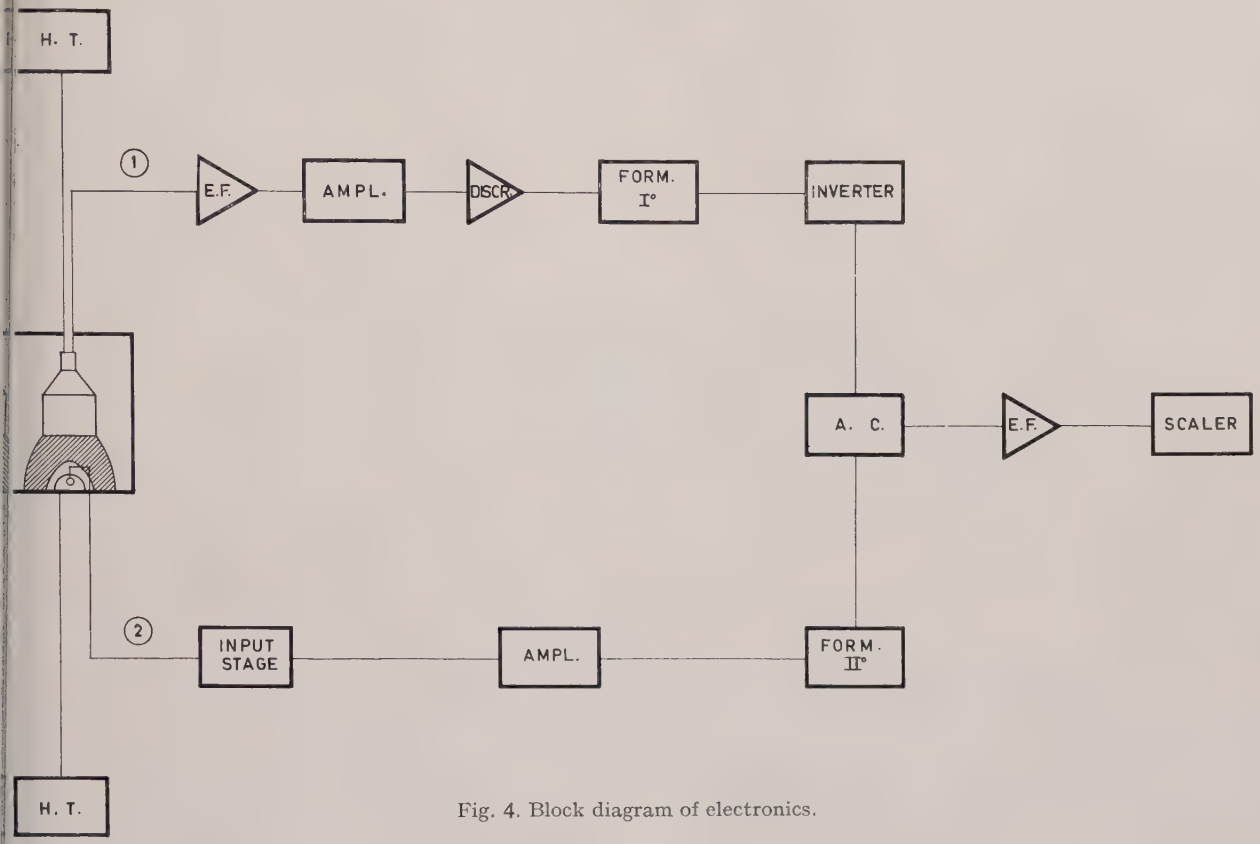

Fig. 4. Block diagram of electronics.

Pulses coming from the gas-flow counter are emitter-followed and feed and amplifier, so as to increase their amplitude until a pulse shaper similar to the one situated in the scintillation channel can be reliably triggered. The pulse shapers are obviously designed so as to produce constant-shape pulses, independently of the input pulses. The pulses thus shaped are sent to an anticoincidence that triggers only in the absence of pulses in channel 1. The anticoincidence output is sent to a scaler, made with transistors and Philips Z-700 U gas tubes, through an emitter follower. As it has been mentioned all the active circuit components are transistors, thereby making it easy to satisfy points b and c above.

$\pm$ 10% and against room temperature variations of $\pm$ 10°C.

3. Results

3.1. THE 2π GAS-FLOW COUNTER

The counter has been made in various versions that differ only for the enclosure system. The last type, made by lucite (fig. 5), is particularly convenient, and allows a speedy insertion of the radioactive sample. The cathode consists of an internal stratum of graphite (aquadag) that is a "clean" material, i.e. exempt from radioactive impurities, such as lucite is. The anode consists of a tungsten wire, bent in the shape of a ring, 12 mm in diameter. The useful internal diameter of the counter is 4 cm.

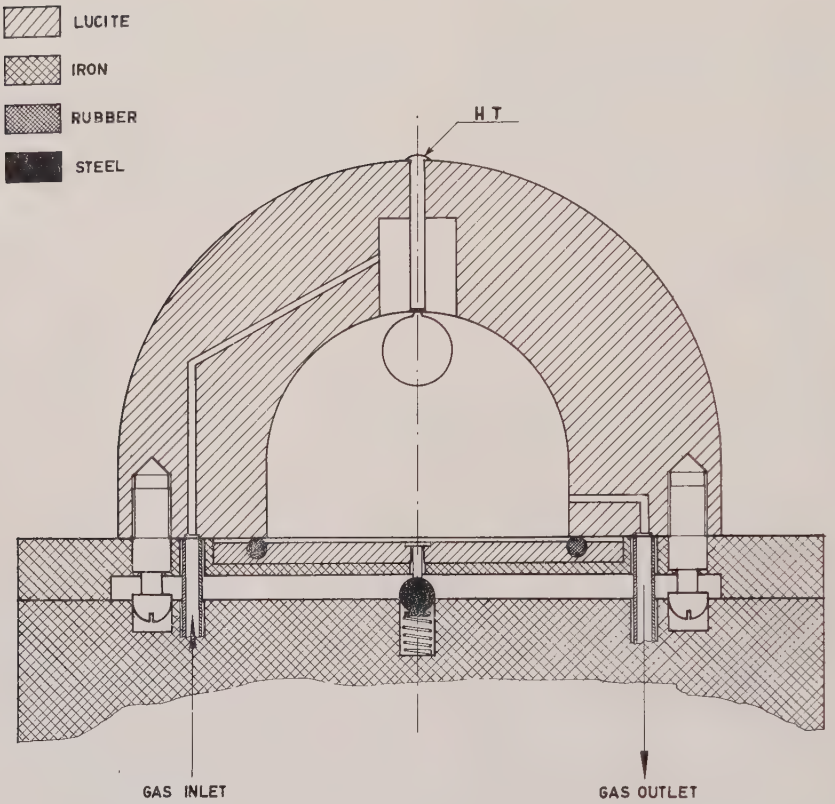

Fig. 5. Gas flow counter.

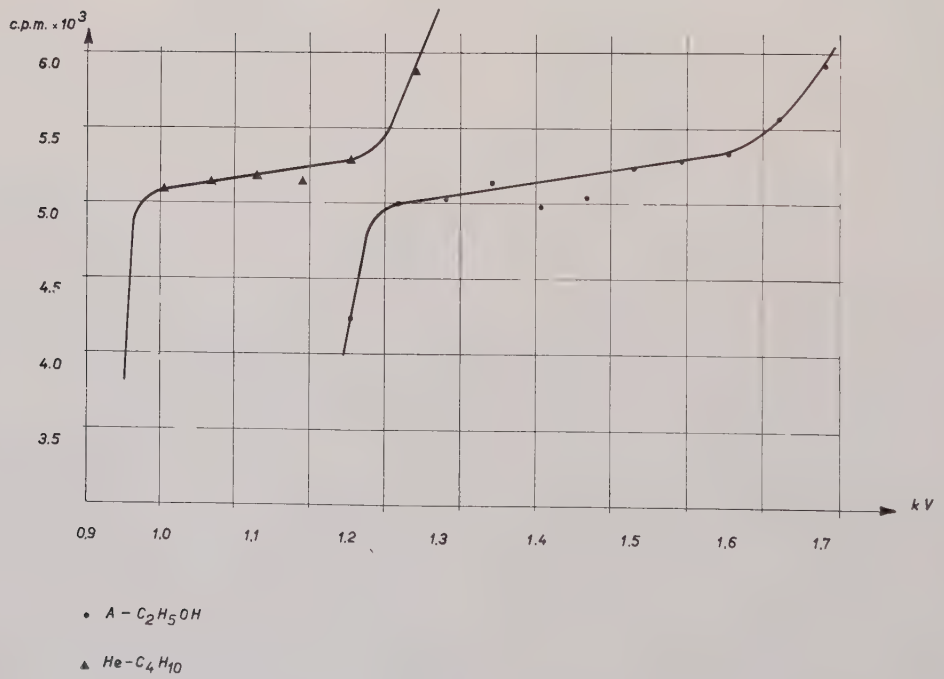

Fig. 6. Geiger zone plateaus for two different gas mixtures.

e counter can work both as a Geiger and as a portional counter, by changing the gas and the unter voltage. The mixtures we have tested in ing the counter in the Geiger region were He-

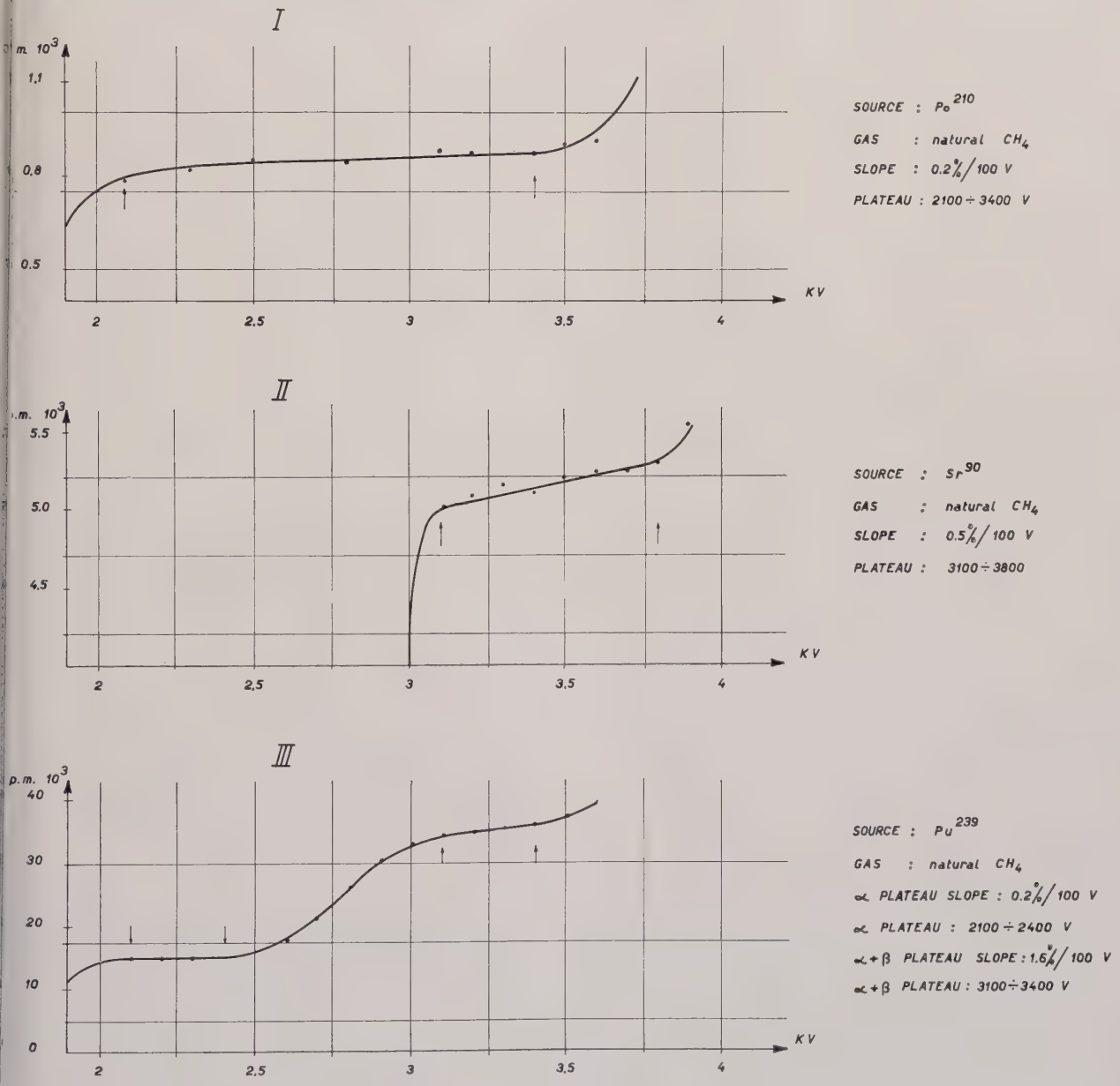

Fig. 7. Alpha and beta plateaus obtained with various sources: (I) Po^{210}; (II) Sr^{90}; (III) Pu^{239}.

sobuthane and argon-alcohol. In fig. 6 the Geiger-one plateaus if the two gases are shown: the slope s 1.8%/100 V, while the lengths were 200 V and 350 V respectively.

The counter is used in the proportional mode, as it has been mentioned: it shows an alpha and a beta plateau.

In fig. 7 the alpha and beta plateaus are shown. The first (curve 1) has a slope of 0.2%/100 V, calculated for a plateau length of 1300 V. The second (curve II) has a slope of 0.5%/100 V, calculated for a length of 700 V. The two plateaus have, as it can be seen, a common working-voltage range of 3100 ÷ 3400 V in which alpha and beta particles may be

simultaneously counted: this is shown by curve III.

The curve was obtained using a Pu^{239} source. The first plateau is the one in which only alpha particles are detected, the second allows detection of both alphas and electrons. Slopes are 0.2%/100 V and 1.6%/100 V respectively. A set of measurements has been made furthermore, designed to determine the other characteristics of the counter[7]) so as to establish its behaviour with sources of different type: conducting, non conducting, dry, damp, of small and of large dimensions. In fig. 8 plateaus obtained with a calibrated Sr^{90} source type SIRC 1 (Amersham) are shown; the source was bare, or covered with mylar (0.8 mg/cm^2 thickness) graphitated or ungraphitated. The slopes of the plateaus are practically the same. Covering mylar with graphite seems to have improved only the counting efficiency. The errors drawn are the average of deviations. When the source is a soft beta emitter, e.g. C^{14}, then graphite diminishes instead of increasing, the detection efficiency, due to absorption (see fig. 9). The source of C^{14} used was a disk (2.5 cm diameter) of poly (methyl – C^{14}

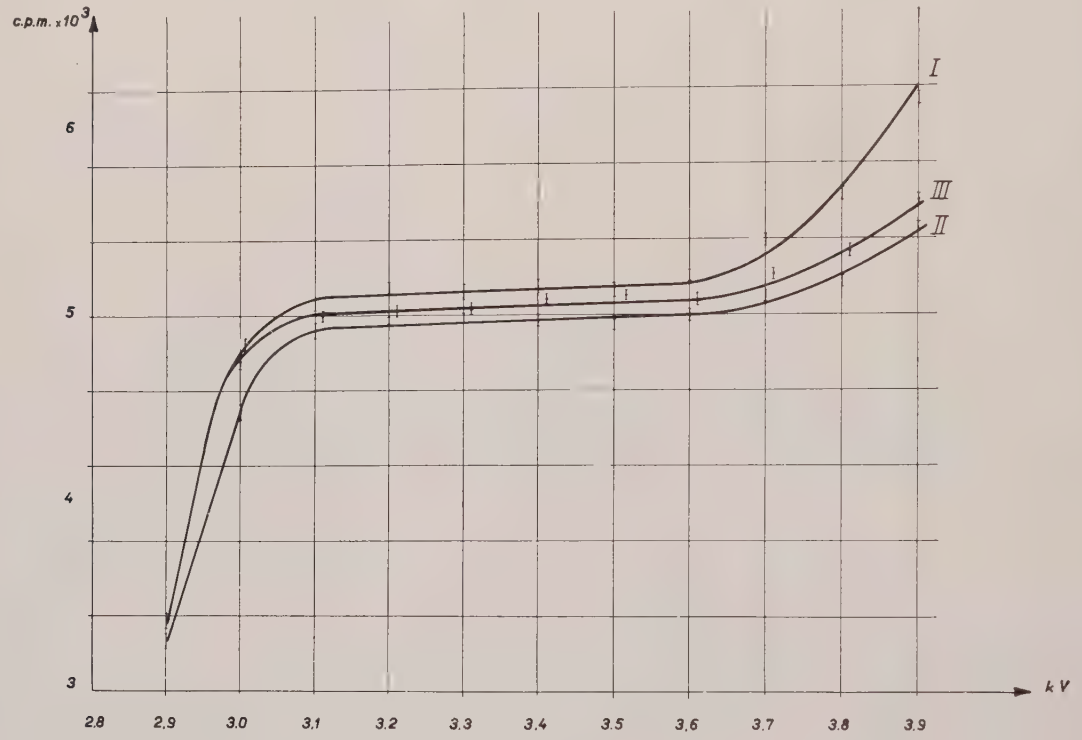

Fig. 8. Plateaus obtained with a calibrated Sr^{90} source type SIRC 1 (Amersham). — (I) Free source, (II) Source covered with mylar, (III) Source covered with graphitated mylar.

methacrylate $(C_5H_8O_2)_x$ type CFR 3 (Amersham). The plateaus of fig. 9, relative to the ungraphitated source (curve I) and the graphitated one (curve III) show quite clearly that the counting rate due to sources made by insulating material is not affected by irregularities. This result is confirmed by the plateau obtained with the Sr^{90} source covered with untreated mylar (fig. 8). The CH_4 counter can count wet sources as well: this has been established comparing the plateau obtained under normal conditions with the Sr^{90} SIRC 1 source with the

[7]) J. S. Nader, G. R. Hagee and L. R. Setter, Nucleonics **12** No. 4 (1954) 29.

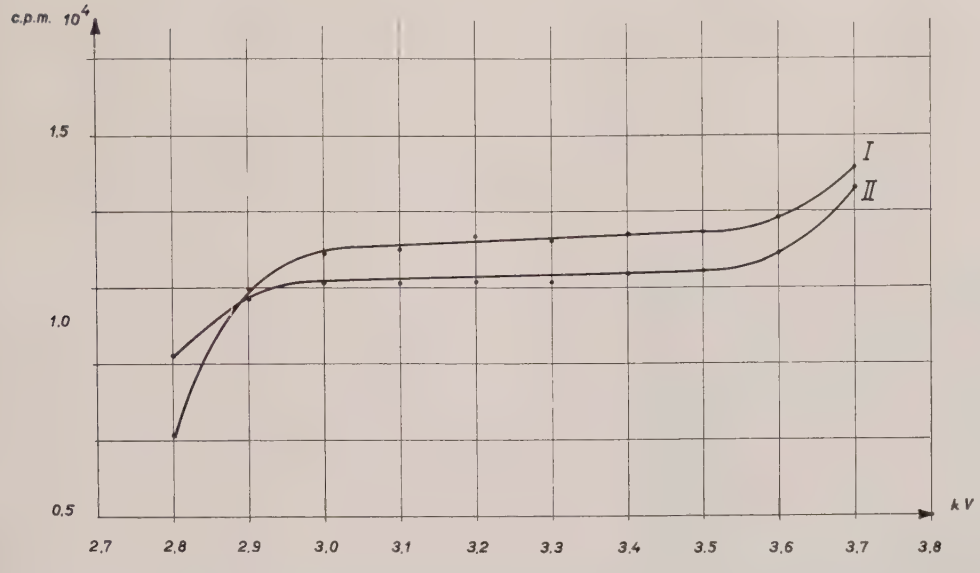

Fig. 9. Plateaus obtained with a C^{14} source type CFR 3 (Amersham)—(I) Ungraphitated source; (II) Graphitated source.

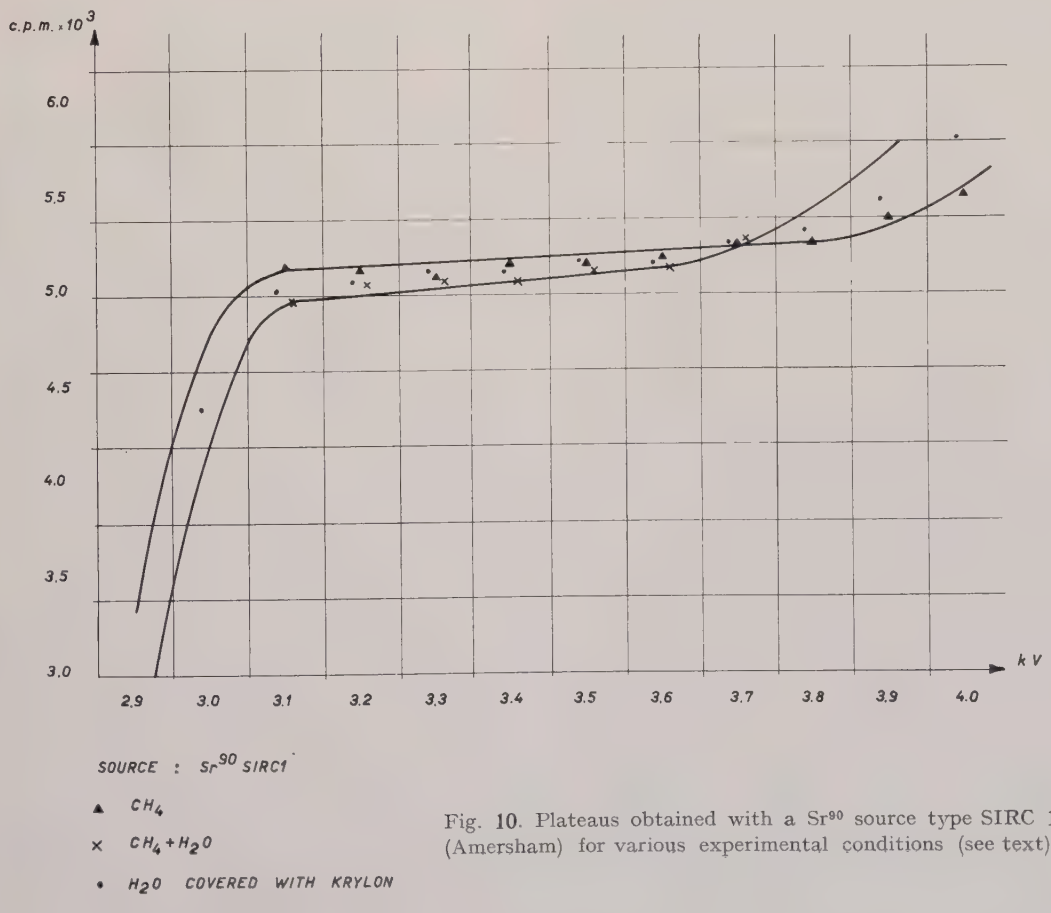

Fig. 10. Plateaus obtained with a Sr^{90} source type SIRC 1 (Amersham) for various experimental conditions (see text).

plateau obtained from the same source put into a basin of water, 2 mm deep and of 33 mm internal diameter (fig. 10). The slope of the plateau is still satisfactory[4]). Covering the water with a stratum of Krylon results improve, and the plateau has a slope intermediate between the preceding ones.

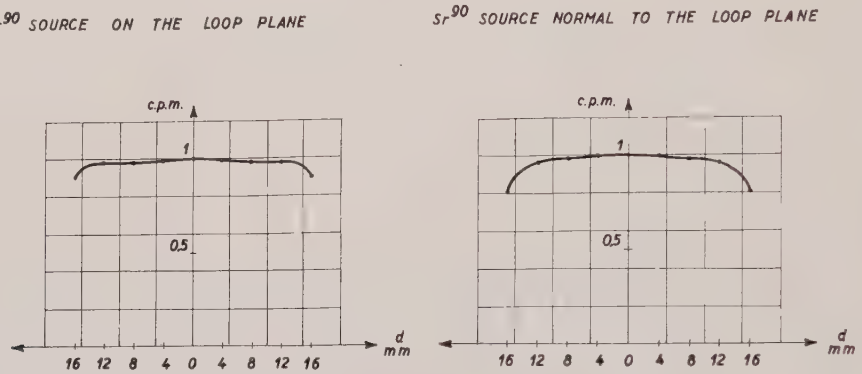

Fig. 11. Counter efficiency against source position.

Finally, with a point Sr^{90} source, the variation of the counter efficiency with position was evaluated; this was done by moving the source along two diameters, one in the loop's plane and the other in the normal one. During the tests the source was raised by 4 mm with respect to the plane of the base of the counter. Fig. 11 shows the results of the measurements. As it can be seen counting efficiency is higher than 95% also for an extended source (32 mm in diameter), assuming 100% efficiency at the counter's center. As it has been mentioned above, the counter allows obsolute measurements to be made; the electronics also allow high counting rates to be handled. Therefore beta sources calibrated at Amersham were measured. In table 1 results are compared with the calibration records. Agreement is good, as it can be seen.

Values of half-life assumed for the sources decay calculation, were taken from the "Radioisotope Data"[8]).

The percentage error given by the authors is the average of deviations. The sources used were al 10 mm in diameter. They were placed at the center of the counter's base, therefore no corrections fo detection efficiency were made.

3.2. BACKGROUND

The instrument with an iron shielding 20 cm thick, has a background of 0.64 ± 0.03 c.p.m measured in the basement of the Institute o Physics of Bologna; with the iron shielding reduced to 10 cm and the spacing between the gas-flow and the scintillation counter filled with mercury, the background was 0.62 ± 0.03 c.p.m.[9]).

Background measurements were also made with shieldings of various nature and with the A.C

[8]) R. A. Allen, D. B. Smith and J. E. Hiscott, Radioisotope Data, AERE, Harwell, Report, R 2938, Second Edition.

[9]) A. Molik, R. W. P. Drever and S. C. Curran, Proc. Roy Soc. A **239** (1957) 433.

TABLE 1

Isotope	Energy (MeV)	H.L. (years)	Amersham				Authors c.p.m. on 14.7.1961
			Code	Date of test	c.pm.	c.p.m. on 14.7.1961	
Pm^{147}	0.22	2.6	PHRC 1	16.9.1960	$4.18 \times 10^3 \pm 5\%$	$3.36 \times 10^3 \pm 5\%$	$3.52 \times 10^3 \pm 1\%$
Tl^{204}	0.77	3.9	TERC 1	29.8.1960	$4.01 \times 10^3 \pm 5\%$	$3.43 \times 10^3 \pm 5\%$	$3.48 \times 10^3 \pm 1\%$
Pb^{210}	1.17†	21	RBRC 1	29.8.1960	$3.02 \times 10^3 \pm 5\%$	$2.93 \times 10^3 \pm 5\%$	$2.93 \times 10^3 \pm 1\%$
Sr^{90}	2.22†	28	SIRC 1	6.2.1959	$5.41 \times 10^3 \pm 5\%$	$5.09 \times 10^3 \pm 5\%$	$5.18 \times 10^3 \pm 1\%$

† See "Radioactive Source" Catalogue issued by the Radiochemical Centre, Amersham.

unter shown in fig. 3a. For example, with the position of fig. 12 we have used 10 cm thick iron d outside this, 20 cm of lead on the top and m on the other sides. The results of measure-nts corresponding to the various shielding ar-ngements and for the two plateaus, alpha and ta, are shown in tables 2 and 3.

TABLE 2

Beta plateau			
Shield	Background (c.p.m.)	P	Time
C + D	1.07 ± 0.04	0.1	960′
C + D + A	1.02 ± 0.04	0.15	1080′
C + D + A + B	0.72 ± 0.03	0.2	1440′
C + D + A + B without antic.	12.2 ± 0.1		
Free	48.3 ± 0.7		

TABLE 3

Alpha plateau			
Shield	Background (c.p.m.)	P	Time
C + D + A + B	0.137 ± 0.007	0.7	2160′
C + D + A + B without antic.	0.153 ± 0.007	0.7	2160′

With the complete shielding the background is .72 ± 0.03 c.p.m., in the Geiger region or in the roportional beta region; in the alpha proportional egion, background is about one fifth's as much.

The results of the Pearson's Chi-square test[2]) elative to each measurement are shown in the hird column (P) of table 2; these tests are made on ach set of measurements so as to guarantee *posteriori* that spurious events have not been ecorded. In the fourth column, the total time of ach measurement is shown. From the table one an calculate the relative intensity of each com-onent of the background: cosmic radiation 23.6%) and surrounding radioactivity (75%). These are in good agreement with values quoted by other authors[1,10,11]).

Finally, the device's sensitivity is

$$A_{\min} = 0.2 \text{ c.p.m.}$$

for counting times of 1000 min and for a background counting rate of 0.6 c.p.m. The above result has been determined assuming that the difference

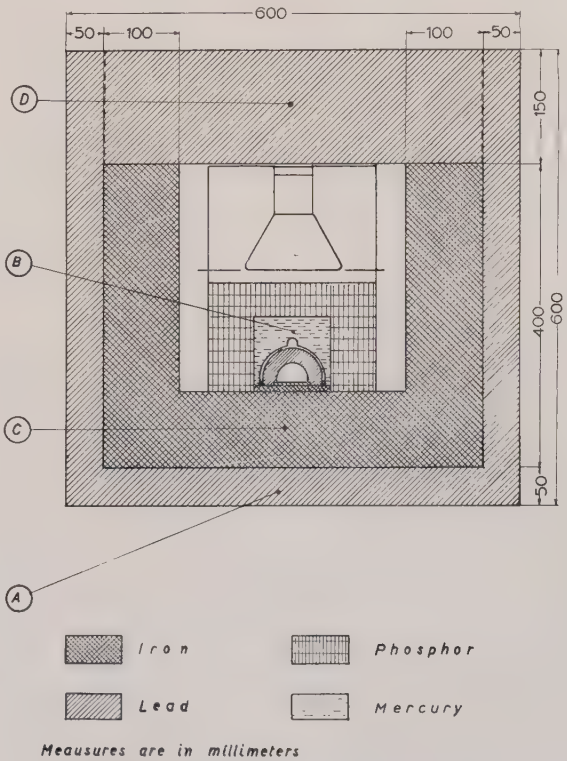

Fig. 12. Counters shielded by iron and lead.

between the two counting rates (background and source) is statistically meaningful when it exceeds by at least three times the standard error on the difference itself and furthermore that the same time interval is employed in measuring the sample and the background.

The very useful collaboration of Mr. R. Degli Esposti, Mr. P. I. L. Lembo and Dr. M. Radicchi is gratefully acknowledged.

10) W. R. Looscmore, Atomic **8** (1957) 97.
11) J. L. Kulp and L. E. Tyron, Phys. Rev. **23**, No. 6 (1952) 296.

NUCLEAR INSTRUMENTS AND METHODS 14 (1961) 24–32; NORTH-HOLLAND PUBLISHING CO.

PULSE SHAPE DISCRIMINATION

L. VARGA

Central Research Institute for Physics, Budapest†

Received 27 May 1961

Pulse shape discrimination methods used up to the present are discussed, considering in particular to what extent the possibilities offered by the shape of the scintillation decay are being exploited. A new method is then described which utilizes in a statistically optimum way and by simplest means the information obtainable from the various pulse shapes. The application of this method to the discrimination between proton and deuteron scintillation response of CsI(Tl) crystals is described. Finally, some special cases in which the separation can be improved still further are considered.

1. Introduction

It is known that a number of scintillators respond to the absorption of particles which differ in mass or in charge by the emission of light pulses of various durations. This scintillation can usually be described as the sum of two exponentials in which the time constants differ by one order of magnitude. Although more components may be involved, their contribution to the total number of photons is less than a few per cent[1]). The intensity ratio of the two essential components depends on the mass and charge of the particle absorbed by the phosphor in question. In this respect organic and inorganic detectors behave differently. It has been shown by the experiments of Owen[2,3]) that in organic phosphors the slow component of the scintillation excited by protons is twice as intense as that due to electrons. The decay constants of the fast and slow components of organic phosphors are independent of the mass or charge of the exciting particle[2,3,4]) within the experimental error. This opinion is not shared by Wright[5]), his results, however, must have been affected by his neglecting the presence of the slow component. The case is usually reversed for inorganic scintillators: for the latter it is the particle of higher mean ionization density which induces scintillations with a lower ionization density[2,6]). A further difference between organic and inorganic phosphors is that for the latter the mean life of the fast component varies with the ionization density of the exciting particle though this has so far been verified satisfactorily for CsI(Tl) only. Summarizing we may state the following: if a particle of average ionization density $\bar{\rho}_i$ is absorbed by a scintillator, in the resulting scintillation the number of photons emitted in the time interval Δt will be

$$N_i(t)\Delta t = [a(\bar{\rho}_i)\, e^{-t/\alpha(\bar{\rho}_i)} + b(\bar{\rho}_i)\, e^{-t/\beta}]\, \Delta t\,. \qquad (1)$$

If the phosphor is organic, α and β are constants independent of $\bar{\rho}_i$, and by normalizing to

$$N_1(t=0) = N_2(t=0) = \ldots = N_i(t=0) - \ldots$$

we have

$$b(\bar{\rho}_1) < b(\bar{\rho}_2) < \ldots < b(\bar{\rho}_i) < \ldots$$

when

$$\bar{\rho}_1 < \bar{\rho}_2 < \ldots < \bar{\rho}_i < \ldots$$

With the use of inorganic phosphors only β will be independent of $\bar{\rho}_i$, and normalized as above,

$$b(\bar{\rho}_1) > b(\bar{\rho}_2) > \ldots > b(\bar{\rho}_i) > \ldots$$

if

$$\bar{\rho}_1 < \bar{\rho}_2 < \ldots < \bar{\rho}_i < \ldots$$

In pulse shape discrimination we are usually confronted with the problem of identifying the

[1]) F. B. Harrison, Nucleonics **12** (1954) 24.
[2]) R. B. Owen, Nucleonics **17** (1959) 92.
[3]) R. B. Owen, Proceedings of International Symposium on Nuclear Electronics, Paris, 1958. Published by International Atomic Energy Agency, Vienna.
[4]) H. Kallman and G. J. Brucker, Phys. Rev. **108** (1957) 1122.
[5]) G. T. Wright, Proc. Phys. Soc. B**69** (1956) 358.
[6]) R. S. Storey, W. Jack and A. Ward, Proc. Phys. Soc. B**72** (1959) 523.

† Some of the work reported here was carried out during the author's I.A.E.A.-sponsored stay at the CISE Laboratory, Milano, Italy.

rticle responsible for the scintillation from the ne distribution of the N_0 photons arriving at the otocathode per scintillation. By plotting the ntillation decay curves for two particles, rmalized to

$$\frac{1}{N_0}\int_0^\infty N(t)\,\mathrm{d}t = 1\,,$$

oducing the same total number of photons (fig. 1), is easy to realise which data are available for the lution of the problem. As seen from the figure, for scintillation producing in total N_0 photons, the

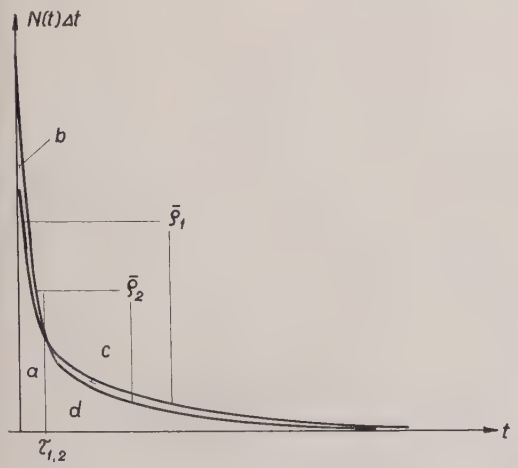

ig. 1. Typical decay curves normalized to the same area intercting each other at a time $\tau_{1,2}$. $\bar{\rho}_1$, $\bar{\rho}_2$ are the mean ionization ensities, a and d denote the common area, the areas b and c contain the information.

ontribution up to a certain time $\tau_{1,2}$ of the particle with ionization density $\bar{\rho}_1$ is $N_0 b$ more while after his time it is $N_0 c$ less than that of the particle with onization density $\bar{\rho}_2$. It is this value $N_0(b + c)$ in he number of photons which distinguishes the particle characterized by $\bar{\rho}_1$ from the particle with $_2$ if they produce in total the same number of photons per scintillation.

The ratios shown in fig. 1 hold for organic phosphors with the restriction that $\bar{\rho}_1 > \bar{\rho}_2$. Essenially, the picture is acceptable for inorganic crystals too, except that $\bar{\rho}_1 < \bar{\rho}_2$. The diagram is somewhat modified also by the dependence of the fast time constant on $\bar{\rho}_i$.

2. On the Various Discrimination Methods

Let us now consider to what extent the information obtainable from the pulse shape, as described above, is made use of by the various methods of particle discrimination. Not too many authors have tackled this problem, and every one of them has used a different approach.

The highly interesting space charge method of Owen[2,3]) consists in the use of a plate dynode potential in the multiplier which suppresses in organic phosphors the slow component of the scintillation response to γ-particles by means of the space charge due to the high intensity current pulse of the fast component. For protons, on the other hand, the relatively weaker fast component cannot assert itself against the more intensive slow component. The procedure is very simple. It is, however, rather difficult to show by calculation to what extent the information is being exploited, nevertheless it is obvious that only a small part of the multiplier current corresponding to the number $N_0 c$ of photons can be affected by the space charge of the current due to $N_0 b$ (fig. 1). In addition, as the author realized, the repeated space charge effects due to statistical fluctuation in the slow component are rather disturbing, particularly for low energy particles.

In the same paper[2]) Owen describes an alternative circuit by which the voltage pulse proportional to the total number of photons is compared to the pulse height of the plate current. This, however, makes the situation even worse than before, since the current pulse height being determined by a relatively small number of photons emitted in the vicinity of the peak, is subject to even higher statistical fluctuations.

A circuit which, in respect to working principle and efficiency, is quite similar to Owen's latter design, was developed by Brooks[7]) using a different approach. This author assumed the mean lives T_p resp. T_γ of the fast components in the scintillation responses of anthracene to protons and γ particles to be different from each other. He had some reason to do this considering the esperiment of Wright[5]). Yet, even if the values obtained by Kallmann and Brucker, showing T_γ to be equal within the experimental error to T_α, did not convince Brooks, Owen's experiment verified unambiguously that for organic phosphors $T_\gamma = T_\mathrm{p}$. Notwithstanding this ap-

[7]) F. D. Brooks, Nucl. Instr. and Meth. 4 (1959) 151.

proach, the method of Brooks proved to be successful owing to the fact that the slow component (0.370 μsec) is already approximately integrated by the $R_dC \sim 1$ μsec circuit of the dynode, while the $R_aC \sim 2 \times 10^{-8}$ sec plate circuit delivers a pulse proportional to the multiplier current. By comparing the two voltages, a pulse "h" was obtained which was proportional to the difference in current amplitude between proton and γ induced scintillations containing the same number of photons (fig. 1). If the subtracting circuit is set in such a way that the positive pulse coming from the dynode extinguishes the negative current pulse delivered by an electron coming from the plate, we obtain the positive "h" for the proton pulse of lower amplitude. We should like to remark that although Brook's measurement does not verify his assumption that $T_p \neq T_\gamma$, this does not diminish the applicability of his method.

A method was developed by Robertson and Ward[8]) for discrimination in CsI(Tl) crystals. Their work was based on the results of Storey *et al.*[6]) who have shown the time constants of the fast components in the scintillation responses to α particles T_α and to electrons T_β to be very different. The difference in the intensities of the slow components was not exploited by their method, although this would have improved the discrimination efficiency.

Forte[9]) too has assumed the existence of the relations illustrated in fig. 1. His procedure, however, needs some modifications. The use of a diode prior to the complete evaluation of the information constitutes rather a drawback. Owing to nonlinearity it responds differently to small and large pulses and, in addition, it starts at a rather undetermined level with the rectification of the pulses which in any case have rather low amplitudes. Furthermore, a considerable loss in amplitude is caused by the integrating circuit. The arrangement as described permits only a very low counting rate. It is to be regretted that the author has given only a qualitative analysis of the discrimination efficiency of the method, since this does not show how far the otherwise accurate underlying principle has been approached by the circuit arrangement.

A common disadvantage of all above methods, perhaps with the exception of that used by Robertson and Ward, is their applying rather slow circuits which cannot work with as high counting rates as it would be inherently possible with scintillators. Therefore, it was thought useful to develop a new method which, in addition to fully exploiting all information available for the identification of particles, makes it possible to work with the optimum counting rate.

3. Theoretical Considerations

Let us start by considering fig. 1. If the scintillator is struck by one of the particles of type $1, 2, \ldots i \ldots$ (with ionisation densities $\bar{\rho}_1 < \bar{\rho}_2 < \ldots < \bar{\rho}_i < \ldots$) then a pulse similar in shape to the curves seen in fig. 1 will be obtained when normalizing again to the total number of photons produced by the scintillation. In the figure only the scintillation decays of the responses to particles with ionization densities $\bar{\rho}_1$ and $\bar{\rho}_2$, respectively, are shown. Now we have to deal with the separation of the particles from the particles denoted by $i - 1$ and $i + 1$ respectively. First, we shall consider the problem of distinguishing between the scintillation response to particles i from that to particles $i - 1$. The decay curves of the two particles intersect at the time $\tau_{i-1,i}$ for scintillations producing an identical number of photons. The number of photoelectrons produced by the two scintillations at the photocathode is given by $N_0 \cdot A_i$ and $N_0 \cdot A_{i-1}$ before and by $N_0 \cdot B_i$ and $N_0 \cdot B_{i-1}$ after the time $\tau_{i-1,i}$ respectively. The difference in the number of photoelectrons before and after $\tau_{i-1,i}$ is given for both particles by

$$S'_i = N_0(A_i - B_i) \quad \text{and} \quad S_{i-1} = N_0(A_{i-1} - B_{i-1}) , \qquad (2)$$

the difference between these two quantities being

$$D'_{i-1,i} = N_0[A_i - A_{i-1} + B_{i-1} - B_i] . \qquad (3)$$

This leads by using the notations of fig. 1 to

$$D'_{i-1,i} = N_0(b + c)$$

and

$$S'_i = N_0(a - d + b) \text{ and } S'_{i-1} = N_0(a - d - c)$$

respectively.

[8]) J. C. Robertson and A. Ward, Proc. Phys. Soc. B**73** (1959) 523.

[9]) M. Forte, Nuovo Cimento: Suppl. Ser. **10**, No. 2 (1958) 378.

That is to say, that the values obtained for S'_i and S'_{i-1} differ from each other by the quantity $\Delta_{i-1,i}$ which is precisely all the information available for discrimination. It is rather unfortunate that S'_i and S'_{i-1} contain additively also the number of electrons $N_0(a-d)$, so that due to the statistical fluctuation in the latter, the effect of the relatively small differences $N_0 b$ and $N_0 c$ may be blurred. Therefore, instead of using eqs. (2), it seems more convenient to substract the number of electrons arriving after the time $\tau_{i-1,i}$ multiplied by an arbitrary factor η from the number of electrons arriving prior to this time. Then we have

$$\Delta_{i-1,i} = N_0[(A_i - A_{i-1}) + \eta(B_{i-1} - B_i)] = N_0(b + \eta c) \,. \quad (4)$$

This factor η has to be so chosen that the relative error in the value $D_{i-1,i} = S_i - S_{i-1}$ is kept at a minimum. In calculating η, we shall exploit the fact that the photoelectrons produced by the photons of the scintillation obey a Poisson distribution, thus

$$\Delta D_{i-1,i} = \sqrt{N_0} \cdot \sqrt{A_i + A_{i-1} + \eta^2 (B_i - B_{i-1})} \,. \quad (5)$$

Furthermore, it follows from

$$\frac{\mathrm{d}\Delta D_{i-1,i}/D_{i-1,i}}{\mathrm{d}\eta} = 0$$

that

$$\eta_{\mathrm{opt}} = \frac{A_i + A_{i-1}}{B_i + B_{i-1}} \frac{B_{i-1} - B_i}{A_i - A_{i-1}} \,.$$

As a result of normalization $B_{i-1} - B_i = c = b = A_i - A_{i-1}$, hence

$$\eta_{\mathrm{opt}} = \frac{A_i + A_{i-1}}{B_i + B_{i-1}} \,. \quad (6)$$

This means that the relative error in the value of the difference between S_i and S_{i-1} will be minimized by weighting the number of photoelectrons arriving after the time $\tau_{i-1,i}$ with the ratio of the average number of photoelectrons produced by the scintillations of the two kinds of particles before and after this time. By doing so

$$S_i = N_0 \frac{A_i B_{i-1} - A_{i-1} B_i}{B_i + B_{i-1}} \text{ and } S_{i-1} = N_0 \frac{A_{i-1} B_i - A_i B_{i-1}}{B_i + B_{i-1}} \quad (7)$$

that is

$$S_{i-1} = -S_i \,. \quad (8)$$

Thus if we use the weighting factor η_{opt} now obtained, the discriminating pulses S will be of opposite sign for the two kinds (denoted by i and $i-1$) of particles.

Some calculations can be made as to the threshold energy for discrimination. If we accept Brooks[7]) definition of the resolution for pulse shape discrimination, the lower limit is given by N_0 as calculated form the expression

$$\frac{\Delta D_{i-1,i}}{|S|} = 1 \,. \quad (9)$$

From this we obtain

$$N_0 = 2 \frac{A_i + A_{i-1}}{B_i + B_{i-1}} \left(2 \frac{B_i}{A_i - A_{i-1}} + 1\right)^2 \,. \quad (10)$$

When starting from Owen's[2,3]) experimental data of unknown accuracy relating to antracen, the graphically determined values of A and B give $N_0 = 90$ which corresponds to electron and proton energies of 90 keV and 350 keV, respectively.

4. Application of the Method

Let us consider now the circuit in fig. 2. There is sufficiently high resistance in the anode of the multiplier to give together with the stray capacity a time constant permitting the integration of the

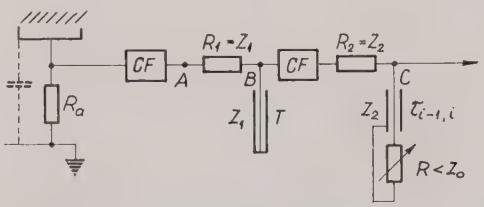

Fig. 2. Diagram showing the discrimination arrangement. CF cathode follower.

charge induced by the scintillation and assumed to be amplified without distortion by the multiplier. Using a cathode follower, the multiplier is coupled to a shorted cable reflecting the pulses with a delay time T. T is equal to the duration of the scintillation, thus at point B after a time delay $2T$ reckoned from the start of the pulse we are again at zero level. It is obvious that the dead time is $2T$. Up to now the pulse has been only shaped, the actual pulse shape discrimination is to follow. Essentially, this is done by means of a cable closed by a resistance R reflecting the pulses at the time $\tau_{i-1,i}$ the cable being connected to the output B of the shaping cable through a cathode follower, as seen above. What happens at point C? The reflection occurring

at the end of the cable of characteristic impedance Z_0 and being closed by R, is

$$p = \frac{R - Z_0}{R + Z_0}. \tag{11}$$

In fig. 3 we analyse the pulse of a particle with ionization density $\bar{\rho}_i$ as taken from the point C in fig. 2. The pulse shape from $t = 0$ up to the time $\tau_{i-1,i}$ follows that of the integral of the charge collected by this time at the anode. At this point, however, a break occurs caused by the return of the

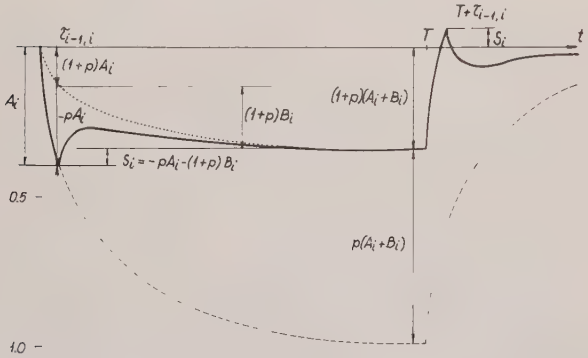

Fig. 3. Time variation of the voltage appearing in point B (dotted line) and that appearing in point C (full line) of fig. 2. The line marked by small dots is the $(1 + p)$-fold of the dotted line.

initial pulse multiplied by $p (p < 0$ in the figure) from the shorted cable. The resultant pulse can be now considered as the superposition of two parts: the initial one multiplied by $1 + p$ and the same multiplied by $-p$ and shaped by the shorted cable with reflection time $\tau_{i-1,i}$. Thus at the time $\tau_{i-1,i}$ the pulse is given by $(1 + p)A_i$ plus $-pA_i$. It is seen from the figure that

$$S_i = -A_i p - (1 + p)B_i. \tag{12}$$

As observed previously, the optimum discrimination will be obtained if the condition

$$S_i = A_i - \eta_{\text{opt}} B_i$$

is satisfied. From this we have

$$p = -\frac{1}{1 + \eta_{\text{opt}}} < 0. \tag{13}$$

By comparing (13) with (11), it follows that

$$R = \frac{\eta_{\text{opt}}}{2 + \eta_{\text{opt}}} Z_0. \tag{14}$$

The size of the discriminating pulse S_i is given by the difference between the maximum occurring at the time $\tau_{i-1,i}$ and the integrated pulse built up during the time T. This difference is given for the time $\tau_{i-1,i}$ in the mirror image of the ascending part of our pulse. Such is the case if prior to the time $\tau_{i-1,i}$ the particle producing a higher number of photoelectrons has been absorbed by the crystal. Now, if the crystal is struck by the other particle we have S_{i-1} which owing to (8) does not become positive by the time $T + \tau_{i-1,i}$, but remains negative because of $S_{i-1} = -S_i$. Two such pulse shapes are seen in fig. 4. From (7) it is apparent that S_i and S_{i-1} are proportional to N_0 and thus to the energy and therefore the points S_i and S_{i-1} lie along straight lines in the S-energy coordinate system having identical absolute values but slopes of opposite sign, provided in the scintillation the ratio of fast to slow photons and the average lifetimes of the two components are independent of the energy. It is seen that in this simple way discriminating pulses are obtained only for the particle responsible for the fast component of relatively higher intensity, that is with the use of organic phosphors for particles with lower and with inorganic phosphors for those with the higher ionization density.

If the crystal is struck by more than two kinds of particles, a further cable, similar to the previous one, has to be coupled to the cathode follower

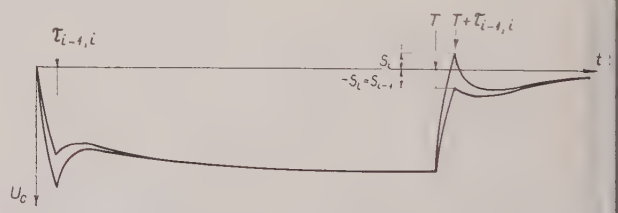

Fig. 4. Pulse shapes in point C of fig. 2 for two particles of different ionization densities.

Since the cut-off time $\tau_{i-1,i}$ as well as the reflection coefficient have been chosen so as to obtain the optimum separation of two kinds of particles, the same circuit cannot discriminate between A_i and A_{i+1} as well. In order to separate the scintillation response of the particle with ionization density $\bar{\rho}_i$ from that characterized by $\bar{\rho}_{i+1}$, a cable with delay time $\tau_{i,i+1}$ and circuited by $R_{i,i+1}$ is required. These latter values are determined by the difference in pulse shape of the two particles in question. In the first stage positive discriminating pulses S are

ained for all incident particles (denoted by $+1, \ldots$) which produce integral curves of her slope than that of the particles with ionization density ρ_{i-1}, while in the second stage the lses S will be negative but for particles denoted $i+1, i+2, \ldots$. The anticoincidence of the lses $+S$ in the two circuits occurs thus precisely the absorption of the particle i in question.

Experiment on CsI(Tl) Crystal

The measurements of Storey, Jack and Ward[7]) ve full information on the pulse shape of the ntillation of CsI(Tl) crystals. The time constant the fast component is shown by their measurement to be decreasing exponentially with increasing ean ionization density. Furthermore, it is possible to calculate from their measurement the ratio the total number of slow to fast photons

$$\int_0^\infty slow \, dt \Big/ \int_0^\infty fast \, dt \qquad (15)$$

shown in fig. 5. From these two data the pulse ape of particles with any ionization density can e determined. Thus, for instance, the pulse shapes

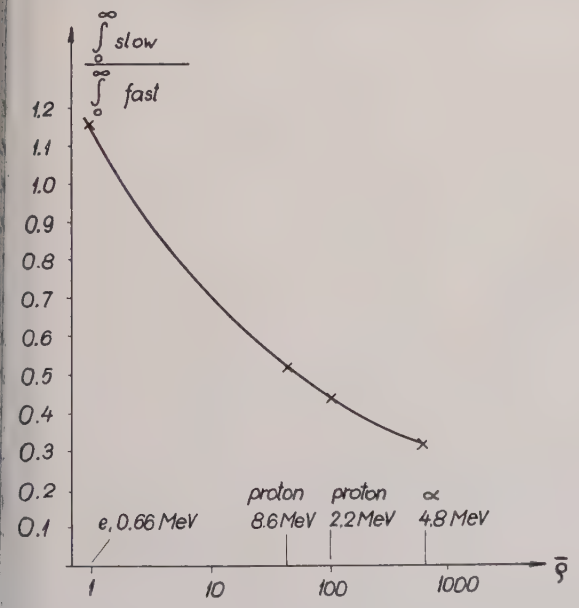

ig. 5. Ratio of photons belonging to the slow and fast component of scintillation corresponding to different mean ionization densities on the basis of the dates given in[6]).

f 2.2 MeV protons and of 2.26 MeV deuterons of dentical scintillation responses, further those of 8.6 MeV protons and of their counterparts the 8.85 MeV deuterons, can be calculated as follows:

$$N_{p,2.2}(t)\Delta t = (1.33\, e^{-t/0.52} + 0.044\, e^{-t/7.0})\, \Delta t\,, \qquad (16a)$$

$$N_{d,2.26}(t)\Delta t = (1.48\, e^{-t/0.48} + 0.041\, e^{-t/7.0})\, \Delta t\,, \qquad (16b)$$

$$N_{p,8.6}(t)\Delta t = (1.074\, e^{-t/0.6} + 0.051\, e^{-t/7.0})\, \Delta t\,, \qquad (16c)$$

$$N_{d,8.85}(t)\Delta t = (1.225\, e^{-t/0.56} + 0.046\, e^{-t/7.0})\, \Delta t\,. \qquad (16d)$$

The response curves of the 2.2 MeV particles intersect at $\tau_{dp} = 0.66\ \mu$sec. Now, the values A and B and the factor η_{opt} can be calculated from (16a)

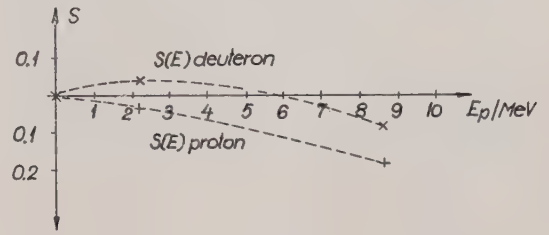

Fig. 6. Discriminating pulses relating to proton and deuteron in dependence on the energy of the proton. The reflexion coefficient was chosen so as to obtain optimum discrimination between proton of 2.2 MeV energy and deuterons of the same scintillation efficiency.

and (16b), which values in turn yield the discriminating pulses $S_i = S_{d,2.26}$ and $S_{i-1} = S_{p,2.2}$ irrespective of their absolute values, since the total number N_0 of the photoelectrons is irrelevant in this problem. The discriminating pulses for 8.6 MeV protons and those for deuterons corresponding from the point of view of scintillation efficiency to these protons can be determined from (16c) and (16d), though it has to be taken into account that τ_{dp} and R_{dp} have been chosen for the optimum discrimination of 2.2 MeV particles. The results of our calculations are shown in fig. 6. These two sets of points may be completed by our knowledge that $S_p = S_d = 0$ for $E = 0$. It is immediately apparent that $S_d(E) \neq kE \neq S_p(E)$. This problem has been investigated experimentally and the result is shown in fig. 7. The pictures were taken by irradiating a deuterized paraffin layer with 14 MeV neutrons. The aluminium plate supporting the paraffin was mounted on 1.5 mm thick CsI(Tl) phosphor. α particles were obtained from the Al(n, α) reactions, deuterons, from the elastic scattering and protons from both the Al(n,p) and the D(n,p) reactions. Owing to the (n,γ) radiation of the surroundings γ-pulses too were obtained. The scintillations were

detected by a Dumont 6292 photomultiplier. From the point C in fig. 2 the pulses were transmitted to the vertical amplifier of a Tektronix type 515A oscilloscope, while the pulses coming from the first cathode follower and delayed for $t \geqslant \tau_{dp}$ were being

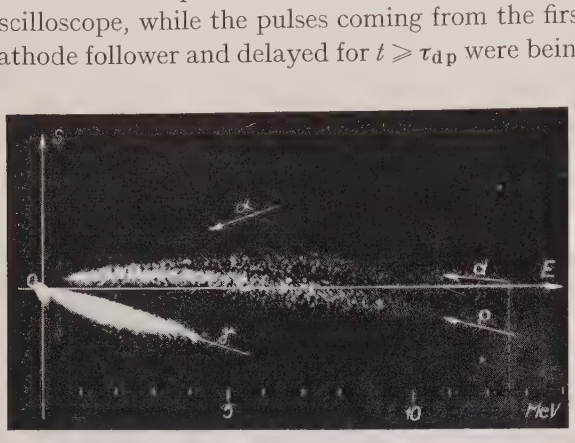

Fig. 7. Photograph of oscilloscope obtained for various particles incident simultaneously using the arrangement of fig. 2.

passed to the horizontal amplifier. The electron beam of the oscilloscope was opened at $T + \tau_{dp}$ and kept open for $t \simeq 50$ mμsec. The best photographs were obtained with $T = 3$ μsec and $\tau_{dp} \simeq 0.5$ μsec. The number of α particles is relatifely low. The upper limit of the γ line is quite sharp, the lower limit, however, is blurred and broadened since only a small fraction of fast electron energy is lost to the crystal and such scintillation appear at lower energies. In consequence of the lower average ionization densities, the S is more negative than for electrons having the same photon yield but being completely absorbed by the scintillator. It is also apparent that the discriminating pulses for α and γ-induced scintillation showing a great difference in fast component versus lifetime curves, lie, in terms of the energy, on an approximately straight line. The deuteron and proton lines are curved. Usually, however, a reflection coefficient differing from the optimum can be found for which the two curves rise above the energy axis, so that above a given energy and as compared to a certain $U > 0$ discrimination level, we have $|S_p| < U < |S_d|$. The energy scale was calculated for the maximum deuteron energy possible upon bombardment with 14 MeV neutrons. Proton-deuteron discrimination seems to be feasible above $\sim$ 3 MeV. Their separation from the γ, p, α background can be achieved with the aid of the arrangement shown in fig. 8. The second cathode follower is coupled to two cables of delay time τ_d and τ_{dp} and closed by impedances R_{dp} and $R_{d\alpha}$. The input of these cables is connected to the discriminator. The necessity for this arrangement has been already discussed in connection with the d–p discrimination, yet it is not superfluous for the α–d channel either, since, though the discriminator of the d–p channel delivers a pulse for each discriminating S above the preset level, thus for S_α too, no signals are obtained for α particles having lower S than the discrimination level set for the d–p channel. It follows from the above that by discriminating subsequently in the α–d channel at 0 volt, anticoincidences would be brought about by pulses which, though produced by α particles, could be identified as deuterons since their S appears between 0 and U_{dp}.

Considering that, usually, the energies of the discriminated particles have also to be measured, it is useful to wait for the scintillation to die out. Sometimes, however, a higher counting rate is required even at the expense of analysis and separation. In this case the time T has to be reduced which necessitates some modification also fo τ. If we have to

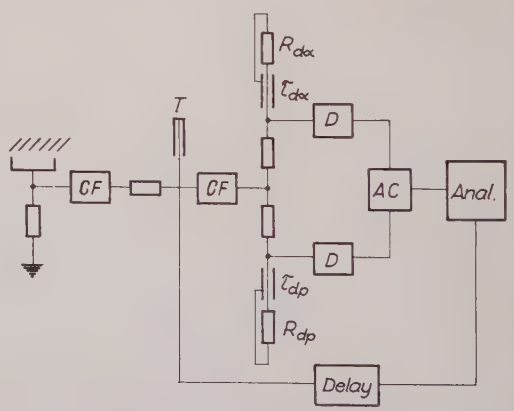

Fig. 8. Block diagram of circuit selecting one type of particle from among the different components of the background.

work extremely fast, the arrangement shown in fig. 9 may be convenient, although only scintillations of very short duration would then give positive discriminating pulses, if the reflecting resistance R is suitably chosen and $R_a = Z_0$. The length of the cable is determined by the requirement that the reflected wave should return at

ie about the mathematical mean value of the ay contants of the fast components of the ticles to be discriminated. For α–γ discrimina- n in Cs(Tl) it is about ~ 0.56 μsec.

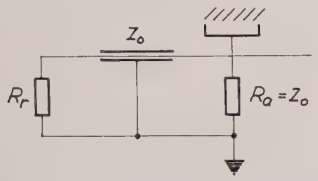

Fig. 9. Simple circuit for fast discrimination.

Reduction of the Threshold Energies for Discrimination

n special cases when the incident beam of ticles is well collimated, the method can be im- oved by suitably combining the informations ob- ned from the measurement of dE/dx with the ape discrimination. It is obvious that, similar to e discriminating pulses S being meaningless with- t the measurement of the energy (total number of otons), the particle will be determined by dE/dx ly if we know the energy of the particle which es—to a foil of given thickness—the amount of ergy $\rho \Delta x$ ($\rho = dE/dx$). Now, since in the course shape discrimination the particle energy has al- ady been determined, we have only to combine e knowledge of these three experimental values. Let us use a scintillator foil for the measurement ρ. A particle of energy E_0 loses the fraction $\Sigma = \rho \Delta x$ of its energy. $E_0 - \Delta E$ be absorbed by e analysing crystal. The number of photoelectrons oduced in the foil per scintillation be n. This rrent be amplified by a factor k in a multiplier d possibly with the help of other electronical vices. The other scintillator deliver N photo- ectrons proportional in number to the energy $_0 - \Delta E$ and this be multiplied by k'. In accord- nce with the previous denotation for the arrival of e particle denoted by i, we obtain a quantity $n_i + k'N_i$. What is the difference in the composi- on of these two equal quantities $kn_{i-1} + k'N_{i-1} = n_i + k'N_i$ obtained for particles i and $i - 1$, spectively? If $\bar{\rho}_i > \bar{\rho}_{i-1}$ it follows that $n_i > n_{i-1}$ nd by choosing a suitable inorganic measuring rystal we have $S_i > S_{i-1}$ as well.

Let us choose a foil the scintillation decay of which is much faster than that of the measuring crystal. It should be fast enough to permit the scintillation to die out completely prior to the time τ characteristic for the analyzer. This requirement is fully met by coupling an organic scintillator foil with an inorganic measuring crystal. In this case the sign of $A_i - A_{i-1}$ will be the same as that of $n_i - n_{i-1}$. This means that virtually only the information "b" in fig. 1 increases in accordance with $n_i - n_{i-1}$. It has to be kept in mind that owing to the change in normalization $\tau_{i-1,i}$ needs some correction which will induce some change in η_{opt} as well.

We calculate now in the same way as above

$$\eta^* = \frac{k}{k'} \frac{n_i + n_{i-1}}{N_i B_i^* + N_{i-1} B_{i-1}^*} + \frac{N_i A_i^* + N_{i-1} A_{i-1}^*}{N_i B_i^* + N_{i-1} B_{i-1}^*} \quad . \quad (17)$$

The terms with asterisk correspond to those, used in the previous treatment, though differing from them as regards their normalization and in consequence of the new $\tau_{i-1,i}$. The second term of the expression for η^* is incidentally the perfect analogue of η_{opt}. Further, it can be readily shown that

$$S_i^* = \frac{(kn_i + k'N_i A_i^*) N_{i-1} B_{i-1} - (kn_{i-1} + k'N_{i-1} A_{i-1}^*) N_i B_i^*}{N_i B_i^* + N_{i-1} B_{i-1}^*} = > S_{i-1}^* \, . \quad (18)$$

Assuming in a rough approximation the qnantities A and B to be independent of energy, and N to be proportional to E, while n to $1/E$, it becomes apparent that $S^*(E)$ is the superposition of a hyperbola and a straight line. The weight factors of the superposition can be influenced both by the foil thickness Δx and the multiplying factors k and k'. The k (amplification of the channel ρ) however, energy loss ΔE in order to determine the spectra more accurately, it is obvious that the optimum setting is $k = k'$.

It is to be noted that even ΔE cannot be arbitrarily small. In the calculation of η^* the Landau effect has not been taken into account; this means that ΔE must be higher by an order of magnitude than the maximum energy which can be transferred from the particle detected to an electron of the foil. If this condition is not satisfied, the Landau effect has to be calculated too.

7. Telescope

The above considerations can be applied without any alteration to the so-called telescopes. The previously used proportional counter-crystal detector combination is now being replaced at an ever increasing rate by scintillator foil-crystal analyser arrangement. It is to be noted that the above results will hold only if the detectors conform to the above requirements. By adding the integrated pulses of the two multipliers and transmitting this sum pulse to the shape discriminator, we obtain with corrections $\tau \to \tau^*$ and $\eta_{opt} \to \eta^*$ the results of the preceding paragraph.

8. Shape Discrimination with Sandwich-detectors

Similarly, the above considerations are readily applicable to the plastic phosphor-inorganic crystal sandwich arrangement. This combination has been

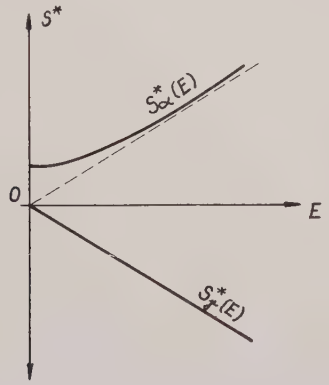

Fig. 10. When combining the measurement of dE/dx with pulse shape discrimination, the pulses for α particles can be separated from those of γ rays even at low energies.

experimentally tested by the author. A plastic foil of about 1 mg/cm^2 was mounted on a CsI(Tl) crystal plate and irradiated with the α rays of a Po^{210} source. The α radiation released the electrons in the CsI crystal so that they were not affected by the foil, the discriminating straight line $S^*(E)$ however, rose above its previous level as it is seen in fig. 10. In this case the condition $k = k'$ is automatically satisfied, since both scintillations are counted by the same multiplier, thus the circuit shown in fig. 2 may be kept unaltered but for k and R.

Something has to be said also on the part played by the multipliers. Actually, no fast multipliers are needed for the integration, nevertheless it is desirable that the multiplier should sufficiently weakly respond to any variation in the emission of the light pulses since it is the rise time of the integrated pulse which is exploited for discrimination.

This means that only a minimum fraction of the charge collected prior to time τ should be permitted to pass into the subsequent time interval because of the distortion caused by the multiplier. This problem does not arise with "slow" scintillators such as CsI, NaI etc. For faster organic phosphors however, the choice of the multiplier becomes of considerable importance. If the distortion due to the multiplier becomes appreciable, the optimum conditions for discrimination had better be determined from the time distribution of the charge collected on the anode than from the parameters of the scintillation decay. This does not involve additional work, since our present knowledge of the scintillation mechanism still requires the experimental correction of the predicted data.

Acknowledgement

I take this opportunity to express again my thanks to the International Atomic Energy Agency for sponsoring my study abroad. Thanks are due to the Nuclear Physics Department of the C.I.S.E., in particular, to Prof. U. Facchini for continued interest in my work as well as to Prof. E. Gatti for helpful discussions.

UCLEAR INSTRUMENTS AND METHODS 14 (1961) 33–37; NORTH-HOLLAND PUBLISHING CO.

SOME NEW PROPOSALS FOR DESIGN OF COMPTON SPECTROSCOPES

MILORAD MLADJENOVIĆ†

Centro Studi Nucleari Della Casaccia, Roma

Received 26 July 1961

me new possibilities of using inhomogenous magnetic field tors for Compton spectroscopy are discussed. Among them e spectrographs for (n, γ) measurements, spectroscopes for point gamma sources, and a large radiator, intermediate focus Compton spectrometer, with Siegbahn-Swartholm field.

Introduction

Many of the neutron capture gamma-ray spectra an be resolved only with spectroscopes having esolutions of the order of a few pro mille. While at w energies crystal spectrometers give probably ne best results, Compton spectroscopes seem to ave some advantages at energies over 2–3 MeV. he development of Compton spectrometers has een rather slow [1–3]) and only recently the resolu- ion "barrier" of a few percent has been overpassed nd some designs with an order of magnitude better esolution have been reported. Thus Groshev *et al.*[4]) escribe a large Compton spectrometer, consisting f two magnetic sectors and having resolution of .3%. Lee-Whiting presented a very thorough heoretical discussion of a new type of single nagnet Compton spectrometer, which should have resolution of 0.2%[5]). A resolution of 0.3% was lso achieved by Motz *et al.*[6]) with a Siegbahn- wartholm double-focusing spectrometer, using a γ–β coincidence arrangement.

There are many possible types of Compton pectroscopes, and only a few of them have been sed up to now. On the other hand, the requirements ary from one laboratory to another, so that there s a need to develop various types, optimising some articular characteristics in each of them. For nstance the neutron fluxes may vary by several rders of magnitude. With a low flux reactor, one as to optimise the luminosity, while with very igh fluxes one can sacrifice some luminosity to ain on the resolution. In general, with low fluxes it s preferable to use spectrographs, detecting a part of the spectrum simultaneously. Another factor of importance is the availability of other beta-and gamma-spectroscopes in the laboratory, since a greater number allows a finer specialisation of each.

Having in mind the need for diverse types, we shall consider in this paper some new possibilities to improve various characteristics of Compton spectroscopes. General properties may be sufficiently well illustrated by confining the discussion to approximations of the first order. The calculation of second order properties would have allowed a more precise and more usefull discussion, but would have much delayed the publication of the paper.

2. Use of Sector Pole Pieces

The background in Compton spectrometers is generally so high that counting has to be done with some coincidence arrangement. The second Geiger counter can be placed either behind the first one, in a telescopic set-up, or in the intermediate focus, if it exists. In both cases the effects due to scattering of electrons at low energies have to be considered. Another method developed by Motz and collaborators[6]) is to measure the coincidences between electrons and backscattered photons. This has

† On leave from University of Belgrade.

[1–3]) The development of Compton spectroscopes was reviewed recently by:

[1]) G. A. Bartholomew, J. W. Knowles and G. E. Lee-Whiting, Report on Progres in Physics, Vol. **23** (1960) 453.

[2]) M. Mladjenović, Nucl. Instr. and Meth. **10** (1961) 1.

[3]) M. Mladjenović, Reports of CNEN, Rome, 1961 (in press.)

[4]) L. Groshev, A. Demidov, V. Lucenko and A. Malov, Izvestia **27** (1960) 791.

[5]) G. E. Lee-Whiting, Canad. J. Phys. **38** (1960) 720.

[6]) H. T. Motz, R. E. Carter and W. D. Barfield, IAEA Symposium on pile neutron research, Vienna (1960).

advantages over the other two methods, the most important being that the lower energy electrons scattered in the radiator so as to enter the acceptance slit, are not counted. The line remains narrower and the resolution is improved. In the Motz arrangement, however, the coincidence counting rate is relatively low, because the gamma counter subtends a small solid angle, detecting only a minor part of gamma rays backscattered between angles ϑ and $\vartheta + d\vartheta$. An improvement would be achieved by the use of a detector in form of a ring, coaxial with the gamma beam. The space necessary for such arrangement may be obtained by cutting out the part of polepieces through which the electron beam is not passing. Then there is also enough space on the electron detection side, which is especially important in spectrographs. Fig. 1 shows how the sector arrangements would look like in the spectrometer used by Motz *et al.*[6]), and in the one proposed by Lee-Whiting[5]).

It appears therefore that sector pole-pieces are generally more convenient in Compton spectroscopy. Modifications from the classical design are then required and we shall discuss them briefly.

a) In a typical double-focusing spectrometer the beam-free space is used to place the magnetic field measuring device at equilibrium radius. This is not possible with sector pole-pieces. One should then use two field-measuring devices, at different radii, getting thereby an additional possibility to control the field gradient.

b) Circular symmetry of the field is perturbed near the sector edges. This effect could probably be somewhat reduced by the shimming, so that it would be safe to place the radiator and the exit slit at a distance from the edges equal to pole piece separation.

c) The construction of the vacuum chamber becomes somewhat more complicated, because side walls with pole piece profile have to be made.

One could conclude that sector magnets do not introduce serious difficulties, but only demand a more careful machining and adjustment.

3. Spectrographs

The generally low counting rate of Compton electrons favorises the use of spectrographs, in which a part of the spectrum is detected simultaneously. Thus, Motz *et al.*[6]) have four scintillation counters in the focal plane of a double-focusing

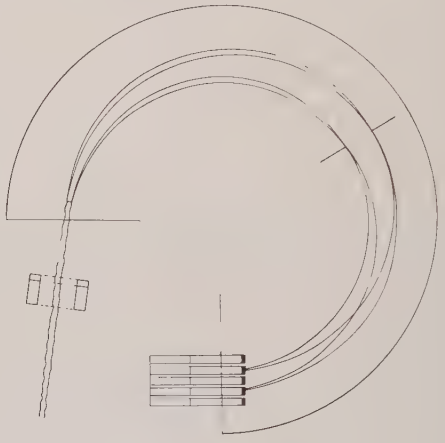

Fig. 1. Sector versions of a) Motz double-focusing spectrometer of Siegbahn-Swartholm type.

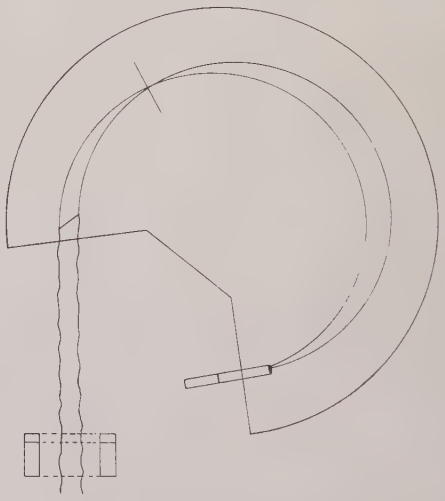

b) Lee-Whiting spectrometer.

spectrograph. It could be expected that in future semiconductor detectors turn out to be more convenient for this purpose, since they take much less space and are not sensitive to the magnetic field, as are the photomultiplyers. Electron sensitive semiconductor detectors were reported recently[7]), and the development has advanced such that sensitive surfaces larger than 1 cm^2 can be obtained. In a high resolution Compton spectroscope with an

[7]) Solid State Radiation Detectors, IRE Trans nucl. Sc (USA) vol. NS-8 (1961).

equilibrium radius of 50 cm, the dimensions of exit slit might be about 5 mm radially, and nm axially. At least 8–10 detectors could thus placed within a relatively small distance $\rho = r - r_0)/r_0 = \pm 0.04$ from the equilibrium path. such small distances the line widths should not ease appreciably. It is possible that fields with ger focal planes can be found, so that greater nber of detectors can be used, but for that, ond and third order solutions have to be worked , as it was done by Huber[8]) for beta-spectro-phs.

All the best Compton spectrometers have large iators and intermediate radial focuses. In ctrographs it would be complicated to work with ermediate radial focuses, although in principle it not impossible. In the following we shall only sider the spectrographs without the inter-diate radial focus.

The field geometry is connected with the radia-s shape and relative area, and one would like to ose it so that the area is large and the shape as ple as possible. These requirements are in neral satisfied by "half-wave" solutions, in ich the radiator-detector angle ϕ is given by

$$\phi = \tfrac{1}{2}\phi_r = \tfrac{1}{2}\phi_z n$$

n = uneven whole number
ϕ_z = axial focusing angle
ϕ_r = radial focusing angle.

The advantages of half-wave solution is that:

1. The largest radiator can be used for a given aximum radial and axial departure from the uilibrium orbit.
2. The radiator is flat and placed perpendicularly the gamma-ray beam.

The simplest solution is

$$n = 1 \qquad \phi_r = \phi_z = 255° \qquad \phi = 127°$$

rresponding to a sector with Siegbahn-Swartholm ld. Since angle ϕ is relatively small, it is essential use e–γ coincidence arrangement, in order to ppress the background. Two possible geometries such a spectrograph are shown in fig. 2. The ectron emission angles are then determined by mma detectors, and baffles are primarily em-

[8]) H. Wield and O. Huber, Helv. Phys. Acta **29** (1957) 224.

ployed to reduce the scattering. This is especially important in the case of the spectrograph shown in fig. 2a, where the radiator is in the field, because

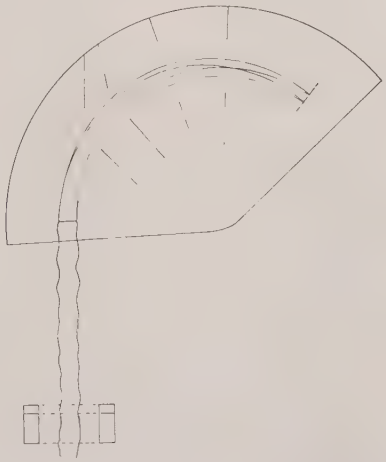

Fig. 2. Sector spectrograph with Siegbahn-Swartholm field.
a) Radiator inside the field.

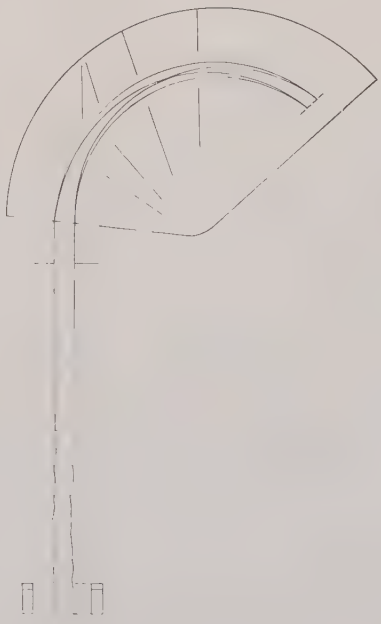

b) Radiator in field free region.

the entrance slit would influence the line shape and focal plane position. The single counting rate in the electron detector would be lower in the type shown in fig. 2b, which has another operational convenience that the radiator orientation and shape are not important at all.

$$n = 3 \qquad \phi_r = 570° \qquad \phi_z = 190° \qquad \phi = 285°.$$

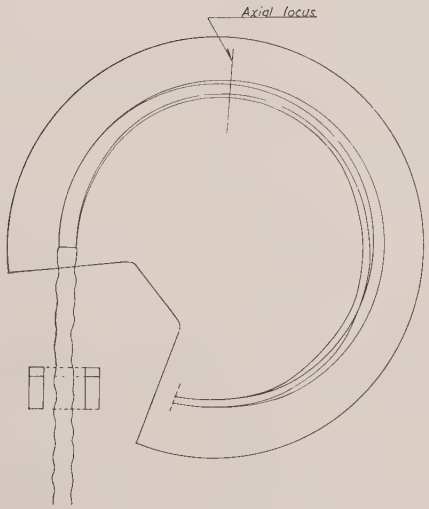

Fig. 3.
Large dispersion spectrograph with intermediate axial focus.

The next half-wave solution is (fig. 3)

There is an intermediate axial focus after the electron beam has rotated through 95°, which helps to reduce the background and control the resolution. The dispersion of this field is very high, five times higher than the dispersion of the Siegbahn-Swartholm type. It should be preferably used with high-flux reactors, which allow fine collimation of both, gamma-ray and electron beams. The contribution of the electron-energy spread to the line width can then be minimised.

4. Point Source Compton Spectroscopes

Compton line measurement of gamma-ray spectra of radioactive isotopes may happen to be most convenient in cases where the crystal diffraction spectrometer is not available and external photo conversion measurement is handicapped by large Compton background. Special Compton spectrometers were developed for that purpose, but obviously it would be interesting to have spectrometers which are good for both, Compton line, as well as the internal and external conversion measurement. One of the types which can be adapted for such dual purpose measurements is a spectrometer developed for beta-ray measurements by Sakai *et al.*[9]) and by Kaminskii and Kaganskii[10]).

[9]) M. Sakai, H. Ikegami and T. Yamazaki, INSJ-10 (1958).
[10]) D. L. Kaminskii and M. G. Kaganskii, PTE (1959) No. 1, 32.

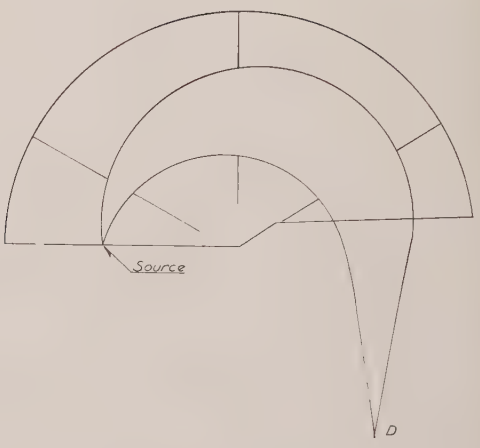

Fig. 4. Point source spectroscopes. a) Sakai's sector beta spectrometer.

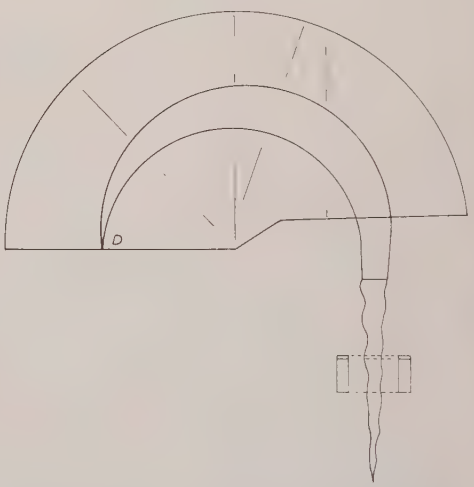

b) Compton version of the same spectrometer.

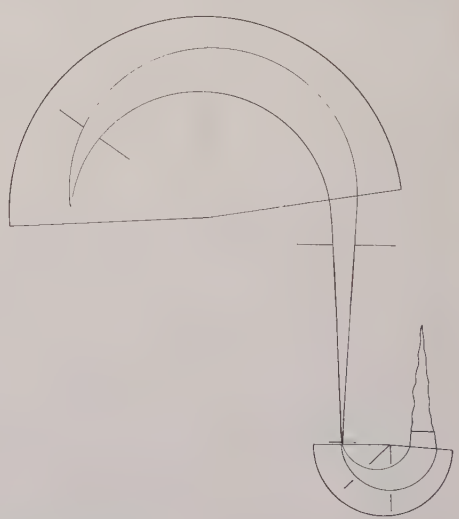

c) Two-sector spectrometer with intermediate focus.

t is a 180° sector with Siegbahn-Swartholm l. (fig. 4). The source is inside and the detector side of the field, in order to get a larger trans- sion. By inverting the positions of the detector l the source, the same apparatus can serve as a ge radiator Compton spectrometer (fig. 4b). The iator is placed some distance from the source. ce it is in the field-free region, its exact shape l orientation are not important. The use of an ular gamma-ray detector is quite essential to vent the line broadening by lower energy elec- ns and to reduce the background. It could be o developed as a spectrograph.

The gamma-ray detector is not necessary if other sector is added, as shown in fig. 4c. The ction of the first magnet (which Groshev calls parator") is to produce a small image, which ves as source of the second sector. It should have v dispersion field, higher order focusing and small uilibrium radius. Unfortunately, no convenient lf-wave sector of $\phi \leqslant 180°$ can be made with low spersing fields. Fig. 4c shows an arrangement th Siegbahn-Swartholm field. It should be entioned that coupling of two sectors into one ectrometer, reprents some operational diffi- lties.

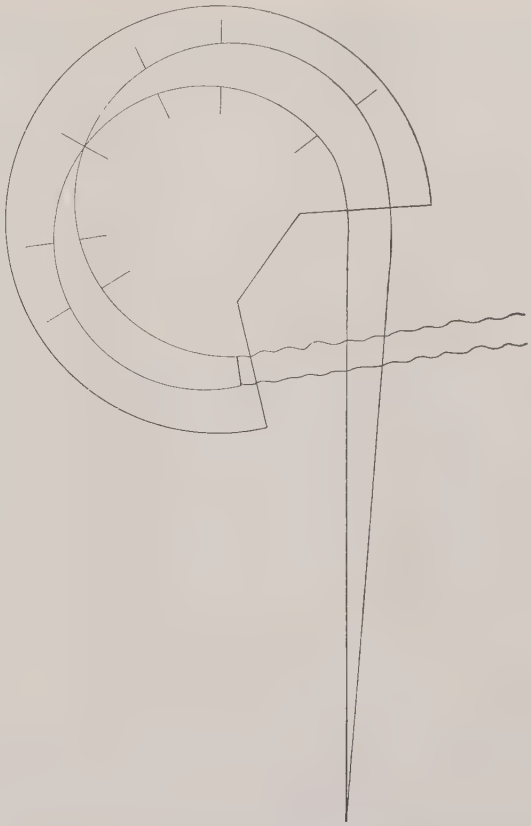

Fig. 5. Compton spectrometer with intermediate focus, using a Siegbahn-Swartholm field.

Intermediate Image with Siegbahn-Swartholm Field

A spectrometer with Siegbahn-Swartholm field, nich can be used either as a beta spectrometer or large radiator, intermediate image Compton ectrometer, is now under construction in the aboratory of Applied Nuclear Physics in Rome. ne principle is illustrated in fig. 5. The sector angle the pole pieces is 280°.The electron ejected from flat radiator, placed perpendicularly to the gamma eam, are after half-wave angle of 127° brought to ie intermediate double focus. The final focus is 5 m outside of the magnet. The gamma- and eta-ray beam are crossing each other. This may crease the background, but as some coincidence rangement shall be used, it should not cause any ouble. The intermediate double focus should help uch with background and resolution.

At the end it should be remarked that all the above discussed spectroscopes are made with magnetic sectors. More detailed discussion should include the fringing field effects. Recent theoretical[11]) as well as experimental work[4,9,10,12]) on magnetic sectors serves as an encouragement. There is no doubt that the use of inhomogenous field sectors open up new and interesting possibilities.

Acknowledgements

The present work was done while the author was in Applied Nuclear Physics Laboratory (Rome) under the agreement on the exchange of Scientists between Italian and Yugoslaw Nuclear Energy Commissions. The hospitality and the interest of Prof. S. Sciuti, Director of the Applied Nuclear Physics Laboratory is gratefully acknowledged.

[11]) D. L. Judd and S. A. Bludman, Nucl. Instr. **1** (1957) 46.
[12]) A. V. Cohen, J. A. Cookson and J. L. Wankling, Nucl. Instr. and Meth. **10** (1961) 84.

NUCLEAR INSTRUMENTS AND METHODS **14** (1961) 38–40; NORTH-HOLLAND PUBLISHING CO

SCANNING APPARATUS FOR BUBBLE CHAMBER DATA ANALYSIS†

G. BRUNHART, C. D. GALL, C. VITTITOE, K. SCHNEIDER and V. P. KENNEY

University of Kentucky, Lexington, Kentucky

Received 14 September 1961

The usefulness of automatic equipment for the analysis of bubble chamber film is enhanced when suitable equipment is available for the preliminary scanning of film to locate the events of interest. Desirable criteria for scanning equipment include (1) ease and speed of operation, (2) low cost, and (suitability for use as a simple auxiliary measuring instrumen Two devices which have proved very satisfactory in the respects are described.

1. General Purpose Scanning Machines

Three scanning machines of the type shown in fig. 1 have proven useful in studying 35 mm photographs of pion interactions in the Alvarez 15″ bubble chamber at the Lawrence Radiation Laboratory, as well as in the Adair 14″ chamber at the Brookhaven National Laboratory; they are presently used in scanning film which is to be measured on a Hermes precision film reader.

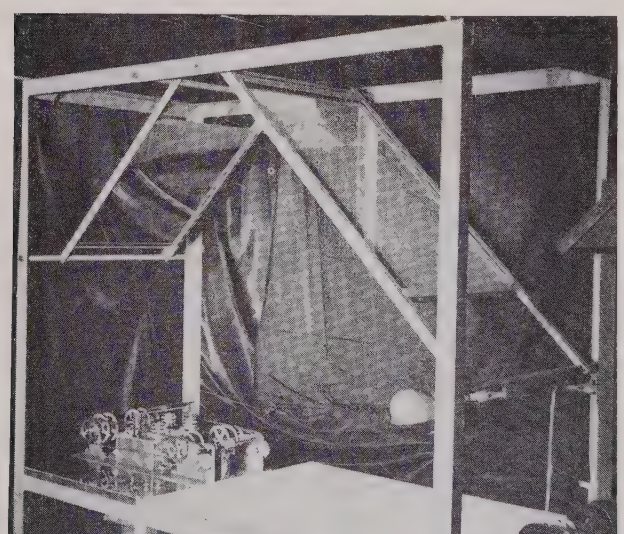

Fig. 1. Overall view of the general purpose scanning machine of the type used at Kentucky. The film advance and projection optics on the left project the bubble chamber film image to be scanned onto the opaque Formica surface at the center.

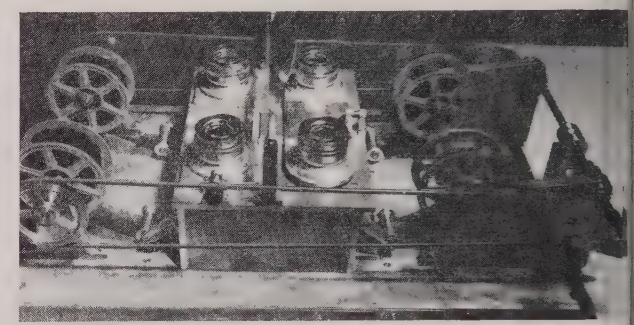

Fig. 2. Film advance and projection optics for the gener purpose scanning machine. Thumbscrews for superimposi stereo images are to be seen in the front and to the right of th projector housing. The mechanical shutter at the top is move by hand to cut off either pair of stereo views.

The film advance and projection optics a mounted for convenience at the operator's sid with the film image projected on a flat Formic surface by means of two front-surface mirro mounted above the screen. For bubble chamb film which contains four stereo images on tw separate rolls of film, the optical system shown i fig. 2 is used. Projection lenses are Componar *f*/4. 105 mm. The four views may be examined singl or in any of four stereo pair combinations, by a propriate selection of projection lamps and th position of a shutter. Film advance is mechanica with a single hand crank used to move either roll film forward or backward. When the control kno is drawn forward, a slotted key on the driveshaf engages the front drive assembly; when pushe

† Supported in part by the National Science Foundation.

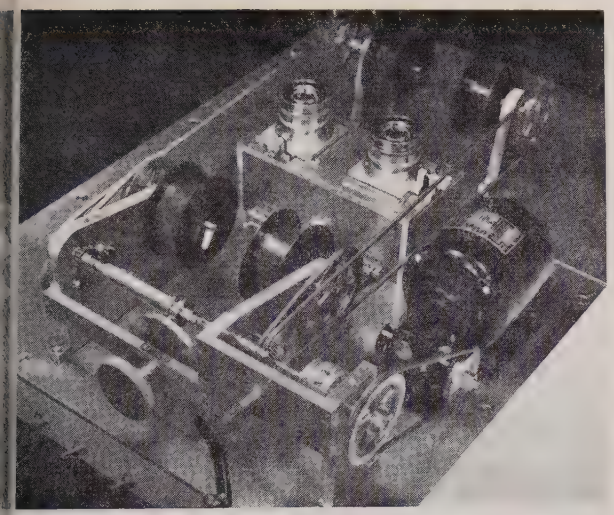

Fig. 3. Two-lens modification, with magnetic clutch and motor drive shown at the right. The hand crank is used for frame-by-frame advance. The knurled knob to the left of the crank engages either the left hand or right hand film advance; the film is clamped in the center position. The shift from forward and backward film advance is accomplished by reversing the position of the idler gears on the crank shaft, which may engage either of two sets of gears to drive the film by means of the pulley system shown.

ack, the rear drive is engaged. In the center osition from which neither roll may be driven, a icroswitch actuates a solenoid to clamp the film rmly against a $\frac{1}{4}''$ optically flat glass plate, which is rced-air cooled.

A most useful feature is the lens motion provided y thumbscrews which permit pairs of lenses to be oved over a range of 2 cm in each of two perpendicular directions. Pairs of stereo views may thus be uperimposed permitting rough, direct measurements in first-order stereo geometry, and the ready dentification of tracks which pass out the front or ack of the chamber. Such preliminary analysis aves considerable time in subsequent machine measurement and computing.

The same basic projector, modified for bubble chamber film in which each stereo view is on a separate roll of film is shown in fig. 3. In this modification a $\frac{1}{20}$ h.p. motor and a magnetic clutch are used to provide a variable-speed film advance for film-rewind and for locating desired frames rapidly. The mechanical hand-crank system continues to prove useful in frame-by-frame advance, though the motor-drive may be used for this purpose as well.

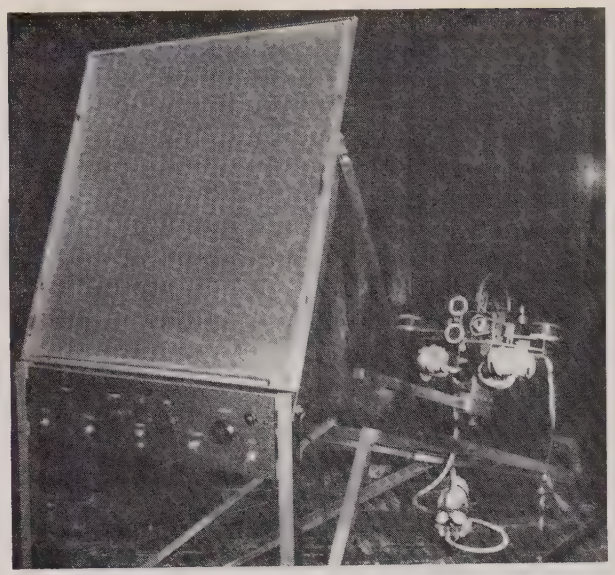

Fig. 4. Overall view of the three-dimension scanning device as viewed from the operator's end, with polaroid films moved out of position. Selsyn motors are used to focus, to move one stereo view vertically and horizontally with respect to the other, and to vary the speed of the film advance, remotely.

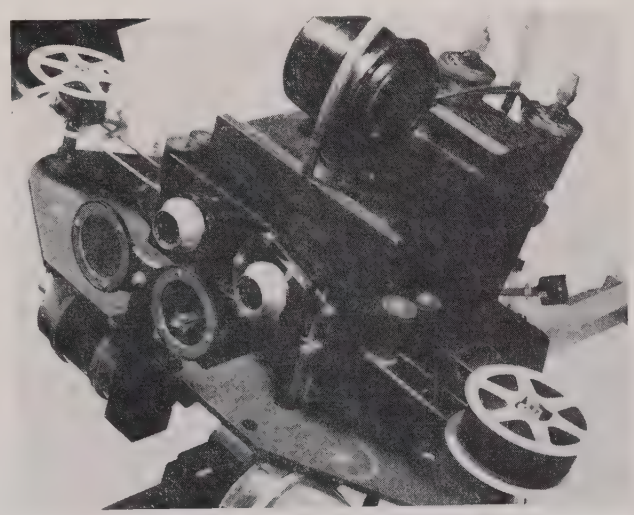

Fig. 5. Projector end of the three-dimension scanning device with polaroid films in place. The right-hand lens is spring mounted and is moved horizontally by pressure of the rollers attached to the brass "pincers" shown. The entire lens mounting is raised or lowered for vertical motion of this view.

2. Three-D Stereo Scanning Machine

For some experiments, it is desirable to employ a scanning device which permits the observer to view each frame in three-dimensional depth. The scanning machine shown in fig. 4 has been used in an experiment in which neutral-pion production

events were selected by scanning for events which were correlated in space with a conversion electron pair from a π^0-decay gamma ray. The stereo effect is provided by simultaneously projecting two stereo views on to a ground-glass screen through separate Polaroid films oriented perpendicularly; the screen is viewed through spectacles provided with appropriately oriented Polaroid films for each eye.

Motion of one lens with respect to the other is provided by springmounting one lens between rollers attached to arms which are connected to a worm-gear to form a type of "pincers", as shown in fig. 5. When the gear at the side is driven, the "pincers" clamp down on the rollers to move the lens horizontally against the tension of the springs. The entire lens assembly is moved in the vertical direction by a separate worm gear; both motions are selsyn-controlled by the observer, who can thereby bring the front-glass fiducial plane, the back-glass plane, or any parallel plane in the chamber into direct superposition, to serve as his reference for 3-D viewing.

The motor-driven film advance system is also controlled by a set of selsyn motors. When the film-advance switch is opened, a solenoid valve permits a vacuum pump to evacuate pump-out grooves behind the film, clamping it in projection position; closing this switch shuts off the vacuum valve and opens the film grooves to a flow of compressed air which serves to free the moving film and prevent the scratching of the soft emulsion surface.

Observers were readily trained to identify events of interest from the spatial orientation of the electron-pair tracks and the primary interaction, as confirmed by subsequent detailed measurements on each separate stereo view. In principle, rough stereoscopic measurements could be made directly with such a projector, by fixing the position of the viewing spectacles and using 3-D parallax techniques; the precision of such measurements are, however, apt to be poor.

CLEAR INSTRUMENTS AND METHODS 14 (1961) 41–47; NORTH-HOLLAND PUBLISHING CO.

DAS RAUMWINKELFILTER, EIN BLENDENSYSTEM ZUR MESSUNG GELADENER TEILCHEN AUS KERNREAKTIONEN

B. CONRAD

I. *Institut f. Experimentalphysik, Hamburg*

Eingegangen am 16. August 1961

method is described to eliminate geometrical errors in asurements of heavy charged particles from nuclear reacns. A constant geometry is given by using a mechanical er, mounted between the target and the detector. With this angement even a three-dimensional target with non-uniform intensity distribution varying in time can be regarded as a point-source in the centre of the target-chamber. The method is well suited for the investigation of angular distributions. In a measurement of the $Li^7(p, \alpha)\alpha$-reaction a geometrical accuracy of 0.1 % was obtained.

Einleitung

Bei allen quantitativen Messungen der Kernysik kommt der Geometrie der Versuchsanordng entscheidende Bedeutung zu. Die Genauigkeit cher Messungen hängt häufig davon ab, ob die n geometrischen Bedingungen hinreiched genau lkulierbar und zeitlich konstant sind. Ein benders durchsichtiges Beispiel dafür sind Kernaktionen, die nur schwere geladene Teilchen einhließen. Hier gibt es Fälle, bei denen die Genauigit vorwiegend durch Geometriefehler begrenzt rd. Eine Verbesserung der Geometrie war bisher imlich nur auf Kosten der Intensität zu erreichen; r eine präzise Messung wird aber gerade eine hohe tensität benötigt, damit die Meßzeiten in erträgchen Grenzen bleiben. Die Suche nach einem Ausg aus diesen Schwierigkeiten war der Anlaß zur ntwicklung eines Blendensystems, basierend auf r geringen Reichweite schwerer geladener Teilen im Bereich kleiner bis mittlerer Energie, das n Folgenden unter der Bezeichnung "Raumnkelfilter" beschrieben wird.

Das Prinzip

Das Raumwinkelfilter besteht im einfachsten all aus einer planparallelen Platte mit Zylinderchern, einem Lochgitter, das vor dem Zähler ontiert wird. Abb. 1 zeigt als Beispiel eine Anordung mit einem Raumwinkelfilter, wie sie zur lessung von α-Teilchen verwendet wurde. Das Filter bewirkt, daß der Detektor von jedem Punkt des Targetbereiches aus unter dem gleichen Raumwinkel gesehen wird. Der Raumwinkel ist damit "stabilisiert" gegen Wanderungen des Ionenstrahles des Beschleunigers auf dem Target. Insbesonde-

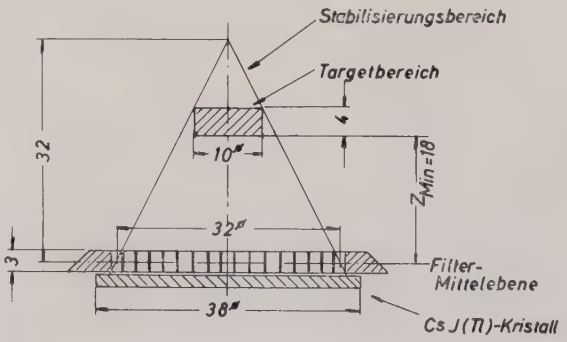

Fig. 1. Beispiel für die Dimensionierung von Targetbereich, Raumwinkelfilter und Zähler. Daten des Zylinderlochfilters: Lochdurchmesser $d = 1.5$ mm; Plattendicke $h = 3.0$ mm; Gitterkonstante $a = 1.8$ mm. Der Feinheitsgrad bei obiger Geometrie ist:

$$n = \frac{d}{h} \cdot Z_{\min} \cdot \frac{1}{a} = 5.$$

re ist die lästige Abstandsabhängigkeit aufgehoben; Abb. 2 zeigt hierzu eine Ausmessung des Filters der Abb. 1 mit einem Po-α-Präparat von 1 mm ϕ in einer Vacuum-Kammer.

Die herkömmlichen Maßnahmen zur Erzielung einer definierten, zeitlich konstanten Geometrie bestehen darin, daß der Ionenstrahl auf dem Target auf einen sehr schmalen Streifen fokussiert wird,

und daß der Detektor in einem relativ großen Abstand aufgestellt wird. Präzisionsmessungen sind aber trotzdem fast ausgeschlossen: soll die Messung eine Genauigkeit von 0.1% haben, und ist der Schwerpunkt der Reaktion auf dem Target in der Zählerrichtung um ± 1 mm unsicher, so müßte der Zählerabstand 2 m betragen. Ein Kristall mit

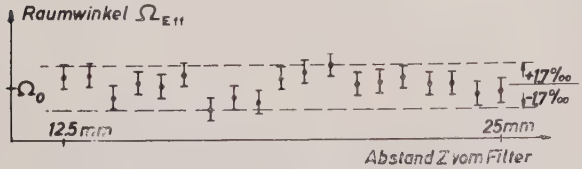

Fig. 2. Abhängigkeit des Raumwinkels Ω_{Eff} vom Abstand Z des „Targetpunktes" vom Filter. Der Abstand variiert im Verhältnis 1:2, trotzdem weicht der Raumwinkel um weniger als ± 1.7‰ vom Mittelwert Ω_0 ab. Ohne Filter würde der Raumwinkel zwischen 25 mm und 12.5 mm Abstand um 120% zunehmen.

einem Durchmesser von 1.5 Zoll würde dann einen Raumwinkel von nur 2.82×10^{-4} sterad erfassen. Die Anordnung der Abb. 1 erzielt mit dem gleichen Kristall einen Raumwinkel von 1.13×10^{-1} sterad, das ist der 400-fache Betrag. Mit Filtern anderer Dimensionierung läßt sich dieser Betrag noch einmal bis auf das Zehnfache steigern, das hier betrachtete Filter hat jedoch einen eingeschränkten Raumwinkelkegel zur Messung höherer Koeffizienten von Winkelverteilungen.

Eine Raumwinkelstabilisierung auf 0.1% ist natürlich nur sinnvoll, wenn der Wirkungsquerschnitt der Reaktion auch die gleiche statistische Genauigkeit erlaubt. Sehr häufig wird das nur durch sehr große Meßzeiten zu erreichen sein; der oben angeführte Intensitäts-Vergleich zeigt jedoch, das dies ohne eine besondere Raumwinkelstabilisierung fast niemals möglich ist. Dabei ist eine solche Meßgenauigkeit in vielen Fällen keineswegs übertrieben groß; bei Winkelverteilungsmessungen ist sie zur Trennung verschiedener Koeffizienten dringend erwünscht. Bei solchen Messungen wird häufig versucht, die Exzentrizität des Schwerpunktes der Reaktion durch "Rund-um-Messungen" auszugleichen; da die meisten Reaktionen jedoch nur *eine* Symmetrieebene haben, kann dadurch auch nur die Abweichung in *einer* Richtung kompensiert werden.

Die Wirkungsweise des Raumwinkelfilters läßt sich an einem Grenzfall einsehen: Das Filter der Abb. 1 sei ein infinitesimal feines Gitter (maßstäbliche Verkleinerung von Lochdurchmesser und Plattendicke). Dieses Gitter hat eine Durchlässigkeit, die nur vom Einfallswinkel α auf seine Oberfläche abhängt, und die oberhalb eines Grenzwinkels α_{max} verschwindet (Teilchenreichweite im Filtermaterial zunächst $= 0$ gesetzt). Bei nicht zu großem Abstand vom Filter (s.u.: "Stabilisierungsbereich") kann die registrierte Intensität also nicht von Lagebeziehungen abhängen. Der "effektive Raumwinkel" ist

$$\Omega_{Eff} = \int D(\alpha)\, d\Omega\,, \qquad (1$$

mit $D(\alpha)$ = Durchlässigkeit als Funktion des Einfallswinkels.

Auch eine andere Ausdrucksweise ist bequem. Das System Kristall-Filter hat ein Ansprechvermögen, das nur vom Winkel α zwischen der Bewegungsrichtung des Teilchens und dem Lot auf den Filter abhängt. Dies ist analog dem Ansprechvermögen eines Kristalls bei der Messung von γ-Quanten. Der wesentliche Unterschied ist, daß hier das Ansprechvermögen auf einen Kreis ganz innerhalb des Kristalles beschränkt ist, und daß dieser Kreis bei einer Bewegung des Targetpunktes "mitwandert". Jeder Punkt des Targets besitzt also seinen "eigenen" Zähler. Das hat zur Folge, daß auch ein räumlich ausgedehntes Target als punktförmig und ideal zentriert angesehen werden kann.

Die Geometrie der Versuchsanordnung ist somit nicht mehr eine Eigenschaft der Lagebeziehungen Target-Zähler, sondern ist eine Eigenschahft des Filters, und ist für einen bestimmten Filtertyp charakteristisch. Man darf daher vom "Raumwinkel eines Filters" oder "Ansprechvermögen eines Filters" (als Funktion des Einfallswinkels) sprechen. Durch diese konstanten Daten wird die numerische Behandlung, speziell von Winkelverteilungen, stark vereinfacht.

3. Übersicht über die möglichen Typen von Raumwinkelfiltern

Als Raumwinkelfilter kann jedes beliebige zweidimensionale Gitter dienen, dessen Durchlässigkeit oberhalb eines Einfallswinkels $\alpha < \frac{1}{2}\pi$ verschwindet. Ein besonders wichtiger Spezialfall sind die Zylinderlochfilter (Abb. 1) deshalb, weil das Ansprech

rmögen rotationssymmetrisch zum Lot ist. Im gemeinen Fall ist das Ansprechvermögen in zwei rschiedenen Richtungen unterschiedlich, die Aushnung des Raumwinkels läßt sich daher in diesen chtungen unterschiedlich dimensionieren; die hfachste Realisierung erfolgt durch zwei gekreuzlineare Gitter ("Schlitzfilter").

Das Filter braucht nicht vor dem Zähler fest zu gen; ein exzentrisch rotierendes, grobes Gitter t die gleichen Stabilisierungseigenschaften wie n sehr feines ortsfestes. Der Grenzfall ist die Begung nur einer einzelnen Elementarzelle gleichäßig über eine Ebene, z.B. eines Detektors mit ngförmigem Bleikollimator. Mit einem solchen ystem ist sogar die Stabilisierung bei der Messung on weicher γ-Strahlung möglich, die Genauigkeit ei zeitlich veränderlicher Quelle ist aber sehr benzt, da nicht genügend rasche Bewegungen erreicht werden können.

Geometrie der Zylinderlochfilter

(Voraussetzungen: 1. Teilchenreichweite im Filrmaterial = 0, keine Streuung. 2. Fehlerfreie itter)

RENZWINKEL

$$\operatorname{tg} \alpha_{\max} = d/h \,. \tag{2}$$

TABILISIERUNGSBEREICH

Das Target muß sich ganz innerhalb eines Kegels nit halbem Öffnungswinkel $\alpha_{\max}$ über dem Filter ls Basis befinden (Vergl. Abb. 1).

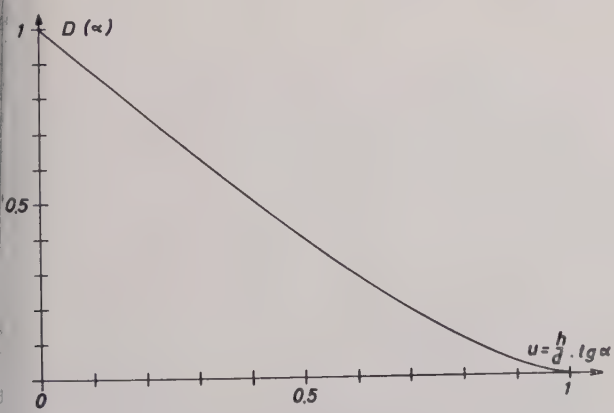

Fig. 3. Durchlässigkeit $D(\alpha)$ bei Zylinderlochfiltern. (Senkrechte Durchlässigkeit D (0) = 1 gesetzt.)

DURCHLÄSSIGKEIT (ANSPRECHVERMÖGEN) (Abb. 3)

$$D(\alpha) = D(0) \cdot \frac{2}{\pi} [\arccos u - u\sqrt{1-u^2}], \quad u = \frac{h}{d} \cdot \operatorname{tg} \alpha \,. \tag{3}$$

Hierbei ist $D(0)$ die senkrechte Durchlässigkeit (bestimmt durch das Loch-Steg-Verhältnis).

CHARAKTERISTISCHER RAUMWINKEL Ω_0

Bezeichnung für den Raumwinkel, den ein Filter im infinitesimalen Grenzfall haben würde. Für die verschiedenen Filtertypen ergeben sich folgende Beträge:

TABELLE 1

Größe des charakteristischen Raumwinkels bei verschiedenen Zylinderlochfiltern

$\operatorname{tg} \alpha_{\max} = d/h$	$\alpha_{\max}$	Charakter. Raumwinkel Ω_0
$\frac{1}{4}$	14.04°	$D(0) \cdot 0.0480$
$\frac{1}{2}$	26.56°	$D(0) \cdot 0.1801$
1	45°	$D(0) \cdot 0.5871$
2	63.43°	$D(0) \cdot 1.462$

Senkrechte Durchlässigkeit $D(0)$ z.B. 0.63.

EFFEKTIVER RAUMWINKEL Ω_{Eff}

Bei grober Gitterstruktur ist der Raumwinkel lokalen Schwankungen unterworfen. Der effektive Raumwinkel ist *im Mittel* jedoch stets gleich dem charakteristischen Raumwinkel. "Im Mittel" heißt: gemittelt über eine zum Filter parallele Fläche von der Größe einer Filter-Elementarzelle. Es existiert auch bei grober Gitterstruktur kein "systematischer" Gang des Raumwinkels mit dem Abstand (Vergl. Abb. 2).

FEINHEITSGRAD

$$n = \frac{d}{h} \cdot \frac{Z_{\min}}{a} \tag{4}$$

a = Gitterkonstante; $Z_{\min}$ ist der kleinste Abstand des Targetbereiches vom Filter. Der Feinheitsgrad bestimmt die maximale Größe der Raumwinkelschwankungen im Targetbereich.

Zahlenbeispiel: Die in Abb. 1 gezeigte Anordnung hat einen Feinheitsgrad $n = 5$.

MAXIMALE SCHWANKUNG

Als obere Schranke für die Schwankung wurde eine Abschätzung gewonnen:

$$\left|\frac{\Omega_{\text{Eff}} - \Omega_0}{\Omega_0}\right| < 0.19n^{-3} \begin{cases} + 0.49n^{-\frac{5}{2}} \text{ (grobe Gitterteilung)} \\ + 0.21n^{-\frac{5}{2}} \text{ (Grenzfall } n \to \infty) \end{cases} \quad (5)$$

(gültig für unbewegte Filter mit Grenzwinkeln bis zu 27°, bis zu Grenzwinkeln von 64° höchstens das Doppelte).

MITTLERE SCHWANKUNG

Die maximale Schwankung bezieht sich auf die Abweichung "Punkt für Punkt". Da mit Raumwinkelfiltern große Targetbereiche verwendet werden können, kompensieren sich diese Abweichungen größtenteils wegen der Regelmäßigkeit der Gitterstruktur. Die mittlere Schwankung ist der Stabilisierungsfehler, der zu erwarten ist, wenn der Brennfleck des Ionenstrahles auf dem Target etwa die Größe einer Filter-Elementarzelle hat. Hierfür gilt eine Abschätzung:

$$\left|\frac{\Omega_{\text{Eff}} - \Omega_0}{\Omega_0}\right| \approx \begin{cases} 0.15n^{-3} \text{ (Grobe Gitterteilung)} \\ 0.11n^{-3} \text{ (Grenzfall } n \to \infty) \end{cases} \quad (6)$$

(gültig bis zu Grenzwinkeln von 27°, bis zu 64° höchstens das Doppelte).

TOTALER STABILISIERUNGSFEHLER

Bis zu Größenverhältnissen von Targetbrennfleck zu Filter-Elementarzelle wie 5:1 sollte sicherheitshalber die mittlere Schwankung als totaler Stabilisierungsfehler angenommen werden. Bei noch größeren Flächenunterschieden tritt jedoch bei jeder denkbaren Ungleichmäßigkeit von Ionenstrahl und Targetdicke weitgehende Kompensation auf, sodaß man für den Stabilisierungsfehler setzen darf

$$\Delta S \approx \sqrt{\frac{E}{F}} \cdot \left|\frac{\Omega_{\text{Eff}} - \Omega_0}{\Omega_0}\right| \quad (7)$$

E = Fläche der Filter-Flementarzelle

F = Fläche des Target-Brennflecks.

5. Zur Realisierung des Prinzips durch Zylinderlochfilter

HERSTELLUNGSTOLERANZEN

Die bei der Herstellung von Zylinderlochfiltern erforderliche Genauigkeit ist sehr unterschiedlich je nach dem d/h-Verhältnis und der Größe der Gitterkonstanten. Ein besonders kritischer Fehler ist die Plattendicke. Der Lochdurchmesser darf streuen, wenn sich dieser Fehler statistisch über die ganze Platte verteilt. Zahlenbeispiel für das Filter der Abb. 1 (Stabilisierung auf 0.1%): Planparallelität auf $\pm$ 1.5 μ.

Zufällige Streuung des Lochdurchmessers $\pm$ 15 μ.

REALER RAUMWINKEL

Der Raumwinkel wird durch die realen Teilcheneigenschaften vergrößert: Die auszublenden Teilchen werden nur unvollständig absorbiert. Sie laufen z.T. durch die Lochkanten ("Absorptionsraumwinkel") und werden z.T. aus den Lochwänden in den Kristall gestreut (der Anteil der gestreuten Teilchen einem "Streuraumwinkel" entsprechend). Die unvollständige Absorption in den Kanten stört die Stabilisierung nicht (Existenz eines Grenzwinkels), die Streuung nur wenig, da nur die große-Winkel-Streuung außerhalb des normalen Grenzwinkelkegels nicht der Stabilisierung unterliegt. Da die beiden Effekte jedoch energieabhängig sind und eine Verfälschung des Spektrums erzeugen, sollten sie möglichst klein gehalten werden.

Für Lochfilter mit $d/h = \frac{1}{2}$ ist das Verhältnis des Absorptionsraumwinkels zum "freien Raumwinkel":

$$\frac{\Omega_A}{\Omega_0} \approx 1.75 \frac{R_0}{d} \quad (8)$$

(R_0 = Reichweite der Teilchen im Filtermaterial).

Eine Verkleinerung des Absorptionsraumwinkels wird durch eine Abrundung der Lochkanten erzielt. Der obige Betrag läßt sich dadurch reduzieren auf:

$$\frac{\Omega_A}{\Omega_0} < \frac{R_0^2}{rd} \quad (9)$$

(r = Radius der Kanten-Abrundung).

Für α-Teilchen von 10 MeV wurde Ω_A/Ω_0 von 1.5×10^{-2} auf weniger als 2.5×10^{-3} verkleinert.

Während der Absorptionsraumwinkel sich durch Vergröberung der Gitterstruktur verkleinern läßt

obei durch Übergang zu rotierenden Filtern sich
. hinreichend kleiner Stabilisierungsfehler er-
ingen läßt), ist der Streuraumwinkel bei einem
stimmten Filtertyp (d/h-Verhältnis, Kantenab-
ndung) nur vom Filtermaterial abhängig. Ab-
nätzungen zeigen, daß der Streueraumwinkel mit
rringerung der Ordnungszahl stark abnimmt,
ährend sich der Absorptionsraumwinkel nur wenig
rgrößert; Filter für eine universelle Anwendung
llten daher aus einem Material von möglichst
edriger Ordnungszahl bestehen.

Messungen zur Abhängigkeit der Streuung von
r Art der verwendeten Teilchen liegen noch nicht
or. Der Streuraumwinkel ist bei α-Teilchen zwi-
hen 2.5 und 10 MeV kleiner als 0.25% des "freien
aumwinkels". (Filter aus Messing, $d/h = \frac{1}{2}$.)

Zur Messung von Winkelverteilungen mit Zylinderlochfiltern

Bei der Messung von Winkelverteilungen mit
wei mit Raumwinkelfiltern versehenen Detektoren
in Monitor, ein drehbarer "Hauptzähler") ist
afür zu sorgen, daß der Meßwinkel θ, nämlich der
Winkel zwischen dem Ionenstrahl und dem Lot auf
em Hauptfilter, hinreichend genau definiert ist.
st die Brennweite des Beschleunigers nicht genü-
end lang im Verhältnis zur Breite des Strahles,
ann ein kleiner Winkelfehler durch rechts-links-
ertauschung eliminiert werden, da bei Messungen
nit Filtern als Geometriefehler nur noch eine
Drehung der Winkelverteilung in Frage kommt.
Diese Korrektur ist bei zu breiten Aperturen wegen
er Möglichkeit zeitlicher Änderungen allerdings
nvollkommen.

UMRECHNUNG AUF PUNKTFÖRMIGEN ZÄHLER

Da große Raumwinkelkegel verwendet werden,
muß eine Verschmierung der Winkelverteilung be-
ücksichtigt werden. Hierbei kann auf Methoden
urückgegriffen werden, die bei der Messung von
γ–γ-Winkelkorrelationen üblich sind. Ein ausge-
lehnter γ-Zähler mit rotationssymmetrischen An-
prechvermögen mißt bei einer genau zentrierten
Punktquelle eine Winkelverteilung (nach Frankel[1])

$$< W(\theta) > = 1 + \sum g_\nu a_\nu P_\nu (\cos\theta) \qquad (10a)$$

anstelle der wirklichen Verteilung:

$$W(\theta) = 1 + \sum a_\nu P_\nu (\cos\theta) \,. \qquad (10b)$$

Die "Schwächungskonstanten" $g_\nu < 1$ hängen nur vom Ansprechvermögen ab.

Einem Raumwinkelfilter sind daher charakteristische Schwächungskonstanten zuzuordnen. Sie lauten:

$$g_\nu = \frac{\int_0^{\alpha_{max}} D(\alpha) \cdot P_\nu (\cos\alpha)\, \mathrm{d}\cos\alpha}{\int_0^{\alpha_{max}} D(\alpha)\, \mathrm{d}\cos\alpha} \,. \qquad (11)$$

Als Beispiel seien die Schwächungskonstanten eines Zylinderlochfilters mit $\alpha_{max} = 28°$ angegeben (abgerundete Lochkanten, die Art der Abrundung beeinflußt $D(\alpha)$ und somit g_ν etwas):

TABELLE 2

Schwächungskonstanten eines Zylinderlochfilters mit einem Grenzwinkel $\alpha_{max} = 28°$

$g_1 = 0.9692$	$g_4 = 0.7253$	$g_7 = 0.3863$
$g_2 = 0.9099$	$g_5 = 0.6134$	
$g_3 = 0.8265$	$g_6 = 0.4980$	

Aus diesen Daten ist ersichtlich, daß ein 28°-Filter noch gut zur Messung von Kugelfunktionen bis P_4 geeignet ist.

CHARAKTERISTISCHE POLYNOME VON ZYLINDERLOCHFILTERN

Bei der Messung von Kernreaktionen muß außerdem die Umrechnung vom Laborsystem auf das Schwerpunktsystem vorgenommen werden. Die verschmierte Verteilung *im Laborsystem* hat dann eine Form:

$$< W(\theta) > = \sum_\nu \sum_{k=0}^{\infty} c_{\nu k}(\theta_{\mathrm{Labor}})\, x^k\, a_\nu P_\nu \,. \qquad (12)$$

Hierbei ist x der bekannte Parameter

$$x = \frac{\text{Geschwindigkeit des Schwerpunktes}}{\text{Geschwindigkeit des beobachteten Teilch. i. Schwpsyst.}}$$

[1]) S. Frankel, Phys. Rev. **83** (1951) 673.

$a_\nu P_\nu$ sind wieder die Glieder der ursprünglichen "punktförmigen" Winkelverteilung im Schwerpunktsystem.

Die $c_{\nu k}$ hängen vom Beobachtungswinkel θ_{Labor} ab. Anstelle der Schwächungskonstanten g_ν ergeben sich also Reihen in x. Da bei Reaktionen mit geladenen Teilchen zumeist $x \ll 1$ ist, braucht man aber nur relativ kurze Polynome zu betrachten, die sich leicht bestimmen lassen. Da diese Polynome vom *Labor*winkel abhängen, der bei Messungen mit Filtern im voraus genau festgelegt werden kann, werden auch nur diskrete Sätze solcher Polynome benötigt, die dann für alle Winkelverteilungsmessungen gültig sind. Einem Zylinderlochfilter sind also charakteristische Polynome zuzuordnen, die die mit ihm im Laborsystem gemessene Winkelverteilung unmittelbar auf die ursprüngliche Verteilung im Schwerpunktsystem zurückführen.

7. Anwendung auf die Winkelverteilung der Reaktion Li^7 (p, α)α

Tabelle 3 und Abb. 4 zeigen Meßwerte für die Koeffizienten A und B der Verteilung

$$W(\theta) = 1 + A \cos^2 \theta + B \cos^4 \theta . \qquad (13)$$

Die Messungen wurden an einem Van de Graaff-

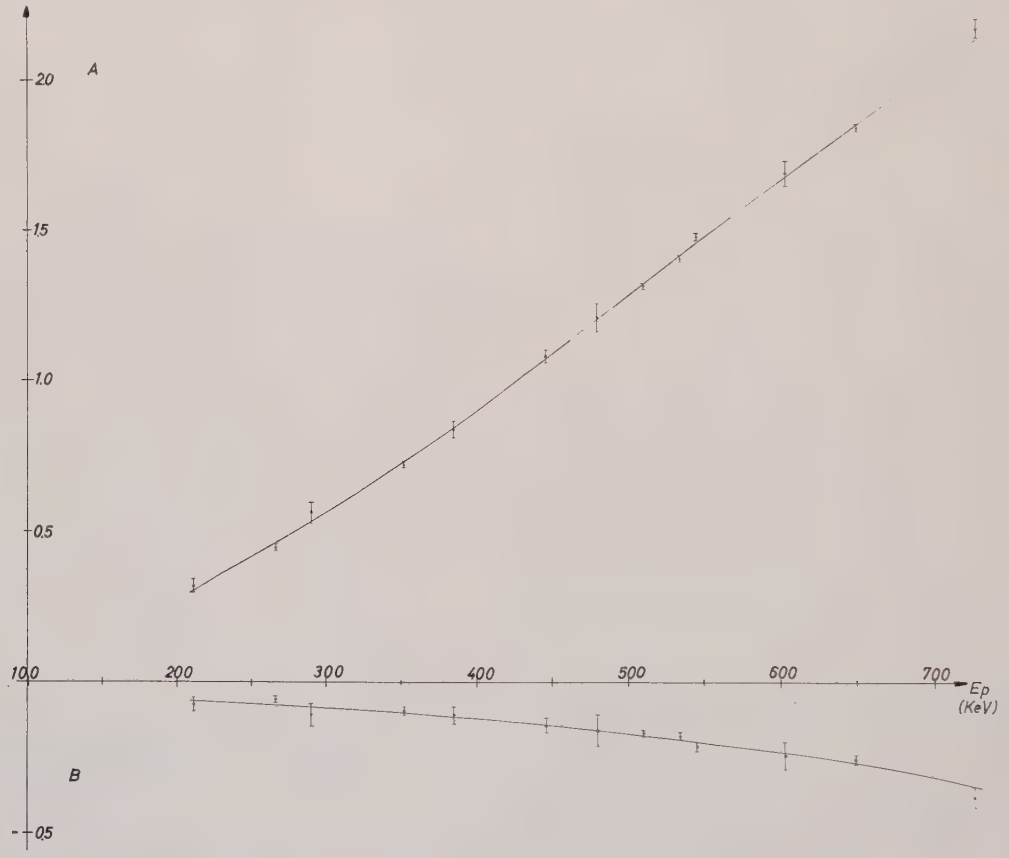

Fig. 4. Mit Raumwinkelfiltern gemessene Koeffizienten A, B der Winkelverteilung der Reaktion Li^7 (p,α) α.

Generator mit einer Targetkammer durchgeführt, die zwei mit Raumwinkelfiltern versehene Detektoren enthielt (Geometrie wie in Abb. 1). Die Winkelverteilung wurde zumeist jeweils aus einer 3-Punkte-Messung bei $\theta_{\text{Labor}} = 0°$, 45° und 90° errechnet. Als charakteristisch für die erreichte Genauigkeit können insbesondere die 3 Werte bei 510, 534 und 545 keV angesehen werden. Die Streuung ist nicht größer als dem statistischen Fehler von weniger als 0.1% für die einzelnen Winkel-Meßwerte entspricht, obwohl verschiedene apparative

Tabelle 3

Raumwinkelfiltern gemessene Koeffizienten der Winkelilung der Reaktion $Li^7(p, \alpha)\alpha$ und ihre mittleren Fehler.

onenergie keV)	$A \pm m_A$	$B \pm m_B$	Targetdicke (keV)
211	0.319 ± 0.022	— 0.073 ± 0.023	40
266	0.446 ± 0.013	— 0.056 ± 0.014	37
292	0.563 ± 0.035	— 0.107 ± 0.037	16
352	0.719 ± 0.011	— 0.092 ± 0.013	26
385	0.835 ± 0.027	— 0.106 ± 0.028	25
446	1.072 ± 0.021	— 0.141 ± 0.024	28
480	1.200 ± 0.049	— 0.156 ± 0.054	25
510	1.306 ± 0.010	— 0.166 ± 0.012	55
534	1.396 ± 0.011	— 0.174 ± 0.013	43
545	1.467 ± 0.013	— 0.210 ± 0.014	43
603	1.675 ± 0.042	— 0.238 ± 0.045	21
649	1.825 ± 0.014	— 0.252 ± 0.016	38
726	2.150 ± 0.031	— 0.372 ± 0.034	18

rameter variiert wurden, um etwaige systemahe Fehler durch eine Auffächerung sichtbar zu chen. Die Messung bei 510 keV wurde über die 4 Punkte $\theta_{\text{Labor}} = 0°$, 30°, 60° und 90° mit einer statistischen Genauigkeit von jeweils 0.07% durchgeführt; die Ausgleichung des Ansatzes (13) war ohne Überschreitung dieser Abweichung möglich.

Die hier erreichte Meßgenauigkeit ist besonders hinsichtlich der Bestimmung des Koeffizienten B von Bedeutung, dessen Betrag im Bereich kleiner Energien bisher nicht genügend genau ermittelt werden konnte[2,3,4]).

Mein besonderer Dank gilt Herrn Prof. Dr. H. Neuert für die Unterstützung bei der Durchführung dieser Arbeit. Der Deutschen Forschungsgemeinschaft und dem Bundesministerium für Atomkernenergie und Wasserwirtschaft danke ich für die Überlassung von Geräten.

[2]) L. H. Martin, J. Bower, D. Dunbar and F. Hirst, Nature **164** (1949) 310.

[3]) F. Talbott, A. Busola und G. Weiffenbach, Phys. Rev. **82** (1951) 1.

[4]) D. K. Cartwright, L. Green and J. Willmott, Phil. Mag. **44** (1953) 1307.

NUCLEAR INSTRUMENTS AND METHODS 14 (1961) 48–52; NORTH-HOLLAND PUBLISHING CO

STATISTICAL ERRORS ARISING FROM USE OF A GATED PULSE TRAIN FOR TOTAL LIVE TIME MEASUREMENT DURING PULSE AMPLITUDE ANALYSIS

M. O. DEIGHTON

Electronics Division, AERE, Harwell, Didcot, Berks., England

Received 25 August 1961

One of the major problems confronting the user of multi-channel pulse analysers, viz. correction of results for counts lost during the analyser dead time, can be overcome automatically by carrying out all counting runs for a known or measured total instrument "live time" rather than for real time as indicated, for example, by a stop-watch. This method avoids much tedious calculation and remains valid even if the analyser dead time varies widely from pulse to pulse.

The preferred method involves gating by the analyser of an accurately timed pulse train, which is then counted by a suitable external scaler. This article considers the statistical questions raised by such a sampling procedure and concludes that a fixed-frequency source at 50 pulses/sec would be satisfactory in most cases.

The use of a beam-current integrator, in conjunction with the "live time" gate, is also considered, since this probably offers the best method of dealing with source intensity fluctuations.

1. Introduction

When analysing a spectrum of random pulses with a multi-channel pulse height analyser, dead-time corrections may need to be applied to the counts recorded in each channel. These take the form

$$\frac{n_k}{n_{kr}} = \frac{1}{1 - n_r\tau} \qquad (1)$$

where

n_k = corrected mean rate in k^{th} channel
n_{kr} = recorded mean count rate in k^{th} channel
n_r = total recorded count rate for the entire analyser
τ = analyser dead time (assumed fixed).

Note that the correction to be applied to individual channel counts is the same percentage for all channels and consequently the errors do not constitute spectrum distorsion, but merely a change of the count rate scale. Nevertheless they often necessitate tedious calculations when the number of channels runs into hundreds. Perhaps the most obvious example is where a background spectrum has to be subtracted from another spectrum, in which case corrections may have to be applied to both before subtraction can legitimately take place.

One way of avoiding the necessity for such corrections is to run the count not for a known real time but rather for an aggregate live time of the analyser, which may be either predetermined or measured. That this automatically effects the desired correction can be seen by writing eq. (1) in the form

$$n_k = \frac{n_{kr}T}{T - n_r\tau T}. \qquad (2)$$

Here T is the total real time of a counting run, hence the denominator above is the difference between total time and dead time, i.e. total live time; the numerator is simply the total number of recorded pulses.

The problem is therefore how to measure such live time and, since accuracy is a prime consideration, the use of a gated timing pulse train of accurately known frequency would seem to be the best practical solution. The experimental assembly (ref.[1])) will be somewhat as sketched in the block diagram, equipment additional to the analyser comprising a source of regularly spaced timing or clock pulses of very short duration, a gate which may be operated by a suitable rectangular wave-form generated within the analyser during each dead period, at least one scaler and, if possible

[1]) C. N. Davey, A Timing Unit with Automatic Dead-time Correction, A.E.R.E. Memorandum to be published.

ns for controlling the analyser from the scaler put and vice versa. (It is to be noted that only re such ancillary equipment is available can one ctly justify the provision of automatic back- und subtraction facilities in the analyser itself.) he essence of this method of measuring live time hat the state of the analyser (i.e. dead or alive) ested by a clock pulse at regular but relatively equent intervals and the results compiled by

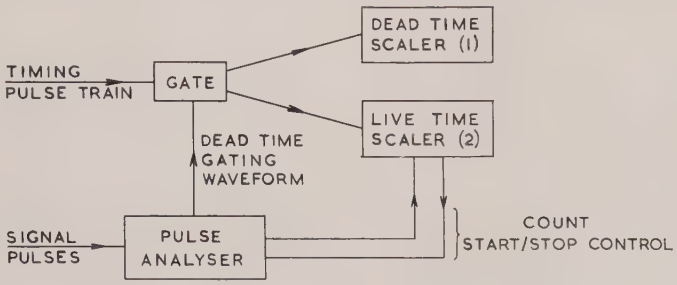

Fig. 1. Block diagram of assembly for measuring total live time of pulse analyser.

e scaler (or scalers). It is therefore a sampling chnique and, as such, subject to statistical in- curacies. Other things being equal, the relative certainty in the total live time measured in this y will decrease as the number of samples is in- eased, i.e. as the clock pulse rate is raised.

There is no significant advantage in increasing e clock rate beyond a certain point, however, nce the signal pulses themselves are random and us even a precisely timed counting experiment ll have statistical uncertainties in the various annel counts, these errors representing the maxi- um attainable accuracy for any given set of ex- rimental conditions. Use of an excessive clock ulse rate, then, while offering only slightly higher verall accuracy, certainly requires a larger count pacity in the live-time scaler and is therefore un- onomic. This remains true even if the primary urce of timing pulses is a high-frequency one .g. a quartz crystal), since one would then employ latively inexpensive fixed-frequency dividers, terposed between this time source and the gate, a preference to the more costly additional aperio- ic frequency dividers which would be needed for ounting gated time pulses.

The purpose of this note is to estimate the magni- ude of uncertainty due to the use of a low clock pulse rate and relate it to the uncertainty inherent even in an accurately timed count of random events. The two sources of random error are independent, so if the clock pulse rate n_c is chosen so that the two errors are of equal percentage, then the total r.m.s. fractional error in the final result will be $\sqrt{2}$ times as much as that due to either source alone. This criterion is employed to define a "minimum recommended clock pulse rate".

2. Statistical Considerations

Let T be the total time occupied by a counting run, of which a fraction p is dead time and a fraction q $(= 1 - p)$ is live time. n_c is the clock pulse rate (regular) and n_k is the mean *input* rate (random) to that analyser channel containing the highest counting rate in the spectral region of interest. Clearly the inherent statistical error is lowest and therefore the uncertainty in total live time as measured by clock pulses (which affects all channels equally) is of maximum importance relative to this peak channel

Two assumptions are made:

(i) that the clock pulse spacing is long compared with a single analyser paralysis period

(ii) that there is no fundamental periodicity in the analyser dead time itself; this restricts the present analysis to machines with random-access stores as opposed to those with recirculating stores (e.g. Hutchinson-Scarrott type).

The effect of these assumptions is that each clock pulse has a probability p of being counted in the dead-time scaler (No. 1 in the figure) and a probability q of being routed to the live-time scaler (No. 2), these probabilities being unaffected by the fate of any earlier pulses, supposing this were known. Consequently, the final distribution of ac-

cumulated counts between the two scalers follows the binomial law.

Thus total pulses counted in dead-time scaler $= pn_cT$ on the average, total pulses counted in live-time scaler $= qn_cT$ on the average, these values each being subject to an r.m.s. statistical error of amount $\sqrt{pqn_cT}$. The sum of the registered counts in both scalers is of course n_cT and is not subject to any statistical uncertainty†, except to the extent of 1 pulse.

Hence the r.m.s. fractional error in the total live time as thus measured is

$$\sigma_T = \pm \frac{\sqrt{pqn_cT}}{qn_cT} = \pm \sqrt{\frac{p}{qn_cT}}. \quad (3)$$

Also the mean total counts *recorded* in the channel located at the spectrum peak will be n_kqT, since qT is the effective mean counting time, hence the inherent r.m.s. statistical variation in this count, expressed as a fraction, will be

$$\sigma_c = \pm \sqrt{\frac{1}{n_kqT}}. \quad (4)$$

This equation, based on the Poisson distribution, is still true even when the analyser is operating at a very high loss rate, for although pulses accepted by the analyser are then nearly regular in real time, nevertheless they are still randomly distributed with respect to live time.

Imposing the condition

$$\sigma_T = \sigma_c,$$

we find $n_c = pn_k$. (5)

This is the result sought. Note that the required clock rate is independent of T, since both errors decrease together and inversely as $\sqrt{T}$. The result stated in eq. (5) may be expressed as follows: there should be, on the average, at least one clock pulse for every signal pulse lost from the peak channel.

Since p is itself roughly proportional to overall input pulse rate, when the losses are fairly small, it follows that the minimum requisite clock pulse rate varies approximately as the *square* of the analyser input rate, for a given spectrum shape. These results are illustrated by some typical figures calculated below.

3. Numerical Example

Let us assume a 100-channel analyser, having a fixed dead time of 250 μs. It is also assumed that the input spectrum has a main peak five times higher than the average level over the 100 channels, i.e. the input pulses to the peak channel are 5% of the total.

On this basis, the figures given in table 1 below have been calculated for four different overall input rates (n p.p.s.) to the analyser.

TABLE 1

Overal input rate to analyser n (in p.p.s.)	Fractional dead time (p)	Mean input rate to peak channel n_k (in p.p.s.)	Recorded rate in peak channel n_{kr} (in c.p.s.)	Minimum recommended clock pulse rate n_c (in p.p.s.)
500	0.11	25	22.2	2.78
1000	0.20	50	40	10
2000	0.33	100	67	33
4000	0.50	200	100	100

In each case p is calculated from

$$p = \frac{n\tau}{1 + n\tau}. \quad (6)$$

The figures in the last column show that, in all cases except the last (where the loss rate is 50%),

† The main purpose of the second scaler, if used, would be to keep an accurate check on the value of n_c.

k pulse rate of 50 pulses/sec should be adequate. e this is the frequency of the A.C. mains supply, convenient to postulate a source of 50 c/s fixed . and the figures in table 2 give data referring to case for the same four input rates as before, it g assumed in each case that the count is carried ntil the live-time scaler reaches 10000 counts for a total nominal live time of 200 seconds).

Table 2

rall input rate n (in p.p.s.)	Total time of counting run T (in sec)	Recorded counts in peak channel	R.m.s. count error σ_c (in %)	R.m.s. error in live time σ_T (in %)	Total r.m.s. error in measured count rate σ_{tot} (in %)
500	225	5000	1.4	0.33	1.45
1000	250	10000	1.0	0.45	1.1
2000	300	20000	0.7	0.58	0.9
4000	400	40000	0.5	0.71	0.87

igures in the fifth column are obtained from (3). It is to be noted that when $qn_cT = 10000$, is simply $\sqrt{p}\,\%$ and the timing error cannot eed 1%.

he final total fractional error or uncertainty, ' is obtained from

$$\sigma_{tot}^2 = \sigma_c^2 + \sigma_T^2 . \qquad (7)$$

It is seen that, even where the measured live time certainty is predominant, the total error in the ak channel is under $\pm$ 1% in the example chosen; other channels the normal statistical errors will ually predominate.

Modified System for Use with Fluctuating Sources

In many experiments the primary source of rticles responsible for signal pulses at the analyser put is a particle accelerator, the output beam rrent of which is subject to quite large fluctuaons during the course of a single experimental run. such instances and assuming the counting rate is w enough to avoid appreciable analyser deadne losses, it is usual to normalise the resulting cumulated channel counts with respect to inteated beam current (i.e. total beam charge). This tegration is performed over the duration of the experiment, the length of which is then only of secondary importance.

One form of beam current integrator that may be used consists of a Faraday cup suitably disposed in the particle beam and connected to an electronic circuit, wherein the collected beam current charges a capacitor C repetitively between defined voltage limits. Each time the capacitor voltage reaches the final limit it is rapidly discharged back to its starting potential and a pulse is simultaneously applied to an electromechanical register. This cycle of events is repeated many times during a counting run, so that, if ΔV is the difference between the capacitor voltage limits and N is the count showing on the register at the end of a run, then the total beam charge used is given by $NC\Delta V$. In a typical instrument[2]) the charge per count $C\Delta V$ may be varied to suit conditions by selecting one of a number of different capacitors, giving values in the range 10^{-9} to 10^{-5} coulomb; a meter is also provided for purposes of interpolation.

An instrument of this kind should be combined with the "live-time integrator" system described earlier, when accurately standardised amplitude spectrum measurements are to be made in the presence both of source intensity fluctuations and of high counting rates with their attendant losses in the analyser. Evidently one requires, for the standardisation of results, a measure of the beam current integrated with respect to time, but integrated only throughout the successive live periods of the analyser, since the beam is effective only during these intervals. This quantity, which may

[2]) E. A. Sayle, A Monitor for Simultaneous Measurement of Current and Total Charge in a Particle Accelerator Beam, (To be published).

be termed the effective integrated beam current, must be carefully distinguished from the product:

(total integrated beam current) × (overall fractional live time). One can readily verify by a few trial calculations that the two are in general different. To obtain the effective integrated beam current it is only necessary to divert the beam current integrator pulses, which normally operate the register, and apply them to the gate input, where previously a timing pulse train was used. The effective integrated beam current is then given by the product of $C\Delta V$ and the number of counts registered by the live-time scaler in the course of an experiment.

The accuracy of this result is subject to two conditions. In the first place, statistical considerations similar to those of Section 2 dictate that the mean pulse rate from the beam current integrator should exceed the mean rate of *loss* of input signal pulses from the analyser channel located at the spectrum peak. This condition ensures that the statistical uncertainty, which is introduced into the effective integrated beam current by this method of measurement, is less than the random errors inherent in the particular counting experiment. A proper choice of capacitor value in the beam current integrator will be needed to fulfil this condition. In the second place, it is assumed that the particle beam fluctuations are essentially slow in comparison with the beam current integrator pulse rate; if this is not the case results obtained in the manner suggested ma be quite misleading.

5. Conclusions

For experiments requiring about 1% accuracy where loss rates in the range 10–50% occur, th gated pulse train method is satisfactory using fixed p.r.f. of 50 p.p.s. and a live-time scaler ca pacity of 10^4 counts. Extended scaler capacity (c a lower clock pulse rate) will however be neede with low input pulse rates to the analyser whic demand longer counting runs.

Note that the essential statistics are the sam whether the count is terminated at some arbitrar time or controlled by the live-time scaler itself.

Finally, it should be observed that the results ob tained in Section 2 are not confined to the case of fixed analyser dead time (such as in the numerica example), but apply also when the dead time varie widely from one input pulse to another.

Acknowledgement

Acknowledgements are due to Mr. E. H. Cook Yarborough and Mr. K. Kandiah, who propose the experimental techniques outlined herein an drew the author's attention to the statistic problem involved. The author would also like t thank Mr. Cooke-Yarborough for many usef comments and criticisms made during preparatio of the manuscript.

NUCLEAR INSTRUMENTS AND METHODS 14 (1961) 53–62; NORTH-HOLLAND PUBLISHING CO.

A NETWORK ANALOGUE FOR A QUADRUPOLE LENS SYSTEM

C. F. COLEMAN

A.E.R.E., Harwell, Didcot, Berks., England

Received 25 August 1961

An analogue model for a system of quadrupole lenses is described. If such a lens system has two planes of symmetry through its axis the action of the system on displacements from the two planes is equivalent to that of two corresponding sets of cylindrical lenses. In the model these cylindrical lenses and the intervening distances are represented by successive parallel and series impedors in an A.C. network. From the model direct information can be obtained on those transformations of elliptical phase space boundaries which are used to describe the transport of particle beams through lens systems. It can be used to investigate the restrictions which slits within the system impose on the available phase space at the input, and leads to a particularly straightforward method for finding a system which will accept a beam with given characteristics and produce an output with waists at specified positions.

Introduction

In beam handling problems one has first to consider the trajectories of individual particles as they pass through the focusing system. If this system is made up of strong focusing quadrupole lenses it will usually have two perpendicular planes of symmetry passing through its axis. The displacement and divergence of a given trajectory from one of these planes at a given distance z along the axis are then related to the corresponding quantities at another distance z' by two homogeneous linear equations. If the displacement and divergence at z are x and p, at z', x' and p', and if the lens system can be represented for deviations from the chosen plane of symmetry by a series of flight paths of lengths $d_1 \ldots d_n$ followed by thin lenses of powers $P_1, \ldots P_{n-1}, 0$, all quantities being measured in consistent units, these equations are

$$\begin{pmatrix} x' \\ p' \end{pmatrix} = \prod_1^n \begin{pmatrix} 1 & 0 \\ -P_i & 1 \end{pmatrix} \begin{pmatrix} 1 & d_i \\ 0 & 1 \end{pmatrix} \begin{pmatrix} x \\ p \end{pmatrix}. \qquad (1)$$

An analogous set of equations holds for displacements from the other plane, and the two sets of displacements are independent. Electrical analogue networks will be described below which make use of the formal similarity between, on the one hand, the matrices describing the effects of a flight path and a thin lens on displacements and divergences, and on the other, those describing the effects of series and parallel impedances on voltages and currents.

In discussing the profile of a beam of particles passing through a strong focusing system Johnson[1]) showed that it was convenient to consider the structure of the beam in certain phase spaces. At a given axial position z these are the two dimensional space defined by the co-ordinates x and p, and a second similar space defined by the displacements and divergences of the trajectories from the other plane of symmetry. The boundary which encloses all points in the x, p phase space representing trajectories of particles contained in the beam transforms as one moves to different points along the axis in such a way that the area enclosed within it always remains constant. If the initial boundary is an ellipse with its centre at the origin of co-ordinates, then the transformed boundary will also be a centred ellipse, though its eccentricity and inclination to the co-ordinate axes will usually have altered. All beams "filling" a given boundary in the x, p phase space have the same profile when projected onto the plane of symmetry normal to that from which the displacements are measured. Over a flight path containing no lenses the profile of a beam which at any one axial position "fills" an elliptical phase space boundary is a hyperbola, and

[1]) K. Johnson, Injection Philosophy for Synchrotrons, CERN-PS/KJ (30th November, 1956).

the minimum of the hyperbola occurs at the axial position where the principal axes of the phase space ellipse coincide with the phase space co-ordinate axes. Such a beam is characterized by its "emittance" E, the area of the phase space ellipse, and by the "blow-up length" Γ, the axial distance from the position of the beam minimum (or "waist") at which the beam width has increased by a factor $\sqrt{2}$.

Beam handling problems, then, involve setting up a system which will take a beam having known parameters (emittances, waists, and blow-up lengths for deviations from both planes of symmetry) and will produce a beam having four assigned properties (waists and blow-up lengths) in the output drift space, where the beam may impinge on a target, or pass on into further equipment, such as the injection section of an accelerator. With a very simple lens system it is practicable to carry out hand calculations of the output beam parameters for a number of different combinations of lens powers and distances in order to get an overall picture of the way in which the system behaves, but such calculations become prohibitive if the system is at all complex. The information must then be obtained from calculations carried out on a digital computer, or a suitable analogue computer, or from measurements made on some analogous system. Montague[2]) has recently described the use of an analogue computer for this purpose, and has obtained results with an accuracy better than 5% for a two lens system. Heyford[3]) has proposed an analogue system using ideal transformers. It will be shown below that certain A.C. networks provide a very direct means of investigating beam handling problems. They are appreciably simpler than Montague's analogue computer, and applied to a four lens system have given results with accuracies of the order of 10%. These errors can be reduced by correcting for losses in the inductive elements.

[2]) B. W. Montague, Phase Space Analogue Computer for Beam Matching Problems CERN 60-24 (25th May, 1960).

[3]) Heyford, private communication.

2. Demonstration of Analogy

2.1. TRAJECTORY TRANSFORMATIONS

Consider a network made up of alternate series and parallel elements and driven by a sinusoidal e.m.f. The voltages and currents at various points in the network will be denoted by symbols such as V and I, which represent complex quantities of the form of $a \exp(i\varepsilon) \exp(i\omega t)$, where ω is the pulsatance of the applied e.m.f. Suppose that all the impedors in the network have the same phase angle ϕ_0,

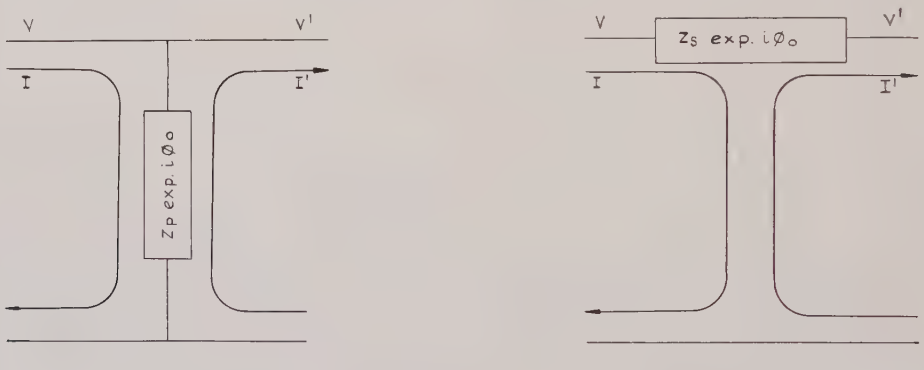

Fig. 1. Current and voltage relations for parallel and series impedances.

that they are all of the form $Z \exp(i\phi_0)$, where Z a real quantity. Then for a parallel impedor $Z_p \exp(i\phi_0)$ one has the equations (fig. 1a).

$$\left.\begin{aligned} V' \exp(-i\phi_0) &= V \exp(-i\phi_0) \\ \text{and} \qquad I' &= Z_p^{-1} V \exp(-i\phi_0) + I \end{aligned}\right\} \quad (2$$

and for a series impedor $Z_s \exp(i\phi_0)$ (fig. 1b)

$$\left.\begin{aligned} V' &= V + Z_s \exp(i\phi_0)\, I \\ \text{or} \qquad V' \exp(-i\phi_0) &= V \exp(-i\phi_0) + Z_s I \\ \text{and} \qquad I' &= I\,. \end{aligned}\right\} \quad (3$$

The parameters x, p and x', p' of a particular trajectory before and after passage through a thin cylindrical lens of diverging power P satisfy the relations

$$\left.\begin{aligned} x' &= x \\ p' &= Px + p \end{aligned}\right\} \qquad (2b)$$

while the corresponding parameters at the beginning and end of a flight path of length d satisfy the equations

$$\left.\begin{aligned} x' &= x + dp \\ p' &= p \end{aligned}\right\} \qquad (3b)$$

Thus the equations relating the values of the electrical quantities $[V \exp(-i\phi_0), I]$ on the two sides of a parallel impedance $Z_p \exp(i\phi_0)$ have real coefficients, and are similar in form to those relating the values of the trajectory parameters (x, p) on the two sides of a thin lens of power Z_p^{-1}, while the equations relating the values of the corresponding electrical quantities on the two sides of a series impedance $Z_s \exp(i\phi_0)$ are similar in form to those relating the values of the trajectory parameters at the two ends of a lens-free flight path of length Z_s. To see how the trajectory parameters themselves are introduced we will consider two special cases.

$\phi_0 = 0$.

The network elements are all resistances. If a positive series resistance R is taken to represent a distance d along a flight path then a positive parallel resistance R' will represent a diverging lens of focal length $R'(d)R^{-1}$, and a negative parallel resistance $-R'$ a converging lens of the same focal length. For a trajectory with parameters x and p we can define the axial distance xp^{-1}. This will be represented by a resistance $xR(pd)^{-1} = R_I$ across the terminals corresponding to the input of the optical system, and will be negative if the trajectory is moving towards the plane of symmetry. If an e.m.f. V_0 applied to the terminals corresponding to the output of the optical system drives a current I_0 through the network, and produces a voltage V_I across the input terminating resistance, then the parameters x', p' of the trajectory on emergence from the optical system are given by $x \mid V_0 \mid / \mid V_I \mid$ and $\mid I_0 \mid / \mid I_I \mid$ or $\mid I_0 \mid Rx / \mid V_I \mid d$. It will be seen that provided frequency independent negative resistances can be obtained this analogy holds independently of the frequency of the driving e.m.f.

b. $\phi_0 = \frac{1}{2}\pi$.

The network elements in this case are all reactances. If we take a series capacitative reactance $(i\omega C)^{-1}$ to represent a flight path of length d then a parallel capacitative reactance $(i\omega C')^{-1}$ will represent a diverging lens of power $C'(dC)^{-1}$ and a parallel inductive reactance a converging lens. In this case an incoming trajectory with parameters x and p will be represented by terminating the input with a reactance $(i\omega C_I)^{-1}$, where

$$C_I = p\, dCx^{-1}.$$

The analogy proceeds as before, except that it holds only for one particular frequency, determined when the inductance to be equivalent to a given value of capacitance is chosen.

2.2. PHASE SPACE TRANSFORMATIONS

If x, p are the parameters of a particular trajectory at a given axial position, then the set of trajectories given by varying s in the relations

$$\left.\begin{aligned} p(s) &= p \exp(is) \\ x(s) &= ix \exp(i\psi) \exp(is) \\ &= ixp^{-1} \exp(i\psi)\, p(s) \end{aligned}\right\} \qquad (4)$$

is represented in phase space by a set of points which form the boundary of a centred ellipse of area $\pi xp \cos\psi$. The forms of the corresponding ellipses at different positions on the axis of the system can be found by following this set of trajectories through the system. The pair of complex quantities $p(s)$ and $x(s)$ can evidently be substituted into the basic matrix relations (1) in place of the pair of real quantities p and x, but whereas the latter represent a particular trajectory, the former represent a particular family of trajectories. They may be regarded as the parameters describing the beam which contains all trajectories falling within the boundary ellipse. It should be noted that this beam is defined only as far as the quantities x and p are concerned, and that no restriction has been

placed on displacements and deviations from the second plane of symmetry, which are independent of x and p. Using relations (4) the standard transformation formulae can easily be derived. Thus it can be shown that if the beam filling the given phase space ellipse diverges from a waist at a distance d back along the axis, and has an emittance E and a blow-up length Γ, then the beam parameters at the waist are

$$\left.\begin{aligned} p'(s) &= p(s) = \sqrt{\Gamma^{-1}E}\exp(is) \\ x'(s) &= i\sqrt{\Gamma E}\exp(is) \end{aligned}\right\} \quad (5)$$

since $p'(s)$ and $x'(s)$ must be in quadrature at the waist. One can then write

$$\left.\begin{aligned} x(s) &= i\Gamma\sec\psi\exp(i\psi)p(s) \\ &= i\sqrt{\Gamma^2+d^2}\exp(i\tan^{-1}d\Gamma^{-1})p(s) \\ &= i\sqrt{\Gamma^2+d^2}\exp(i\tan^{-1}d\Gamma^{-1})\Gamma^{-1}E\exp(is) \end{aligned}\right\} \quad (6)$$

which shows that along the length of the beam its width varies as $d\sqrt{1+\Gamma^2d^{-2}}$, while the angle ψ between the directions of $x(s)$ and $p(s)$ in the Argand diagram varies according to the equation $\tan\psi = d\Gamma^{-1}$. This angle therefore expresses the distance of the particular axial position from the beam waist in terms of the beam blow-up length. Passage through a system containing lenses as well as flight paths, and having a transformation matrix A from the input position z to the output position z'', results in beam parameters at the output of the form

$$\begin{aligned} p''(s) &= \exp(i\theta)p(s) \\ x''(s) &= i\Gamma''\exp(i\psi'')\sec\psi''p''(s)\,, \end{aligned}$$

where Γ'' is the beam blow-up length in the output drift space, and ψ'' defines the position of the output beam waist relative to z''. These quantities and θ, which essentially describes the amount by which the points representing individual trajectories have moved round on the boundary of the phase space ellipse, are given in terms of the parameters of the input beam and of the elements a_{ij} of A by the equations

$$\left.\begin{aligned} \tan\theta &= a_{21}\Gamma(a_{22}-a_{21}\Gamma\tan\psi)^{-1} \\ \tan\psi'' &= [\Gamma a_{21}a_{11}\sec\psi + (a_{22}a_{11} + \\ &\qquad + a_{21}a_{12})\tan\psi + \Gamma^{-1}a_{22}a_{12}] \\ \Gamma'' &= \Gamma(a_{22}^2 - 2a_{22}a_{21}\Gamma\tan\psi + \\ &\qquad + a_{21}^2\Gamma^2\sec^2\psi)^{-1}\,. \end{aligned}\right\} \quad (7)$$

Since the equations governing the transformation of the beam parameters $p(s)$ and $x(s)$ are identical with those (1) which govern the transformations of the trajectory parameters p and x, the analogy mentioned earlier also holds between $p(s)$ and $x(s)$ on the one hand and I and $V\exp(-i\phi_0)$ on the other, but whereas in the original analogy only the peak values of the electrical quantities were related to optical quantities, the parametric variable s now plays a role closely similar to that of the time t in the electrical equations. By suitably choosing the terminating conditions of the electrical network the values of the quantities $V\exp(-i\phi_0)$ and I occurring at the same instant of time can be made to represent a single trajectory, and the Lissajous figure of $V\exp(-i\phi_0)$ against I, suitably scaled, will then reproduce the elliptical boundary of the phase space diagram at the corresponding position in the optical system.

A linear relationship

$$x(s) = i\Gamma\sec\psi\exp(i\psi)\,p(s) \quad (8)$$

between the beam parameters at the input to the lens system defines a particular phase space ellipse at this point, except that the beam emittance remains undetermined. An equivalent relationship at the corresponding end of the electrical network can evidently be enforced by terminating the network with an impedance given by

$$z_T = i\Gamma\sec\psi\exp(i\psi)\,d_0^{-1}z_0 \quad (10)$$

where z_0 is the impedance $Z_0\exp(i\phi_0)$ corresponding to an axial distance d_0. In this analogy, in contrast to that which holds for the trajectory parameters x and p, the phase of z_T does not usually coincide with that of the impedances representing elements of the lens system proper. In fact, if a waist occurs at the optical input, we find for the corresponding value of z_T

$$z_T = i\Gamma\,d_0^{-1}z_0\,, \quad (11)$$

so that in this case the phase of z_T differs by $\frac{1}{2}\pi$ from that of those impedances which represent elements of the lens system, while its magnitude

responds to a length associated with the geo-try of the incoming beam, the blow-up length Γ. he beam waist occurs away from the input the responding z_T can be broken up into two nents in series. The first represents the beam w-up length, and has the value $i\Gamma d_0^{-1} z_0$, while second represents the distance from the waist to input position, and has the same phase as any er impedance representing a flight path, except t it may be negative, since the beam may be verging to a waist at a point beyond the input sition. Thus the physically distinct lengths as-iated with the lens system and with the geo-try of the particle beams are represented in this del by two sets of impedance operators whose ases differ by $\frac{1}{2}\pi$.

Suppose now that the electrical network is set up represent a particular lens system, that it is minated at the appropriate point by an impe-nce z_T which represents the phase-space charac-istics of a particular beam entering the system, d that a sinusoidal e.m.f. V'' applied to the net-rk at the point corresponding to the output of e optical system drives a current I'' into the net-rk. V and I, the corresponding e.m.f. across and rrent into the terminating impedance z_T, satisfy

$$V = z_T I \,.$$

If V'' and I'' are related to V and I by the uations

$$\left.\begin{aligned} I'' &= \lambda \exp(i\alpha) I \\ V'' &= \mu \exp(i\beta) V \end{aligned}\right\} \qquad (12)$$

en $$V'' = \mu\lambda^{-1} \exp i(\beta - \alpha) z_T I'' \,. \qquad (13)$$

If $p''(s)$ and $x''(s)$ are the parameters of the article beam on emergence from the given lens stem, then by following the two sets of equations rough one can see that the phase space ellipse for e emergent beam must be given by the equation

$$''(s) = i\Gamma\mu\lambda^{-1} \sec \Psi \exp i(-\alpha + \beta + \Psi) p''(s) \,. \qquad (14)$$

There will be a waist at the output of the lens stem if

$$-\alpha + \beta + \psi = 0 \qquad (15)$$

that is, if I' and $V' \exp(-i\phi_0)$ are in quadature at the driving point of the electrical network. We shall now consider systems corresponding to particular choice of ϕ_0.

a. $\phi_0 = 0$.

The elements representing the focal lengths of diverging and converging lenses are positive and negative resistances, while the blow-up length at an input waist is represented by a pure reactance, capacitative or inductive, so that the system now becomes frequency dependent. The phase difference between I and V coincides with that between $p(s)$ and $x(s)$. Such a system was proposed by Hereward at C.E.R.N. and built by Vosicki. It is stated in ref.[2]) that it was abandoned because the network becomes unstable when simulating conditions in which a waist occurs inside the lens system.

b. $\phi_0 = \frac{1}{2}\pi$.

The elements representing the focal lengths of diverging and converging lenses are capacitors and inductors, while the blow-up length at an input waist can always be represented by a positive resistance, so that negative resistances are not required. The phase difference between I and V differs by $\frac{1}{2}\pi$ from that between $p(s)$ and $x(s)$, so that a waist occurs at the output of the lens system if the network presents a purely resistive impedance to the driving e.m.f. An analogue network of this kind has been set up for a four lens system, and is described below.

3. Construction of Analogue Network

The analogue network with $\phi_0 = \frac{1}{2}\pi$ was chosen because it avoids the use of negative resistances. Reactances of the kind used to represent the series elements are also needed for about half the parallel elements. Since capacitors with a range of 50 → 1500 pF, good setting accuracy, and low losses were immediately available, but inductors with a comparable performance were not, the former were used to represent the series elements. To restrict stray capacitances to positions where their effects could be calculated, each series element was totally enclosed in a separate cell of a large aluminium shielding box. Thus the only significant strays were

those from each of the two conductors to the shield. By further arranging that in each capacitor one conductor almost completely enclosed the other, the stray capacitance from the inner conductor to the shield was limited to about 3 pF, while the corresponding stray capacitance from the outer conductor was about 30 pF. Within the network these strays could be lumped in with the parallel elements, a process which could not be performed with the $\phi_0 = 0°$ analogue, since the latter has resistive shunt elements. The series elements at the ends of the network were arranged with the output commections to the inner conductors, so that the stray capacitance to the shield could be neglected.

Since suitable variable inductances were not available, units were made up for the purpose. The losses in these elements and mutual inductance effects account for most of the discrepances between results obtained from the analogue system and calculated values. Each inductance consists of an 800 turn coil $3\frac{1}{4}''\phi$ by $1\frac{1}{4}''$ long, made up from four 12 strand Litz wires (0.0028″ conductors) jumble wound together and connected in parallel. A ferrite rod $\frac{1}{2}'' \times \frac{1}{2}'' \times 4''$ is arranged so that it can be moved along the axis of the coil by means of a lead-screw, giving an inductance range from 20 to 70 millihenries with good setting accuracy. The Q of a coil with the core fully out is about 250 on the bench, but drops to about 120 when the coil is mounted in a three sided shielding cell. By using thin multiply-slotted walls for the shielding cells the Q can be brought up to about 180. The Q of a coil so mounted falls to about 120 at the maximum inductance setting, in which the core is symmetrically placed with respect to the coil. Each inductance was calibrated in terms of equivalent capacitance at 33 kc/sec, the frequency of the driving e.m.f. This was done by measuring the parallel capacitance required to produce resonance at a series of settings of the lead screw. The purity of the driving waveform and the setting accuracy of the condensers were such that the resonant fall in the current flowing into the tuned circuit could be followed quite well at Q's as high as 300.

Fig. 2 is a block diagram of the network and its associated circuits, fig. 3 a circuit diagram of the electronic units. The driving e.m.f. was supplied from a Wien bridge oscillator at a level of 2 V. Occasional repetition of a single calibration point for one of the inductances showed that the oscillator frequency was constant to $\sim 0.1\%$, while the purity of the waveform was such that, even when the Lissajous figures became straight lines, no distortion of their shape was apparent. The output from the oscillator is fed through a two way switch either to the network or to a variable resistor mounted on it. The network shield forms the "effective earth" for the elements of the network. This shield is connected to the other end of the variable resistor, and both are returned to the amplifier earth through the primary of a small transformer. The output from the secondary is used to measure the current through the system. At the operating frequency the effective impedance presented by the transformer primary is about 60 Ω which is small compared with typical network impedances of 5 kΩ. The output from the transformer is amplified and fed to the Y plates of an oscilloscope, while the network input voltage is amplified and fed to the X plates. Both amplifiers contain simple capacitative phase shifters with ranges of about 30°, so that the Lissajous figure obtained from the resistor can be displayed as a straight line. When the value of the resistance is changed by a large amount some compensating adjustment of the phase controls is needed, especially if the setting of the oscilloscope amplifiers is altered. Noise on the trace was never troublesome, but the hum superimposed on the current signal was sufficient to blur the zero-phase setting somewhat at the highest values reached by the input impedance ($\sim$ 500 kΩ).

4. Use of Analogue Network

4.1. APPLICATION TO WAIST PROBLEMS

The application of the analogy can most easily be illustrated by showing how it would be used to solve a particular problem. Suppose that a beam has to be transported between two fixed positions, that the beam at the initial position has waists with respect to two perpendicular planes of symmetry, and that the two corresponding blow-up lengths are specified. The problem is to arrange the lens system so that the beam converges to waists with respect

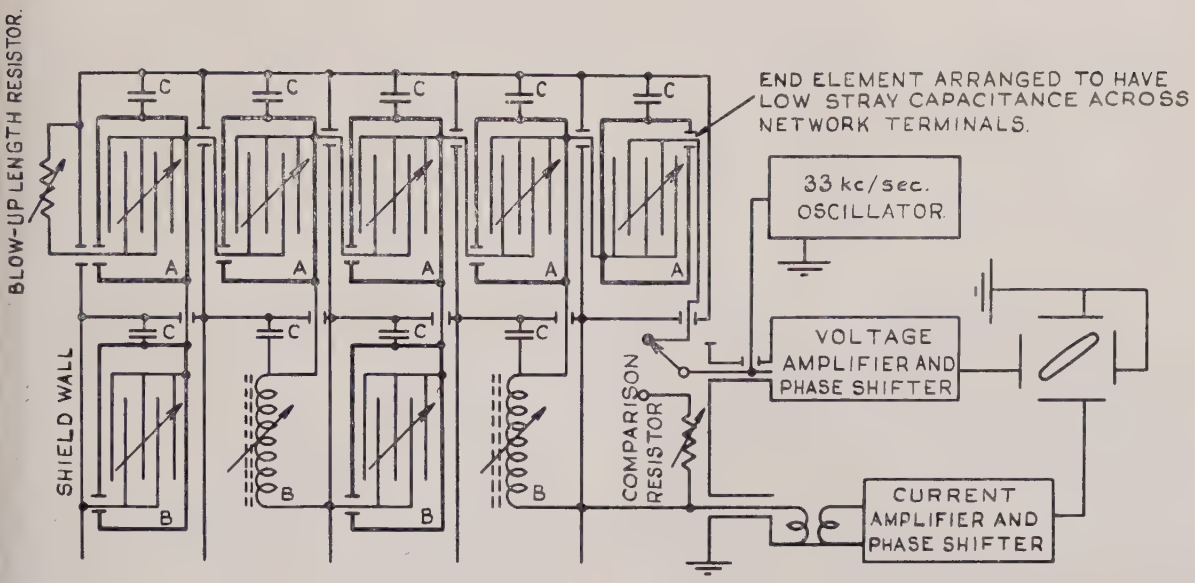
BLOW-UP LENGTH RESISTOR.
END ELEMENT ARRANGED TO HAVE LOW STRAY CAPACITANCE ACROSS NETWORK TERMINALS.
33 kc/sec. OSCILLATOR
VOLTAGE AMPLIFIER AND PHASE SHIFTER
CURRENT AMPLIFIER AND PHASE SHIFTER
COMPARISON RESISTOR
SHIELD WALL
A — ELEMENTS REPRESENTING INTERLENS DISTANCES
B — ELEMENTS REPRESENTING LENSES
C — STRAY CAPACITANCES

Fig. 2. Block diagram of lens system analogue.

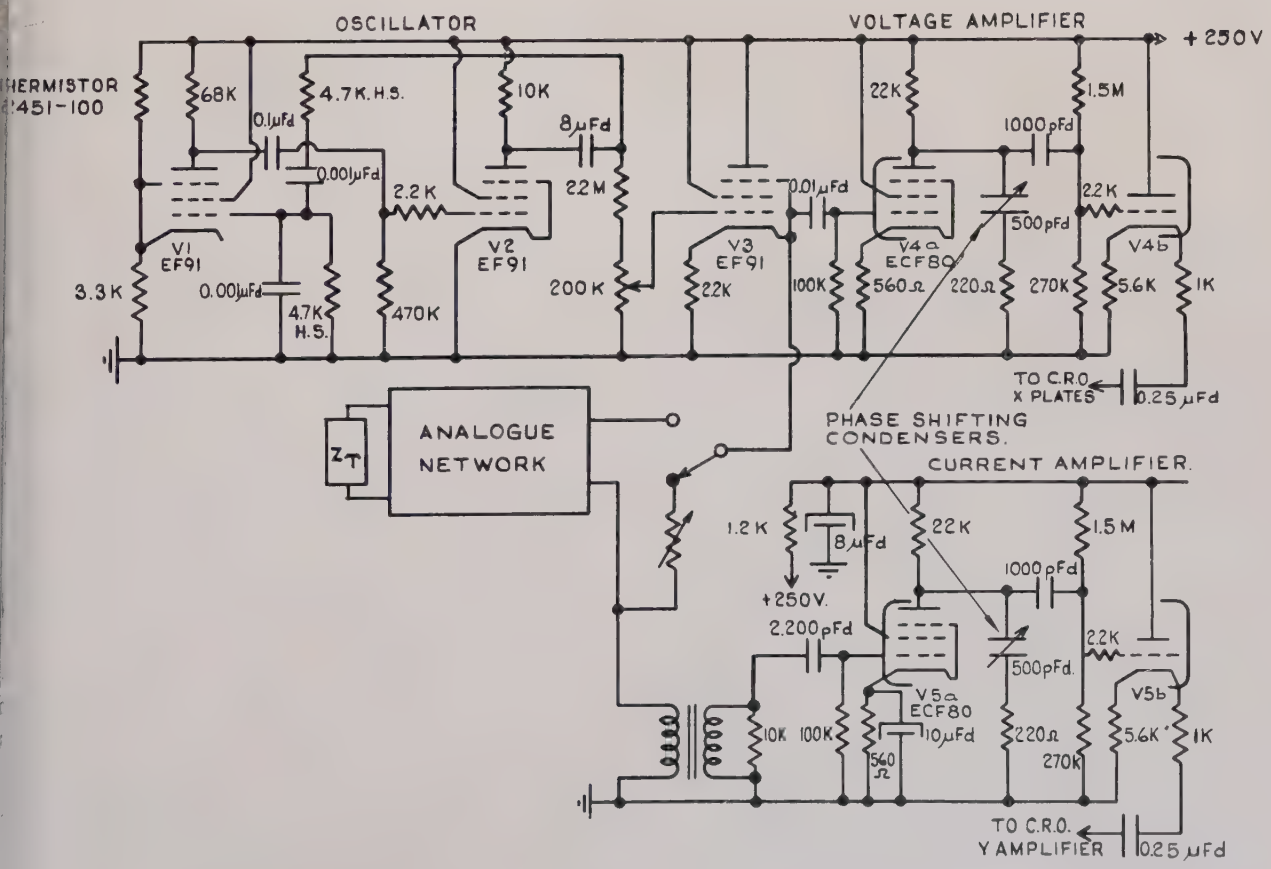

Fig. 3. Circuit diagrams of oscillator, phase shifters, and amplifiers.

to both planes of symmetry at the final position, and to determine the corresponding blow-up lengths at this point. Once a particular order for the focusing and defocusing lenses has been chosen, the analogue network can be set up. The value of the terminating resistance must be chosen to represent one of the given blow-up lengths, but all the other network elements save two, say P_1 and P_2, can be set to any convenient values. With the driving e.m.f. switched to the comparison resistor the phase controls are set to produce a straight line Lissajous figure. The drive is switched to the network, P_1 is set to its lowest value, and P_2 is adjusted till the Lissajous figure becomes a straight line. The input impedance and thus the blow-up length are then found by adjusting the comparison resistance to give a line of the same slope. This procedure is repeated for a series of values of P_1 spanning the required range of this variable (the inductors described have a range of variation of only 3:1), and a curve of P_1 against P_2 is drawn up, labelled at intervals with the corresponding values of the blow-up length. Such a curve (see fig. 4) may have several branches, and there may also be ranges of each variable in which no corresponding values of the other can be found.

It has been assumed that P_1 and P_2 represent lenses or distances, but they may be required to represent two element components such as a doublet or a lens position, variation of which changes the separation of the lens from both of its neighbours. Such a component may be treated as a variable if the two elements are always varied stepwise by corresponding amounts. P_1 is in any case changed stepwise, but P_2 is normally varied continuously till a straight line Lissajous figure is obtained. If P_2 is to be varied stepwise it becomes necessary to measure the phase of the input impedance at each setting, and to determine the correct setting by interpolation, but this is a comparatively time-consuming procedure. It should be noted here that the ratio of the diverging and converging powers of a quadrupole lens is a number greater than unity which depends on the length and power of the lens. For an ideal "hard-edged" quadrupole of nominal power P and length l the diverging and converging powers are given to the first order in lP by the expressions $\mp P\,(1 \pm lP/6)$. The separations of the principal planes to the same approximation are $(\pm l^2P/12)$.

Knowing the power ratio functions for the lenses to be used one can set up a network to represent deviations from the second plane of symmetry, in which P'_1 and P'_2 are the components which correspond to P_1 and P_2 in the original network. Sets of corresponding values of P'_1, P'_2, and the blow-up length are found, converted to equivalent values of P_1 and P_2, and plotted on the P_1P_2 diagram for the first plane of symmetry. The cut or cuts of the curves for the two planes, if they exist, give the values of P_1 and P_2 in the first plane which lead to a double waist at the output point, and the blow-up lengths in the two planes can be read off by interpolation. Fig. 4 shows a set of such curves obtained from the analogue computer, together with corresponding curves obtained by numerical calculation with a Mercury computer, and discrepancies $\sim 10\%$ in the powers obtained from the two sets are apparent. Fig. 5 shows sets of curves for a three lens system in which the effective inductor losses have been increased by the insertion of series resistors. It is clear that these losses can bring about considerable displacements of the curves. The displacement of any particular intersection arising from this cause may be found by measuring the Q's of the inductors at the intersection, halving each by the addition of a suitable series resistor, and with the modified components repeating the readings in the neighbourhood of the intersection. It is easy to show that to a first approximation the original intersection lies half-way between the new intersection and the one which would have been obtained if all the inductors had been ideal. The process must be repeated for each intersection because the equivalent series resistances representing the losses in the inductors vary considerably as the inductances are altered.

4.2. FINDING THE ACCEPTANCE CONDITIONS AT THE INPUT IMPOSED BY THE INTRODUCTION OF SLITS

The existing equipment has not been used for this purpose, but the application is quite straightforward. Since the model employs two independent networks for displacements from the two planes of

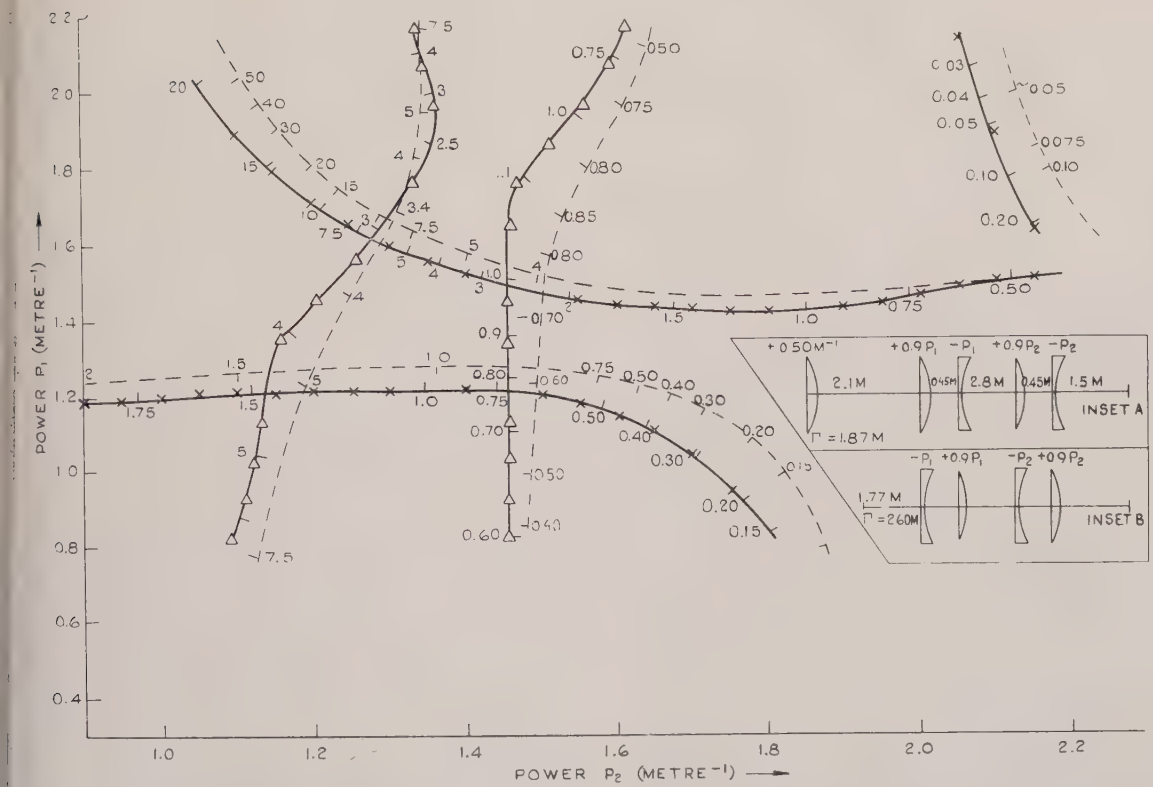

Fig. 4. P_1, P_2 curves obtained from the A.C. analogue and by computation. – – – computed curves. Δ—Δ analogue curves for plane "A". ×–× analogue curves for plane "B"

The curves are labelled with the corresponding values of the blow-up length in metres. Insets A and B show the effective cylindrical lens systems operating for deviations in plane A and plane B.

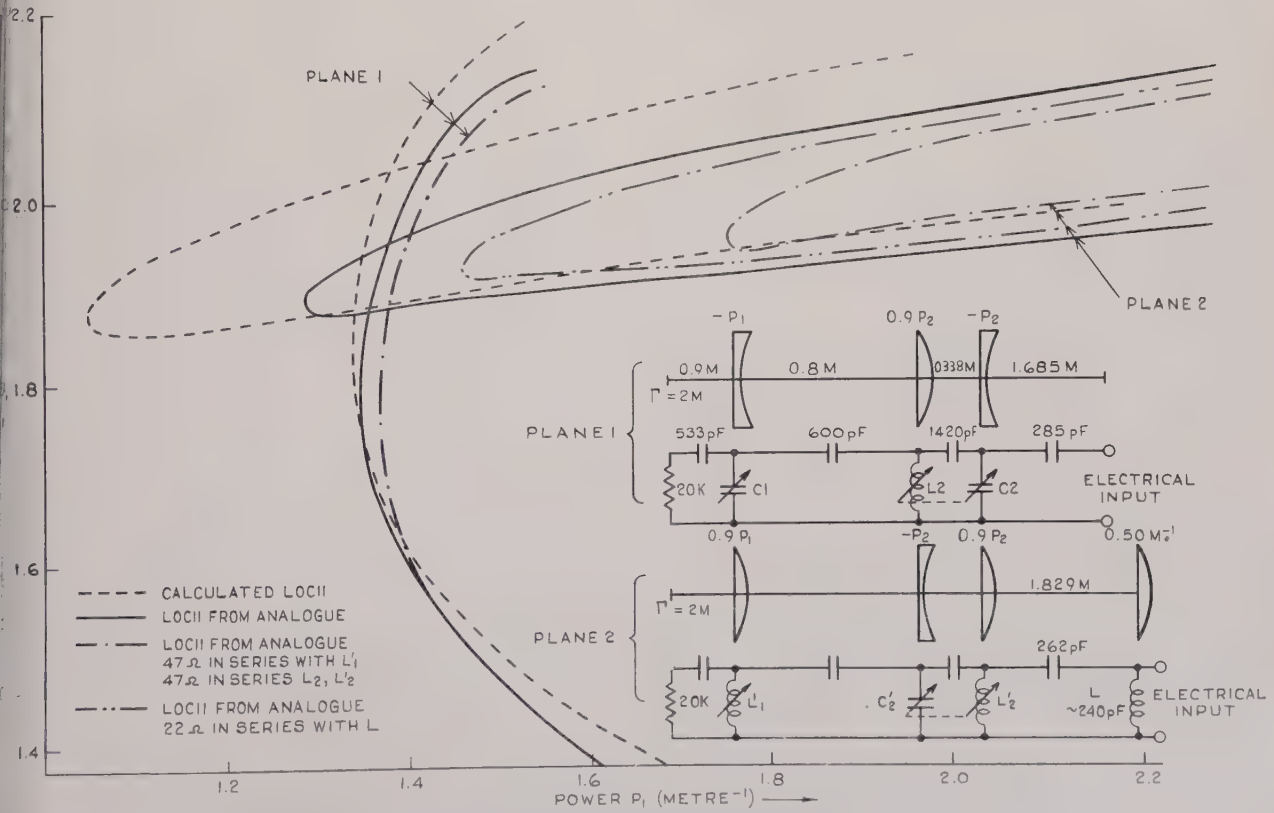

Fig. 5. P_1P_2 curves for a three lens system, showing the effect of inductor losses.

symmetry it can only be used to find the effect of slits whose jaws are parallel to one or other of these planes. The peak e.m.f. at any point in the network corresponds to the maximum displacement at the corresponding position in the lens system, but the effect of a slit in this position cannot be directly represented by the introduction into the electrical network of a biased diode, since the resulting waveform clipping introduces harmonics of the drive frequency, while the analogy holds for the fundamental frequency only. In principle however one can still use such diodes to explore the corresponding limiting contours in the input phase space. Terminating the network with a series of particular values of capacitance C_T selects particular straight lines through the origin of the phase space. For each selection the drive e.m.f. can be increased till clipping just begins to appear. The observed e.m.f. V_T across the terminating capacitance taken with the value C_T then defines a point on the limiting contour. It can however be shown that for a given slit this contour is just a straight line, and the parameters of this line can readily be determined without making use of non-linear elements. If x and p are the parameters of a particular trajectory at the input, while x' and p' are the parameters of the same trajectory at the position of the slit, then a relation of the form

$$x' = a_{11}x + a_{12}p \tag{16}$$

will hold between x', x, and p for all possible trajectories. If x' is limited to the value h by the slit edge the corresponding limiting contour in the input phase space is then

$$h = a_{11}x + a_{12}p\,. \tag{17}$$

For different values of h this represents a series of parallel straight lines, determined completely when a_{11} and a_{12} are known. In the A.C. analogue the equation corresponding to (16) is

$$\mathrm{i}V' = a_{11}\,\mathrm{i}V + a_{12}I\,. \tag{18}$$

By driving the network at the position of the slit, and taking the Lissajous figure of the driving e.m.f. V' when the output terminals are open circuited against the e.m.f. V_{0c} across the output one can obtain a_{11} from the relation

$$V'_{0c} = a_{11}V_{0c}\,. \tag{19}$$

Similarly a_{12} can be found from the relation

$$\mathrm{i}V'_{sc} = a_{12}I_{sc} \tag{20}$$

between the driving e.m.f. V'_{sc} when the output terminals are shortcircuited and the current I_{sc} between them. Thus the defining quantities of (17) can be directly determined. For such measurements the network shield would be earthed directly and a suitably low input impedance for the current measurement could be obtained by feeding into the emitter junction of an emitter follower.

5. Summary

The analogue system described above gives a simple and inexpensive method for investigating the action of lens systems, which may contain slits, on particle beams. Errors $\sim$ 10% in the determination of lens powers have been encountered, which arise from mutual inductance effects and especially from losses in the inductors. A first order correction for inductor losses is described.

LEAR INSTRUMENTS AND METHODS 14 (1961) 63–70; NORTH-HOLLAND PUBLISHING CO.

AN ARRAY OF SOLID STATE COUNTERS WITH DELAY LINE PULSE SORTING†

O. M. BILANIUK, B. B. MARSH, A. K. HAMANN and J. C. HEURTLEY

Department of Physics and Astronomy, University of Rochester, Rochester, New York

Received 14 August 1961

atrix of twenty 2 × 12 mm² surface barrier counters has constructed for use in the image plane of a magnetic trometer. The outputs of individual crystals are displayed predetermined channels of a 400-channel pulse height yzer. This is done by connecting separate crystals to successive sections of a delay line and converting the time difference between signals arriving at the ends of the line into pulse heights. Simple procedures for producing reliable Ge-Au surface barriers and contacts and certain properties of such counters are discussed. Samples of data decoded by this unit are presented.

ntroduction

Although the applicability of semiconductor ices for detection of ionizing radiation has been nted out some time ago[1]), a serious effort to velop and use surface barrier and surface junction nters has begun only recently[2]). The scintillator-otomultiplier combination is, at the time, still rivaled for detection of nuclear radiation of low cific ionization, but this is no longer true for avy nuclear fragments and for charged particles low energy. Perhaps the easiest solid-state detec- to make is the Au-Ge surface barrier counter. e effective depth of such a counter, prepared by aporation of gold onto an etched surface of n-type rmanium or silicon, is of the order of 50 microns. is insures the proportionality between the output lse and the particle energy, with an intrinsic solution better than 1%, to approximately 4 MeV deuterons and 12 MeV for alphas. In these nges, this detector supersedes the scintillation unter both in simplicity and in resolving power. rface junction counters, produced by diffusing osphorus into p-type silicon of high resistivity, ve an effective depth which is an order of magnide larger.[2]). Recent developments with ion ifted P-I-N junctions[3]) promise even larger fective depths.

The usefulness of solid state counters extends over a wider range still when they are used in conjunction with a magnetic spectrometer. This is particularly true for those solid state counters which have a restricted sensitive range but which are very easy to manufacture. Moreover, the use of thick junction counters with a magnetic spectrometer will permit simultaneous resolution both in momentum and in energy of the particles.

A particular application for which the surface barrier counters are well suited is their use in lieu of nuclear emulsions for nuclear spectroscopy. Past attempts to replace emulsions by arrays of scintillation crystals or proportional counters have not led to satisfactory results. In view of their compactness and simplicity of production, the surface barrier counters appear ideally suited for this purpose. The same arrangement is also applicable for direct registry of angular distributions.

† This work was performed under the auspices of the U.S. omic Energy Commission. An inchoate version of this system s been described in an unpublished report (see ref.[6])). The ain features of the present system were reported at the IAEA nference on Nuclear Electronics in Belgrade, Yugoslavia, 1961.

[1]) See "Bibliography on Semiconductor Nuclear Radiation Detectors" (72 references), compiled by J. L. Blankenship, ORNL–2583 (1958).

[2]) Proceedings of the National Meeting on Solid State Radiation Detectors, IRE Transactions on Nuclear Science, Vol. NS-8 (1961);

J. W. T. Dabbs and F. J. Walter, ed., Semiconductor Nuclear Particle Detectors (National Academy of Sciences Report 32, 1961).

[3]) Jacob Benveniste, Rex Booth and A. C. Mitchell, Observations on the Response of a Lithium-drifted Detector to Protons, UCRL Report 6441 (1961);

J. W. Mayer, N. A. Bailey and H. L. Dunlap, Characteristics of Ion Drifted P-I-N Junction Particle Detectors (IAEA Conference on Nuclear Electronics, 1961).

A straightforward way to implement this scheme is to provide each counter of such an array with a separate amplifier and register. Although this is quite feasible using transistorized circuitry[4]), it is apposite to investigate the possibility of reducing the number of amplification channels.

This paper deals with a scheme by which the information from a large number of counters is sorted by using a delay line[5]), a time to pulse height converter, and a multi-channel pulse height analyzer. An array of 20 counters has been built, tested, and used in nuclear reaction studies. The rudimentary version of this system has been described previously in an unpublished report[6]). Work is in progress on extending the array to include 40 and eventually 100 individual channels.

2. Surface Barrier Counters

Since in the present application the particle selection is done by the magnetic spectrometer, ease of manufacture rather than superior resolution and depth are desirable for the counters. While both silicon surface barrier and silicon surface junction counters have been successfully produced in this laboratory, counters chosen for use with the delay line were germanium surface barrier counters because of the simplicity of their production and their reliability over indefinite periods of time.

The detectors in question are made from 40 ohm-cm n-type monocrystalline germanium. The ohmic contact with the n-region is provided by simply soldering the crystal to a backing of Kovar. Kovar has been chosen because its thermal expansion coefficient is close to that of germanium; cracking of crystals upon cooling is thus avoided. The crystals are etched for about one minute in CP4 and washed with tap water. Gold is then evaporated onto the etched surface to a thickness of the order of 100 $\mu g/cm^2$. A mask is used to prevent gold deposits on the edges, which could lead to leakage currents.

Rather than make another ohmic contact with the surface gold layer, a non-ohmic contact is bonded through this layer into the germanium. This is done by spot welding a 0.002″ gold whisker onto the gold covered side of the germanium. Such bonding, accomplished by means of the apparatus shown in fig. 1, results in a clean and mechanically rugged (relatively speaking) rectifying weld between the n-type germanium and the gold wire, and at the same time provides the intended ohmic

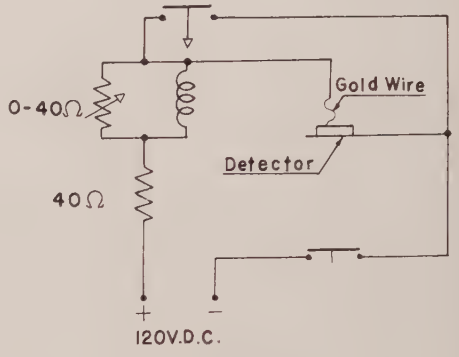

Fig. 1. Control circuit for bonding 0.002″ gold wire to n-type germanium. When the current through the whisker exceeds a value (approx. 2 A) predetermined by the setting of the variable resistor, the relay closes thus shunting the current away from the bond.

contact between the surface layer of gold and the whisker. It is primarily this simplicity of producing durable contacts which in this case outweighs the disadvantage of having to work at liquid nitrogen temperatures. (The Au-Ge counters produced by the simple procedure outlined above have been consistently found to work at room temperature also, but with a signal to noise ratio of only about 10:1, which is an order of magnitude poorer than at low temperatures.)

The counter bank was composed of individually mounted 2 × 12 mm^2 crystals. Multicounter units were also successfully prepared by evaporating gold onto a single piece of germanium or silicon through a grid. Diffused multicounter banks were prepared on a single p-type silicon crystal by using the Kodak metal etch resist (KMER process) for chemical milling of the counter mozaic. Individually mounted counters are preferred, however, because of the possibility of replacing defective units.

[4]) W. C. Parkinson and O. M. Bilaniuk, to be published in Rev. Sci. Instr.

[5]) The use of a delay line in this connection has been suggested independently by W. P. Alford and D. A. Bromley.

[6]) O. M. Bilaniuk and B. B. Marsh, Bull. Am. Phys. Soc. 5 (1960) 226;

O. M. Bilaniuk, A. K. Hamann and B. B. Marsh, A Multichannel Unit of Solid State Counters for Nuclear Spectroscopy, University of Rochester Report, NYO-9026 (1960).

was found that no bias was needed for the Au surface barrier counter to serve as a portional counter of alphas up to 6.5 MeV. If arity of pulse height with energy is not essen-

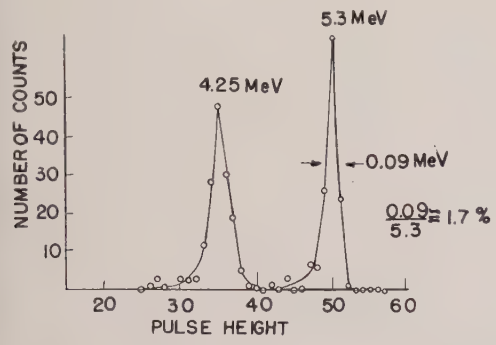

2. Resolution check for one of the counters of the array. 5.3 MeV alpha group comes from a thin Po^{210} source. up at 4.25 MeV is the same group after traversing 1.72 $/cm^2$ of aluminium absorber. The overall resolution is about %. Resolution appeared to be limited not by the counter lf but by the noise level of the conventional electronics used.

l, as in the present application where resolution accomplished by a magnetic spectrometer, one uld expect junction counters to be useful even thout the reverse bias. Thus in the initial tests th the delay line the bias was dispensed with for simplicity. However, the delay line loaded with unbiased detectors showed prohibitive attentuation. Attenuation was considerably reduced when the effective resistance of the counters was increased by reintroducing the reverse bias of a few volts.

Although no special effort was made to achieve high resolution in the counters as such, it was found that their resolution was not limited by themselves but by the noise level of the conventional electronics used, which was of the order of 1.5%. Fig. 2 shows the result of a resolution check on one of the counters of the array. The overall resolution was of the order of 1.7%.

3. Pulse Sorting

The block diagram in fig. 3 shows the components of circuitry used for sorting the information from the individual detectors. The actual electronic circuits are represented in fig. 4.

The detectors, prepared as described in Sec. 2, are all mounted with their n-regions cammon. The gold whiskers bonded onto the individual p-surfaces are connected to successive stages of a lumped delay line. In the original version[6]), the counters themselves constituted all the capacitors of the delay

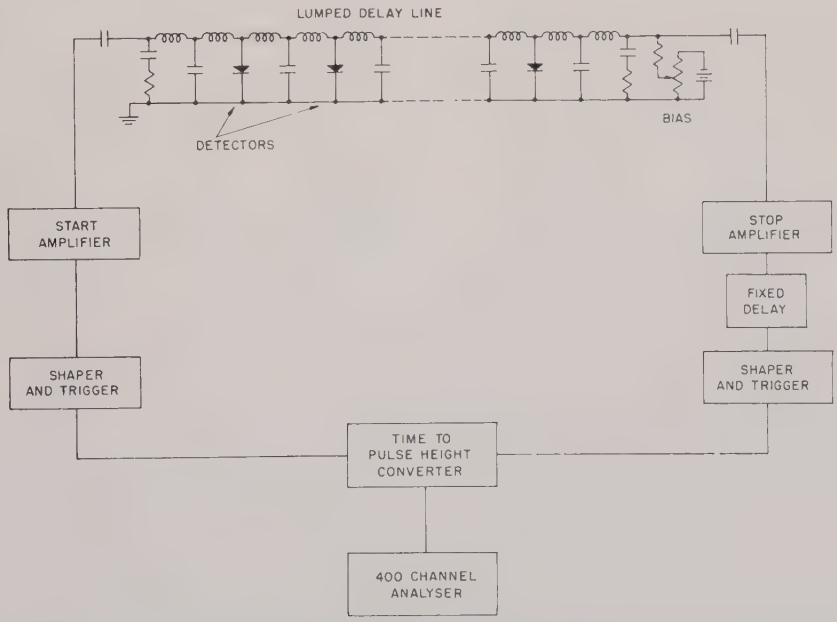

ig. 3. Detector loaded delay line with associated components. It was found that by alternating the detectors with the 60 μF apacitors of the delay line a better signal to noise ratio was obtained. Bias is provided by a battery inserted between the grounded n-bases and the delay line.

line. Better matching was obtained, however, when counters were connected so as to replace alternate capacitors of the line. An equal amount of reverse

ces, a 60 $\mu\mu$F capacitor and the counter. When an ionizing particle strikes a counter, the resulting pulse travels toward both ends of the lumped delay

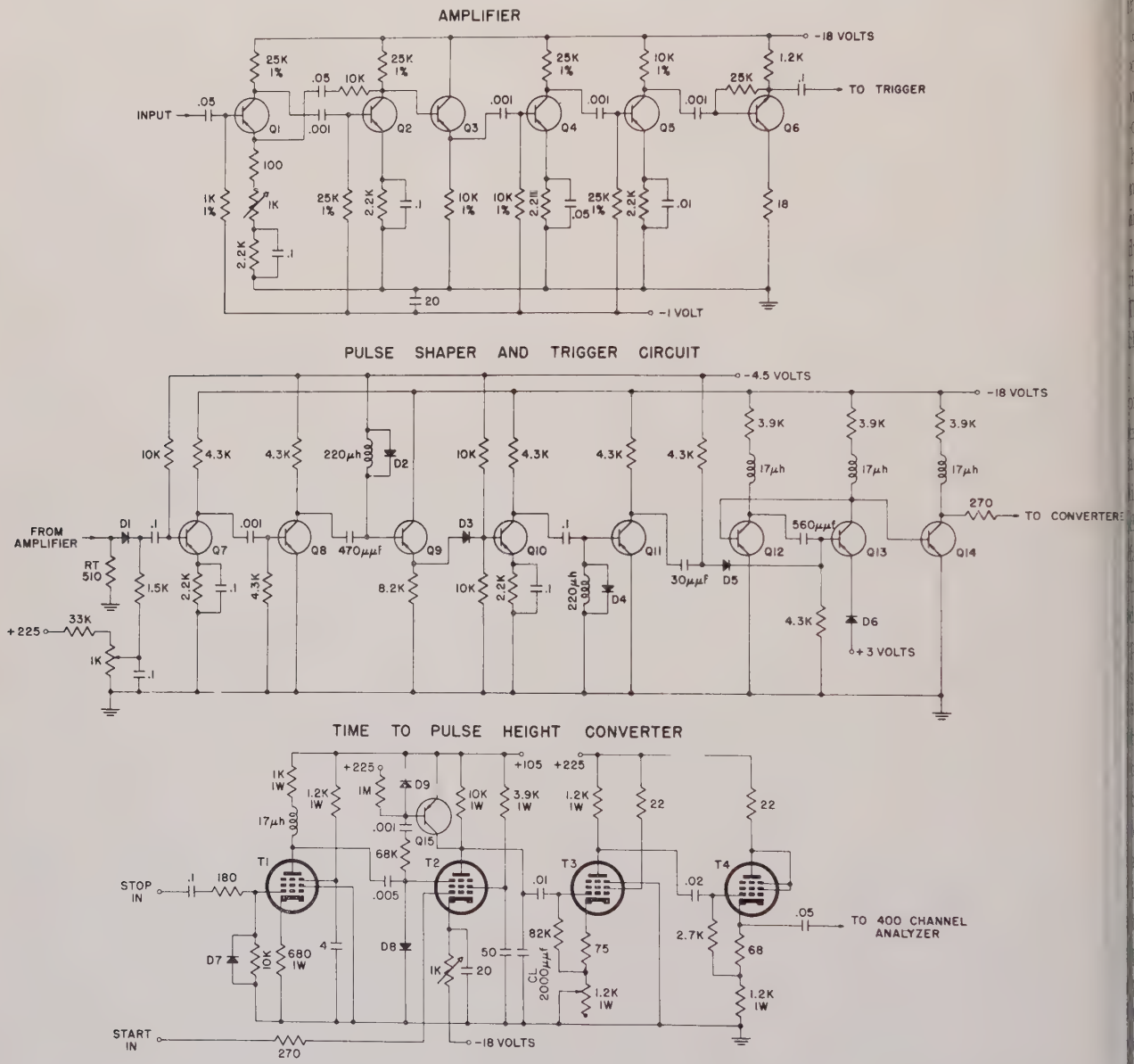

Fig. 4. Amplifier, shaper-trigger, and time-to-pulse-height converter circuitry of the present unit. Transistor Q6 is 2N364; all others are 2N502. All diodes are 1N100. Tube T1, which inverts the stop gate, is 6688. The tube T2, in which the actual time-to-pulse-height conversion takes place, is the 6BN6 beam tube. The inverter amplifier and the cathode follower tubes T3 and T4, are both 6CB6.

bias was applied to all counters by inserting a battery between the grounded n-bases and the delay line, as shown in fig. 3. Each lump of the delay line is thus made up of two 35 μH inductan-

line. Since each lump provides for a delay of $t = 2(LC)^{\frac{1}{2}} = 90$ mμsec, the time lapse between the arrival of this pulse at the two ends of the delay line differs by 180 mμsec for two adjacent counters.

The outputs of the far ends of the delay line are nected into transistor amplifiers with a gain of ut 3000, followed by identical shaping and ger circuits. The stop amplifier includes a fixed ay, slightly greater than the total delay of the nter loaded delay line, to ensure that the stop se always arrives at the time-to-pulse-height verter after the start pulse. The pulse arrives at start and stop gates at different times, deter- ned by the position of the counter on the delay e. The time-to-pulse-height converter then pro- ces a pulse whose height is proportional to the he difference between the start and stop pulses. e output of the converter is displayed on a 400 annel analyzer.

The most important consideration in the design the electronics is that of preserving the time rela- n between the leading edges of the pulses arriving the start and the stop ends of the tapped delay e. This is necessary if the counter resolution of e device is to be high. There are several major ctors which tend to defeat this purpose. First is e presence of noise. The signals at the ends of the lay line are of small magnitude (about 0.1 mV r MeV of energy loss) and noise distorts both their ape and amplitude. Second is the variation in ape of pulses appearing at the ends of the line cause of the frequency response characteristics the delay line. The output pulse originating in a unter near the end of the line has a much sharper ading edge and a slightly greater height than one ising from a counter near the center. This means effect that it is displaced in time slightly, if iggering of the gate generator takes place at some oint of constant amplitude for both shapes of ulses. This effect is pronounced but can be con- olled by using several sections of delay line at the ds as low-pass filters. A third effect is jitter oc- uring in the triggering of the gate generators. It as found that by controlling the shape and mplitude of the triggering pulses, this source of ncertainty was greatly reduced.

Transistors Q1 and Q2 constitute a low noise, edback amplifier in which the bandwidth is quite ndependent of the gain control. (It increases lightly as the closed loop gain is decreased.) It is een that in setting the gain control for lower overall gain by increasing the amount of closed loop feedback, one also decreases the open loop gain by increasing the emitter degeneration in the emitter of Q1. Thus the magnitude of the fedback voltage is quite constant. This form of voltage feedback, from the collector of Q2 to the emitter of Q1, raises the input impedance and lowers the output impedance of the amplifier. The bandwidth for this stage is fixed by the stray circuit wiring capacities and the unit has a rise time of 0.15 μsec. The low value of resistance in the base of Q1, together with the bypassed 2.2 kΩ emitter resistor, serve to stabilize the quiescent operating point of Q1. The purpose of other bypassed emitter resistors occuring in other stages is also for quiescent operating point stabilization. Both Q1 and Q2 are operated at low values of base and collector current for low noise operation.

The output of Q2 is directly coupled to the base of the emitter follower, Q3. This reduces the loading on the collector of Q2 which would occur if it were RC coupled directly to the base of Q4. The resulting pulse is again inverted and amplified in Q5 and passes to the emitter follower stage Q6 which serves as the cable driver. In the stop circuit, another emitter follower has been placed between Q4 and Q5, and the fixed delay inserted at this point.

Passing to the trigger circuit, the pulse proceeds through the diode discriminator D1 which removes the low level noise. The value of the resistor RT was experimentally chosen to present the best matching at the end of the coaxial cable. It is seen that the trigger shaper section is essentially a chain of over driven biased amplifiers, with shaping networks inserted at appropriate points. The purpose of this is to take incoming pulses which vary in shape and amplitude and convert them into pulses of constant shape and amplitude, thus ensuring reliable triggering of the gate generator. Using the pulses appearing at the collector of Q5 to trigger the sweep of a fast scope, it was observed that the time variation in the leading edge of the gate pulse at the collector of Q14 was generally less than 6 mμsec.

After passing through the discriminator, the pulse is amplified and inverted in Q7 which in turn drives Q8 into a region of high current conduction. The effective collector load of Q8 is the 220 μH peaking inductor shunted with a high conductance

diode OA5. This first stage of pulse shaping provides a pulse of relatively constant shape and amplitude. For pulses of interest, Q8 is generally driven to saturation and the peak waveform at the base of Q9 is + 4 V. Diode D3 and associated base circuit resistors of Q10 serve to clip off any negative undershoot occuring in the pulse. Q10 is another shaper inverter stage in which the collector load is another 220 μH coil and the high conductance diode D4, which is shunted with the base-to-emitter diode of Q11. Q11, which is normally off, is driven into a state of high conduction, and the resulting positive pulse occuring at the collector has an amplitude of about 17 V and a rise time of less than 20 mμsec. The pulse is differentiated by the 30 $\mu\mu$F coupling capacitor and 4.3 kΩ resistor, and passes through the iode D5 to the base of Q13. Diode D5 serves two functions. First, as it is reverse biased by nearly 7 V it acts as a clipper so that the differentiated pulse passed is of very short duration and has a very fast rise time. This is excellent for triggering the gate generator. Further, the diode acts as a disconnect element, removing the trigger source from the gate generator during the time it is in operation; it should be noted that the voltage at the base of Q13 goes positive during the time the gate is on.

The gate generator consists of transistors Q12, Q13 and Q14. The collector of Q13 is directly coupled to the base of both Q12 and Q14. Q13 is normally on, thus Q12 and Q14 are normally off. At the moment of triggering and while the gate is on, the base of Q13 is driven highly positive. Under this condition and without the diode D6, the base to emitter junction of Q13 breaks down, thus reducing the reliability of triggering and also making the time duration of the gate highly dependent of the state of the base to emitter junction of the transistor. When diode D6 is inserted it is reverse biased under these conditions and having a higher reverse voltage rating than the transistor junction, it passes little current. Therefore the time duration of the gate pulse is determined only by the biases and the coupling network between Q12 and Q13. The resulting gate pulse at the collector of Q14 has an amplitude of nearly 17 V, a rise time of 12 mμsec, and a fall time of less than 30 mμsec. In the start channel, the pulse goes directly to the first grid of the 6BN6 gated beam tube. In the stop channel the gate is first inverted in T1, which is a shunt compensated amplifier, and then RC coupled to the quadrature grid of T2. Diodes D7 and D8 serve to reduce the change in the quiescent operating point of either T1 or T2 resulting from any average DC bias appearing at the grids of either tube due to grid current or a high pulse counting rate.

The tube in which the actual time to pulse height conversion takes place, T2, is normally biased so that no plate current flows. With the appearance of the start pulse, plate current begins to flow and continues until the stop pulse appears. The change in voltage across CL is nearly proportional to the time during which T2 is passing plate current, since the time constant is large ($\sim$ 15 μsec) compared with the charging time. Transistor Q15, which is normally biased off by the voltage across D9, becomes highly conducting with the appearance of the stop pulse, thus recharging CL in less than 1 μsec. Without this recharging transistor, the counting rate would be limited by the longer recharge time.

Tubes T3 and T4 constitute respectively an inverter amplifier and a cathode follower; the output of the latter goes to the pulse height analyzer.

The choice of components was dictated by reasons of design considerations, availability, and cost. Transistors were used to avoid the problems of microphonics and hum. 2N502 transistors were readily available, they have fast switching times in the proper circuits and are quite uniform in their characteristics. Low noise resistors were used in the first stages of the amplifiers. Voltage supply filtering and decoupling between sections were conventional.

4. Performance of the Unit

The physical layout of the array of counters is shown in fig. 5. It will be noted that the counter base is attached to a cold trap which, in operation, is filled with liquid nitrogen. The signal leads are brought out of the vacuum via a hermetic multi-pin connector.

The above unit and the entire scheme of fig. 3 have been tested by means of a Po^{210} alpha source. A typical result obtained with the 5.3 MeV alphas

shown in fig. 6. Each peak consists of counts registered by an individual predetermined crystal. It will be noted that the decoding is complete. Each

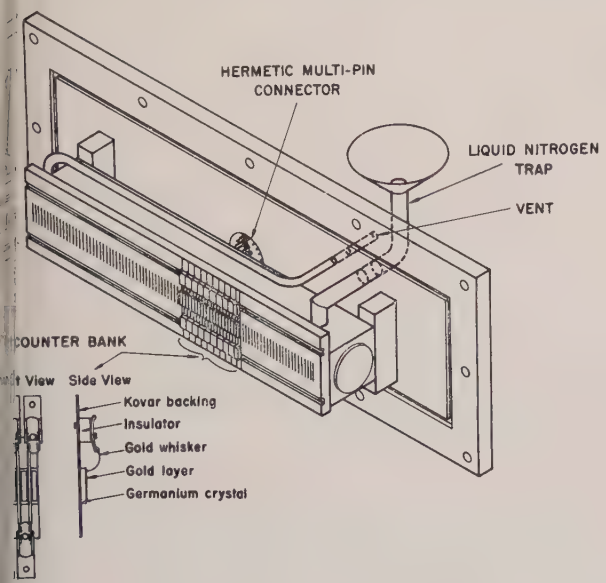

Fig. 5. Isometric view of the present 20-counter array. The counters are mounted on a liquid nitrogen trap. Space is provided for further extension of the array. For clarity, the signal leads connecting the gold whiskers to the hermetic multi-pin connector are not shown in the figure. Detailed front and side views of the counter structure and of their intermeshed arrangement are shown in the lower left hand corner of the figure.

group comprising the counts originating in a given counter is completely resolved from the neighboring groups. This resolution is not spoiled by the slight variation in delays between various sections of the delay line due to the slight variation in the capacitance of these sections.

Since the recovery of the solid state counters is very fast the dead time for the counting will be due entirely to the electronics part of the system. The delay line part of the circuitry is ready to count once every 10 μsec, thus the main limitation for the counting rate does not stem from the multichannel unit but from the 400-channel analyzer which has a dead time of some 200 μsec for every count.

Although the 20 counters of the present array span only 5 cm of the spectrometer image surface, the unit has already been found quite useful. It has been used in the calibration of the new broad range spectrometer at Rochester[7]). It has permitted a direct measurement of the dispersion and resolution of this spectrometer. It is very convenient for quick determination of the energy spread of the d, He^3, or He^4 beams from the Rochester 27″ variable energy cyclotron. The precision measurement of target thickness by beam energy loss can be carried out quite conveniently with this unit. Composition of the target can be determined very easily by observing the resolved groups of beam particles elastically scattered from the various target nuclides, as illustrated by the two lower spectra of fig. 7. The two groups in the upper spectrum of fig. 7 correspond to the ground state doublet of K^{38}, as seen by recording the alphas from the reaction $Ca^{40}(d, \alpha)K^{38}$ by the present 20-channel unit.

While extension to 40 and eventually to 100 channels is required before full use can be made of the potentialities of this unit, it has already been used to collect nuclear data. The angular distribu-

[7]) W. P. Alford, O. M. Bilaniuk and R. A. Hawrylak, Broad Range Nuclear Spectrometer for Use with the Rochester 27″ Cyclotron, University of Rochester Report, NYO-9683 (1961).

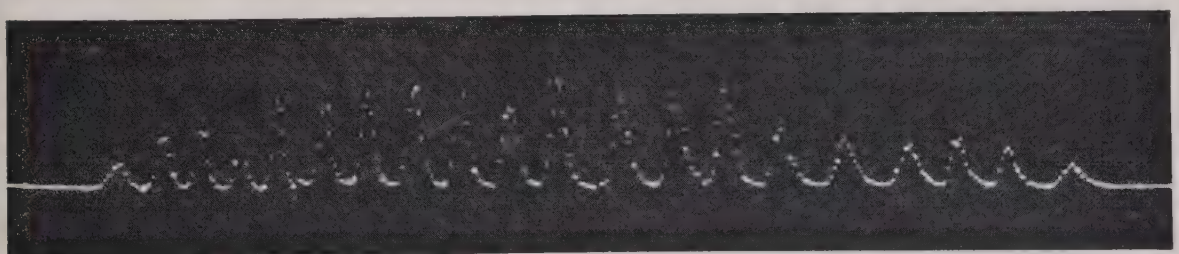

Fig. 6. Decoded information from the counter bank as photographed off the oscilloscope screen of the 400-channel analyzer in a test of the sorting circuitry. In this test a polonium 210 alpha source was placed in front of the counter bank. The peaks, consisting of counts registered by individual detectors, are in a one-to-one correspondence with the detectors of the array. The relative sizes of the groups reflect the solid angle effect.

tion of alpha particles resulting from the $C^{13}(d, \alpha)B^{11}$ (gd. st.) reaction[8]), shown in fig. 8, is an example of data obtained with the present counter array.

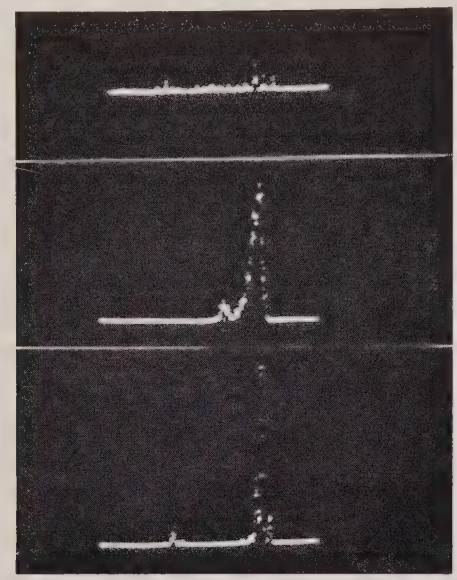

Fig. 7. Sample spectra obtained with the unit, as displayed on the screen of the 400-channel analyzer. The top spectrum, observed with $E_d = 4$ MeV at 30°, shows the two alpha groups resulting from the $Ca^{40}(d, \alpha)K^{28}$ reaction leading to the ground state doublet of K^{38}. The two spectra below were recorded by elastically scattering 4 MeV deuterons, from the gold supported calcium target, into laboratory angles of 30° and 60°, respectively. Relative kinematic shifts of groups, such as above for $Ca^{40}(d, d)$ and $Au^{197}(d, d)$, permit positive identification of target nuclides.

Although attenuation of the signals in the delay line becomes severe when the number of counters is considerably increased, it appears that in its present state the array can be extended to include 40 counters. Larger signals are needed to drive more than 50 stages. Since the prospects are good that

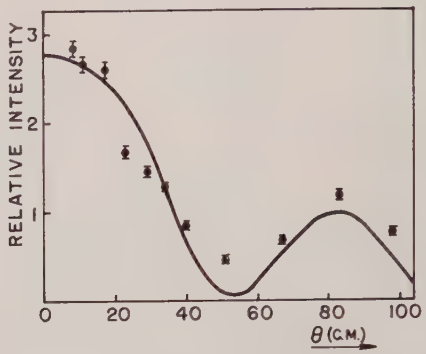

Fig. 8. Angular distribution of alphas in the double pick-up $C^{13}(d, \alpha)B^{11}$ (gd. st.) reaction at $E_d = 3.45$ MeV as recorded by the counter array. For a discussion of this result see ref.[8]).

solid stage avalanche counters, with a multiplication factor of > 20, will be developed[9]), the extension to 100 or even more channels may become practical without basic changes in the present sorting circuitry.

Acknowledgement

It is a pleasure to thank Dr. W. Parker Alford for the many valuable discussions of the problems encountered in this work.

[8]) W. P. Alford, O. M. Bilaniuk and B. B. Marsh, Proceedings of the Rutherford Jubilee International Conference, Manchester, 1961.

[9]) J. W. Mayer, private communication.

CLEAR INSTRUMENTS AND METHODS 14 (1961) 71–75; NORTH-HOLLAND PUBLISHING CO.

RAPID CARRIER FREE SEPARATION TECHNIQUE

W. C. PARKER† and Y. GRUNDITZ

Institute of Physics, University of Uppsala, Uppsala

Received 25 August 1961

Apparatus and technique are described for the rapid carrier-free separation of radioactive nuclides not isotopic with the target material. The principle employed, that of fractionation of volatilization at reduced pressures, has been developed to a reasonable degree of efficiency in so much that comparable yields with those chemical techniques normally enployed have been obtained. Added advantages are that a far shorter period of time is required for the separation, contamination of the sample, from foreign material, is reduced to a minimum, and finally, both the separation and deposition are achieved in a single operation. At the present time the following samples have been prepared: Hg, I, As, Zn, Ag and Au.

Introduction

Finston and Miskel[1]) have previously reported the application of volatilization fractionation to the separation of radioactive materials. The above authors have pointed out the possibility of achieving extremely rapid separations by means of "flash-distillation". Spiess[2]) fractionated astatine from a mixture of astatine and polonium on a platinum ribbon, the separation requiring less than 0.5 sec. Ramos and Finston[1]) separated up to 10 g of bismuth from 10 mg of uranium by vacuum distillation of the bismuth at 800°C. The separation required less than one hour and greater than 99.99% of the bismuth was volatilized.

Sherwin[3]) has described apparatus and technique for the separation and deposition of pure samples of P^{32}, Sr^{90} and Y^{90}, used in an investigation concerning neutrino recoil esperiments[4]). The sample requirements in this particular case were such that the utmost care was necessary to avoid thick layers of active material. The technique developed by Sherwin overcame this difficulty and provided suitable samples.

Carrier-free separations of mercury[5,6,7]) and of astatine[8,9]) have also been reported in the literature based on volatilization fractionation.

In the present work some effort has been made to reduce the solid angle subtended by the vapour source, containing the material, thus increasing the collection probability for a given area.

2. Apparatus (low temperature)

The apparatus employed for the separation of, comparatively, low temperature radioactive fractions has been previously described[6]) and only a short description will be given at the present time.

The greater part of the device consists of a dewar flask formed by the insertion of a small metal cup within another of a larger dimension. Two vacuum connections are situated on the outside of the larger cup, one for evacuation purposes, the other for connection of a quartz tube target holder. Passing through the latter connection, and screwed into the bottom of the smaller cup, is a copper "cold finger" for supporting and cooling the catcher material. The apparatus is evacuated by means of a rotary pump to a pressure of approximately 0.1 mm Hg and the target material heated externally by means

† Present address: Department of Physics, Chalmers University of Technology, Gothenburg, Sweden.

[1]) H. L. Finston and J. Miskel, Annual Rev. Nucl. Sci. **5** (1955) 269.
[2]) F. N. Spiess, Phys. Rev. **94** (1954) 1292.
[3]) C. W. Sherwin, Rev. Sci. Instr. **22** (1951) 339.
[4]) C. W. Sherwin, Phys. Rev. **73** (1948) 1173.
[5]) R. W. Fink and E. O. Wiig, J. Am. Chem. Soc. **74** (1952) 2457.
[6]) W. C. Parker, Nucl. Instr. and Meth. **8** (1960) 354.
[7]) J. Halter and H. Slätis (Private communication).
[8]) E. H. Appelman, Nucl. Sci. Series, NAS-Ns 3012 (March, 1960) p. 10.
[9]) W. Forsling *et al.*, Arkiv för Fysik **19**, No. 7 (1961).

of a micro-burner, placed under the lower tip of the quartz tube. Fig. 1 shows the general arrangement employed.

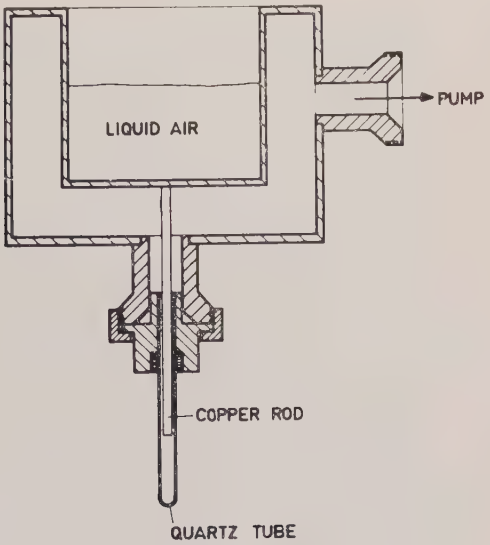

Fig. 1. Low temperature separation apparatus.

2.1. EXPERIMENTAL

Using the low temperature apparatus the active fractions given in table 1 were investigated. With the exception of tellurium, all of the targets were in the form of metal foils, 0.1 mm thick, which were first cut into thin strips and measured with a G-M

TABLE 1

Nuclide	Target	Melting point (M.P.) Target	Evaporation point (E.P.) Nuclide	Backing
As^{73}	Germanium	959	400	M + Ag
Hg^{198}	Gold	1063	—	M + Au*
I^{131}	Tellurium	452	—	M + Ag*
Zn^{63}	Copper	1083	(sub) 343	M + Ag

* The ultra thin backing described in section 2.2 were also employed for the nuclides Hg^{195} and I^{131}.

tube in order to determine which would give the highest yield. The tellurium was in the form of spectroscopically pure metal powder, placed in an air-tight plastic container for irradiation purposes. It should be pointed out that rather than risk the severe contamination, possibly resulting from the sudden removal of the lid of the container, the material was first knocked over to one side of the container and a sharp sewing needle inserted through that side left free of target material. A controlled amount of the target could then be transferred, by gently tapping, into the quartz tube of the volatilizer and the activity measured. In their turn, the metal foil targets were measured in the same manner.

2.2. CATCHER TECHNIQUE

The backings employed as catchers were prepared in one of two ways[10]): (a) evaporation in vacuum of the required metal onto a 0.9 mg/cm² mylar film over an area determined by the spectrometer requirements. In our particular case a sample diameter of between two and four millimeters was that usually specified. After the deposition of the metal spot, the copper cold finger, mentioned in section 2, was smeared with a small amount of vacuum grease and pressed into intimate contact with the back side of the mylar film. The surplus mylar was pleated along the sides of the finger and later held in position by the quartz tube.

Using the second technique (b) a thin uniform layer of white domestic washing soap was spread evenly over the tip of the cold finger. When dry the finger was placed in the evaporation chamber and the required metal deposited on the surface of the soap. On completion of the separation deposition the finger was removed from the apparatus and submerged in warm water, causing the soap to dissolve and the thin metal foil to float on the surface, from which it was later removed by raising a thin zapon film, mounted on an aluminium ring gently into contact with the foil.

Using the latter technique for preparation of the backing it was found possible to have a metal spot of gold of only some 4 μg/cm² and to support this with a zapon film 10 μg/cm², followed by an additional substrate of some 5 μg/cm², giving a total backing thickness of only 19 μg/cm², arrived at using an instrument for thin film thickness determination, working on the principle of α particle absorption[11]). However, the author would like to

[10]) W. C. Parker *et al.*, Nucl. Instr. and Meth. **7** (1960) 22
[11]) De Croes, Parker and Sevier, Nucl. Instr. and Meth. **7** (1960) 160.

t out that a considerable amount of practice is ssary before undertaking such preparations.

RESULTS

ollection efficiencies for mylar backings, with without a conducting layer, used in the aration of mercury isotopes from their gold ets, as found by Petterson[12]), were ~ 50% 10–20% respectively.

or the separation and consequent deposition of from tellurium advantage was taken of the -iodide's ability to form silveriodide and silver, d as the metal substrate on mylar. A separation osition time of some 2–3 min was employed and approximate yield of 20% obtained. A careful asurement of the various I^{131} samples was under- en, and the samples placed in an evacuated mber for a period of three hours. At the end of s time no apparent decrease in activity was nd to have taken place i.e., no free iodide had atilized out of the sample. It will be remembered t the metal substrate was restricted to a maxi- m of 4 mm diameter. For this reason it was essary to evaporate a thin, conducting metal n over the entire surface of the mylar, so as to ke grounding of the sample possible. This last ocedure was carried out for all of the samples pared.

When dealing with the nuclides As^{73} and Zn^{63}, ficulty was experienced in preventing the sepa- ed fraction condensing in the immediate inity of the target material. Attempts at in- asing the temperature resulted in the targets lting and a negligible collection efficiency. One planation for the latter might be the great surface nsion of the molten target, preventing the conti- ation of the separation. The problem was finally ercome by lagging the quartz tube with asbestos ing, resulting in a better heat distribution for e tube.

Backings used for the two nuclides just dealt th were of both types described above. However, noticable difference in efficiency was found as far collection was concerned, this latter being tween 25 and 30% for every four out of five mples produced.

[12]) B-G. Petterson *et al.*, Nucl. Phys. **24** (1961) 243.

3. Apparatus (high temperature)

The arrangement used for high temperature separations can be seen in fig. 2, and has the following construction. A base plate with a diameter of 250 mm is divided in two parts by means of a

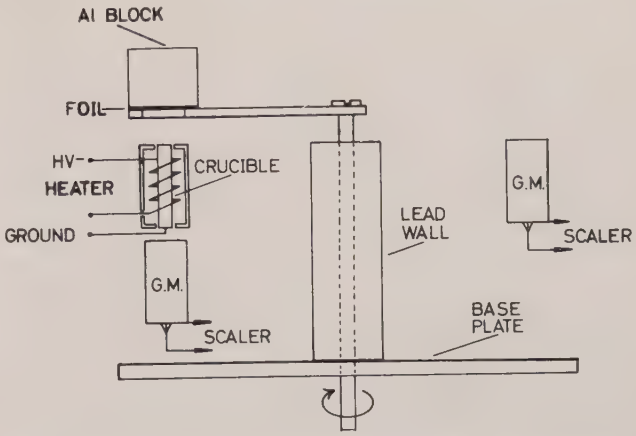

Fig. 2. High temperature separation apparatus. Cross-section view showing heating arrangement (electron bombardment), detector displacement and adjustable columns.

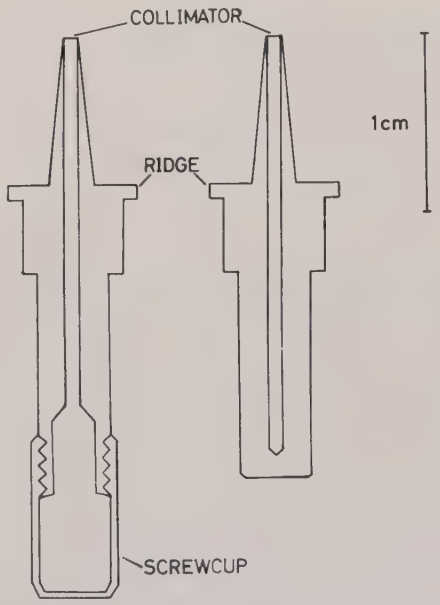

Fig. 3. Crucible construction. Two examples of crucible construction employed for work in the region 2000° C -2500° C for targets of thin wire or foil.

lead wall 40 mm thick. On the left hand side of this wall are situated the heating arrangement, employing electron bombardment, and immediately

under this, a G-M detector mounted on an adjustable column. On the right hand side of the wall is a second G-M detector and the necessary electrical connections for temperature measurement, etc. Passing through the lead wall is a second column, which can be both raised, lowered and rotated. The purpose of this column is to support the backing material employed as catcher.

The crucibles, or vapour sources, used for containing the target material when in metal foil or wire form, are shown in fig. 3, and have been described in detail previously[13]). For powder

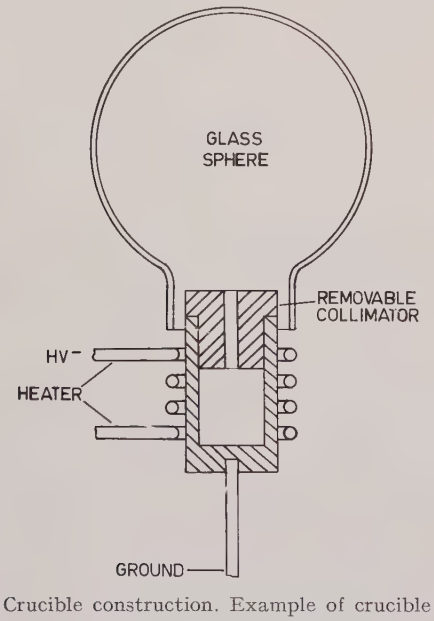

Fig. 4. Crucible construction. Example of crucible employed for powder targets together with the special catcher arrangement described above.

targets the arrangement shown in fig. 4 was found best, however, because of the sacrifice in collimation the catcher normally used had to be replaced, as shown, by a round bottomed reaction flask, thus ensuring the collection of the greater part of the vapourised fraction. The two former crucible types were constructed of tantalum and the latter from high purity graphite. The crucibles were electrically grounded and the tungsten heater kept at high voltage negative.

3.1. EXPERIMENTAL

In table 2 are given the materials reported here. Three of the targets, rhodium, platinum and palladium, were in the form of thin metal foils 0.1 mm thick, while the ruthenium was in the form of spectroscopically pure powder. The technique employed

TABLE 2

Nuclide	Target	M.P. Target	Nuclide E.P.	Backing
Ag^{105}	Rhodium	1967	1047	Al (600 μg/cm
Ag^{107}	Palladium	1555	1047	Al (600 μg/cm
Au^{197}	Platinum	1774	1465	Al (600 μg/cm
Au^{195}	Platinum	1774	1465	Al (600 μg/cm
Rh^{103}	Ruthenium	2500	2149	Al (600 μg/cm

M.P. Melting point
E.P. Evaporation point at V.P. = 10 microns Hg.

for transferring this powder to the crucible was the same as that described for tellurium. After the suitable division of the target concerned, the activity was loaded in a crucible and the activity measured by placing the latter at a given distance above the second G-M detector. The crucible was then placed within the heating assembly, and the activity again measured with the first detector. The described arrangement makes possible the continues monitoring of both the amount of activity leaving the crucible and, also, the percentage of the activity collected by the backing. A typical run would proceed as follows. The crucible containing the activity would be heated to a given temperature for a period of 60 sec. On the crucible cooling, the rotatable backing support is turned 180° bringing the backing over the second detector, and an activity present measured. With the backing remaining in the same position the crucible measured by detector one, and from the difference in the measured activity the efficiency calculated

3.2. CATCHER TECHNIQUE

The backing material used as catcher for the part of the reported work, took the form of aluminium foil 600 μg/cm^2. These foils were both supported and cooled by being pressed into intimate contact with a polished aluminium block, previously smeared with a small amount of vacuum grease

[13]) W. C. Parker, Nucl. Instr. and Meth. **5** (1959) 142.

perature tests, with this method of support, wed that the foils could withstand radiated heat n a crucible heated to a temperature of 2500°C distance of only two millimeters. This last is parable to thin foils of aluminium oxide having hickness of 25 $\mu g/cm^2$, which are capable of standing the same temperature and require no ling[14]).

RESULTS

Due to poor temperature control initial attempts separating Au^{195} from platinum resulted in only of the active fraction being collected. As previously mentioned, this is thought to be due to the t that the target, if allowed, to melt, prevents tinued volatilizing of the active fraction because of surface tension. In this particular instance other explanation might be the crucible material, in this case carbon, which is known to form h temperature carbides with the platinum tals[15]). As to whether or not this was the cause s, at the present time, not been investigated, ce all other attempts were made using tantalum cibles and the target material kept in unmolten m. The gold activities, regardless of the production method employed (see table 2), showed no preference as far as separation efficiency was concerned i.e., approximately 20% of the total active ld content present in the target could be collected a single 60 sec period.

The separation of Ag^{107} from paladium targets llowed almost exactly the same lines as that scribed for gold isotopes, with the difference that a lower temperature could be used. However, for the separation of Ag^{105} from rhodium, one of the heating periods resulted in a 100% separation collection efficiency. It could only be concluded that the exact temperature and time conditions had been satisfied. In any case, it proved impossible to reproduce this excellent result, the efficiency dropping down to the usual 20%.

Because of the excessive out-gassing brought about by the high temperature necessary for the separation of Rh^{103} from ruthenium, the great increase in pressure is thought to have been responsible for the failure in attempting to separate this nuclide. Only on one occasion could any measurable activity be detected, and this proved to be less than 0.5% of the total activity present.

It seems probable that this form of separation technique could be developed to a very high degree of efficiency for both metals and metal compounds, since it is certainly capable of producing carrier-free samples in the true sense of the meaning.

The authors should like to thank Professor K. Siegbahn for following the progress of this work with encouraging interest. One of us, W.C.P., wishes to take this opportunity of expressing his gratitude to Professor Siegbahn for all the kindness and encouragement shown towards him during his stay at the Institute of Physics, Uppsala.

[14]) K. D. Sevier and W. C. Parker, Nucl. Instr. and Meth. **6** (1960) 218.

[15]) L. Holland, Vacuum Deposition of Thin Films (Chapman and Hall, London, 1952).

NUCLEAR INSTRUMENTS AND METHODS **14** (1961) 76–78; NORTH-HOLLAND PUBLISHING CO

STABILIZING A SCINTILLATION SPECTROMETER BY MEANS OF A LOW FREQUENCY MODULATED LIGHT SOURCE

H. J. RIJKS

Reactor Instituut Delft

Received 18 September 1961

The variation in multiplication of a photomultiplier, even if high voltage and temperature are constant, makes it difficult to measure a gamma energy-spectrum accurately.

This paper deals with a method of stabilizing the gain of a photomultiplier by means of a light source modulated by 50 cp mains frequency, which is rather constant.

A gain stabilization better than 1% in 24 hours has bee achieved.

1. Introduction

It has been known for some time that changes in photomultiplier gain occur when the tube current changes[1,2,3]), apart from other effects as aging, temperature variations, changes in voltage distribution between the dynodes and instabilities of the high voltage supply. De Waard published a stabilization method, based on count-rate feedback and control of the high voltage supply[4]). In this case it is necessary to introduce a radioactive source as a reference which gives a photopeak above the spectrum to be measured. A shift of this photopeak results in a signal which controls the high voltage. This method involves that the spectrum to be measured is distorted by Compton-pulses from the reference source and that sum-pulses can effect the reference photopeak. Haun and Kamke[5]) developed a stabilization method by using a pulsed light source which gives a specific line; therefore the contribution of Compton-pulses in the spectrum to be measured can be neglected.

To avoid additional Compton-pulses from the stabilization method it is also possible to introduce as a reference a light source modulated with a low frequency which does not pass the pulse amplifier. The use of an amplifier with a not too low cut-off frequency makes this possible.

The reference signal is amplified in a peaked amplifier. The difference between the signal and a constant DC voltage controls the high voltage supply.

2. Principle of Operation

The mains frequency (50 cps) on the continent i rather constant; therefore this frequency was use to trigger a univibrator. The univibrator drives a output pentode in the cathode circuit of which small bulb with a short heat response is placed. T avoid againg of the bulb the current is limited t about 60% of the nominal value. The bulb is place in the base of the scintillation probe. The 50 cp light pulse, which is reasonably sinusoidal, i colour-filtered to match the spectral sensitivity c the photo-cathode. By means of a lightpipe an glass disc which is mounted between photo-cathod and scintillation-crystal the light pulse is guided t the photo-cathode. The photomultiplier outpu pulse is fed into a peaked amplifier and rectifie As the modulation of light depth is frequenc dependent, the frequency response of the amplifie is chosen to correct for the effect of mains fre quency variations. The difference between rectifie signal and a constant DC voltage is fed into a D amplifier. The high voltage is obtained with the ai of a 20 kcps oscillator, which is controlled by th DC amplifier output. Obviously the stabilization i

[1]) L. Cathey, I.R.E. Transactions on Nucl. Science (De 1958).

[2]) R. D. Connor and M. K. Hussein, Nucl. Instr. and Met **6** (1960) 337.

[3]) P. R. Bell, R. C. Davis and W. Bernstein, Rev. Sci. Inst **26** (1955) 726.

[4]) H. de Waard, Nucleonics **13** (1955) 36.

[5]) S. Haun and D. Kamke, Nucl. Instr. and Meth. **8** (196 331.

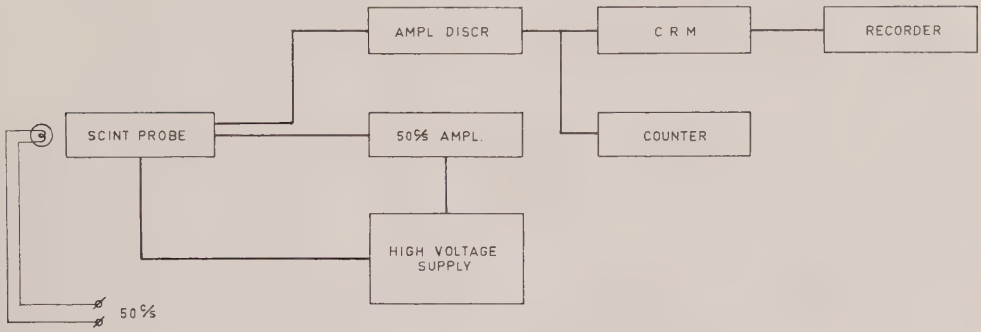

Fig. 1. Block diagram of the stabilization circuit.

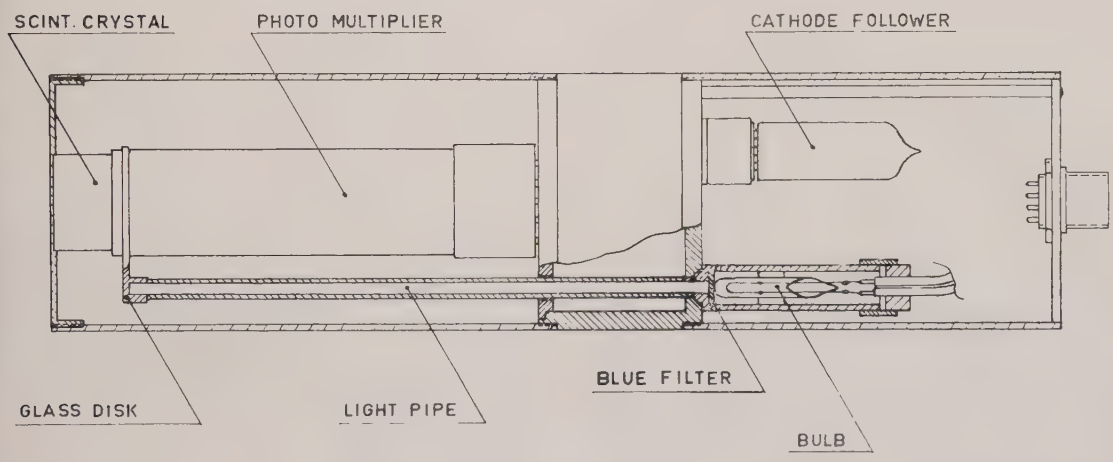

Fig. 2. Construction details of the scintillation proble.

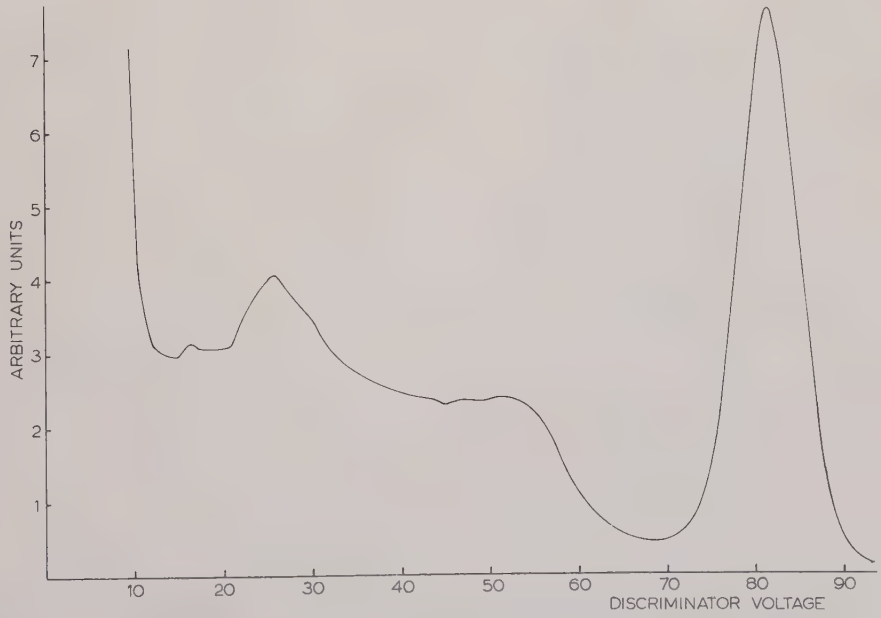

Fig. 3. Measured Cs^{137} spectrum.

independent of the position of the photopeaks to be measured, which can be considered as an advantage over the methods mentioned in[4]) and[5]).

3. Circuit Description and Performance

The univibrator and power pentode are placed in the high voltage unit. To obtain a sinusoidal light pulse a capacitor is connected parallel to the bulb. The 300 V DC must be stabilized better than 10^5 in order to get a constant light amplitude of the light source. When the gamma count-rate is excessive high, an increase of the reference output signal occurs. Its influence can be decreased by choosing a larger amplitude of the light pulse.

A disdavantage of this method is that the amount of noise in the low energy part of the gamma spectrum increases with light amplitude, so a compromise must be made between increased noise and count-rate.

No noticeable distortion of the reference signal occurred at 600000 cpm above 40 keV. At this setting the background without shielding was 4440 cpm and above 70 keV 3590 cpm.

The sinusoidal pulses do not pass the amplifier (Franklin, model 348) so the 50 cps pulses are not counted in the counting channel.

After warming up a stability better than 1% in 24 hours has been achieved.

At the above mentioned setting and pulse rate, which is considered rather high, the spectrum below 90 keV is not usable, due to increase of noise. This effect, the glass disc and probably the phen mena mentioned by Bell, Davis and Bernstein results in a decrease of the resolution. The us photomultiplier (Dumont 6292) had a resolution 8.9% on the Cs^{137} photopeak; with modulat light source this value increased to 9.5% at 1100

It has been difficult to shield the circuit again the 50 cps mains pick-up, but as long as this pick- is constant and small with respect to the signal, does not affect the stabilization.

Another noticeable effect was the displaceme of the bulbfilament in its suspensions as a result a mechanical shock of the scintillation probe whi resulted in a changing light output. A bulb had be individually selected in order to get rid of th effect.

4. Final Remarks

A better gain stabilization which however is mo expensive can be achieved if the univibrator triggered by a more stable frequency than t mains frequency which varies about $\pm$ 4%. It advisable to choose this frequency lower than 50 c to avoid difficulties with pick-up.

Acknowledgement

The author wishes to extend his sincere thanks prof. dr. ir. J. B. le Poole and ir. C. J. van Daat laar for their useful discussions and helpful ide and to Mr. C. A. van der Werve under whose sup vision the electronic instrumentation was bui

CLEAR INSTRUMENTS AND METHODS 14 (1961) 79–82; NORTH-HOLLAND PUBLISHING CO.

QUANTITATIVE MEASUREMENTS OF ION BEAM PROPERTIES

P. H. ROSE, A. B. WITTKOWER, R. P. BASTIDE and A. GALEJS

High Voltage Engineering Corporation, Burlington, Massachusetts

Received 4 September 1961

evice is described which can be used to determine the profile, position and emittance of beams of charged or neutral particles

Introduction

The instrumentation of the positive ion D.C. accelerators used in nuclear research has traditionally been elementary, largely because of the inherent simplicity of the D.C. acceleration. Now that extensive beam handling systems are coming into use and the accelerators are more complex, some quantitative means of measuring the ion beam becomes desperative. Of the traditional methods, viewing the luminescence of a beam on a quartz plate is common. However, apart from the disadvantage that the beam is intercepted, the information obtained depends upon the interpretation of the observer.

Nielsen has described a quantitative tool called a beam scanner[1]); an insulated wire is moved through the ion beam and the resultant current to the wire is measured. The collected current is used to generate a voltage which is displayed as the vertical movement of an oscilloscope trace with the time base synchronized to the position of the probe.

In this paper a scanner will be described which

[1]) K. O. Nielsen and O. Skilbreid, Nucl. Instr. **1** (1957) 159.

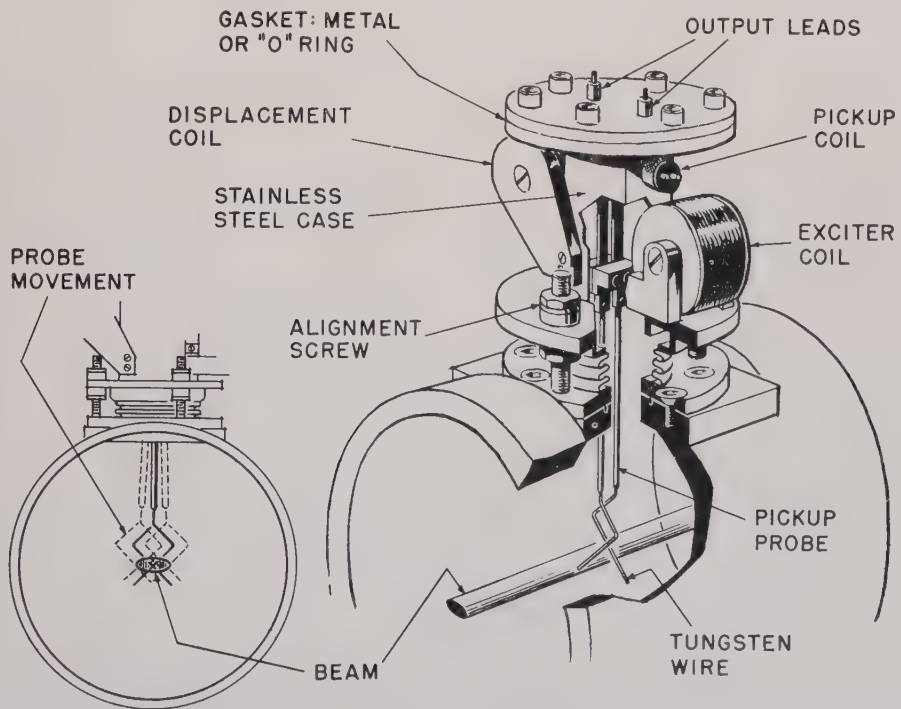

Fig. 1. The vibrating beam scanner.

simultaneously measures the beam in the horizontal and vertical directions. In particular, this beam scanner has been used to measure the position and focus of positive, negative and neutral† ion beams, the energy stability of an accelerator and the measurement of the emittance††[2]) of an ion beam. The measurement of beam emittance, the fundamental property of an ion beam, has previously proved to

ments which may otherwise act as apertures in th system along the beam path can then be matche to the emittance of the beam at these points i order to obtain an optimum system.

2. Description

Fig. 1 shows the beam scanner which can give th profile of the beam horizontally and verticall

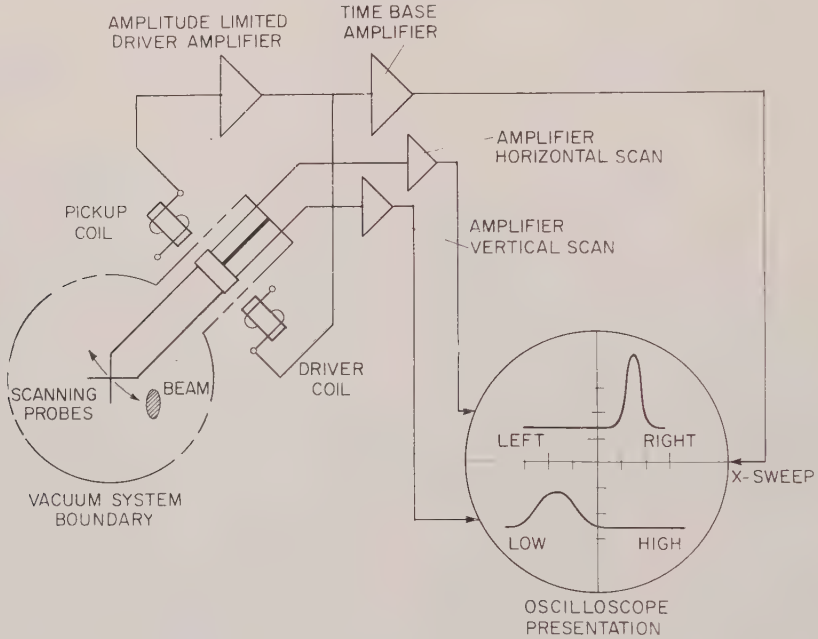

Fig. 2. Schematic of display circuit and typical beam profile.

be quantitatively difficult. The emittance of the beam completely determines its properties, i.e. diameter, divergence and charge density at any plane in the system. The acceptance†††[3]) of physical ele-

† The neutral beams are observed by the emission of secondary electrons from the wire struck by the beam.

†† The emittance of a beam is defined as the area it occupies in phase space. In its simplest form, phase space is a plane described by the totality of points (r, p_r) where r and p_r are the radius and radial momentum of a particle in a rotationally symmetric system. If V is the beam energy then $p_r \cong r' \sqrt{2V}$ where r' is the slope of the trajectory of the particle. The invariance of emittance is a direct consequence of Hamiltonian mechanics.

††† The complementary concept to beam emittance is component acceptance. This is defined as the area in phase space which an idealized beam would fill if it could just pass through the component without losses.

†††† By a judicious choice of probe thickness and oscillation frequency the interception can be reduced to $< 0.1\,\%$ in order to probe beams of high power density.

simultaneously by inclining the vibrating reeds 45° to the vertical. The reeds are excited into res nance by an electromagnet. The change of flux in pickup coil is used to provide the exciting signal ar also to monitor the peak amplitude of the vibrati which is held to a constant level. The probes mo through an arc of 3.8 cm. Since the amplitude vibration generates the x-sweep of the oscilloscop uniform velocity is not required to achieve a line display. The scanner vibrates at its natural fr quency which is typically 15 c/s and intercep $<2\%$ of a 1 centimeter diameter beam††††. When n in use the scanner may be left in the rest position

[2]) P. A. Surrock, Static and Dynamic Electron Optics (Ca bridge University Press, Cambridge, 1955).

[3]) D. L. Judd, Conceptual Advances in Accelerators, Annu Review of Nuclear Science **8** (1958) 181 (Annual Reviews, Inc

ld by an electromagnet at an extreme position out beam.

A schematic of the circuit employed is shown in . 2 which also shows a typical beam profile, as easured by this scanner, displayed on a dual trace

preferably using a microalignment telescope. The beam scanner makes it possible to check the location of the ion beam to equivalent precision and to correct the beam position if necessary. At the same time the focus can be examined and adjusted. Most

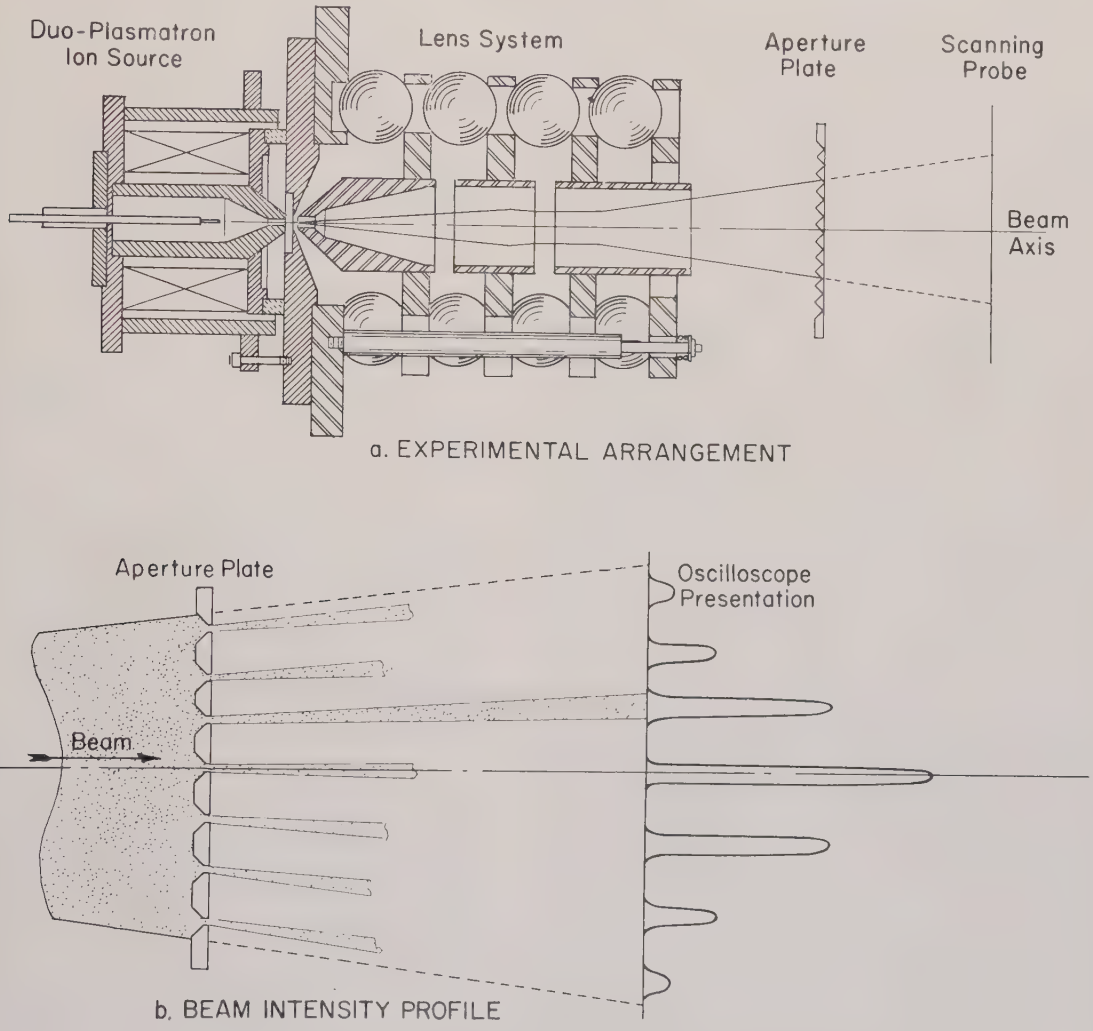

Fig. 3. Schematic of emittance measuring apparatus.

cilloscope. The position of the beam with refernce to the scanner, which may be aligned to the celerator axis, is also given by this display.

Application

The scanner can be used in two ways; either utinely to assist in the operation of an accelerator, r experimentally to examine its performance. The rger accelerators of today are aligned optically,

important, both these observations can be made without interrupting the beam and this is perhaps the most outstanding advantage of these devices.

Stabilization of an electrostatic generator is generally achieved by taking corrective signals from the image slits of an analysing magnet. For efficient stabilization these slits must intercept a part of the beam, usually at least 10%. An electronic system working from the signal produced by a scanner can

stabilize an accelerator just as effectively with a much lower interception. It must be pointed out that slits have a definite advantage if the stabilization system is inadequate, for particles of an energy which differ grossly from the median energy are lost on the slits before reaching the target†.

The scanner has been used successfully over an energy range of from 100 eV to 10 MeV and a current range of from 1 mμA to 30 mA. The position and spot size of charged particle beams and neutral beams have been varied and observed, and beam profiles varying in width from 0.040 inch to 1.5 inches have been measured. However, the measurement of beam emittance and the application of the scanner to this task is of particular interest in view of the usual tediousness of this measurement. An experiment in which the emittance of a 10 keV, 1 mA positive hydrogen ion beam was measured will now be described. The beam was extracted through a 0.010 inch exit aperture of a duoplasmatron ion source, and the focus of the beam was controlled by a three element unipotential lens. The beam passed through a series of small equispaced apertures in a plate, such that the beam was sampled at several radii r_i across the beam diameter. The scanner was placed 4 inches behind the apertures, and the beam profile was recorded (fig. 3).

† Often the energy stability of a beam must be measured. The scanner can be used effectively for this purpose by mounting it beyond an analyzing magnet. An energy ripple is immediately measurable by observing the variation of position with time on the oscilloscope screen.

By a geometric construction, the maximum and minimum beam angles from each, aperture can b computed, giving the values of r'_i, lying upon th envelope of the emittance diagram at radius r_i

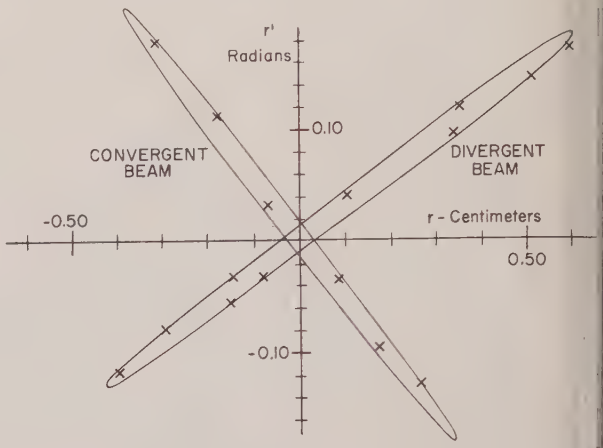

Fig. 4. The phase space diagram of a 10 keV positive hydrog ion beam.

(fig. 4). By varying the focus voltage on the lens, beam converging or diverging at the aperture w studied and an average value of the emittance w found to be 0.016 radian-cm at a beam energy 10 keV. It is interesting to note that the linearity the axis of the phase space contour denotes a optical system free from distortion.

Acknowledgements

The authors wish to thank Dr. R. J. Van d Graaff for his interest and helpful suggestions.

CLEAR INSTRUMENTS AND METHODS 14 (1961) 83–86; NORTH-HOLLAND PUBLISHING CO.

TRAGBARER PULSGENERATOR FÜR PRÜFZWECKE

THOMAS FRIESE

Mitteilung aus dem Hahn-Meitner-Institut für Kernforschung Berlin, Sektor Kernchemie, Abt. Elektronik, Germany

Eingegangen am 26. Juli 1961

A small portable pulse generator was built for testing and calibrating radiation detection instruments. The thermal drift of eleven calibrated frequencies ist less than 1% between 0°C and 45°C. The pulse amplitude is adjustable continuously from 0 V to ± 10 V, the pulse duration is 1 μs. The compensation of the thermal frequency drift of the blocking oscillator is described.

1. Einleitung

Für die routinemässige Überprüfung und Eichung von Strahlungsmessgeräten ist ein kleiner tragbarer Pulsgenerator zweckmässig, vor allem, wenn die Geräte in Überwachungsanlagen fest eingebaut sind. Die Inkonstanz der Pulsfrequenz soll kleiner als ± 1 % und die Pulshöhe zwischen 0 und ± 10 V kontinuierlich einstellbar sein, da Diskriminatoren in mit Röhren bestückten Geräten meist eine untere Ansprechschwelle von 5 V haben. Eine Pulsbreite von 1 μs mit Ansteigs- und Abfallzeiten von 0.1 μs ist gut geeignet zur Prüfung von Geräten, die Geiger-Müller-Zählrohrimpulse oder Szintillationszählerimpulse verarbeiten.

2. Blockschaltbild des Pulsgenerators

Bild 1 zeigt das Blockschaltbild des Pulsgenerators. Ein Sperrschwinger kann auf 12 verschiedene Festfrequenzen eingestellt werden. Fünf dieser Frequenzen werden mit der einfachen oder doppelten Netzfrequenz synchronisiert und haben dadurch eine der Netzfrequenz entsprechende Inkonstanz. Die Festfrequenzen sind so gewählt, dass bei den handelsüblichen Strahlungsmessgeräten mit integrierender Anzeige für einige Bereiche Vollausschlag erreicht wird.

Der Sperrschwinger triggert eine monostabile Kippstufe, die einen negativen 1 μs-Puls erzeugt, dessen Höhe von 0 bis etwa − 10.5 V kontinuierlich eingestellt werden kann. Dieser Puls steuert einen Ausgangsverstärker, aus dem wahlweise positive oder negative Pulse von maximal 10 V Höhe entnommen werden können. Ein nachfolgender Stufenabschwächer mit einem Innenwiderstand von 100 Ohm verkleinert den Puls im geeichten Verhältnis 1:10:100:1000 ± 1%.

3. Schaltung des Pulsgenerators

Bild 2 zeigt die Schaltung des Pulsgenerators. Bei Verwendung grosser Kondensatoren C_i zur Erzielung langer Kippzeiten des Sperrschwingers (Tl) muss W1:W2 > 1 sein, da dann genügend Ladung in den Kondensator fliesst. Zur Strombegrenzung wird in die Emitter-Leitung ein kleiner Widerstand geschaltet. Zur Erlangung einer kurzen Erholzeit wird die Dämpfungsdiode D parallel zur niederohmigen Seite des Transformators geschaltet und das restliche, auf der Basisseite störende Ausschwingen mit einem Widerstand gedämpft.

Der Emitterreststrom von T1 verringert mit steigender Temperatur die Zeitkonstante. Bei 35°C beträgt der der Emitterstromzunahme äquivalente Ersatzwiderstand gegenüber dem bei 20°C gemessenen Wert etwa 10 MOhm, was für $R_i = 50$ kOhm bereits einen Fehler von 0.5% zur Folge hat. Zur Verringerung dieses Einflusses wurde zwischen Emitter und *RC*-Zeitkonstantenglied eine Siliziumdiode 0A 127 geschaltet, deren Sperrstrom weniger als 1/100 des Sperrstroms des Transistors beträgt. Die verbleibende Temperaturabhängigkeit der Frequenz ist gegeben durch die Temperaturkoeffizienten von R_i und C_i und die Temperaturabhängigkeit des Transistors. Die Hersteller geben folgende Temperaturkoeffizienten an:

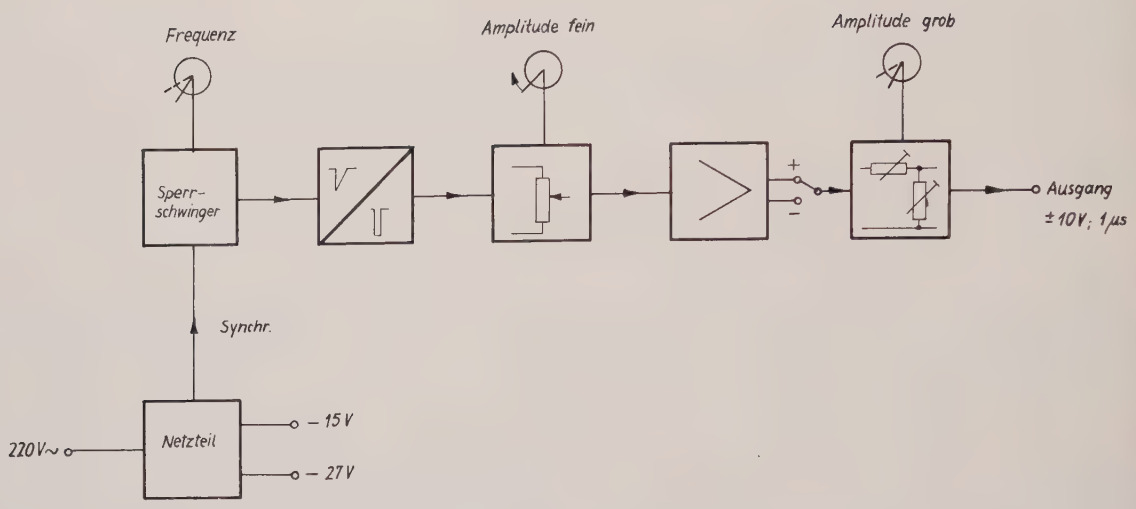

Bild 1. Blockschaltbild des Pulsgenerators.

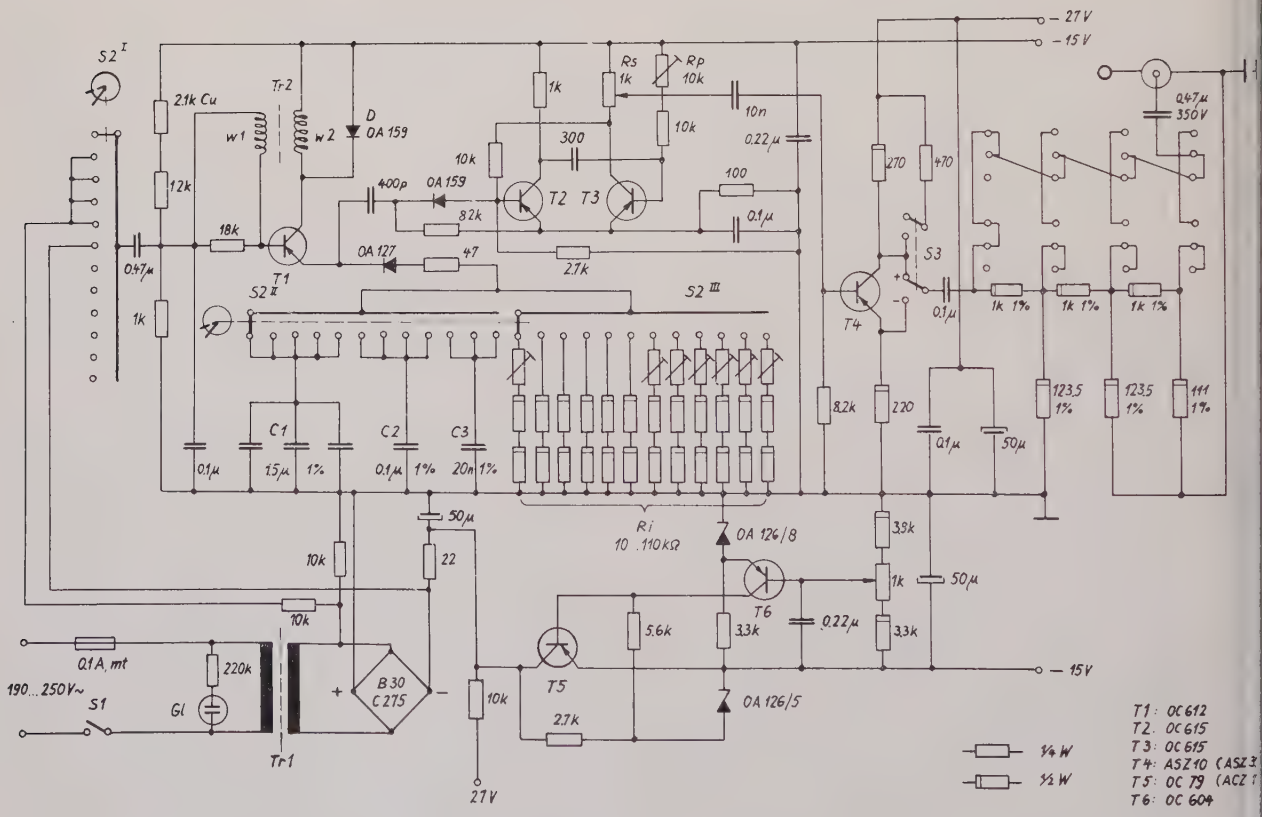

Bild 2. Schaltbild des Pulsgenerators.

	zeitl. Inkonstanz	Temperaturkoeffizient
Kohleschichtwiderstand $\frac{1}{2}$ W	—	ca. -0.5×10^{-3}/°C
Styroflex-Kondensatoren (S.u.H.)	ca. $\pm$ 0.3 %	ca. -0.15×10^{-3}/°C
MKL-Kondensatoren b. 800 Hz (S.u.H.)	ca. $\pm$ 2 %	ca. $+0.9 \times 10^{-3}$/°C

Eine Temperaturerhöhung des Transistors bewirkt eine Frequenzerhöhung, da er bei höherer Temperatur in der Sperrschwingerschaltung eher öffnet wird. In der Schaltung wird zur Erzeugung der Frequenzen von 5 Hz bis einschliesslich 50 Hz ein MKL-Kondensator verwendet. Da die Frequenzen 10; 16.6; 25 und 50 Hz netzsynchronisiert sind, spielt der Temperaturgang dieser Zeitkonstanten keine Rolle. Die Sperrschwingereigenfrequenzen liegen 5 $\pm$ 2% unter den synchronisierten Frequenzen. Die Frequenz 5 Hz kann für Eichzwecke nicht empfohlen werden, zumal die zeitliche Inkonstanz von MKL-Kondensatoren gross ist. Zur Erzeugung der Frequenzen über 100 Hz, die nicht synchronisiert sind, dienen Styroflex-Kondensatoren.

Die Temperaturabhängigkeit der Frequenz kann durch eine temperaturabhängige Basisvorspannung kompensiert werden. Eine Verringerung der Basisvorspannung bewirkt eine Frequenzerniedrigung. Es wurde experimentell ermittelt, dass ein Temperaturkoeffizient des oberen Basisteilerwiderstandes von $+$ 0.26%/°C den Temperaturkoeffizienten der Frequenz im Mittel nahezu aufhebt. Der Widerstand von Kupfer hat einen Temperaturkoeffizienten von $+$ 0.4%/°C. Ersetzt man im oberen Basisteilerwiderstand einen Teil $\alpha = 0.26/0.4$ durch einen Kupferwiderstand, so erhält man einen Gesamtwiderstand mit einem Temperaturkoeffizienten von ca. $+$ 0.26%/°C. (Der Einfluss des T_k des Schichtwiderstandes wurde hierbei vernachlässigt.) Der auf diese Weise temperaturkompensierte Sperrschwinger zeichnet sich durch gute Frequenzstabilität im Bereich zwischen 0°C und $+$ 45°C aus. Bild 3 zeigt die relative Änderung einiger Frequenzen in Abhängigkeit von der Temperatur. Gegen Transistorwechsel ist die Schaltung weitgehend unempfindlich.

Die negative, steile Flanke des Emitterpulses von T1 wird differenziert und triggert die monostabile Kippstufe T2, T3. Die Pulsbreite kann an R_p zwischen 0.8 μs und 1.4 μs eingestellt werden. Am

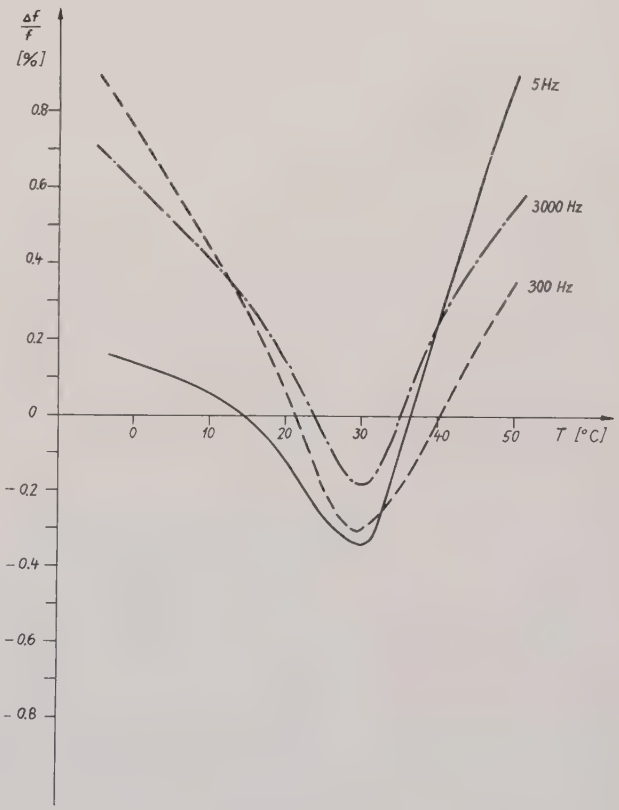

Bild 3. Temperaturabhängigkeit einiger Frequenzen.

Kollektorwiderstand R_s von T3 wird ein zwischen 0 und ca. $-$ 10.5 V einstellbarer Puls abgegriffen.

Der negative Puls steuert den als Emitterfolger geschalteten Transistor T4, aus dessen Emitter oder Kollektor wahlweise ein negativer oder positiver Puls ausgekoppelt wird. Der nachfolgende 100-Ohm-Kettenteiler wird über einen Drucktastensatz an die Ausgangsbuchse geschaltet. Der Druck-

tastensatz ist so geschaltet, dass die Längskapazität möglichst klein ist. Der Ausgang ist mit einem Kondensator abgeblockt, damit der Puls an beliebigen Stellen einer Schaltung eingespeist werden kann.

Die Einstellung des negativen Ausgangspulses auf maximal − 10 V erfolgt durch Justierung der Betriebsspannung − 15 V, des positiven auf maximal + 10 V durch Abgleich des Kollektorwiderstandes des T4. In Stellung "negative Ausgangspulse" des Schalters S3 wird der Kollektorwiderstand (270 Ohm) durch Parallelschalten von 470 Ohm auf etwa 170 Ohm verringert, damit auch bei einer Netzspannung von 190 V die Kollektorspannung gross genug bleibt. (Die Betriebsspannung für T4 ist nicht stabilisiert.)

Im Netzteil liegt vor dem Ladekondensator ein Widerstand von 22 Ohm, vor dem die zur Synchronisierung des Sperrschwingers erforderliche 100-Hz-Spannung abgenommen wird. Die Spannung für den Transistor T4 ist nicht stabilisiert, sondern wird nur gut gesiebt. Der Siebwiderstand kann gross sein, da das Tastverhältnis des Pulsgenerators höchstens 1:330 ist und folglich nur ein kleiner mittlerer Strom zur Ausgangsstufe fliesst. Die Betriebsspannung − 15 V wird in einer üblichen Regelschaltung stabilisiert.

Technische Daten

Ausgangspuls:	max. 10 V ± 3 % positiv oder negativ kontinuierlich von 0 an einstellbar
Abschwächer:	1:10:100:1000 ± 1 %
Innenwiderstand:	bei Abschwächung 10, 100, 1000 fach: R_i = 100 Ohm
Pulsdauer:	1 µs ± 10 % (justierbar 0.8 bis 1.4 µs)
Anstiegs- und Abfallzeit:	0.1 µs

Frequenzen und Genauigkeit

Imp/sec	Imp/min	Inkonstanz
5	300	± 2 %
10	600	netzsynchronisiert
16,66	1 000	
25	1 500	
50	3 000	
100	6 000	
166,6	10 000	± 1 %
300	18 000	
500	30 000	
1 000	60 000	
1 666	100 000	
3 000	180 000	

Betriebstemperaturbereich: 0° C bis + 45° C
Netzspannung: 190 V bis 250 V
Leistungsaufnahme: 3.5 VA.

Bild 4. Pulsgenerator für Prüfzwecke.

UCLEAR INSTRUMENTS AND METHODS 14 (1961) 87–93; NORTH-HOLLAND PUBLISHING CO.

A MECHANISM OF THE PROPAGATION OF GEIGER DISCHARGE IN HALOGEN-QUENCHED G. M. COUNTERS

JUICHI AKUTSU

The Institute of Physical and Chemical Research, Tokyo, Japan

Received 10 August 1961

mechanism of the propagation of the Geiger discharge parallel the anode wire, i.e., the cause of successive avalanche which llowed the first avalanche initiated by an ionizing particle in logen counters has been studied theoretically. The results tained elucidate that successive avalanches in argon-bromine unters are due to the secondary electrons produced in the gas t not the photoelectrons produced at the cathode, although the Geiger discharge is not confined to the region of the gas volume where the first avalanche is formed and photons created in the avalanche can cause photoionization at some distance from the point of origin. This may account for the experimental results that the cathode does not play a part in the mechanism of argon-iodine counters as reported by van Zoonen.

Introduction

Some of the characteristic behaviors[1]) of gas scharges in halogen counters consist in the facts hat the halogen molecules capture electrons in the ischarge process, that the discharge is not localized n the region of the anode wire, and that the break-own potentials are much lower. In these behaviors, he difference in the localization phenomenon of the ischarges between argon-bromine or neon-argon-romine counters and ordinary argon-alcohol ounters will arise from two causes: one is the ifference in partial pressure of bromine and alcohol apor, the other is the difference in absorption oefficient of bromine[2]) and alcohol[3]) vapor for J.V. photons. Hence, in argon-bromine counters, J.V. photons generated in the first avalanche will pread widely within the counter envelope. The fact hat halogen counters do not show the localization f discharges have been proved experimentally by Vilkening and Kanne[4]), and by Liebson and riedman[5]). From the experiments on mutual igni-ion with the system of two electrodes in line, iebson and Friedman[5]) concluded that the econdary mechanism in halogen counters is caused y the photoemission at cathode. Van Zoonen[6]), owever, showed that the above conclusion seemed ot to be inevitable by the experiments with two ounters having a cylinder as cathode and helically ound wire as cathode, which are enclosed in one glass envelope. In this paper it is aimed at to know whether the spread of the discharge along the wire in halogen counters is due to the photoeffect at cathode or to the photoionization in gas, or to the both effects. A theory for argon-bromine counters has been developed by considering the following subjects: electron loss[7]) by electron capture with halogen molecules, electron multiplication by cumulative ionization, relation between the first avalanche and the second one at the threshold of Geiger discharges, and estimation of an average value of α/E (α is Townsend coefficient in ion pairs per cm and E is the field strength in V per cm) in the limited range of E/P (P is the total pressure in mm Hg) for argon-bromine mixture.

2. Number of Ions Generated in an Avalanche in Halogen Counters

Considering the geometry of a coaxial cylinder, the radii of the cathode and anode are put b and a

[1]) K. van Duuren, A. J. M. Jaspers and J. Hermsen, Nucleonics **17** (1959) 86.

[2]) D. Porett, Proc. Roy. Soc. (London) A **162** (1937) 414.

[3]) F. Alder, E. Baldinger, P. Huber and F. Metzger, Helv. Phys. Acta **20** (1947) 73.

[4]) M. H. Wilkening and W. R. Kanne, Phys. Rev. **62** (1942) 534.

[5]) S. H. Liebson and H. Friedman, Rev. Sci. Instr. **19** (1948) 303.

[6]) D. van Zoonen, Appl. Sci. Res. B **4** (1955) 237.

[7]) K. Shinohara and J. Akutsu, J. Sci. Res. Inst. (Tokyo) **47** (1953) 80.

respectively and they are maintained at potentials zero and V respectively. In such a counter, the number of electrons produced at any distance from the anode wire will be decreased by electron capture on collisions with bromine molecules and increased by cumulative ionization on collisions with argon atoms and halogen molecules at the region of the anode wire when the electrons are accelerated towards the wire by electric field.

In order to simplify the calculation on the decrease in the number of electrons by the effect of electron capture in a halogen counter, it is assumed[7]) that the drift velocity of electrons is proportional to E/P for the range of interest in a Geiger counter, and that the electron attachment probability h per collision between an electron and a bromine molecule is constant for E/P of the range. Then, in drifting over the distance Δr towards the central wire, the decrease of n electrons at r from the center, which is due to the effect of electron capture by bromine molecules, is given by[7])

$$(\Delta n)_{\mathrm{D}} = n\left(h\frac{\sigma_1}{\sigma}\frac{1.32\times10^{15}\,PP_1}{k_0^2\,E}\right)\Delta r\,, \qquad (1)$$

where σ_1 is collision cross section of bromine molecules, σ mean collision cross section of bromine molecules or argon atoms, k_0 electron mobility at 1 mm Hg, P_1 partial pressure of bromine vapor in mm Hg, and the field strength is given by $E = V/r \ln(b/a)$ in V/cm.

At higher field near the central wire, the electrons may obtain enough energy from the electric field at which the electrons cause ionization by collisions with bromine molecules or argon atoms. Thus electron multiplication takes place very close to the wire surface. Then, in drifting over the distance Δr towards the central wire, the increase of n electrons at the distance r from the center, which is due to the cumulative ionization by collisions, is represented as follows:

$$(\Delta n)_{\mathrm{I}} = n\alpha\Delta r \qquad (2)$$

where α is the mean number of ion pairs formed per unit length along the field and is so-called the first Townsend coefficient. In an argon-bromine counter α is simply defined in accordance with Wilkinson's theory[8]), as

$$\alpha = CE\,, \qquad (3)$$

where C is a proportional constant, and this value will be discussed in section 4. Equation (2) would thus be re-written as

$$(\Delta n)_{\mathrm{I}} = nCE\Delta r\,. \qquad (4)$$

From (1) and (4), the total number of electron increment in drifting over Δr towards the central wire of the number n of electrons produced in a halogen counter may be expressed by

$$\Delta n = (\Delta n)_{\mathrm{I}} + (\Delta n)_{\mathrm{D}} = \left(\frac{CV}{\ln(b/a)}\frac{1}{r} - \frac{G\cdot PP_1}{V}r\right)n\Delta r\,, \qquad (5)$$

where

$$G = h\frac{\sigma_1}{\sigma}\frac{1.32\times10^{15}}{k_0^2}\ln(b/a)\,. \qquad (6)$$

Integrating (5), we get

$$N = S(R)\,\mathrm{d}R\left(\frac{R}{a}\right)^{CV/\ln(b/a)}\cdot\exp\left\{-G\frac{PP_1}{2V}(R^2-a^2)\right\} \qquad (7)$$

where N is the total number of electrons arriving at the wire surface, $S(R)\,\mathrm{d}R$ is the number of electrons produced between R and $R+\mathrm{d}R$, the distance R being measured from the wire, and $S(R)$ is electron density. This value of N would be equal to the number of ions produced in an avalanche if the effect of electron capture by bromine molecules in the high field near the anode wire is neglected.

3. Relation between the First Avalanche $N(1)$ and the Second One $N(2)$

Denoting the electron, the argon atom and the bromine molecule by e, Ar and Br_2 respectively, the main reactions which cause primarily ionization or excitation in the first avalanche are expressed by the following equations:

(A) $\mathrm{e} + \mathrm{Ar} \rightarrow \mathrm{Ar}^+ + \mathrm{e} + \mathrm{e}$
(ionization of argon atom)

(B) $\mathrm{e} + \mathrm{Ar} \rightarrow \mathrm{Ar}^* + \mathrm{e}$
(excitation of argon atom)

(C) $\mathrm{e} + \mathrm{Br}_2 \rightarrow \mathrm{Br}_2^+ + \mathrm{e} + \mathrm{e}$
(ionization of bromine molecule)

In these reactions it seems hardly to cause ionition by the process (A) at the Geiger threshold ıce the ionization potential of argon atom 15.7 eV higher than that of bromine molecule 12.8 eV†. ccordingly, from the processes (B) and (C), it may found in the first avalanche that the ionization ll mainly occur by electron impact with bromine olecules and the excitation by electron impact th argon atoms. Thus the large number of excited gon atoms and ions will be produced in the first alanche formed near the anode wire. These cited argon atoms or ions will act to generate the otoelectrons in the gas or at the cathode by some otoelectric process, e.g., by U.V. photons and sonance photons[6]). These photoelectrons will use the second avalanche. In order to cause the eiger discharge, it may be said that there is a obability per ion of the first avalanche that photoectrons will be generated. Let $\varepsilon_g(R)$ be the probality per ion of the first avalanche to generate otoelectrons by the photoionization in the gas, nd ε_c be the probability per ion of the first avanche to generate another photoelectrons by the hotoemission at the cathode. If the photoelectrons hich may cause the successive avalanches are due photons from the excited argon atoms, some of ıch photons will be absorbed in the gases to cause hotoionization and the remainder of the photons ill reach the cathode to cause photoemission.

Since the absorption coefficient of the gases for ıe photons created in the first avalanche in the rgon-bromine counter seems to be very small, it an be assumed that $\varepsilon_g(R)$ is not dependent on the adial distance from the wire R, namely, $\varepsilon_g(R) = \varepsilon_g$.

We then have $S(R) = \varepsilon_g N(1)$ and $\varepsilon_c N(1)$ for the hotoelectrons produced in the gas and at the athode respectively. Considering that all of such hotoelectrons will contribute to the generation of he second avalanche, the number of electrons roduced in the second avalanche may be reresented from (7) as follows:

$$N(2) = \int_a^R \varepsilon_g N(1) \left(\frac{R}{a}\right)^{CV/\ln(b/a)} \cdot \exp\left\{ - G \frac{PP_1}{2V} (R^2 - a^2) \right\} \mathrm{d}R + \varepsilon_c N(1) \left(\frac{b}{a}\right)^{CV/\ln(b/a)} \cdot \exp\left\{ - G \frac{PP_1}{2V} (b^2 - a^2) \right\} = N_g + N_c , \quad (8)$$

where N_g is the number of electrons reaching the wire from a region in the gas in which photoelectrons $\varepsilon_g N(1)$ are produced, being subjected to both effects of electrons capture and electrons multiplication on their way; N_c is the number of electrons reaching the wire from the cathode at which photoelectrons $\varepsilon_c N(1)$ are produced, being subjected to both effects of electron capture and electron multiplication on their way.

In order to cause the Geiger discharge, it is required that the number of ions $N(2)$ contained in the second avalanche is equal to or larger[8]) than $N(1)$ contained in the first one. The condition of Geiger threshold would be satisfied with

$$N(1) = N(2) , \quad (9)$$

by neglecting the statistical fluctuations in the production of avalanche. If the avalanche breeding in the Geiger discharge is due to only the photoelectrons produced at the cathode, (9) becomes

$$N(1) = N(2) = N_c ,$$

since $N_g = 0$ in (8).

We thus have

$$\left(\frac{b}{a}\right)^{CV_t/\ln(b/a)} \cdot \exp\left\{ - G \frac{PP_1}{2V_t} (b^2 - a^2) \right\} = \frac{1}{\varepsilon_c} , \quad (10)$$

where V_t is Geiger threshold voltage.

Next, if the avalanche breeding in the Geiger discharge is started only by the photoelectrons produced in gas volume, the relations $N_c = 0$,

[8]) D. H. Wilkinson, Phys. Rev. **74** (1948) 1417.

† It should be noted that a substantial decrease in breakdown voltage for argon-bromine mixture in comparison with pure argon is attributable to Penning's effect, and that the ionization potential for Br_2 is in the range between 9.91 eV and 11.55 eV, according to Kuiper and van Zoonen (J. Kuiper and D. van Zoonen, Appl. Sci. Res. B **4** (1954) 235).

$N(1) = N(2) = N_g$ and $V = V_t$ may be substituted in (8). Thus, in this case, we obtain

$$\int_a^R \left(\frac{R}{a}\right)^{CV_t/\ln(b/a)} \cdot \exp\left\{-G\frac{PP_1}{2V_t}(R^2 - a^2)\right\} dR = \frac{1}{\varepsilon_g}. \tag{11}$$

4. Limit Value of α/E in Argon Bromine Mixture

In previous section 2, the relation between α/P and E/P for argon containing some bromine vapor was assumed to be linear in a rough approximation, in order to simplify the calculation within the limited range of E/P in which electron multiplication occurs. This approximation may be a very rough one, since the relation between α/P and E/P for argon-bromine mixtures does not seem to be well known. It is, however, seen from the studies of Gill and Pidduck[9]), of Ayres[10]) on argon contaminated[11]) with some impurities, and of Kruithof and Penning [12]) on pure argon that the zero point of α/P on the curve of α/P is more close to the origin and the slope of the curve have a tendency to be smaller than that of pure argon, as shown in fig. 1.

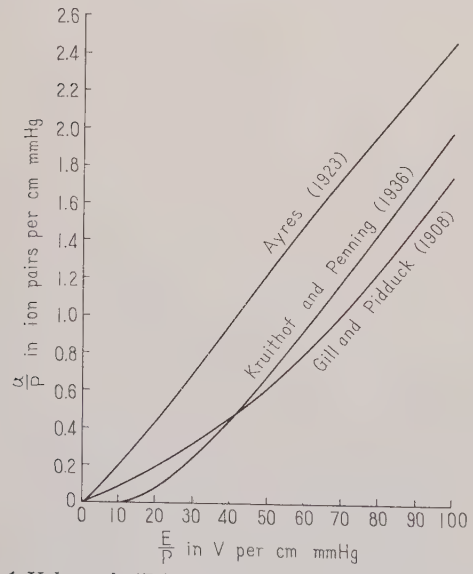

Fig. 1. Values of α/P for argon contaminated by some impurities and for pure argon as a function of E/P. It is shown in the figure that the values of α/P argon as a function of E/P were revised in chronological order (see refs.[9–11]).

Then we have reasonably taken as

$$\frac{\alpha}{P} = C\frac{E}{P} \quad \text{or} \quad \alpha = CE,$$

where C is a proportional constant corresponding to the slope of a straight line, which is drawn from the origin as the average inclination in the α/P curve for E/P of interested range. The value of C is looked upon as an average value of $\alpha/E = \eta$ which is generally some function of E/P. The values of η for various gases or gas mixtures have been investigated[13]) by many researchers. Among them the study of neon-argon mixtures by Kruithof and Penning[14]) is of particular interest, since the values of η for these mixtures shown at low values of E/P are largest than those for other gases[15]). It has been shown in their studies[14]) that an increase of argon in neon causes an apparent increase of η for E/P lower than 100 V/cm mm Hg, but the maximum value of η is not above 0.04 V^{-1}.

It is known that the breakdown potentials of argon-bromine counters[16]) are higher than those of neon-argon counters[15]). Therefore, the maximum value of η for argon-bromine mixture must be lower than that of neon-argon mixtures, for the same range of E/P, since gases or gas mixtures which have high values of η produce low breakdown potential. Thus C for argon-bromine mixtures must be lower than 0.04 V^{-1} in lower range of E/P.

5. Comparison of Experimental and Theoretical Results

Table 1 shows the experimental data which have been obtained in a previous work[7]) by using a conventional end-window counter having $a =$ 0.25 mm (anode radius), $b = 12.5$ mm (cathode radius), and $l = 30$ mm (effective length of anode wire). It is shown in the table that the threshold voltage V_t is increased as the total pressure P of argon is increased under a constant pressure at $P_1 = 1$ mm Hg of bromine vapor.

The calculated values of E/P at Geiger threshold for our counters are shown in fig. 2. From the figure, the range of E/P in which Geiger discharge

[9]) E. W. B. Gill and F. B. Pidduck, Phil. Mag. **16** (1908) 280.
[10]) T. L. R. Ayres, Phil. Mag. **45** (1923) 383.
[11]) F. M. Penning and C. C. J. Addink, Physica **1** (1934) 1007.
[12]) A. A. Kruithof and F. M. Penning, Physica **4** (1937) 430.
[13]) L. B. Loeb, Basic Processes of Gaseous Electronic (University of California Berkeley and Los Angeles, 1955) Ch. 8.
[14]) A. A. Kruithof and F. M. Penning, Physica **3** (1936) 515.
[15]) J. A. Simpson, Jr., Rev. Sci. Instr. **21** (1950) 558.
[16]) D. van Zoonen, Appl. Sci. Res. B **3** (1952) 1.

Table 1

perimental data for a conventional end-window counter ed with argon-bromine mixtures, having $a = 0.025$ cm iode radius), $b = 1.25$ cm (cathode radius) and $l = 3$ cm (effective length of anode wire)

Trial No.	Partial pressure of bromine vapor P_1 (mm Hg)	Total pressure of added argon to bromine vapor P (mm Hg)	Threshold voltage V_t(V)
1	1.0	100	550
2	1.0	220	640
3	1.0	339	700
4	1.0	460	750
5	1.0	570	800
6	1.0	624	820

reaks out is found to be from 10 to 60 V/cm mm Hg. In (6) G may be given as a constant value by utting $a = 0.025$ cm, $b = 1.25$ cm, and

$$\frac{h}{k_0^2}\frac{\sigma_1}{\sigma} = 8.0 \times 10^{-15}\ (\mathrm{V\ sec/cm^2\ mm\ Hg})^2 .$$

Ve thus have $G = 41.4\ \mathrm{V/cm^2\ (mm\ Hg)^2}$ for our ounters.

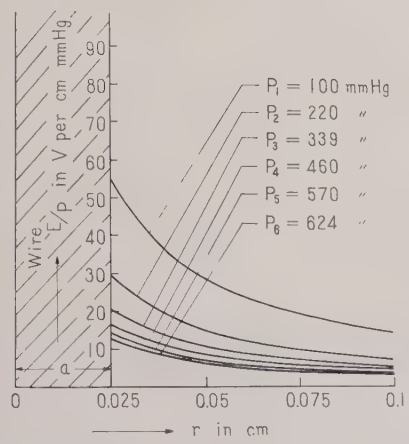

ig. 2. Values of E/P near the anode wire at the Geiger threshold or our counters as a function of the distance from the wire. he curves have been obtained by computation from the experimental results as shown in table 1.

Substituting the numerical values for a, b, P_1 nd G, and those for V_t corresponding to P in Table 1 respectively into (10) on the assumption hat the avalanche breeding in halogen counters at Geiger threshold occurs only by the photoelectrons reated at the cathode, we obtain six simultaneous equations including C and ε_c as unknown values.

If the values of C and ε_c are independent of the argon pressure P, these algebraical equations can be solved by means of the method of least squares. We can thus obtain $C = 0.07\ \mathrm{V^{-1}}$ and $\varepsilon_c = 10^{-15}$.

However, such values of C and ε_c seem to be unreasonable for the following reason:

(1) $C = 0.07\ \mathrm{V^{-1}}$ for argon-bromine mixtures is much larger than the expected value $C < 0.04\ \mathrm{V^{-1}}$, as was discussed in section 4.

(2) $\varepsilon_c = 10^{-15}$ is so small as a probability per ion of the first avalanche to generate the photoelectrons at the cathode surface.

These results suggest that the avalanche breeding at Geiger threshold can not be produced only by the photoelectrons created at the cathode by the photoemission.

Next it is assumed that the avalanche breeding at Geiger threshold occurs only by the photoelectrons produced in the gas. Then (11) will be applied to the experimental results.

Substituting the numerical values for a, b, P_1, G and P, and those for V_t corresponding to P in table 1 respectively into (11), we have six integral equations including C and ε_g as unknown values. The solution can be obtained by keeping ε_g constant in the graphical integration and by choosing a plausible value of C lower than $0.04\ \mathrm{V^{-1}}$. The results obtained for $C = 0.013\ \mathrm{V^{-1}}$ are shown in table 2. It seems to be satisfactory for our counters since ε_g is approximately constant and does not depend on P. The value of $C = 0.013\ \mathrm{V^{-1}}$ also seems to be reasonable as discussed in section 4.

In consequence, it seems to be plausible for our

Table 2

Value of e_g, the probability per ion of the first avalanche to generate photoelectrons by photoionization in the gas. It seems to be approximately constant, namely, ε_g (mean) $= 1.54 \times 10^{-2}$

Trial No.	P (mm Hg)	$1/\varepsilon_g$	ε_g ($\times 10^{-2}$)
1	100	64	1.56
2	220	65	1.54
3	339	59	1.69
4	460	64	1.56
5	570	71	1.43
6	624	71	1.43

The pressure of bromine is kept constantly at $P_1 = 1$ mm Hg.

counters that avalanche breeding occurs only by the photoelectrons from the gas, but does not occur by those from the cathode. This result agrees with van Zoonen's results for argon-iodine counters that the cathode does not play a role for avalanche breeding.

6. Discussion

The electron increment per unit length $\Delta n/\Delta r$ as a function of the distance r from the center of the wire can be calculated by (5). In case of $n = 1$ for our counters is shown in fig. 3, in which the $\Delta n/\Delta r$ vs. r curve intersets at R_0 with the abscissa. This R_0 can be easily obtained from (5) as the distance where the electron increment is equal to the electron decrement, namely,

$$R_0 = \frac{V}{\ln(b/a)} \sqrt{\frac{C}{G'PP_1}}, \qquad (12)$$

where

$$G' = h\frac{\sigma_1}{\sigma}\frac{1.32 \times 10^{15}}{k_0^2} = 10.6\,\mathrm{V/cm^2 \cdot (mmHg)^2}\,.$$

In fig. 3 it is evident that the left region of R_0 is sensitive for the counting, but the right region of R_0 is insensitive.

The propriety of the above may be checked by applying (12) to the experimental results by van Zoonen[17]) shown in fig. 4. In obtaining the results that show the radial sensitivity in an argon-bromine counter obtained by X-ray, the numerical values of $V = 1360$ V, $P = 600$ mm Hg, $P_1 = 0.6$ mm Hg, $a = 0.05$ cm, $b = 0.95$ cm, and $C = 0.013\ \mathrm{V^{-1}}$ are substituted into (12). We thus have $R_0 = 0.86$ cm.

The result is in a good agreement with the experimental result by van Zoonen shown in fig. 4. Now it can be seen that the photo-electrons from the cathode do not contribute to generating the successive avalanche, although the photoelectrons may be generated at the cathode. This is the reason why the mechanism of avalanche breeding is attributed only to the photoelectrons produced in the gas for the halogen counters.

It is, however, not simply considered that avalanche breeding in halogen counters causes only by the photoionization in the gas, because the distance R_0 depends on many factors as was seen in (12), such as the counter voltage V, the bromine

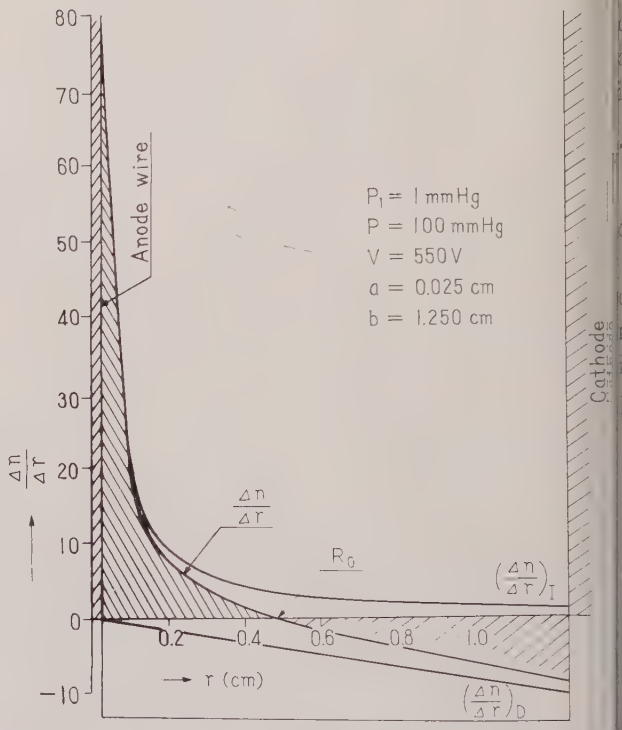

Fig. 3. Electron increment per unit length $\Delta n/\Delta r$ in a halogen counter as a function of the distance r from the center of the wire. R_0 shows the distance where the electron increment $(\Delta n/\Delta r)_I$ is equal to the electron decrement $(\Delta n/\Delta r)_D$.

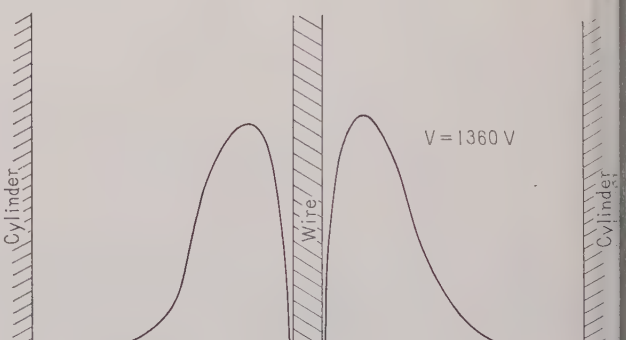

Fig. 4. Radial sensitivity for counter voltage $V = 1360$ V of a mica-window counter (argon pressure $P = 600$ mm Hg, bromine pressure $P_1 = 0.6$ mm Hg, anode wire radius $a = 0.05$ cm, and cathode radius $b = 0.95$ cm) obtained by directing through a mica-window the counter with X-ray beam parallel to the anode wire (see ref.[17]).

[17]) D. van Zoonen, Appl. Sci. Res. B **4** (1954) 196.

essure P_1, the total pressure P, the cathode dius b, and the anode radius a. Accordingly, the ntribution to the avalanche breeding of photo- ectrons from the cathode would be possible to cur, since R_0 shifts towards the cathode when V d a are increased and b, P and P_1 are decreased (12).

Conclusion

A theory for the avalanche breeding in the Geiger scharge in the halogen counter is developed.

By applying this theory to an experimental result tained in our counter filled with argon-bromine ixtures, it is deduced that the avalanche breeding argon-bromine counters is caused only by the notoelectrons produced in the gas.

This result agrees with the experimental results by van Zoonen for argon-iodine counters.

The theory is further capable of elucidating the fact that the above result is not solely acceptable, since the contribution to the avalanche breeding of the photoelectrons produced at the cathode is possible to occur by relying on many factors, i.e., the counter voltage, the counter dimension, and the counter filling.

Acknowledgements

The author wishes to express his gratitude to Dr. K. Shinohara for his kind guidance as well as to Dr. F. Yamasaki for his helpful discussions and to Professor M. Kimura for his advice and encouragement.

NUCLEAR INSTRUMENTS AND METHODS **14** (1961) 94–96; NORTH-HOLLAND PUBLISHING CO.

SINGLE SAMPLE SPIN GENERATOR SPECTROMETER

K. V. VLADIMIRSKY and B. A. LABZOV

P.N. Lebedev Institute of Physics of the Academy of Sciences of USSR, Moscow

Received 21 August 1961

Resonance conditions in the high-resolution nuclear magnetic resonance spectrometer are stabilized by a self-excited electronic circuit, frequency of oscillation being controlled by one of the lines of the sample under study. A very small width of this control line increases considerably the precision with which frequency follows the unstable field. Changes in the magnet's field configuration do not influence the results of the chemical shift measurements because both for the stabilization and recording of the spectrum the same sample is used.

1. High-resolution nuclear magnetic resonance requires both high magnetic field homogeneity and precise control of the magnetic field strength-frequency relationship. The field homogeneity is attained by the magnet construction improvement, thermostating of the yoke, shimming with auxiliary coils. The sample spinning gives a considerable improvement in resolution too. Resonance condition stabilization methods known at present are less satisfactory because they do not correspond in precision to the minimum line width.

In the spectrometers in which the field-frequency relationship is maintained by the independent stabilization of both quantities, a good long time stability can not be attained at all. Better performance reveal the spectrometers in which nuclear magnetic resonance of the second auxiliary specimen is used. In this way the possibility arises of maintaining the field-frequency relationship without seeking the high grade stability of both quantities separately. For this purpose the automatic frequency control[1]), proton stabilizer[2,3]) superregenerator in a coherent mode of operation[4]) are used. In Varian A-60 spectrometer a version of "spin generator" proposed by Schmelzer[5]) is used. In principle, application of the "maser" type apparatus[6]) is also possible. The static precision of all of the above-mentioned stabilizing devices is sufficient for high-resolving spectrometers. It seems that the spin generator is the best rapid-operating device.

It must be mentioned, however, that in two sample spectrometers the high stability is not insured by the very principle of operation. The chemical shift cannot be found directly but as a difference of a number of quantities of the different origin but the same order of magnitude. The results depend on the difference in field at the two sample sites, on some (unknown) fraction of the control line width, and on the parameters of the sweeping coils. Besides, the above mentioned methods of the field homogenization do give a good uniformity in some near vicinity of one arbitrary chosen point that is in *one* sample only. In two sample spectrometers the control sample would be located in the field with worse homogeneity than that in the sample under study, which diminishes sufficiently the precision of the stabilization. So the use of the separate sample for the stabilization purposes can give the precision of measurements necessary at the present resolution level at the cost of a number of parametric stabilization measures and of some calibrations only. Further improvement of the

[1]) E. B. Backer and L. W. Burd, Rev. Sci. Instr. **28** (1957) 313.

[2]) M. E. Packard, Rev. Sci. Instr. **19** (1948) 435.

[3]) K. V. Vladamirsky and B. A. Labzov, Pribory i Tekhnika Eksperimenta USSR (1961) N4.

[4]) R. V. Pound and R. Freeman, Rev. Sci. Instr. **31** (1960) 96;
R. Freeman and R. V. Pound, Rev. Sci. Instr. **31** (1960) 103

[5]) Schmelzer, Lectures on the theory and design of an alternating gradient proton-synchrotron (1953).

[6]) K. V. Vladimirsky, JETP USSR **33** (1957) 532; Nucl. Instr. **1** (1957) 329.

olution by using this method of stabilization is dly possible.

2. We constructed and tested a spectrometer ich to a considerable extent is free from the ove-mentioned shortages (fig. 1). For the spec- um study and for the precise stabilization, a

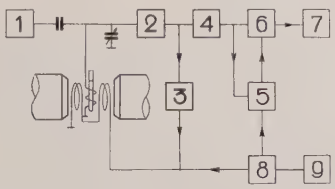

g. 1. Block diagram of the NMR spectrometer: 1. r.f. oscillator eceiver; 3. limiting amplifier; 4. linear amplifier; 5. balanced odulator; 6. synchronous detector; 7. recorder; 8. a.f. generator; 9. crystal calibrator.

ngle sample is used†. The strongest of the lines is e control one and is used for the stabilization by e spin generator method. The rest of the lines are corded by using a double modulation. The control e can be one of the substance under investigation of another substance. Tetramethylsylane is the ost convenient[7]) as its line lies outside most of the ectra.

Our apparatus and circuitry includes few unusual ements. Rollin type detector operating at 36,27 c/s is used[8]). Its tuned circuit is loosely coupled to e crystal-controlled r.f. oscillator. The receiver nverts the amplitude modulation of the r.f. oltage across the tuned circuit to an audio fre- uency signal. Oscillation of the spin generator type excited by the amplified output of the receiver eing applied to the modulating coils. The magnetic eld H_0 is regulated so that the resonance frequency f the control line is about 2 kc/s higher then that f a r.f. oscillator. The frequency of oscillation is etermined by the resonance condition for mo- ulated fields[9]).

$$\gamma H_0 = \omega_0 + n\Omega\,, \qquad (1)$$

where γH_0 is the resonance frequency in the d.c. eld, ω_0-frequency of the r.f. oscillator, Ω-frequen- y of modulation, n-any integer. In our case $n = 1$ that is the first side band is used. The

† The second sample with a broad line is used in a proton tabilizer[3]) for the preliminary stabilization.

precision with which the frequency of oscillation fits eq. (1) depends essentially upon the line width. In the most important case of a very small line width the sample characteristics are the main source of the phase changes in the feedback loop and the frequency of oscillation fits eq. (1) very closely. The frequency of oscillation supplements the r.f. oscillator frequency up to the exact resonance value, which makes it possible to use such a selfexcited system for the precision stabilization purposes.

The main point in the realization of such a mode of operation of the spin generator is the stability of oscillation controlled by a narrow line, obtained from matter with large value of the relaxation time. Without some special measures the selfexcitement process proceeds to the interrupted oscillation.

In our case a high degree of the oscillation stability is insured by the insertion of a noninerted nonlinearity—of a limiting amplifier—in the feedback loop. High precision in the field strength—frequency control can be obtained without very high parameters of the receiver, amplifier and modulating coils. With the line width of 1 c/s and the amplifier band width of only 1 kc/s, the stabilization ratio will be $\sim 10^3$. Fast action is secured by noninertial change of the magnetic moment precession frequency with the field.

Experimentally, the high precision of the stabilization is confirmed immediately by the constancy of the amplitude of the control signal. As far as precision of the preliminary stabilization permitted, the close fit of the frequency of oscillation to eq. (1) was studied. The most essential approbation of the precision of the control is the very good reproducibility of the spectra obtained (see below). Of some interest are the unsteady modes of operation of the spin generator. Thus, when the amplitude of modulation were increased beyond the stability limits, samples with two strong lines give the oscillation controlled by the two lines in turn. The frequency difference gives immediately the

[7]) G. Tiers, J. Phys. Chem. **62** (1958) 1151.
[8]) B. V. Rollin, Nature **158** (1946) 669.
[9]) K. V. Vladimirsky, Doklady Ak. Nauk USSR **58** (1947) 1625;
K. Halbach, Helv. Phys. Acta **29** (1956) 37;
K. V. Vladimirsky, JETP USSR **33** (1957) 529.

chemical shift between the lines, and the periodicity of two modes depends on the relaxation phenomena in two spin systems.

3. The application of the spin generator for stabilization in our spectrometer is based on the fact that the spin generator operating steadily on single narrow line does it equally well with a total spectrum of narrow lines. In the last case, the spin generator oscillates on the frequency of the strongest line and the rest of these do not violate the spin generator operation because the resonance condition (1) for these lines is not fulfilled. To study these lines, it is necessary to make the resonance conditions for the second line too. It is attained by using the double modulation. Besides of the spin generator oscillation, the second modulation frequency Ω_1 equal to the frequency difference between the control line and the other one is applied to the modulating coils. In this way the combination tones $\Omega \pm \Omega_1$ of the double modulation are used to excite the signal of the second line. The same results gives the amplitude modulation of the limiting amplifier output too. The resonance frequency differences are sufficiently stable as the field instability is small enough ($\sim 10^{-6}$ in our case). It is clear therefore that the modulation frequency Ω_1 can give a very stable scale for the chemical shift measurements.

A synchronous detection of the signals is used. The balanced modulator (fig. 1) gives the reference signal with the frequencies $\Omega \pm \Omega_1$ and at the same time removes the zero displacement due to the control signal. The d.c. signal at the output of the synchronous detector is recorded in the usual way. The nonlinear effects, possible in the spin generator and in receiving circuitry, are small when the control signal is strong enough and do not prevent the precise chemical shift measurements.

When recording the spectrum the modulation frequency is swept slowly. The frequency marks are made with the use of a crystal calibrator which permits the direct evaluation of the chemical shift in c/s. Because the control line width is small, the stabilization error is also small, and the values obtained in this way are very close to the chemical

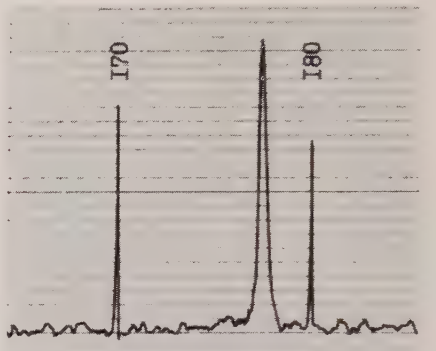

Fig. 2. Methyl group line in toluene. Frequency marks in c/s.

shift of the lines against the control one. The maximum precision can be obtained by the usual internal standard method.

As an example, fig. 2 shows the recording of the methyl group line in toluene. Phenyl group line was used as the control one. The reproducibility of such recordings is very high, better than 10^{-8}.

So far, the single sample stabilization method gives very promising results with the apparatus not specially built and very far from being perfect. High stability of the spectrometer and the presence of the control signal at the output of the receiver do improve essentially the resolution practically realised, as for the best results it is enough to adjust for the maximum control signal strength. To estimate the perspectives, it is important that the precision of the stabilization obtained grows up with the resolution. It seems probable that in the future this will give a possibility to attain the resolution exeeding the so far accesible 10^{-8}.

CLEAR INSTRUMENTS AND METHODS 14 (1961) 97–100; NORTH-HOLLAND PUBLISHING CO.

INVESTIGATION OF THE NUCLEAR CASCADE IN SHIELDING MATERIALS

A. CITRON and L. HOFFMANN

CERN, Geneva

and

C. PASSOW

DESY, Hamburg, Germany

Received 2 September 1961

e build-up of the nuclear cascade and its subsequent at- uation has been measured in two types of concrete and earth ng as primary radiation protons from the CERN-PS. From a row and a wide beam experiment we find the following lower its for characteristics of the cascade:

(i) there is a region of a full width of 550 g cm^{-2} in which the intensity increases by a factor of 3, and drops down again to the initial value.

(ii) this is followed by a nearly exponential decrease of the intensity of the radiation with an attenuation length of 145 ± 10 g cm^{-2}.

Introduction

In the attenuation of radiation in shielding walls high energy accelerators the "nuclear cascade" ays an important part. By this we mean a mode propagation of high energy radiation through atter, in which the primary particles provoke uclear interactions of such nature, that one or ore secondary particles are ejected of an energy fficient to induce similar nuclear reactions and so through several generations. Calculations have own that this phenomenon is of primary impor- nce not only for shielding proton accelerators in e GeV region[1,2]), but even for electron accelera- rs of this energy[2,3]).

In the present paper two experiments are escribed which were designed to study this nuclear scade. Both measurements were carried out at e CERN proton synchrotron. The evaluation of sults took place partly at DESY in Hamburg, rtly at CERN. 24 GeV/c protons were made to ll on absorbers composed of concrete and, in one se, earth. The development of the cascade inside ese absorbers was measured with the help of uclear emulsions, (Ilford G5).

Wide Beam Experiment

Fig. 1 gives the dimensions of the absorber and ie position (I . . . IX) of the nuclear emulsions in this experiment. For the various materials used, the density and the mean free path (mfp) for nuclear interactions are listed in table 1.

TABLE 1

Material	Density (g cm^{-3})	Nuclear mfp.* (g cm^{-2})	Nuclear mfp.* (cm)
Iron	7.9	142	18)
Baryte concrete	3.6	137	38
Ordinary concrete	2.5	103	44
Earth	1.6	104	65

* The values for the nuclear mfp (g cm^{-2}) are based on the geometrical cross section, i.e. they are calculated from the expression:

$$37 \frac{1}{\sum_i n_i A_i^{-1/3}}$$

A_i: atomic weight of element i
n_i: percentage by weight of element i.

[1]) W. Gentner and A. Citron, CERN-PS/WG 3 1954 (unpublished).

W. Gentner, A. Citron and A. Sittkus, Strahlentherapie **94** (1954) 23.

[2]) Conference on Shielding of High-Energy Accelerators, New-York, 1957;

G. K. O'Neill, Monte Carlo Calculations, p. 89;

B. J. Moyer, Build-up Factors, p. 96;

E. Crosbie, 12.5-BeV Proton Synchrotron, p. 167;

W. K. H. Panofsky and others, Shielding Work at Stanford Univ., p. 199.

[3]) C. Passow, DESY, 1959, Physikalische Grundlagen zur Besprechung des Strahlenschutzes für Hochenergie-Beschleuniger (unpublished).

The momentum spectrum[4]) of the charged part of the incident beam, the "scattered out proton beam", is given in fig. 2. The beam was not well collimated. In the horizontal plane its width (at half-intensity) was $\pm$ 12 cm, in the vertical plane

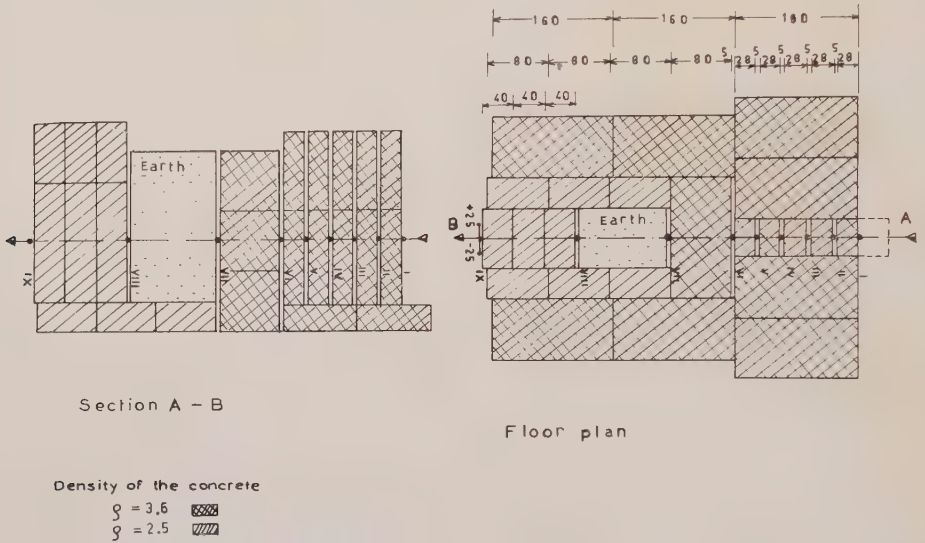

Fig. 1. Geometrical arrangement of the absorber and position of plates, in the wide beam experiment. Dimensions in cm

$\pm$ 4 cm. The time of exposure in the various positions was chosen according to the dose expected. The beam intensity was monitored throughout the exposure. The plate in position IX was spoilt in processing. The results given for this point are interpolated between those in position IX – 25 and IX + 25.

All plates were scanned for stars (events with 2 or more prongs). At each positions 150 stars were evaluated and the volume in which they were found was recorded. They were classified as "neutral stars" (without visible primary) and "charged stars". In position IX stars, of which all prongs go in a direction roughly opposite to that of the incident beam, were not counted. These (about 10% of all stars) were considered to be caused by background particles, which had not passed the full absorber thickness.

The results are given in fig. 3. The total number of stars reaches a maximum at a depth of 180 g cm^{-2}, or 1.3 mfp in heavy concrete. Here the density of stars is three times that found in positon I (in front of the absorber). This density drops to the initial value at a depth of 550 g cm^{-2} (4 mfp) (end of the "transition region"). From here on the drop is nearly exponential, with an attenuation length of 145 $\pm$ 10 g cm^{-2} (1.06 $\pm$ 0.07 mfp) ("absorption region"). The uncertainty in the absorption length is caused mainly by lack of information about the composition of the absorbers used (iron parts, water content).

The fraction of neutral stars (fig. 3b) depends initially (position I) on the composition of the incident beam. Already in the transition region it reaches a value (0.64 $\pm$ 0.1), which does not change any more throughout the absorption region. It is thus characteristic for the cascade process. A stronger predominance of neutral stars due to the ionisation losses of the charged particles is expected for absorber thicknesses greater than those used in this experiment. It should be remarked that the classification into neutral and charged stars becomes less unambiguous at greater absorber depths, since the generating particle may be incident at a considerable angle with the initial beam direction, and may thus be taken for a secondary particle.

3. Narrow Beam Experiment

In this experiment only heavy concrete was used as an absorber. The positions of the plates can be

[4]) A. Ashmore, G. Cocconi, N. Diddens and A. M. Wetherell, CERN, SC Internal report 60–11 (1960) (unpublished).

d off the relevant abscissa scale in fig. 3 (A . . G). beam was momentum analysed and had a mentum of 20 GeV/c $\pm$ 3%, but also contained he neutral particles. It was collimated to an izontal halfwidth of $\pm$ 0.9 cm and a vertical fwidth of $\pm$ 3.1 cm. The scanning procedure was

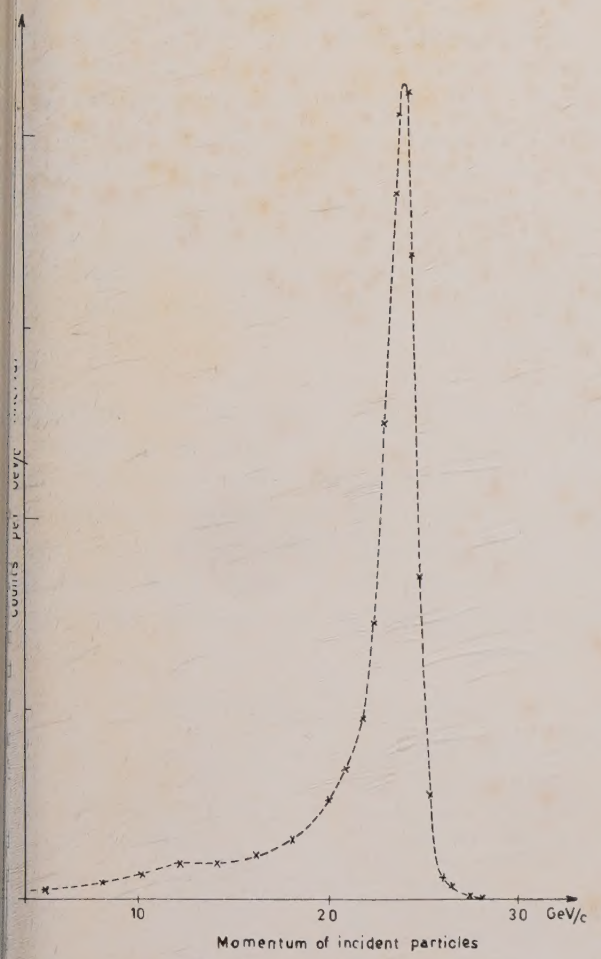

g. 2. Momentum spectrum of the charged part of the incident beam, according to[4]). Geometrical resolution $\pm$ 2.9%.

nilar to that adopted in the wide beam experiment. Since in this case the dimensions of the ates are not small compared to the beam dimensions, it is important to find in each plate the gion of maximum track density, which is taken be on the axis of the cascade. A zone corsponding to the halfwidth of the beam incident the first plate was scanned in each position.

The result is included in fig. 3. It is seen that the ildup is less pronounced in this case. The flat maximum is reached at about 150 g cm^{-2} already, the transition region ends at 300 g cm^{-2}. In the absorption region the attenuation length is 115 $\pm$ 15 g cm^{-2}, which corresponds to 0.84 $\pm$ 0.11 mfp, in heavy concrete.

The fraction of neutral stars (fig. 3b) is initially

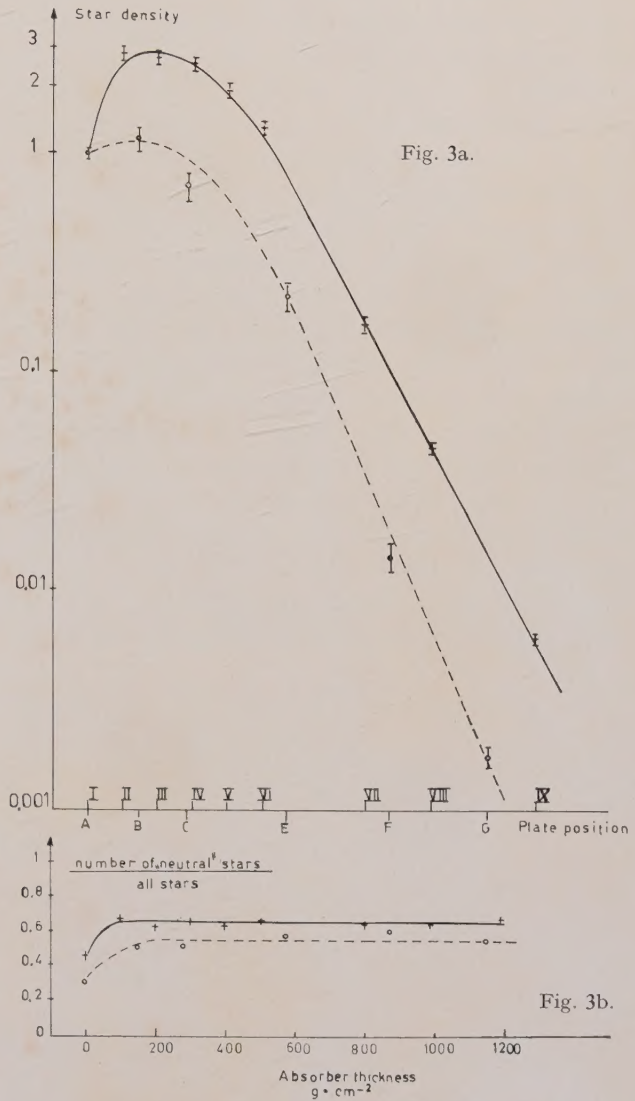

Fig. 3a.

Fig. 3b.

Fig. 3a. Density of stars per unit volume and per particle incident on the absorber as a function of absorber thickness, measured in g cm^{-2}, normalized to the value at zero absorber thickness. The full line refers to the wide beam experiment, the broken one to the narrow beam experiment. The positions of the plates are indicated. Roman numerals refer to the wide beam, capital letters to the narrow beam exposure.

Fig. 3b. Fraction of stars without visible primary, as a function of absorber thickness, measured in g cm^{-2}. Crosses refer to the wide beam, circles to the narrow beam experiment.

lower than in the wide beam experiment, but reaches the equilibrium value of 0.55 ± 0.1 soon.

4. Discussion

In fig. 3, the absorber thickness is measured in g cm^{-2}. If, instead, the mfp values of table 1 are used as units of absorber thickness, the absorption curve in earth and light concrete is shallower than that in heavy concrete. Therefore, between these two samples the cross section for star processes seems to depend on the atomic weight (A) not like $A^{\frac{2}{3}}$, as assumed in table 1, but more like A, in which case the mfp (g cm^{-2}) is independent of A.

The much stronger apparent absorption in the narrow beam experiment is explained by the fact that in this case the dimensions of the incident beam are much smaller than the width over which the nuclear cascade spreads the particles after a few interactions. (Typical angles are of the order of several degrees.) This results in a dilution of the beam, which is superimposed on its attenuation. This geometric dilution is also present in the wide beam experiment, but less pronounced. The true attenuation would be obtained, if the incident beam would be wider, both in the horizontal and the vertical plane, than the lateral distance, over which particles from one point at the beginning of the cas cade are spread at the last stage of the cascade obser ved. This is not quite fulfilled in either experiment *In this sense the attenuation length found in the wid beam experiment has to be taken as a lower limit fo the true attenuation length.* The same is true for th width of the transition region, etc.

Failing an experiment with a very wide beam th dilution can be corrected for, if it is accuratel known. This necessitates an investigation of th lateral structure of the cascade. An experiment o this line is planned. It should also avoid some othe shortcomings of the present measurements, such a the lack of information about the neutral com ponent of the beam and about the composition c the absorber, the influence of stray radiation on th last plates, etc.

The authors wish to express their gratitude t members of the MPS division, in particular Mi Geibel, for their collaboration in the preparatio and execution of the experiments. We enjoyed th collaboration of Dr. Ballam in the second experi ment. We also wish to thank Prof. Teucher fo making available to us scanning work in hi laboratory.

NORTH-HOLLAND BOOKS

FROM THE SERIES IN PHYSICS

General Editors:

J. DE BOER, Professor of Physics, University of Amsterdam
H. BRINKMAN, Professor of Physics, University of Groningen
H. B. G. CASIMIR, Director of the Philips' Laboratories, Eindhoven

Monographs:

B. BAK, Elementary Introduction to Molecular Spectra
H. C. BRINKMAN, Application of Spinor Invariants in Atomic Physics
H. G. VAN BUEREN, Imperfections in Crystals
S. R. DE GROOT, Thermodynamics of Irreversible Processes
E. A. GUGGENHEIM, Thermodynamics
E. A. GUGGENHEIM, Boltzmann's Distribution Law
E. A. GUGGENHEIM and J. E. PRUE, Physicochemical Calculations
D. TER HAAR, Elements of Hamiltonian Mechanics
H. JONES, The Theory of Brillouin Zones and Electronic States in Crystals
H. A. KRAMERS, Quantum Mechanics
H. A. KRAMERS, The Foundations of Quantum Theory
J. G. LINHART, Plasma Physics
J. MCCONNELL, Quantum Particle Dynamics
A. MERCIER, Analytical and Canonical Formalism in Physics
A. MESSIAH, Quantum Mechanics, Volume I
I. PRIGOGINE, The Molecular Theory of Solutions
S. RAIMES, The Wave Mechanics of Electrons in Metals
E. G. RICHARDSON, Relaxation Spectrometry
P. ROMAN, Theory of Elementary Particles
M.E. ROSE, Internal Conversion Coefficients
J. L. SYNGE, Relativity: The Special Theory
J. L. SYNGE, Relativity: The General Theory
J. L. SYNGE, The Relativistic Gas
A. VAŠÍČEK, Optics of Thin Films
A. H. WAPSTRA, G. J. NYGH and R. VAN LIESHOUT, Nuclear Spectroscopy Tables

Edited Volumes:

D. A. BROMLEY and E. W. VOGT (editors), Proceedings of the International Conference on Nuclear Structure (Kingston, 1960)
P. M. ENDT and M. DEMEUR (editors), Nuclear Reactions, Vol. I
C. J. GORTER (editor), Progress in Low Temperature Physics, Volumes I–III
H. KALLMAN BIJL (editor), Space Research (Proceedings of the First International Space Science Symposium, Nice, 1960)
H. J. LIPKIN (editor), Proceedings of the Rehovoth Conference on Nuclear Structure
N. R. NILSSON (editor), Proceedings of the Fourth International Conference on Ionization Phenomena in Gases (Uppsala, 1959)
K. SIEGBAHN (editor), Beta- and Gamma-Ray Spectroscopy
Symposium on Solid State diffusion (Colloque sur la diffusion á l'état solide, Saclay, 1958)
3e Colloque de Métallurgie, sur la Corrosion (Saclay, 1959)
Turning Points in Physics, A Series of Lectures given at Oxford University in Trinity Term 1958
J. G. WILSON and S. A. WOUTHUYSEN (editors), Progress in Elementary Particle and Cosmic Ray Physics. Volumes I–V
E. WOLF (editor), Progress in Optics, Volume I

BALTH, VAN DER POL, Selected Scientific Papers
P. EHRENFEST, Collected Scientific Papers

FILED IN STACKS

NORTH-HOLLAND BOOKS

PROGRESS IN LOW TEMPERATURE PHYSICS

Editor
C. J. GORTER
University of Leyden

VOLUME III

Vortex lines in liquid helium II . . . . . W. F. VINEN
Helium ions in liquid helium II . . . . . G. CARERI
The nature of the λ-transition in liquid helium . . . . . M. J. BUCKINGHAM and W. M. FAIRBANK
Liquid and solid ^{3}He . . . . . E. R. GRILLY and E. F. HAMMEL
^{3}He Cryostats . . . . . K. W. TACONIS
Recent developments in superconductivity . . . J. BARDEEN and J. R. SCHRIEFFER
Electron resonances in metals . . . . . M. Ya. AZBEL' and I. M. LIFSHITZ
Orientation of atomic nuclei at low temperatures II . . . . . W. J. HUISKAMP and H. A. TOLHOEK
Solid state masers . . . . . N. BLOEMBERGEN
The equation of state and the transport properties of the hydrogenic molecules. . . . . J. J. M. BEENAKKER
Some solid-gas equilibria at low temperatures . . . . . Z. DOKOUPIL

1961 6 × 9″ XII + 495 pp. 185 ill. 2 plates Gld. 48.— (96s.)

VOLUME I
1955 6×9″ XII + 418 pp.
100 ill. Gld. 30.50 (61s.)

VOLUME II
1957 6×9″ XII + 480 pp.
180 ill. Gld. 42.— (84s.)

From reviews

'The great merit of the book is that it is a veritable mine of information for anyone interested in this field. There are, for example, over 800 references in it.'
British Journal of Applied Physics

' . . . the book deserves to become a much used source for workers in low-temperature and atomic physics.'
Nuclear Instruments and Methods

NORTH-HOLLAND PUBLISHING COMPANY — AMSTERDAM

Sole distributors for U.S.A.: Interscience Publishers Inc. — New York